In the Name of God, the Compassionate, the Merciful.

AMORPHOUS METAL CORES IN MEDIUM FREQUENCY POWER TRANSFORMER

Thesis

submitted to the

University of Salford for the degree

of

Doctor of Philosophy

by

Morteza Razaz

Department of Electronic and Electrical Engineering

University of Salford

Salford M5 4WT England

June 1993

DEDICATED

To the memory of my father who provided me with support and encouragement during my years of study. Also to my dearest mother, brothers and sisters and to my wife and children for their encouragement and patience.

CONTENTS

	Page No.
CONTENTS	i
ACKNOWLEDGEMENTS	vi
LIST OF SYMBLS	vii
SUMMARY	x
CHAPTER 1: INTRODUCTION	1
1.1 Transformer	1
1.2 Power transformer	2
1.2.1 Mains frequency power transformer	2
1.2.2 Aircraft power supplies 400 Hz	3
1.2.3 Switched-Mode power supplies	6
1.3 Core materials	8
1.4 Aims of present investigation	13
CHAPTER 2: TRANSFORMER THEORY AND EQUIVALENT CIRCUITS	15
2.1 The ideal transformer	15
2.2 Linear equivalent circuit of two-winding transformer	24
2.3 Transformer with sinusoidal excitation	32
2.4 Transformer core losses	36
2.5 Approximate equivalent circuits	37
CHAPTER 3: TRANSFORMER DESIGN	41
3.1 Factors influence's transformer design	41
3.1.1 Transformer specification	41
3.1.2 Leakage reactance	44
3.1.3 Effect of frequency	47
3.2 General core design	49

3.2.1 Strip-wound core in grain-oriented silicon-iron 49
3.2.2 Built up laminated transformer 52
3.3 Transformer winding 55
CHAPTER 4: TRANSFORMER CORE LOSSES 57
4.1 Core losses 57
4.2 Hysteresis loss 58
4.3 Eddy current loss 62
4.3.1 Anomalous loss 68
4.3 The effect of applied stress on power loss 69
CHAPTER 5: TRANSFORMER CORE MATERIAL 73
5.1 Core material 73
5.1.1 History of transformer core material 73
5.1.2 Conventional grain-oriented silicon-iron (CGO) 77
5.1.3 High permeability grain-oriented silicon-iron (HIB) 80
5.1.4 Laser scribed high permeability grain-oriented silicon-iron (ZDKH) 85
5.2 Amorphous materials 86
5.2.1 Production of amorphous material 87
5.2.2 The gun technique 88
5.2.3 Piston-and-anvil and double piston technique 89
5.2.4 Centrifuge and rotary splat quencher technique 92
5.2.5 Torsion catapult technique 92
5.2.6 Plasma-jet spray technique 93

5.2.7 Filamentary casting technique 94

5.2.8 Melt extraction technique 98

CHAPTER 6: APPLICATION OF AMORPHOUS MATERIAL 101

6.1 Introduction 101

6.1.1 Power devices 101

6.1.2 Amorphous materials in machines 106

6.1.3 Wound type core distribution transformer 107

6.1.4 First prototype amorphous transformer core development in the UK 112

6.1.5 Commercial production 115

6.2 Electronic devices 117

6.2.1 Magnetic shielding 117

6.2.2 Cable shielding 118

6.2.3 Delay lines 120

6.2.4 Magnetic heads 120

CHAPTER 7: TRANSFORMER CORE DESIGN, MANUFACTURE AND TEST 122

7.1 General design considerations 122

7.1.1 design comparison silicon-iron with amorphous metal core 122

7.1.2 Choice of amorphous material and type of construction 125

7.1.3 Transformer core dimension 128

7.2 Transformer core manufacture and annealing 129

7.2.1 Core winding 129

7.2.2 Purpose of core annealing 131

7.2.3 General condition for annealing process 133

7.2.3.1 Preparation of core 133

7.2.3.2 Annealing atmosphere 134

7.2.3.3 Temperature cycle 134

7.2.3.4 Handling after annealing 135

7.2.3.5 Application of field during annealing process 135

7.2.4 Annealing process under laboratory conditions 136

7.3 Transformer core test 145

7.3.1 Test circuit apparatus 145

7.3.2 Core test measurements using Voltech power analyser 145

7.3.3 Primary and secondary windings for test cores 150

7.4 Comparison of core loss and exciting power of Metglas 2605-S2 with silicon-iron 152

7.5 Comparison of core loss Metglas 2605-S3A with 2605-S2 160

7.6 Comparison of core loss and exciting power with sinusoidal and square wave-excitation 165

7.7 Building factor 178

7.8 Effect of temperature on core losses 185

7.9 Effect of temperature on hysteresis loop Metglas 2605-S2 192

7.10 Separation of core losses 195

7.10.1 Core losses components 195

7.10.2 Separation of losses 195

7.10.3 Determination of hysteresis loop DC method 196

7.10.4 Oscilloscope display of hysteresis loop 199

7.10.5 Results of core loss separation 202

7.11 Comparison of the B/H loop of Metglas 2605-S2 with 2605-S3A 209
7.12 Core protection postanneal 212
7.13 Effect of clamping pressure on the core losses 213
7.14 Effect of applying adhesive to cores 227
7.14.1 Effect of temperature on the B/H loop on core treated with adhesive 234
7.15 Core temperature rise 238
7.15.1 Amorphous Metglas 2605-S2 core 238
7.15.2 Silicon-iron core 244
7.16 Summary and Assessment of Test Results 247
7.16.1 Introduction 247
7.16.2 Comparison of Metglas 1605-S2, 2605-S3A and silicon-iron core losses and exciting VA 247
7.16.3 Annealing process 261
7.16.4 Mechanical stresses 263
7.16.5 Core treated with adhesive 264
7.16.6 Separation of losses 273
7.16.7 Core temperature rise without and with heat sink 279
CHAPTER 8: CONCLUSIONS 281
REFERENCES 284
PUBLICATION 296
APPENDIXES 300

ACKNOWLEDGEMENTS

First and foremost I would like to express my gratitude and sincere thanks to my supervisor Mr K.T. Williams for the help, guidance and encouragement given throughout theresearch project.

I would also like to express my appreciation to Dr. G.H. Cooke for his valuable and helpful discussion throughout the course of this investigation.

Special thanks are also conveyed to all the library, departments workshop for their co-operation throughout the duration of the research project.

I would also thank members of my family for their patience and encouragement during my study: my late father, dearest mother, brothers, sisters and to my wife and children.

Finally, I also wish to gratefully thank the Iranian Government and University of Ahwas for their financial support.

List of Symbols

Symbol	Description	Unit
A	area	m^2
A_{Cu}	total copper cross-section per winding	m^2
A_{Fe}	core leg cross-section area	m^2
A_W	window area	m^2
B	flux density	T
B_r	remanence	T
b_{cen}	distance between centres of core legs	mm
b_{Fe}	half the width of core window	mm
b_1, b_2	radial width of windings	mm
b_o	radial clearance between core low-and high voltage windings	mm
b_{o1}	radial clearance between core leg and low-voltage windings	mm
b_{o2}	radial clearance between high-voltage windings	mm
b_W	width of core window	mm
b_x	reactive width of windings	mm
C	capacitance	F
D	mean path length	m
d	diameter of circle circumscribing core circle	mm
E.C.S.A	effective cross section area	m^2
e, E	electromotive force	V
f	frequency	Hz
F	magnetomotive force	A

H	magnetic field intensity	A/m
H_c	coercivity	A/m
h_w	height of core window	mm
h_{o1}, h_{o2}	axial clearance between low-and high voltage windings and core yoke	mm
i, I	current	A
J	current density	A/m^2
K_w	space factor due to insulation and conductor	
L	inductance	H
L_c	assumed equal height of low- and high voltage windings	mm
L_{mt}	mean circumference of the duct between the primary and secondary coils	mm
M.P.C.	mean path of core	m
N	number of turns	-
P_h	power dissipated in hysteresis loss	W/kg
P_{ec}	eddy current loss	W/m^3
R	resistance	Ω
S	transformer rating	VA
s_1, s_2	length of mean turn of winding	mm
s	$= 1/2(s_1 + s_2)$	mm
v, V	potential difference	V
Wt.C.	weight of core	kg
X	reactance	Ω
%X	percentage reactance	
Z	impedence	Ω
%Z	percentage impedance	

$\Re$	reluctance	A/Wb
σ	metal density	kg/m^3
λ	flux linkage	Wb
ρ	electrical resistivity	Ωm
ϕ, Φ	magnetic flux	Wb
ω	angular frequency	rad/s
η	anomaly factor	

SUMMARY

Theoretical designs have been carried out which demonstrate the possible weight and volume reductions to be obtained when using amorphous metal in place of silicon-iron for the core material in medium frequency power transformers. The amorphous metal provides such savings by its ability to operate at high flux densities without excessive core losses. The reduced core size also benefits the winding size, the overall reduction in weight and volume is particularly appropriate for rail and air borne power supply equipment. Of the various amorphous metal alloys available in ribbon form, two were selected for evaluation for the frequency band 50 to 3000 Hz. Several cores were built suitable for use in a 3 kHz 20 kVA transformer using purpose built core winding facilities. The wound cores, after annealing, were subjected to a comprehensive series of tests using both sinusoidal and square wave supply voltages. The thesis contains a valuable analysis of the results obtained and related to the magnetic properties of amorphous metal. The effect of mechanical stresses has also been investigated. The wound amorphous ribbon cores were found to be slightly flexible and prone to flaking, as a consequence several methods of core protection were investigated. Temperature rise tests have been conducted on the completed cores and various methods of heat dissipation tried.

The research has shown the viability of the use of amorphous metal for the cores of medium frequency power transformers.

CHAPTER 1

INTRODUCTION

1.1 Transformer

A transformer transforms alternating voltage and currents from high to low values or vice versa. Transformers are used extensively in all branches of electrical engineering from large power transformers rated at hundreds of MVA and weighing several hundred tons to miniature signal transformers used in electronic amplifiers and weighing only a few grams.

A transformer consists essentially of a magnetic core upon which are wound two distinct sets of coils suitably located with respect to each other and termed the primary and the secondary. The primary winding is that winding to which the supply voltage is applied, the other winding to which the load is connected is termed the secondary winding.

Developments in transformer design in recent years have largely focused on the new core materials now available. The new materials have implications in the design for the whole spectrum of transformer applications. The transformer type under consideration in this project falls into the category of power transformer for which the low loss amorphous alloy core material developed over last 10 years has a particular

application.

1.2 Power Transformers

Power transformers are used in a wide range of applications with wide variations of winding voltages, currents and power. The term power transformer may be applied to transformers used in applications where the ratings exceed several hundred watts. The operating frequency of power transformers now extends beyond the mains frequency of 50/60 Hz to frequencies in the kilohertz range. The higher frequencies have become possible as a result of the developments in power semiconductor switches.

1.2.1 Mains Frequency Power Transformers

Transformers for use in power applications at mains frequency step up or step down the voltages and currents to make possible an economic distribution of power between the power source and the consumer. The term power transformer at mains frequency in general refers to the transformers in the chain from the generating station to the first distribution point.

Nowadays, the largest power transformers are rated up to 1300 MVA, (400 kV, 3250 A), they are about 10 m in height and weigh about 400 tons (half of which is the weight of the core). These transformers step-up the voltage of the

generators to that of the transmission system.

While there is no generally recognised definition, a distribution transformer may be defined as a transformer used to supply power, for general purposes, at final distribution voltage levels from the higher-voltage distribution system. The minimum rating is usually regarded as 5kVA but the maximum is somewhat indefinite. For public supply purposes, ratings rarely exceed 1MVA, however, industrial sub-stations frequently have higher ratings, 3 MVA is normally the practical limit for loading at medium voltage.

The amorphous alloys at mains frequency will in the first instance find application in small distribution transformers, in particular single phase types used in remote locations where the loading is light and maximum benefit is obtained from the lower core losses.

1.2.2 Aircraft Power Supplies 400 Hz

To reduce the size and weight of the generators and transformers used in airborne power supplies, a higher operating frequency is used, namely 400 Hz rather than the standard mains frequency of 50/60 Hz. The frequency of 400 Hz was chosen originally taking into account the limitations of the core materials available at the time.

The core losses associated with the earlier core

materials resulted in low operating flux densities being used.

The advent of the new amorphous alloys provides the possibility for further weight reductions to be achieved by the use of a higher core flux density without incurring prohibitive losses.

As an example Boll and Warlimont [1] have calculated the maximum power capacity of a toroidal transformer based on identical core dimensions using iron-based amorphous alloy and grain-oriented silicon-steel strip of thickness 0.1 mm and 0.3 mm. Fig. 1.1 shows the dependence of the power output on the peak induction at 400 Hz, the ambient temperature assumed is 40°C, the temperature rise 75°C. The amorphous metal used was Metglas $Fe_{81}B_{13.5}Si_{3.5}C_2$ with 90 mm O.D., 50 mm I.D., and 25 mm width, a maximum power output of 780 VA is possible with the amorphous material compared with 650 VA for a silicon-steel core of 0.1 mm strip thickness and 480 VA for 0.3 mm thickness with same dimensions. Consequently, the power output for the amorphous alloy can be increased by 20% or 60% when compared with o.1 mm and 0.3 mm silicon steel respectively, or for a given rating the core weight and volume can be reduced.

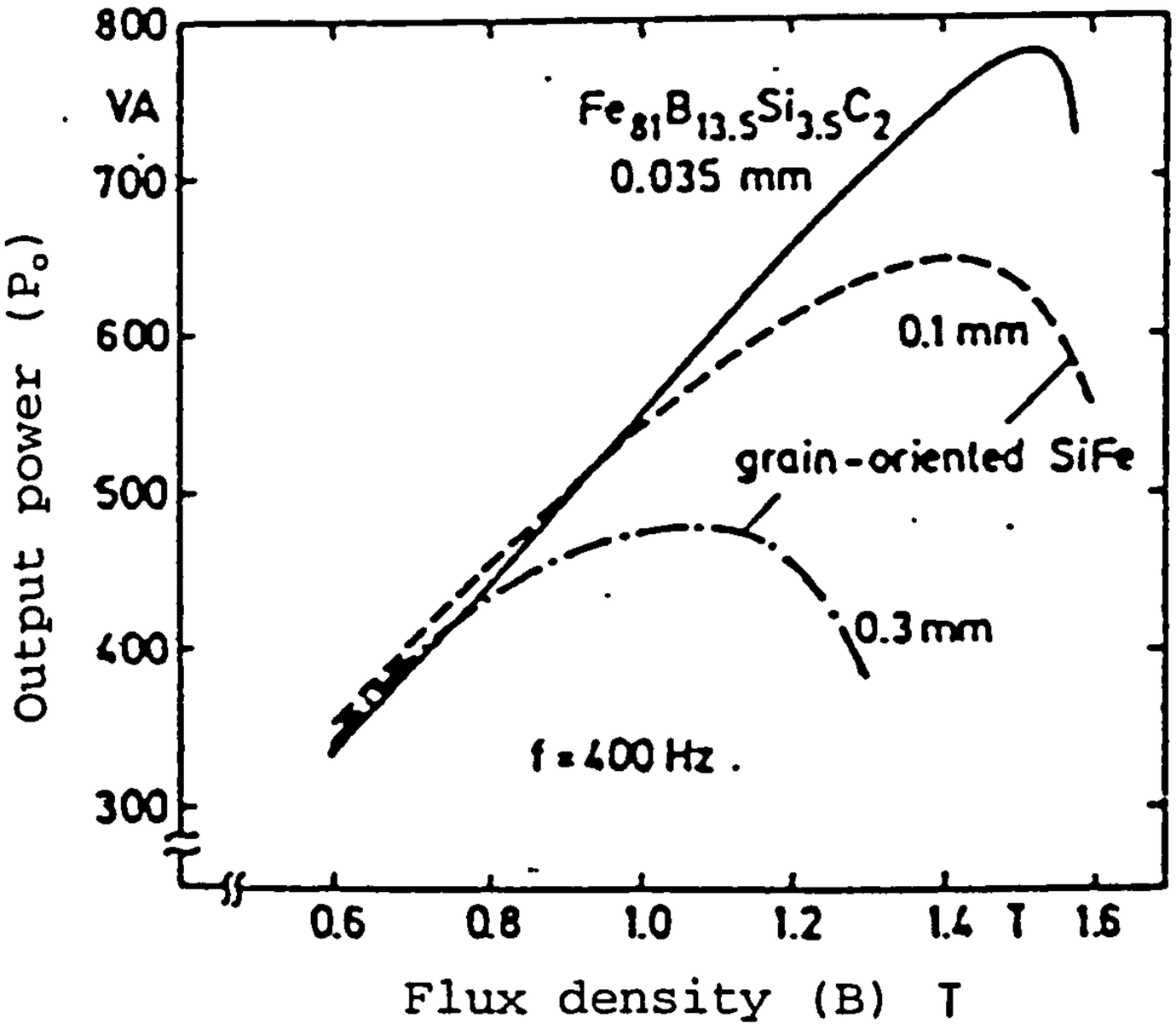

Fig.1.1 Output power (P_o) of transformers with toroidal wound core versus flux density (B) [1].

1.2.3 Switched-Mode Power Supplies

Switched-mode power supplies are rapidly replacing the standard mains power supplies (d.c. power supply) to an increasing extent. This growing market requires magnetic components operating at 10 to 200 kHz, the magnetic components include transformers, inductors and magnetic switches. The magnetic materials in these varied applications are required to operate at high saturation induction together with low losses. Other requirements are low effective permeability in filter inductors which carry a dc current and a high remanence and a low saturated permeability in switching applications.

The new amorphous alloys have properties which make them attractive in various magnetic components. At high frequencies core losses are dominated by eddy currents, thin ribbon and high resistivities are commonly used methods to limit these losses. Amorphous materials are cast as thin ribbons and have resistivities about three times those of the nickel iron crystalline alloys. These characteristics make amorphous alloys of advantage in high frequency applications. Amorphous alloys can be selected which are superior to nickel-iron tapes and ferrites [2]. Chen [3] has compared the losses of conventional materials with amorphous alloys over a large frequency range, see Fig.1.2 and found that the advantage of amorphous alloys over ferrites extends to higher and higher frequencies when higher operating flux densities

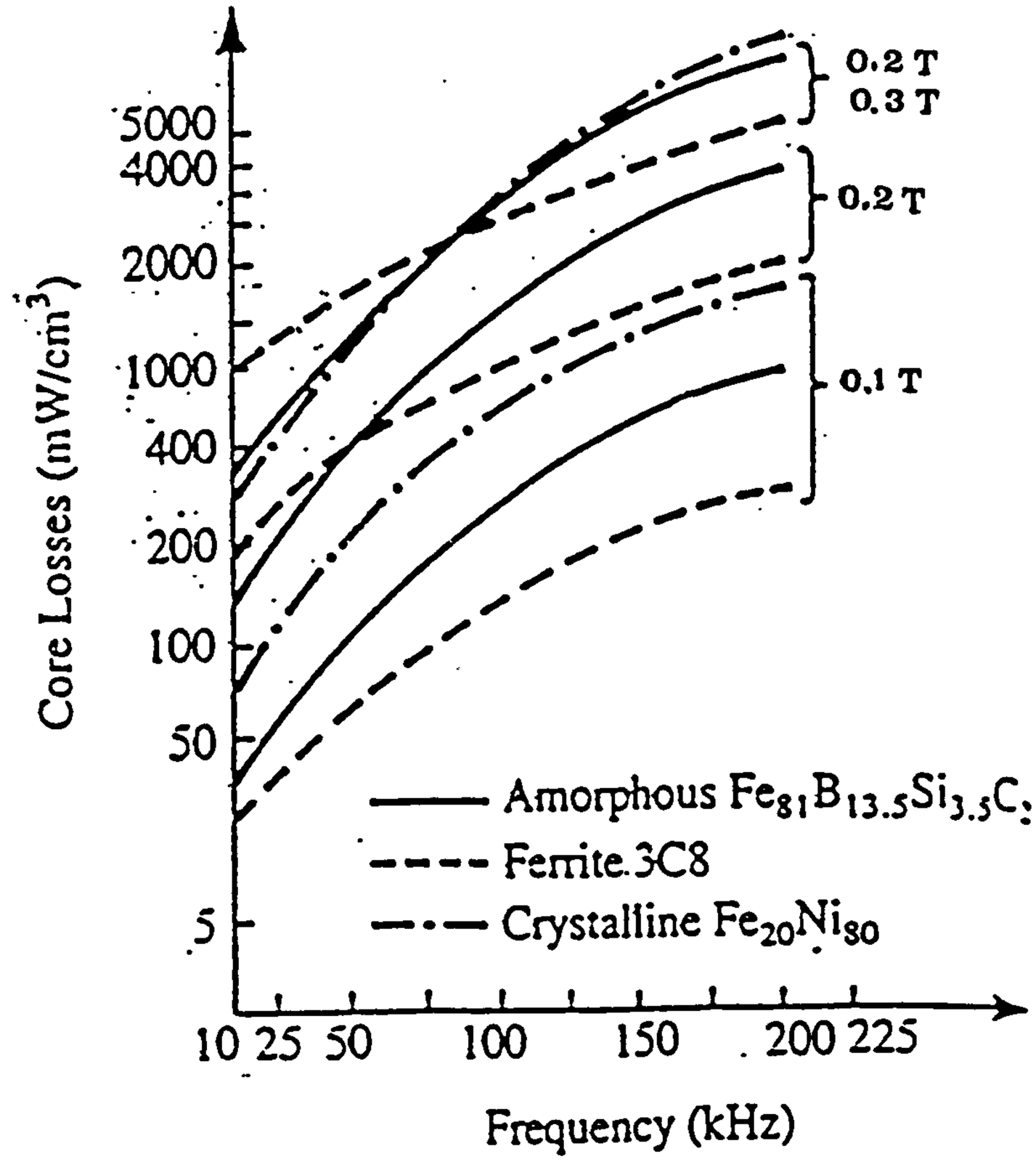

Fig. 1.2 Comparison of core losses versus frequency of amorphous $Fe_{81}B_{13.5}Si_{3.5}C_2$ with Ferrites 3C8 and crystalline $Fe_{20}Ni_{80}$ [3].

are used. At low flux densities for example 0.1 T, the core loss of the ferrite is less than the amorphous alloy over the frequency range 0/200 kHz. However at the higher flux density level of 0.2 and 0.3 T, the amorphous alloys have lower losses than ferrite at frequencies up to 50 kHz and 80 kHz, respectively. Amorphous alloys therefore have an application in SMPS and other similar applications of inverter type drive transformers where the frequency is limited to the lower levels.

1.3 Core Materials

The most generally desired characteristics of all soft magnetic materials are high saturation flux density, high permeability, low coercivity and low loss. The materials in common use up to the 1970,s are given in Table 1.1 together with their main magnetic parameters.

Recent developments in soft magnetic materials, to a large extent have been driven by the demand for still lower iron losses. In Table 1.1 category (A), steel lamination (low C) material is used in inexpensive fhp motors and non-oriented (2% Si) is used in large hp high efficiency motors [4]. Grain oriented (GO) 3 % Si-steel is still the most important soft magnetic material for distribution and power transformers, characterized by its low losses and high induction with low magnetisation. Through improved crystal

Category	B_s (T)	ρ ($\mu\Omega$-cm)	μ_{max}	Typical core loss (W/kg) (f/B_m, Hz/T)
A. Steel lamination(Low C)	2.2	0.4		2.0 (60/1.0)
non-oriented (2%Si)	2.1	0.35		2.7 (60/1.0)
convent.grain oriented (CGO M-4)	2.0	0.48	5,000	0.9 (60/1.5)
high grain oriented (HGO)	2.0	0.45		1.2 (60/1.7)
B. Fe-(Ni,Co) 40-50Ni	1.6	0.48	150,000	110 (50k/0.2
77-80Ni(square permalloy)	1.1	0.55	150,000	40 (50k/0.2)
79Ni-4Mo (4-79 Mo permalloy, superalloy)	0.8	0.58	10^6	33 (50k/0.2)
49Co-2V (permendur, superendur)	2.3	0.35	50,000	2.2 (60/2.0)
C. Ferrite MnZn	0.5	$2x10^6$	6,000	35 (50k/0.2)
NiZn	0.35	10^{10}	4,000	

Table 1.1 Main group of soft magnetic material.

orientation, the introduction of high permeability grain oriented (HGO) steel has brought about further significant steps in loss reduction, particularly at high induction [5].

In category (B) Fe-(Ni,Co) material such as 77-80Ni (square permalloy) has high permeability, commonly used as a thin ribbon. 79Ni-4Mo (4-79 Mo permalloy, supermalloy) has the highest permeability and lowest core loss of any metallic material. In addition, 49Co-2V (permendur, supermendur) has the highest saturation induction of commercial soft magnetic material.

In category (C), ferrimagnetic oxides or ferrites as they are usually known, have been developed as practical magnetic materials over the course of the last forty five years. During this time their use has become established in many branches of electronics and communication. They now embrace a very wide diversity of compositions, properties and applications, their general use is at high frequencies and low flux densities. Ferrite material such as the MnZn material is used in electronic power supply transformers and inductors. NiZn is used at very high frequencies in the MHz range. In general ferrite materials are used in wide range of applications including high frequency transformers, inductors, wide band transformers, pulse transformers and ferrite antennas.

In the 1970's a new class of soft magnetic material

become available with advent of amorphous metals produced by rapid solidification techniques. Table 1.2 lists the three types of amorphous metal alloys currently available from one manufacturer (Metglas alloys, Allied-Signal) together with their main magnetic parameters [6]. Each of the three amorphous metal alloys have particular characteristics which determine their application.

(I) Iron Based amorphous such as Metglas 2605S-2, can be used in mains frequency power and distribution transformers, inductors, motors and ground fault interrupters. Iron-Based type Metglas 2605SC and 2605CO is suitable for use in pulse transformers, magnetic switches. In addition, Iron-Based amorphous ribbon types, Metglas 2605S-3A and 2605SM, have application in medium frequency transformers, current transformers and high sensitivity ground fault interrupter cores.

(II) Nickel-Iron Based amorphous ribbon such as 2826MB can be used in shielding, magnetic field sensors, recording heads, earth leakage cores and sensors.

(III) Cobalt-Based amorphus alloys Metglas 2705M, 2714A are being used in special application with smaller mass such as, high frequency inverter transformers, high frequency magnetic amplifiers, recording heads, sensors and flexible shielding.

Alloy	B_s (T)	C.L. (W/kg) (f/B_m, Hz/T)	DC H_c (A/m, annealed)	Transition Metals used	Typical characrteristic
(I) Iron-Based					
2605-S2	1.56	0.21 60/1.4	1.6		Low loss Low VA Low cost High induction 50-60 Hz
2605SC	1.61	5.9 1k/1.4	3.0		Higher induction than S2 but higher loss 50-60 Hz
2605CO	1.80	o.4 60/1.5	3.5	Fe(Co)	High B_s 400 Hz
2605S-3A	1.41	60 25k/.4	<1	Fe(Cr)	Low loss at 10-200 kHz; High μ_m at 50-60 Hz
(II) Nikel-Iron-Based					
2826MB	0.88		0.4	FeNi	High μ_m
(III) Cobalt-Based					
2705M	0.7		0.8(as cast)	Co	Best as-cast properties
2714A	0.55	5 100k/.2	0.3	Co	High squareness at high freq.for saturable reactors

Table **1.2** Commercially available amorphohus alloys.

The amorphous alloys now available provide an alternative choice to the various steels and ferrites previously available. The choice of a suitable magnetic material for any application will depend on many factors apart from the magnetic characteristics. The initial material cost (usually quantity dependent), ease of manufacture, assembly, service life, are just a few of the factors to be considered. This research project investigates one such application of a medium frequency power transformer.

1.4 Aims of Present Investigation

The project is concerned with the investigation of the use of amorphous metal material for power transformer cores operating at medium frequencies, in particular for a transformer of rating 20 kVA, and an operating frequency in the range of 1-3 kHz. This particular frequency range is chosen as a consequence of the interest of a manufacturer in inverter fed transformers operating at these frequencies. The performance of the transformer design is to be examined for both sinusoidal and square wave voltage supplies. The rating of 20 kVA chosen for the transformer is also at the behest of the manufacturer. One application of the transformer is for power supplies on railway vehicles and hence low weight is a desirable factor. The use of this low loss amorphous material is to be evaluated and compared with conventional silicon iron core material normally used for this frequency range.

Transformer with silicon iron cores used in power applications up to 3 kHz are normally designed to operate with low flux densities to minimise the core losses and the subsequent temperature rise in the core and winding. The markedly lower core losses associated with amorphous metal permits the use of higher core flux densities. A higher flux density will in turn permit a reduction in the size and weight of the core and winding.

The benefits of using amorphous material in the cores of transformers are highlighted by a detailed design study for a common rating of 20 kVA. The values of maximum core flux density chosen for use in the study are based on current practice for steel cores, suitable values for the amorphous cores are determined by inspection of the amorphous metal characteristics supplied by the manufacturer. There are a number of amorphous alloys available each suitable for a particular application, the design study compared two of these amorphous alloys.

The effect of the choice of supply frequency on the transformer design is also compared by carrying out the design study for both 1 kHz and 3 kHz operating frequencies. The results of the design studies will determine the parameters of the transformer cores to be assembled and tested.

Chapter 2

Transformer Theory and Equivalent Circuits [7]

2.1 The Ideal Transformer

A transformer consists of a magnetic system in which a time-varying flux links two or more coils. Its purpose is to transfer electrical energy from one circuit to another, usually without any electrical connection between the two circuits. Usually the potential difference at which the energy leaves one circuit is different from the potential difference at which it enters the other. Therefore, all that is strictly necessary for transformer action to take place is that two coils are so positioned that some of the flux produced by current in one coil links some of the turns of the other coil. The arrangement in Fig. 2.1 thus constitutes a transformer, and some transformers employed in communications equipment are no more elaborate than this. In transformers employed in power circuits, it is necessary to ensure that energy shall not be wasted. To this aim, the coils are arranged on a ferromagnetic core in such way that a large flux is produced in the core by a current in any one coil, and as much of that as possible links as many of the turns as possible of the other coils on the core. Fig. 2.2 represents a transformer consisting of two coils on a ferromagnetic core. In practice, a designer would not

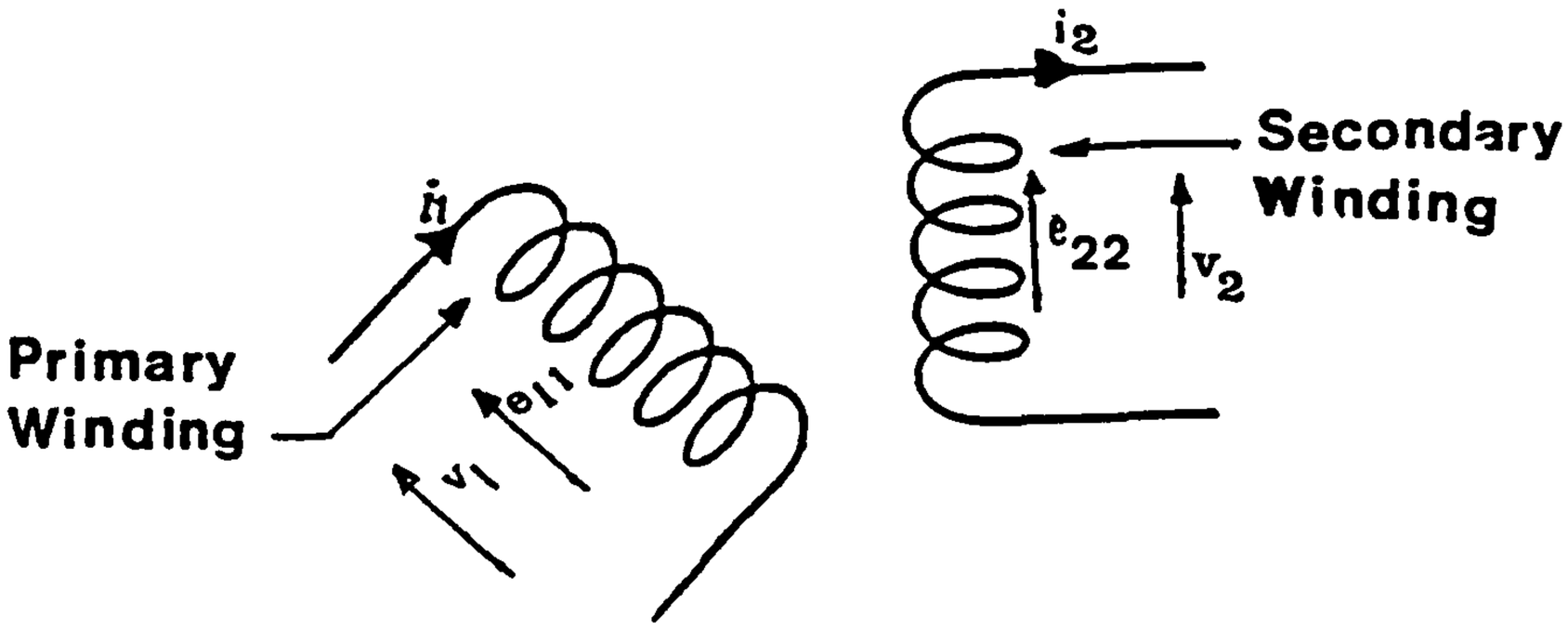

Fig. 2.1 Principle of action of a transformer.

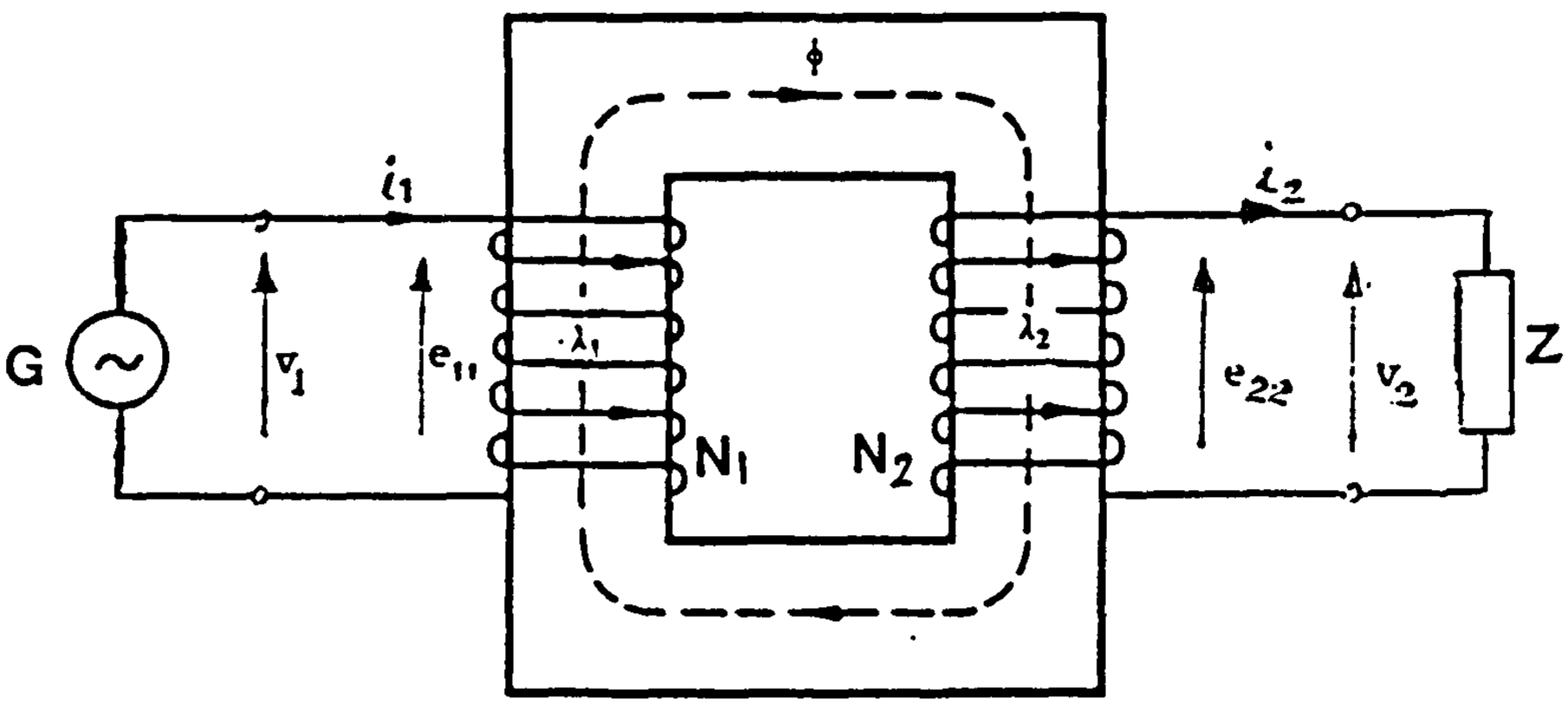

Fig. 2.2 Basic two-winding power transformer.

normally build a transformer as simple as this, for reasons that will become clearer in the discussion to follow.

If the behavior of the transformer is to be analyzed, then a mathematical model of it must be constructed. The first model that will be derived for the transformer is the ideal transformer, for which it is assumed that:

1. The winding resistances are negligible.
2. All magnetic flux is confined to the ferromagnetic core.
3. The relative permeability of the core material is so high that negligible mmf is required to establish the flux in the core.
4. The core losses are negligible.

In Fig. 2.2 if a potential difference v_1 is applied to the terminals of winding N_1, then current i_1 will flow in that winding. The resulting mmf $N_1 i_1$ will produce flux ϕ in the core and a flux linkage λ_1 of winding N_1. If v_1 varies in time, then i_1, ϕ, and λ_1 will vary in time, and an emf e_{11} will be induced in winding N_1, where

$$e_{11} = \frac{d\lambda_1}{dt} \quad (volt) \tag{2.1}$$

If the current and therefore the flux are increasing, the emf induced in the coil will oppose the change in current (Lenz's law) and will act in the direction shown in Fig. 2.2. Since it is assumed that all the flux is confined to the core, and

hence is linking all turns of winding N_1, then

$$\lambda_1 = N_1 \phi \quad (Wb\text{-}turn) \tag{2.2}$$

and

$$e_{11} = N_1 \frac{d\phi}{dt} \quad (volt) \tag{2.3}$$

Furthermore, since the resistance of winding N_1 is assumed to be negligible, then

$$v_1 = e_{11} \quad (volt) \tag{2.4}$$

Flux ϕ will also link winding N_2, producing a flux linkage λ_2. If the flux is inceasing, an emf, e_{22}, will be induced in winding N_2 acting in the direction shown in Fig. 2.2 and of magnitude

$$e_{22} = \frac{d\lambda_2}{dt} = N_2 \frac{d\phi}{dt} \quad (volt) \tag{2.5}$$

If a passive external load circuit is connected to the terminals of winding N_2, then e_{22} will cause current i_2 to flow as shown in Fig.2.2. Since the resistance of winding N_2 is assumed to be negligible, it follows that

$$v_2 = e_{22} \quad (volt) \tag{2.6}$$

Therefore, by virtue of the first two assumptions,

$$\frac{v_1}{v_2} = \frac{e_{11}}{e_{22}} = \frac{N_1}{N_2} \tag{2.7}$$

that is, the potential ratio is equal to the turns ratio, and

$$v_1 = \frac{N_1}{N_2} v_2 \quad (volt) \tag{2.8}$$

The net mmf acting on the core at any instant is

$$F = N_1 i_1 - N_2 i_2 \quad (A) \tag{2.9}$$

By assumption 3,

$$N_1 i_1 - N_2 i_2 = 0 \tag{2.10}$$

This assumption is equivalent to representing the λ-i loop of the core by a straight line coincident with the λ axis. From Eq.(2.10),

$$i_1 = \frac{N_2}{N_1} i_2 \tag{2.11}$$

Therefore no current can exist in winding N_1 unless there is a corresponding current in winding N_2, current i_2, so to speak, "calls current i_1 into existence." The current ratio is thus the inverse of the turns ratio.

From Eq. (2.8) and (2.11)

$$v_1 i_1 = v_2 i_2 \quad (W) \tag{2.12}$$

that is

$$\textit{Instant. power input} = \textit{Instant. power output} \tag{2.13}$$

This is to be anticipated, since assumption 1, and 4 abolish all losses and energy storage in the transformer. If potential difference v_1 is a sinusoidal function of time, then the system made up of the source, the transformer, and the connected passive circuit may be represented by a diagram showing the rms or effective magnitudes of the variables. Such a diagram is given in Fig. 2.3, where the ideal transformer is represented simply as two coils, N_1 and N_2 with dots used to represents the directions in which coils N_1 and N_2 are wound on the core. Phasor equations may be written directly from Eqs.(2.8) and (2.11). They are

$$\overline{V}_1 = \frac{N_1}{N_2}\overline{V}_2 \quad (volt) \tag{2.14}$$

$$\overline{I}_1 = \frac{N_2}{N_1}\overline{I}_2 \qquad (A) \qquad (2.15)$$

from which

$$\frac{\overline{V}_1}{\overline{I}_1} = [\frac{N_1}{N_2}]^2 \frac{\overline{V}_2}{\overline{I}_2} = [\frac{N_1}{N_2}]^2 \overline{Z}_L \qquad (\Omega) \qquad (2.16)$$

where

$$\overline{Z}_L = \frac{\overline{V}_2}{\overline{I}_2} \qquad (\Omega) \qquad (2.17)$$

Z_L is the impedance of the passive circuit connected to the terminals of winding N_2. According to equation (2.16) the system may be represented by the circuit diagram shown in Fig. 2.4, in which the ideal transformer and connected passive load circuit are replaced by an impedance Z'_L where:

$$\overline{Z}'_L = [\frac{N_1}{N_2}]^2 \overline{Z}_L \qquad (\Omega) \qquad (2.18)$$

The impedance Z'_L is said to be " Z_L referred to the N_1-turn side of the transformer." Therefore the turns ratio of the transformer may be employed to change the effective impedance of the load imposed upon the source. This property of the transformer may be utilised, to obtain maximum power

transfer. Fig. 2.5 illustrates a situation where, in order to obtain maximum power transfer from a source of internal impedance Z_s to a load of resistive impedance Z_L, it is essential to choose the turns ratio such that

$$Z_L' = [\frac{N_1}{N_2}]^2 Z_L = Z_s \quad (\Omega) \tag{2.19}$$

For maximum power transfer when Z_L may be complex,

$$\overline{Z}_L' = \overline{Z}_s^* \quad (\Omega) \tag{2.20}$$

where Z_s^* is the conjugate of Z_s.

In a practical situation, where the direction of energy flow through a transformer is known, it is customary to designate one winding the primary and the other the secondary. The primary winding is the one to which the source of energy is connected. Energy flows into the primary winding. The secondary winding is the one to which the load network is connected. Energy flows out of the secondary winding. In general, one winding is designed for a higher potential difference than the other, although isolating transformers, which are employed simply to separate two circuits electrically may have similar windings.

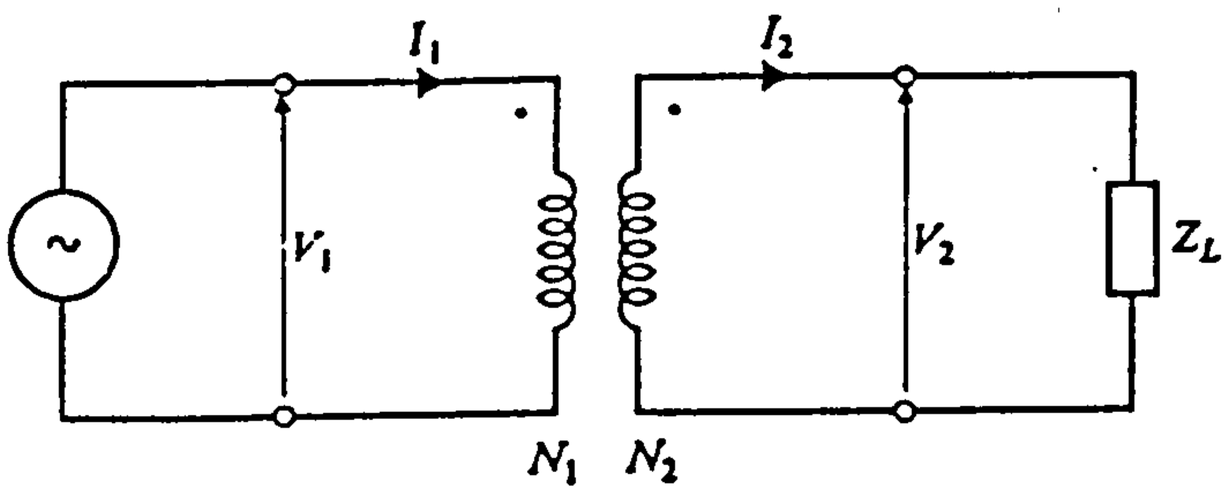

Fig. **2.3** Circuit diagram of ideal transformer.

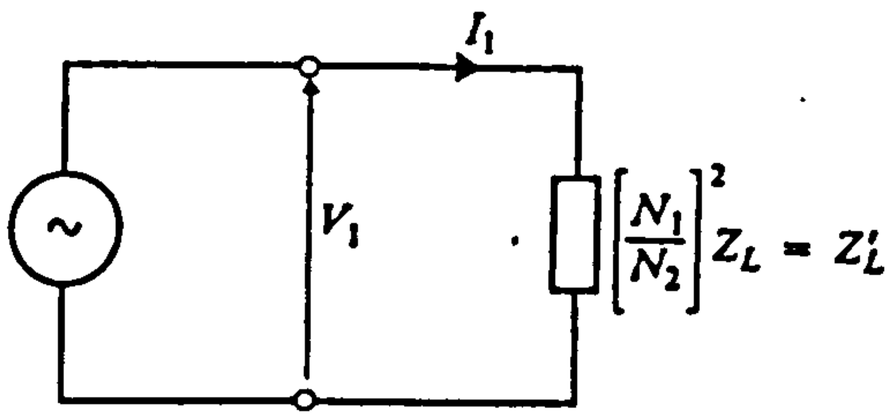

Fig. **2.4** In the ideal transformer load-circuit impedance referred to supply side.

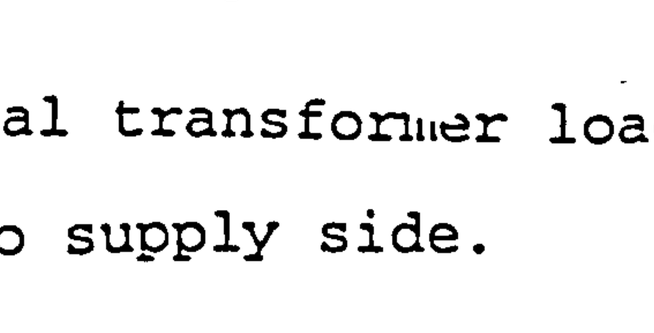

Fig. **2.5** Maximum power transfer.

2.2 Linear Equivalent Circuit of a Two-Winding Transformer

The ideal transformer is not an adequate accurate model for all purposes and when a more accurate prediction of transformer behavior is needed, a model which corresponds more closely to the physical system must be employed. This means that the assumptions and estimatation made must be less radical than those made in deriving the ideal transformer model. A model which is capable of giving very accurate prediction of transformer behaviour under most operating conditions is obtained when the following assumptions are made:

1. Winding resistances may be represented by lumped parameters at the terminals of the windings.

2. The flux produced by the mmf of one winding may be divided into two parts:

   a) Leakage flux linking all of the turns of the winding producing the mmf, but none of the turns of the other winding.

   b) Mutual flux linking all turns of both windings.

3. The permeability of the core is constant.

4. Core losses are negligible

Assumptions 1 and 4 are identical with the assumptions made in deriving the ideal transformer model. Fig.2.6 illustrates the consequences of assumptions 1 and 2, where the magnetic system at the centre of the diagram represents the transformer deprived of its winding resistance. The

magnetic system is therefore no longer a pictorial representation of a real transformer. The leakage fluxes produced by the two windings are given the symbols ϕ_{l1} and ϕ_{l2}. Their directions are consistent with the directions of i_1 and i_2. The mutual flux, which links both windings and is produced by their resultant mmf, is given the symbol ϕ_m. If reluctance of the core is $\Re_m$, then

$$\phi_m = \frac{N_1 i_1 - N_2 i_2}{\Re_m} \quad (Wb) \qquad (2.21)$$

The fluxes ϕ_m, ϕ_{l1}, and ϕ_{l2} in Fig.2.6 are all positive when $N_1 i_1 > N_2 i_2$. Fig.2.7 illustrates the consequences of assumptions 3 and 4, which represents a model of the B-H "loop" of core material or, altermativively, the ϕ-i loop for the core and one of the windings. Since core losses are assumed zero, the loop has zero area. Since permeability is assumed constant, there is a linear relationship between ϕ and i, and it is from this assumed linear relationship that the name linear equivalent circuit is taken. When both windings are carrying current, the flux linking winding N_1 is

$$\phi_1 = \phi_{l1} + \phi_m \quad (Wb) \qquad (2.22)$$

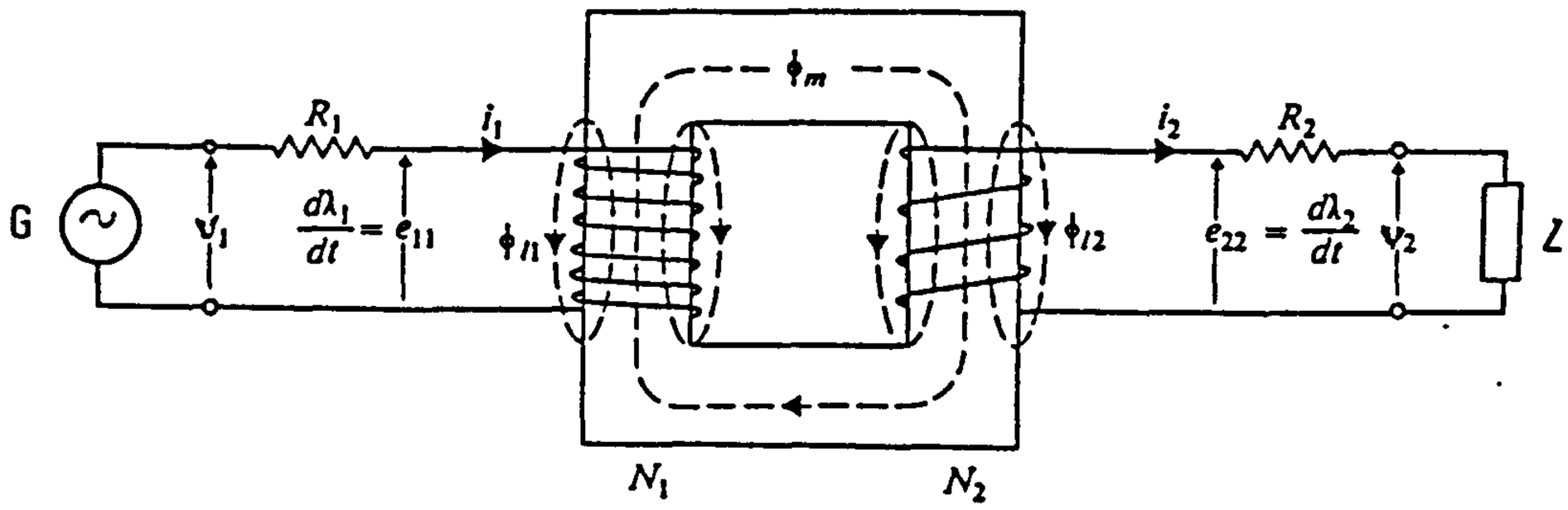

Fig. 2.6 Transformer circuit diagram consequences of assumptions 1 and 2.

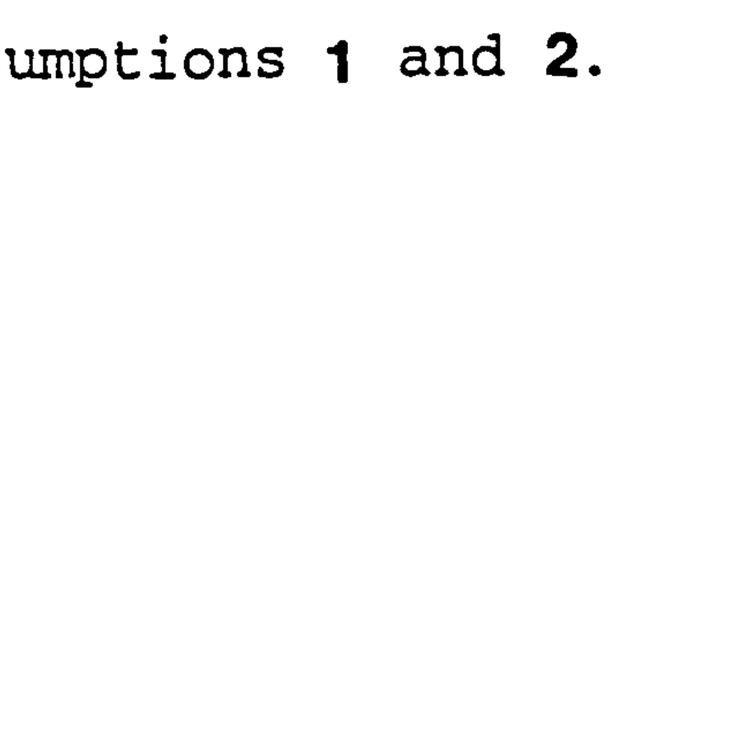

Fig. 2.7 Consequences of assumptions:(3) the permeability of the core is constant,(4) Core losses are negligible.

Similarly, the flux linking winding N_2 is

$$\phi_2 = -\phi_{12} + \phi_m \quad (Wb) \tag{2.23}$$

Since the total flux linkages of winding N_1 and N_2 are

$$\lambda_1 = N_1\phi_1 \quad , \quad \lambda_2 = N_2\phi_2 \quad (Wb) \tag{2.24}$$

then from Fig. 2.6,

$$v_1 = R_1 i_1 + e_{11} = R_1 i_1 + \frac{d\lambda_1}{dt} \quad (volt) \tag{2.25}$$

and

$$v_2 = -R_2 i_2 + e_{22} = -R_2 i_2 + \frac{d\lambda_2}{dt} \quad (volt) \tag{2.26}$$

The emf's induced in the two windings may, from Eqs. (2.22)-(2.24), also be expressed by

$$e_{11} = \frac{d\lambda_1}{dt} = N_1 \frac{d\phi_{11}}{dt} + N_1 \frac{d\phi_m}{dt} \quad (volt) \tag{2.27}$$

$$e_{22} = \frac{d\lambda_2}{dt} = -N_2\frac{d\phi_{12}}{dt} + N_2\frac{d\phi_m}{dt} \quad (volt) \qquad (2.28)$$

Leakage inductances of the two windings may be defined as follows:

$$L_{11} = \frac{N_1\phi_{11}}{i_1} \quad , \quad L_{12} = \frac{N_2\phi_{12}}{i_2} \quad (H) \qquad (2.29)$$

The emf's induced in the windings by the mutual flux ϕ_m may be designated

$$N_1\frac{d\phi_m}{dt} = e_1 \quad , \quad N_2\frac{d\phi_m}{dt} = e_2 \quad (volt) \qquad (2.30)$$

Substitution from Eqs. (2.27)-(2.30) in Eqs. (2.25) and (2.26) then yields

$$v_1 = R_1 i_1 + L_{11}\frac{di_1}{dt} + e_1 \quad (volt) \qquad (2.31)$$

$$v_2 = -R_2 i_2 - L_{12}\frac{di_2}{dt} + e_2 \quad (volt) \qquad (2.32)$$

The circuit diagram in Fig.2.8 take into account these last two relationships, where the magnetic system at the

centre of the diagram represents the transformer deprived of its properties of winding resistance and of winding leakage inductance. From Eq. (2.30),

$$\frac{e_1}{e_2} = \frac{N_1}{N_2} \qquad (2.33)$$

These emf's are in the same ratio as the terminal potential differences of an ideal transformer with turns N_1 and N_2. They may be considered to be the terminal potential differences of the "ideal transformer" in Fig.2.8. This "transformer" is not ideal, however, since the net mmf acting on the core is not zero, due to the fact that the permeability of the core is not infinite.

Let i'_m be the current that would be required in the N_1 winding alone to produce the mutual flux ϕ_m. This may be called the magnetizing current referred to winding N_1. Then

$$N_1 i'_m = N_1 i_1 - N_2 i_2 \quad (A) \qquad (2.34)$$

from which

$$i_1 = i'_m + \frac{N_2}{N_1} i_2 \quad (A) \qquad (2.35)$$

Since i'_m is a current that produces flux, it must flow in an inductive circuit. Thus Eqs. (2.33) and (2.35) may be considered to describe a circuit consisting of an ideal transformer with an inductance connected across the N_1 winding in which i'_m flows. This circuit is shown in Fig.2.9. The requirement that the resultant mmf on the core of the ideal transformer shall be zero is met, since

$$N_1 [\frac{N_2}{N_1} i_2] - N_2 i_2 = 0 \qquad (2.36)$$

The inductance in Fig. 2.10 may be defined as

$$L'_m = \frac{N_1 \dot{\phi}_m}{i'_m} = \frac{N_1^2}{\Re_m} \quad (H) \qquad (2.37)$$

and this is termed the magnetizing inductance of the transformer referred to the N_1 winding.

The complete equivalent circuit may now be produced by substituting the circuit shown in Fig. 2.9 for the "nearly ideal" transformer shown in Fig.2.8, therefore obtaining the circuit shown in Fig.2.10. If it had been assumed initially that the magnetizing current was i''_m flowing in winding N_2 alone, then an inductance L''_m would have been obtained, defined by the equation:

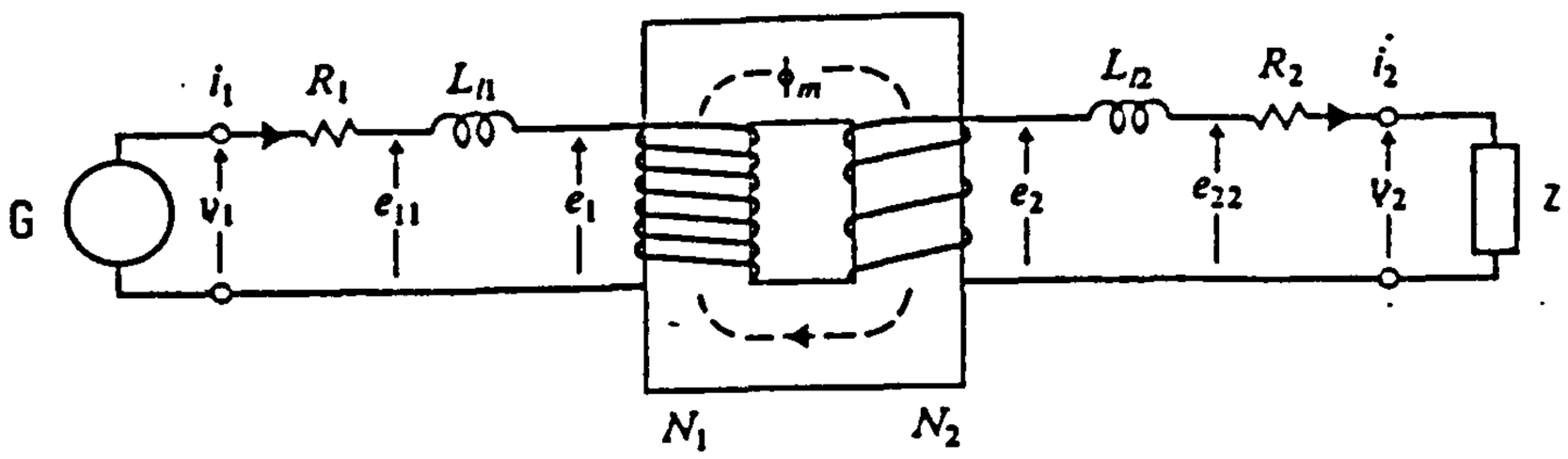

Fig. **2.8** Introduction of leakage inductances.

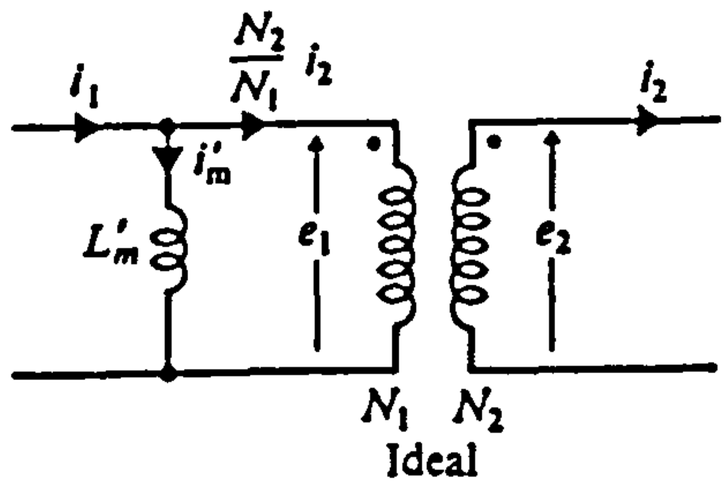

Fig. **2.9** Circuit described by 2.33 and 2.35.equations·

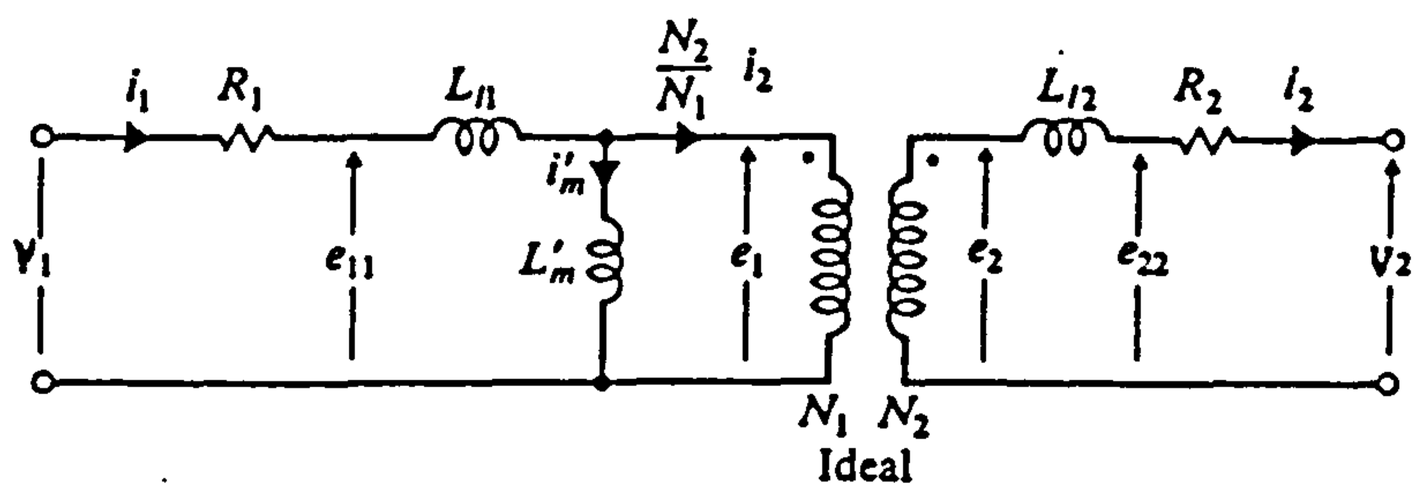

Fig. **2.10** Circuit diagram of transformer linear equivalent circuit.

$$L_m'' = \frac{N_2 \phi_m}{i_m''} = \frac{N_2^2}{\mathcal{R}_m} \quad (H) \tag{2.38}$$

and this inductance would have been connected across the N_2-turn winding.

Since, on the basis of the assumptions made,

$$N_1 i_m' = N_2 i_m'' \quad (A) \tag{2.39}$$

then from Eqs. (2.37) -(2.39),

$$\frac{L_m'}{L_m''} = \left[\frac{N_1}{N_2}\right]^2 \tag{2.40}$$

Therefore, L_m'' is the magnetizing inductance L_m' referred to winding N_2.

2.3 Transformer with Sinusoidal Excitation

When v_1 applied by an energy source to the terminals of winding N_1 of the transformer is a sinusoidal function of time, and a linear network is connected to the terminals of winding N_2, then the entire system may be represented by the circuits of Fig.2.11(a), in which all the variables are all sinusoidal functions of time. The rms values of the variables are shown on the circuit, and the inductances have been replaced by the

reactances for the frequency at which the transformer is operating. For instance,

$$X_{11} = 2\pi f L_{11} = \omega L_{11} \quad (\Omega) \tag{2.41}$$

For the direction of energy flow shown, winding N_1 may be referred to as the "primary" winding and N_2 as the "secondary". The analysis of the circuit may be simplified by referring the variables and parameters on one side of the ideal transformer to the other. For example, when all the secondary quantities are referred to primary side, the circuit shown in Fig.2.11(b) is obtained. The magnitudes of the referred quantities may be obtained from Eqs.(2.8), (2.11), (2.18).

$$\bar{E}_2' = \frac{N_1}{N_2}\bar{E}_2 \equiv \bar{E}_1 \quad (volt) \tag{2.42}$$

$$\bar{V}_2' = \frac{N_1}{N_2}\bar{V}_2 \quad (volt) \tag{2.43}$$

$$\bar{I}_2' = \frac{N_2}{N_1}\bar{I}_2 \quad (A) \tag{2.44}$$

$$\bar{Z}_L' = [\frac{N_1}{N_2}]^2\bar{Z}_L \quad (\Omega) \tag{2.45}$$

$$X'_{12} = \left[\frac{N_1}{N_2}\right]^2 X_{12} \quad (\Omega) \tag{2.46}$$

$$R'_2 = \left[\frac{N_1}{N_2}\right]^2 R_2 \quad (\Omega) \tag{2.47}$$

After these transformations have been made, the secondary terminals of the ideal transformer are short-circuited, making the potential difference between its primary terminal zero. Thus these terminals may also be considered to be short-circuited, and the ideal transformer is eliminated from the equivalent circuit.

In a similar manner, everthing on the primary side of the transformer, including the source, may be referred to the secondary side, giving the circuit in Fig.2.11(c), where the ideal transformer again disappears from the equivalent circuit. The choice of whether to refer all quantities to primary, Fig.2.11(b), or to the secondary, Fig. 2.11(c), depends on the problem that is being solved. A phasor diagram for the equivalent circuit referred to the primary side of the transformer is shown in Fig.2.12. In drawing the phasor diagram it has been assumed that the load circuit possesses both resistance and inductance, and therefore operates at a lagging power factor. Since, in carrying out calculations concerning a transformer, the point of chief interest is the effect of the transformer on the load circuit, the phasor of V'_2 is therefore employed as the reference phasor in the diagram.

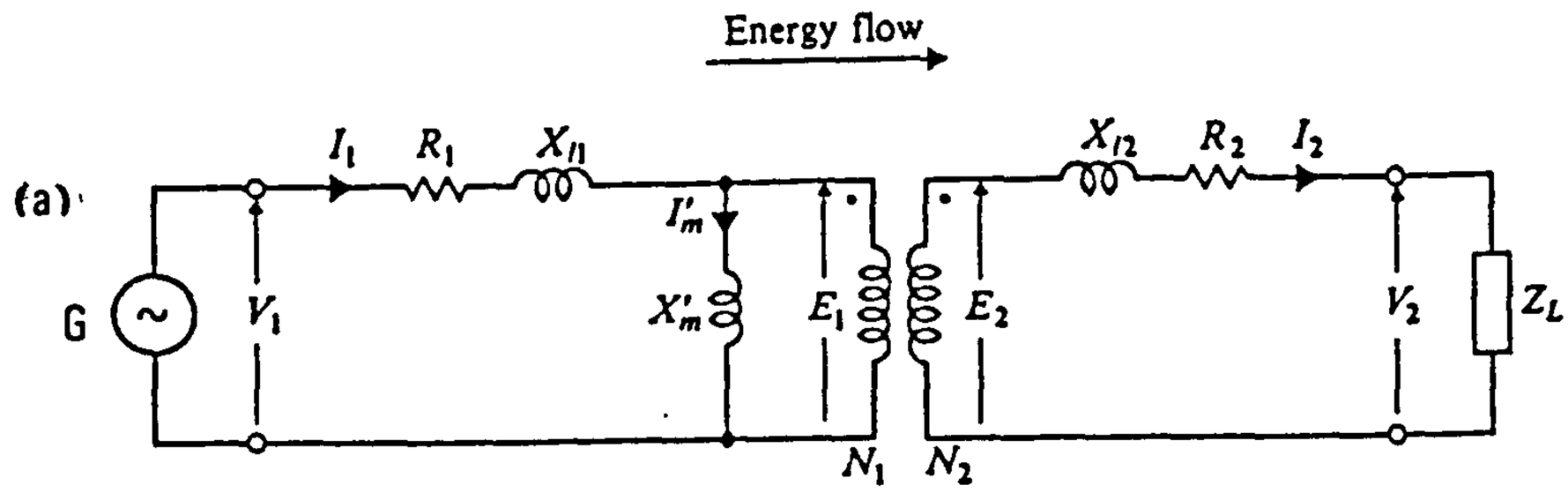

Fig 2.11(a)(b)(c) :
Equivalent circuits for transformers with sinusoidal excitation.

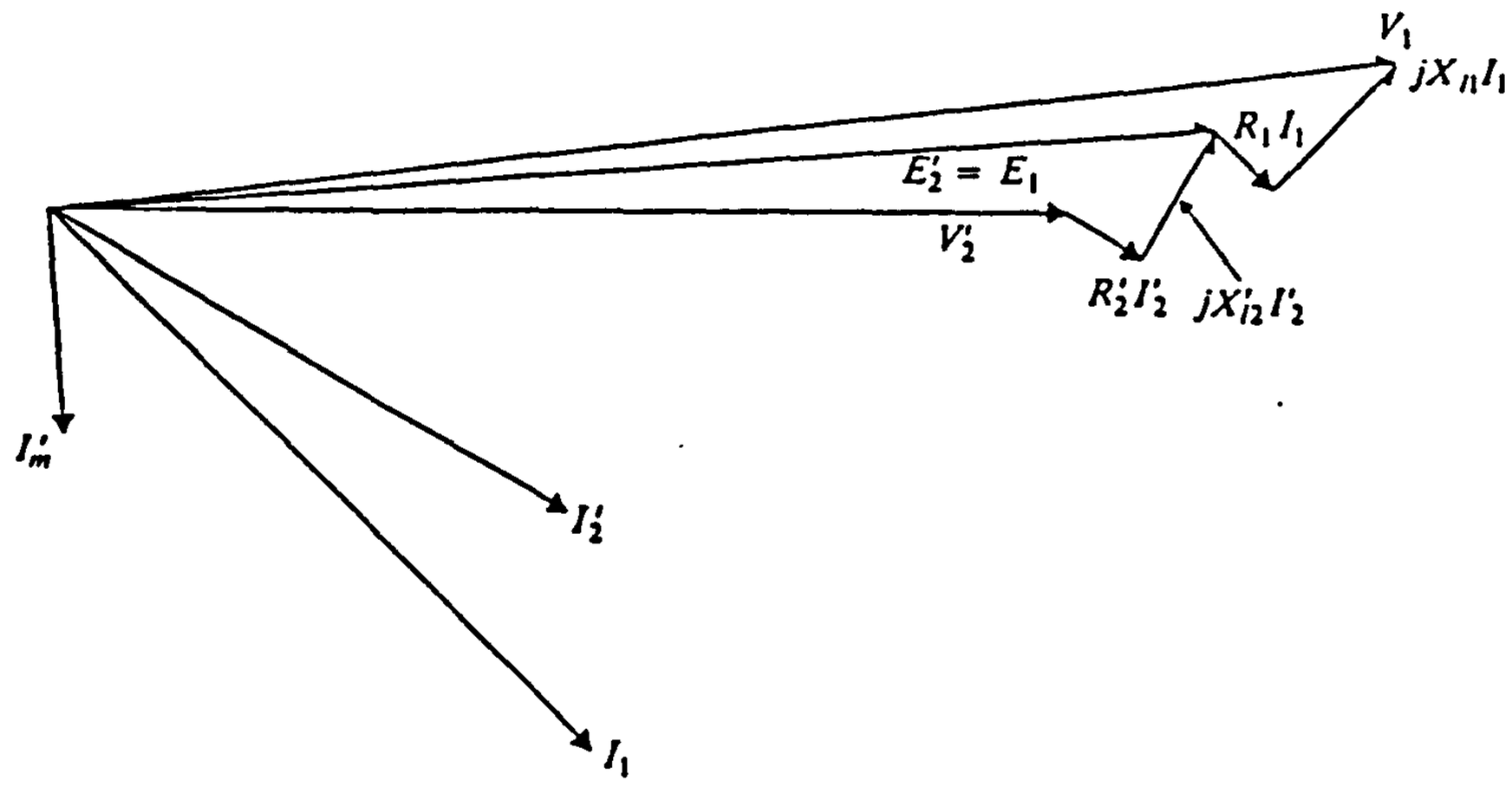

Fig. 2.12 Phasor diagram for system of Fig.2.11(b), referred all quantities to the primary.

That is,

$$\overline{V_2'} = V_2' \angle 0 \quad (volt) \tag{2.48}$$

The effects of winding resistances and leakage reactances are greatly exaggerated in Fig.2.12, as also is the magnitude of the magnetizing current. In practice these quantities are so small that the phasors representing their effects are of the same order of magnitude as would be the drafting error in attempting to draw Fig.2.12 to scale. The phasor diagram is therefore merely a useful guide to the calculation of the magnitudes of the variables in the circuit.

2.4 Transformer Core Losses

Core losses occur in a transformer for the same reasons as they occur in an inductive reactor, and this process will be described in Sections 4.1 and 4.2 (hysteresis loss and eddy current loss). Moreover, a transformer on no load simply behaves as a high-impedance inductive reactor with no air gap. Under these conditions the transformer exciting current is similar to that of an inductor, being made up of two components: I_m', the magnetizing component; and I_c', the core-loss component. Assuming the components to be sinusoidal, a phasor diagram showing their relationship with the emf induced in the primary winding is therefore that shown in Fig.2.13.

A circuit element R_c' may be added to the transformer equivalent circuit to absorb a power corresponding to that dissipated in core losses. The complete equivalent circuit of transformer in which the zero-core-loss assumption is no longer being made is therefore that shown in Fig.2.14. The corresponding phasor diagram for transformer supplying a load circuit with lagging power factor is shown in Fig.2.15 and should be compared with Fig.2.12. The magnitude of the current I_c' flowing in core-loss element R_c' is greatly exaggerated in the diagram.

2.5 Approximate Equivalent Circuits

It is not often necessary to employ the complete equivalent circuit of Fig.2.14 in order to predict with adequate accuracy the performance of a transformer. The calculations involved in using the equivalent circuit are much reduced if further approximations are made. A series of approximate equivalent circuits appropriate to various required degrees of accuracy of performance prediction are shown in Fig.2.16. Circuits (a) and (b) are based on the assumption that

$$V_1 \simeq E_1 , \quad E_2' \simeq V_2' \quad (volt) \tag{2.49}$$

The magnetizing branch consisting of R_c' and X_m' in parallel

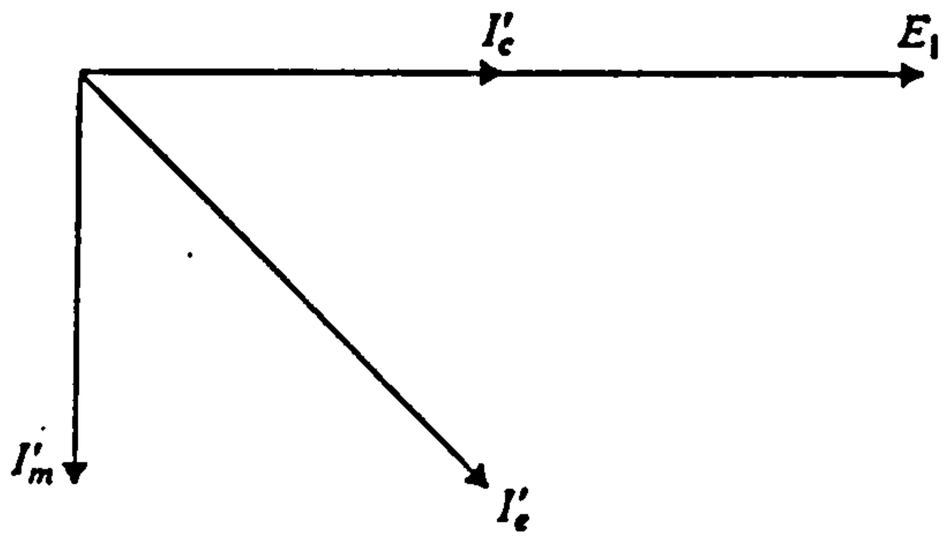

Fig. 2.13 Phasor diagram of transformer exciting current components.

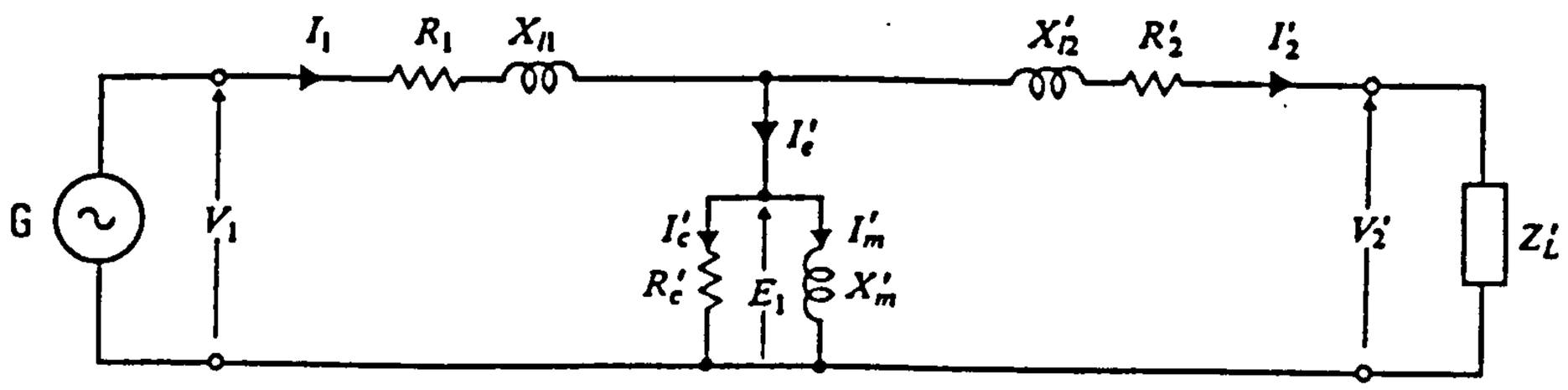

Fig. 2.14 Complete equivalent circuit of a transformer referred to the primary side.

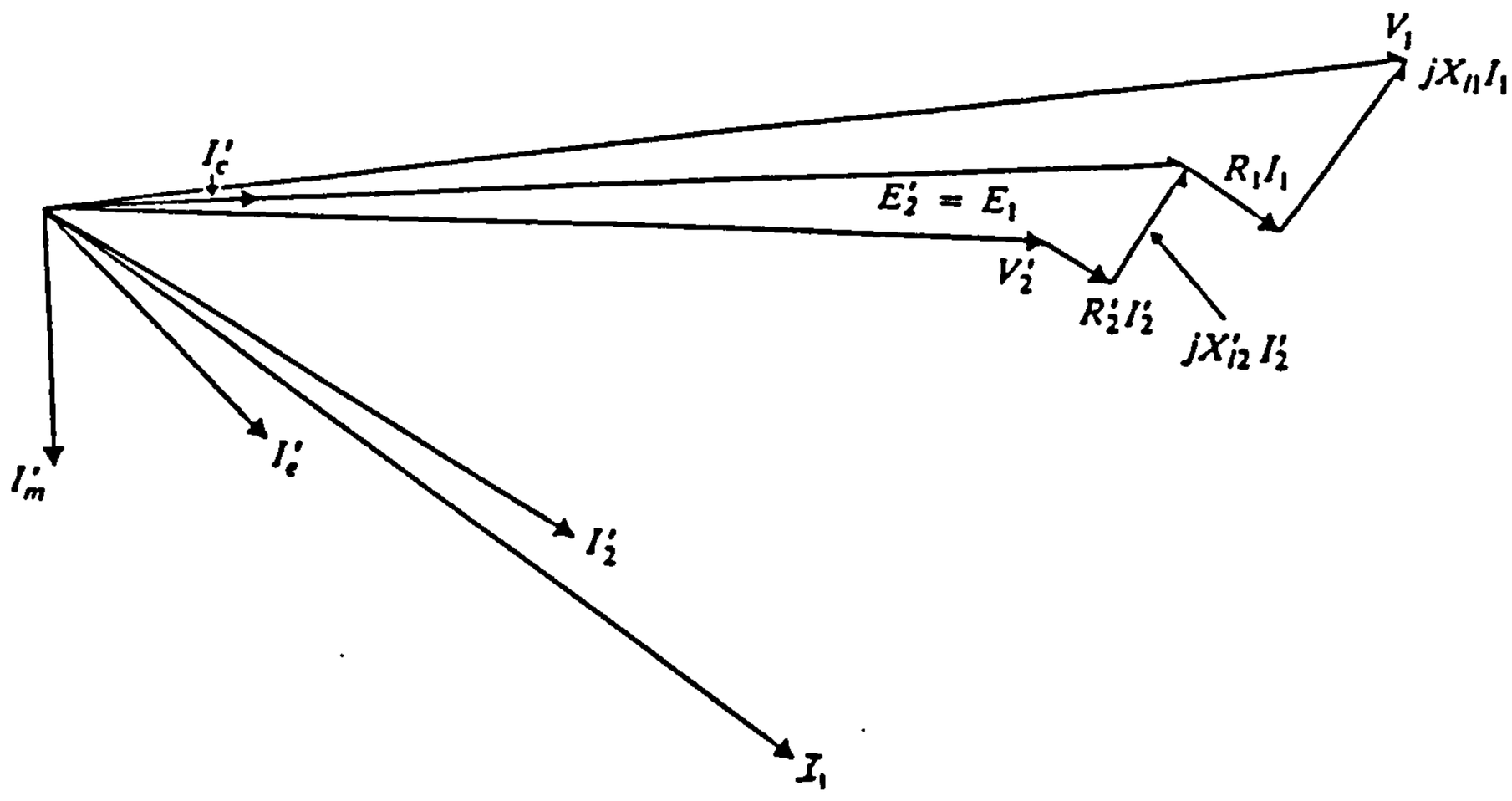

Fig. 2.15 Phasor diagram for circuit of Fig.2.14.

may therefore be connected across the circuit at the point that is most convenient for the problem being solved, and the magnitude of I_e' will not be greatly affected. Circuit (c) is based on the assumption that the exciting current I_e' is negligible in comparison with the winding current I_1. This corresponds to assumption of negligible core loss and very high core permeability. Circuit (c) is usually sufficient for solving for the relationships between V_1 and V_2'. In larger transformers, the resistance R_{eq}' is generally much smaller than the reactance X_{eq}'. Circuit (d) is therefore an sufficient model for the determination of the relationships between V_1 and V_2'. Finally, the potential difference across the leakage reactance may be small enough relative to the applied potential difference to allow the transformer to be represented by the ideal model of circuit (e).

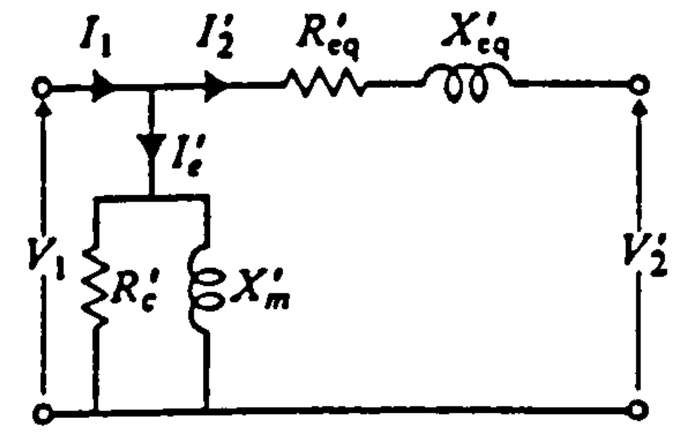

(a)

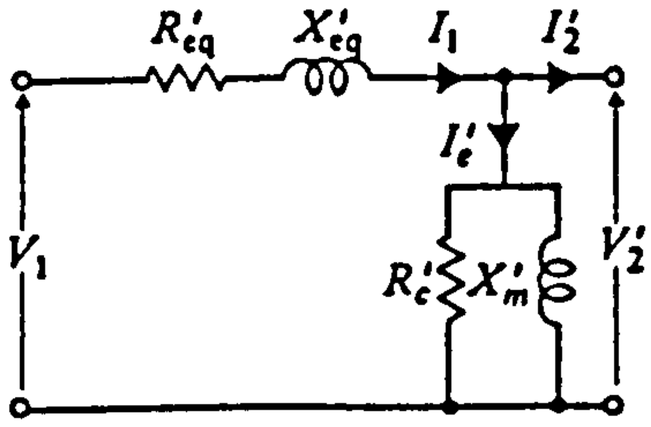

(b)

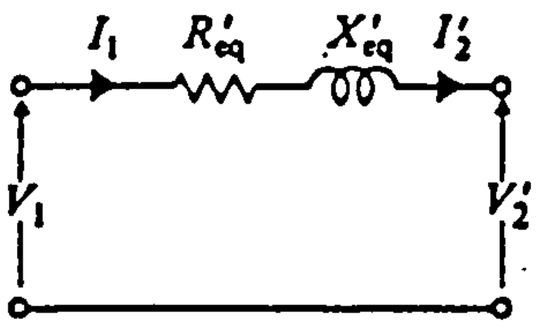

(c)

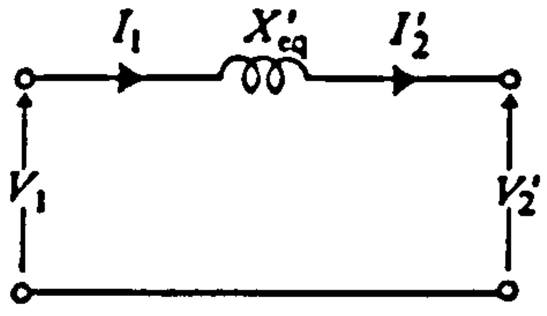

(d)

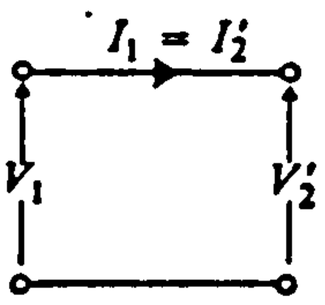

(e)

Fig. 2.16 Approximate equivalent circuit of a transformer.

CHAPTER 3

Transformer Design

3.1 Factors Influence's Transformer Design

3.1.1 Transformer Specification

In the design of a transformer the choice of frame dimensions is the first and the most important stage. The dimension of this frame are determined in accordance with the full technical specification for the transformer in combination with considerations of cost of materials and assembly [8]. Consider the simple two winding transformer shown in Fig.3.1

The rating of a single phase transformer may be expressed in terms of supply frequency f, maximum core flux density B_m, current density J, total core cross-sectional area A_{Fe}, total copper cross-sectional area per winding A_{Cu}

Let S = Transformer rating

$$S = V_1 I_1 = V_2 I_2$$

$$S = \left(\frac{V_1}{N_1}\right)(N_1 I_1) \qquad (3.1)$$

and

$$V_1 = E_1 = 4.44 f B_m A_{Fe} N_1$$

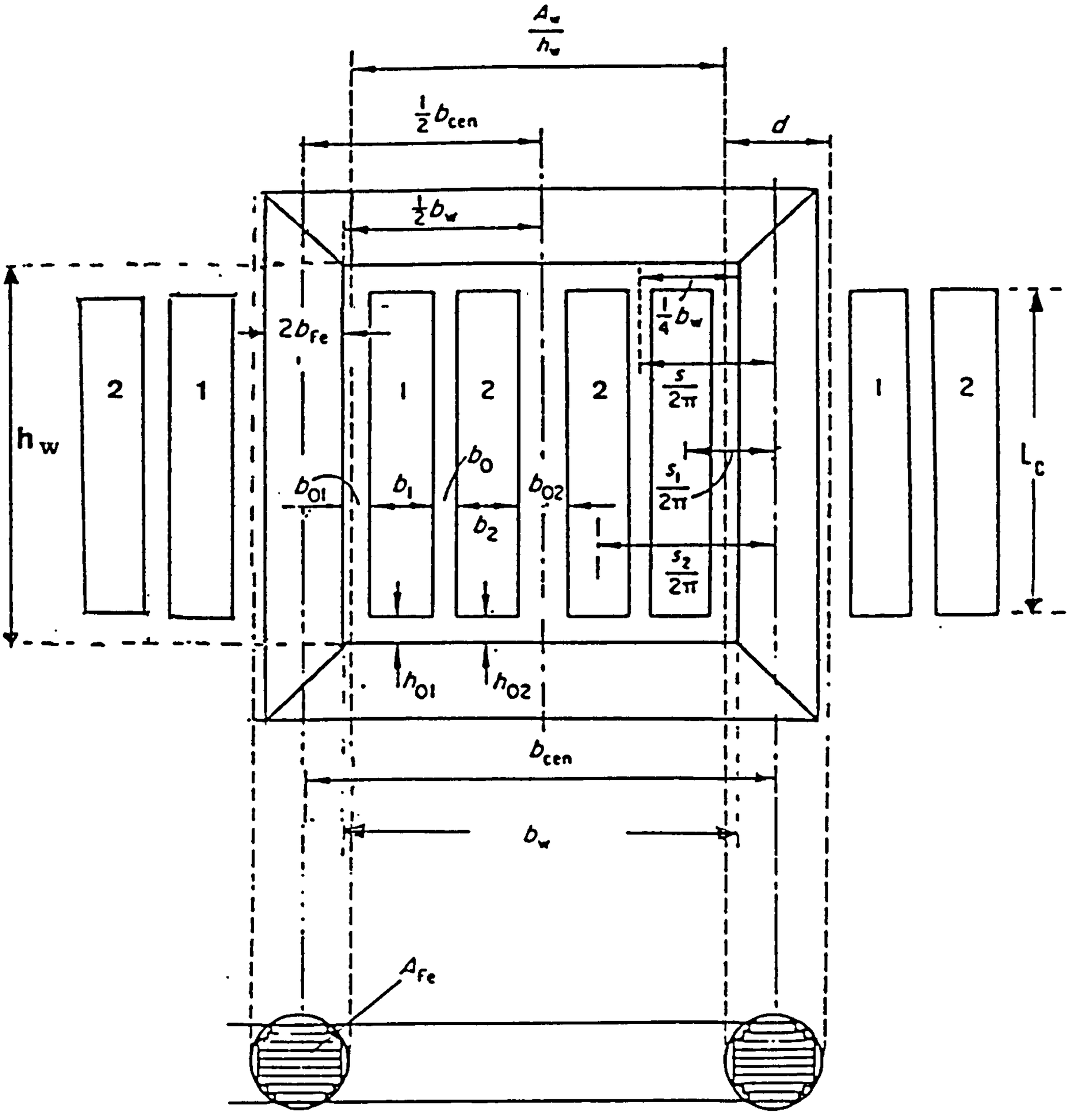

Fig. 3.1 Single phase core-type frame; b_{cen}, distance between leg centres; h_w, window height; b_w, window width; b_{Fe}, half-width of widest core plate; A_{Fe} gross-sectional area; d, diameter of circumscribing core circle; A_w, window area.

or

$$\frac{V_1}{N_1} = \frac{E_1}{N_1} = 4.44 f B_m A_{Fe} \qquad (3.2)$$

Let A_{Cu} = total c.s.a. of copper per winding, $A_{Cu} = A_t N_1$ where A_t is c.s.a. of one turn and N_1 = no of turns

Current density

$$J = \frac{I_1}{A_t} = \frac{I_1 N_1}{A_t N_1} = \frac{I_1 N_1}{A_{Cu}} \qquad (3.3)$$

thus

$$I_1 N_1 = J A_{Cu} \qquad (3.4)$$

Let A_W = window area, then $2A_{Cu} = K_W A_W$ (both windings) where K_W = space factor due to insulation and spacing between conductors.

Hence

$$I_1 N_1 = \frac{J K_W A_W}{2} \qquad (3.5)$$

substituting equations (3.2) and (3.4) into (3.1) gives

$$S = 4.44 f J B_m A_{Fe} A_{Cu} \quad (VA) \qquad (3.6)$$

or expressed in terms of the window area A_w and the window space factor $K_w = 2A_{Cu}/A_w$ gives:

$$S = 2.22 f B_m J A_{Fe} k_w A_w \quad (VA) \qquad (3.7)$$

The current density J and the flux density B_m are commonly termed the specific electrical and magnetic loadings respectively. The choice of the specific loadings is a starting point in design. By choosing J and B_m at or near their upper limits will reduce the material cost of copper and iron to a minimum. The cross-section areas A_{Fe} or A_{Cu} may be varied but not independently, since the product $A_{Fe}xA_w$ for a given rating must remain constant.

However there are a number of other factors to be considered which influence transformer design, for example (a) the leakage reactance on which the regulation of the transformer largely depends (b) the relative volumes of iron and copper which relate directly to A_{Fe} and A_{Cu} respectively and determine the proportion and size of the iron losses and winding resistance losses (c) the material cost of iron and copper.

3.1.2 Leakage Reactance

The transformer specification normally includes a

value for the impedance. The impedance in turn is largely determined by the leakage reactance. The impedance specified relates to the nature of the use of the transformer, a small impedance is required where good voltage regulation is necessary and larger values where the short circuit current needs to be limited.

With reference to the single phase transformer shown in Fig.3.1, the primary and secondary windings comprise two concentric coils of equal length. The leakage reactance of primary and secondary windings may be expressed in terms of the primary winding number of turns by the following equation [9].

$$X = 2\pi f \mu_o N_1^2 [b_o + \frac{(b_1 + b_2)}{3}] (\frac{L_{mt}}{L_c}) \qquad (3.8)$$

where L_{mt} is the mean circumference of the duct between the primary and secondary coils, L_c is the length of windings, b_1 and b_2 are the radial widths of the primary and secondary coils respectively. Let $b_x = b_o + (b_1+b_2)/3$

The per unit leakage reactance in terms of the primary winding is therefore

$$X_{P.U} = \frac{I_1 X}{V_1} = [\frac{2\pi f \mu_o I_1 N_1^2 b_x}{V_1}] (\frac{L_{mt}}{L_c}) \qquad (3.9)$$

The transformer rating $S = V_1 I_1$ and $I_1 = S/V_1$ hence

$$X_{P.U} = \frac{I_1 X}{V_1} = \left[\frac{2\pi f \mu_o S b_x}{\left(\frac{V_1}{N_1}\right)^2}\right]\left(\frac{L_{mt}}{L_c}\right) \qquad (3.10)$$

substituting $V/N = (2\pi/2^{1/2}) f B_m A_{Fe}$ in equation (3.10) gives

$$X_{P.U} = \left[\frac{\mu_o S b_x}{\pi f B_m^2 A_{Fe}^2}\right]\left(\frac{L_{mt}}{L_c}\right) \qquad (3.11)$$

According to the equation (3.10), the value of the P.U reactance for a given rating is dependent on the coil length L_c, the voltage per turn (V/N), the mean turn length L_{mt} and the term b_x. The mean turn length L_{mt} is dependent on the cross-section area of the iron core A_{Fe} and A_{Fe} is itself dependent on the voltage per turn V/N ($V/N = 4.44 f B_m A_{Fe}$). The cross-sectional area of the copper A_{Cu} is also influenced by changes in A_{Fe} for a given rating (see equation $S=2.22 f B_m J A_{Fe} A_{Cu}$). The term b_x is dependent on the radial width of the primary and secondary coils and the radial coil separation.

It is therefore apparent that since all these items are interrelated, the formulation of an economic design is somewhat complex and most manufacturers employ computer aided design methods.

In general, a reduction in reactance is associated with increased mass of iron and increased iron loss, a reduced mass of copper and copper loss and the ratio L_{mt}/L_c is decreased. Conversely, an increase in reactance is associated with reduced iron loss and increased copper loss, and ratio L_{mt}/L_c is increased.

Reactance is thus of fundamental importance in determining the initial dimensions of a design and should be considered at this stage. This is possible, provided an approximate value can be found for b_x.

3.1.3 Effect of Frequency

The induced voltage developed in the coil of a transformer due to a sinusoidally varying magnetic flux is given by:

$$E = 4.44\phi_m f N \qquad (3.12)$$

or

$$E = 4.44 B_m f N A_{Fe} \qquad (3.13)$$

For a given voltage rating various combinations of the values of B_m, A_{Fe}, f, and N may be used to conform with the desired voltage. Normally the operating frequency is also specified

and only the terms B_m, A_{Fe} and N need be considered. In all cases it is appropriate to make maximum use of the core by operating at or near the saturation flux density level of the core material. However another factor associated with the core must be considered before the flux density level is chosen, namely the core losses which are dependent on frequency, the core flux density, the volume of core material, the thickness of the laminations and the core material itself.

The core losses must be kept at a level so that the temperature limits of the core material are not exceeded. At the power frequencies of 50/60 Hz, by choosing a low loss silicon steel core material, suitably laminated, the core loss sustained at the highest values of flux density B_m do not produce excessive core temperatures. Adequate cooling of the core can be obtained by provision of ducts and in some cases by oil immersion. The oil immersion is normally needed in the first instance to cool the transformer windings. The main concern with regard to the core losses sustained at power frequencies is the transformer efficiency, particularly for the larger ratings. It is at the higher operating frequencies that the core losses become excessive , the eddy current loss being proportional to f^2 and hysteresis loss proportional to f. Excessive temperatures are likely to be encountered with steel cores operating at their maximum flux density levels at frequencies much in excess of 100 Hz. The value of B_m must therefore be reduced by either increasing

the core cross-section area A_{Fe} or alternatively by increasing the number of winding turns N.

If the value of B_m is reduced by increasing core cross-section area A_{Fe}, the change in core losses and consequently the core temperature are dependent on several factors,

(a) the dependency of core losses on B_m

(b) the degree by which the volume of the core material is increased

(c) the increase in the core volume is associated with an increase in cooling surface area.

The core losses in a transformer are essentially comprised of two components, the hysteresis loss and the eddy current loss. For a particular frequency the hysteresis loss is dependent on the B_m^n where n is in the range 1.6-2.0 depending on the core material and the eddy current loss depends on B_m^2. The core losses are explained more fully in chapter four.

3.2 General Core Winding Design Feature

3.2.1 Strip-Wound Core in Grain-Oriented Silicon-iron

Strip-wound cores are manufactured by winding the material, in the form of continuous strip, upon a suitably shaped mandrel or former. This method of construction allows full use of the magnetic characteristics of the material, by ensuring that the flux path is always in the rolling direction of the material. This arrangement gives the lowest possible iron loss and is widely used in small distribution

transformers. It has also been applied to large power transformers up to 3.3 MVA in the USA [10], but, since the entire core requires annealing after forming, an expensive manufacturing plant is required. In small power transformers the principle can been extended to three-phase three-limb cores by using three interwound loops. Fig.3.2 (a) and (b) show the wound type cores, single-phase one-loop and single-phase two-loop respectively and Fig.3.2(c) shows a three-phase three-loop interwound core. The latter pattern is not practicable on large cores, since, although there are no corner or joint losses, flux does not readily transfer from one loop to another.

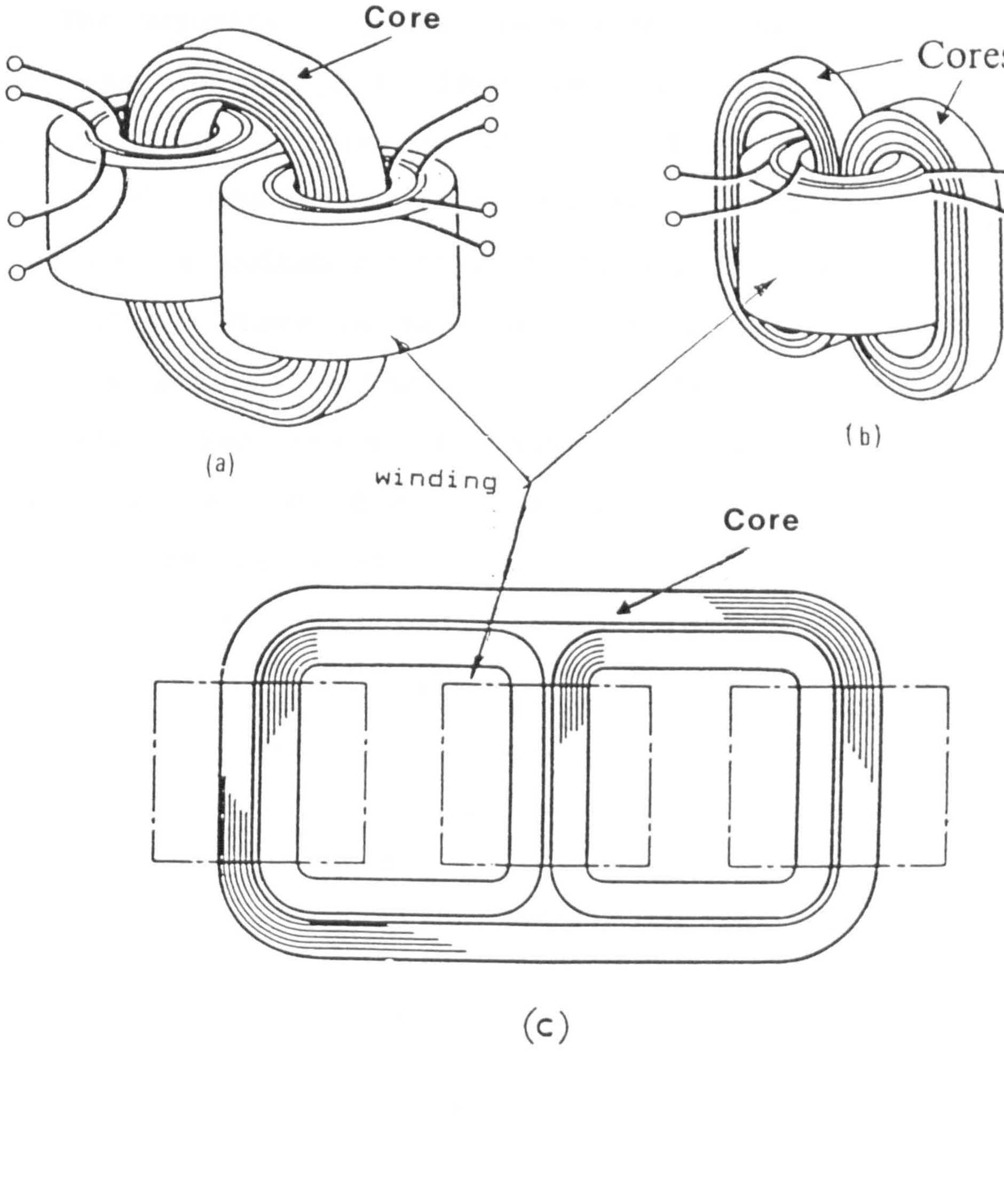

Fig. 3.2 Forms of core built from wound loops; (a) one-phase one-loop; (b) one-phase two-loops; (c) three-phase three-loops.

3.2.2 Built up Laminated Core Transformer

The majority of power transformer cores are built up using pre cut strips to form the limbs and yokes of the various types of cores as shown in Fig.3.3 . The joint between the limbs and the yokes requires particular attention to provide a suitable magnetic circuit with a mechanical construction. There is quite a large range of joint forms available and the method chosen depends on the degree of optimisation required of the magnetic circuit. The majority of cores are assembled with some kind of interleaved joint between limbs and yokes. The three common forms in use are shown in Fig.3.4. The best magnetic properties would be obtained by interleaving alternate laminations, but generally in practice laminations are used interleaved two , three or four at a time, to minimise unevenness caused by variation in laminations thickness or slight bucking of the plates. The windings for transformers are cylindrical in shape, so that the cross-section of the core limbs needs to be made as nearly circular as possible if space is not to be wasted. It is possible to achieve a close approximation to a circular core by using different widths of strips in a stepped arrangement, limited only by the number of different strip widths which the manufacturer is prepared to cut and build. Fig.3.5 illustrates some typical core sections having three, four, seven and fourteen steps respectively.

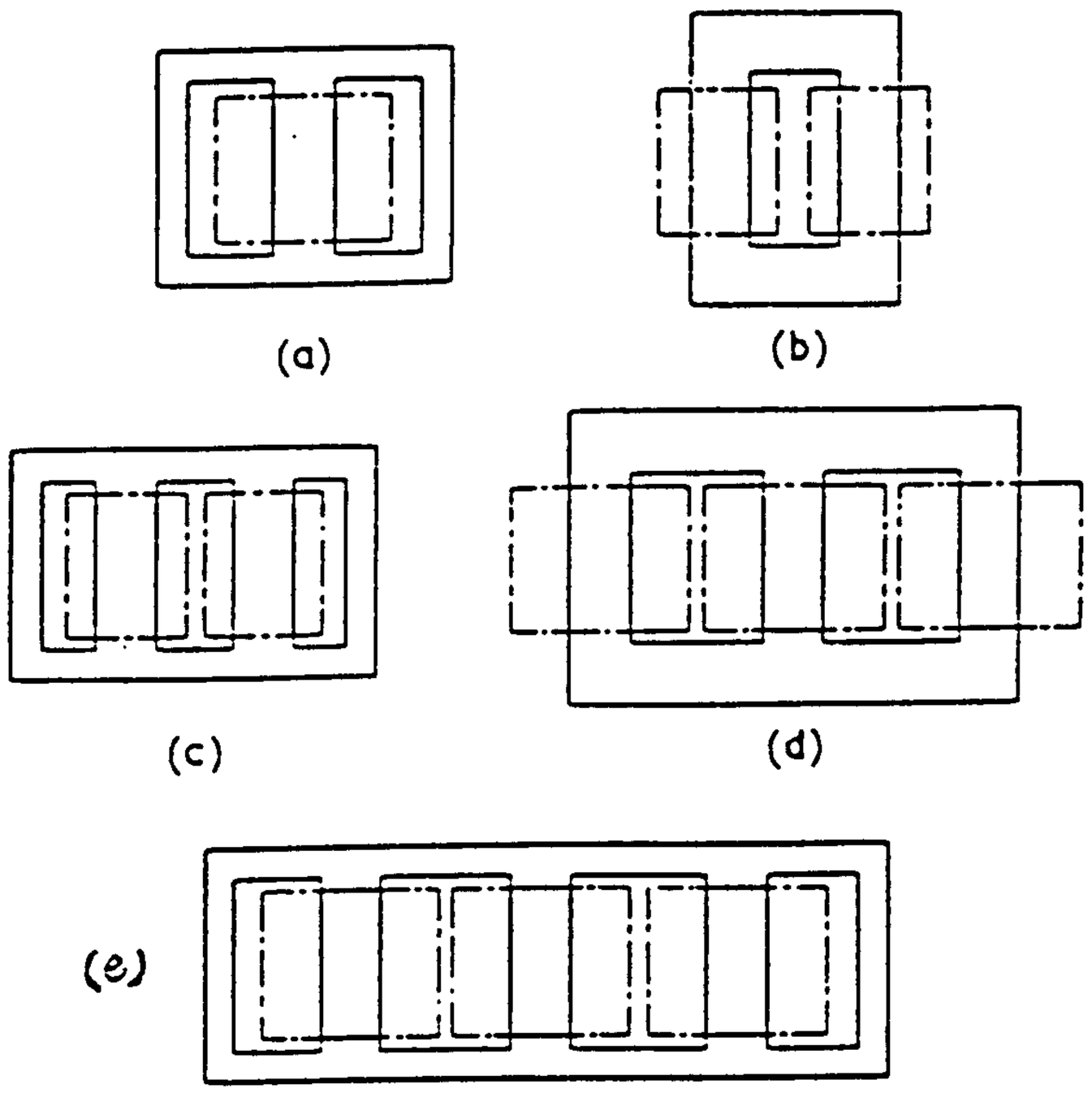

Fig. 3.3 Forms of core built from flat laminations: (a) one-phase, one limb wound with side yoke; (b) one-phase, two limbs wound; (c) one-phase, two limbs wound with side yoke; (d) three-phase three-limb; (e) three-phase five-limb.

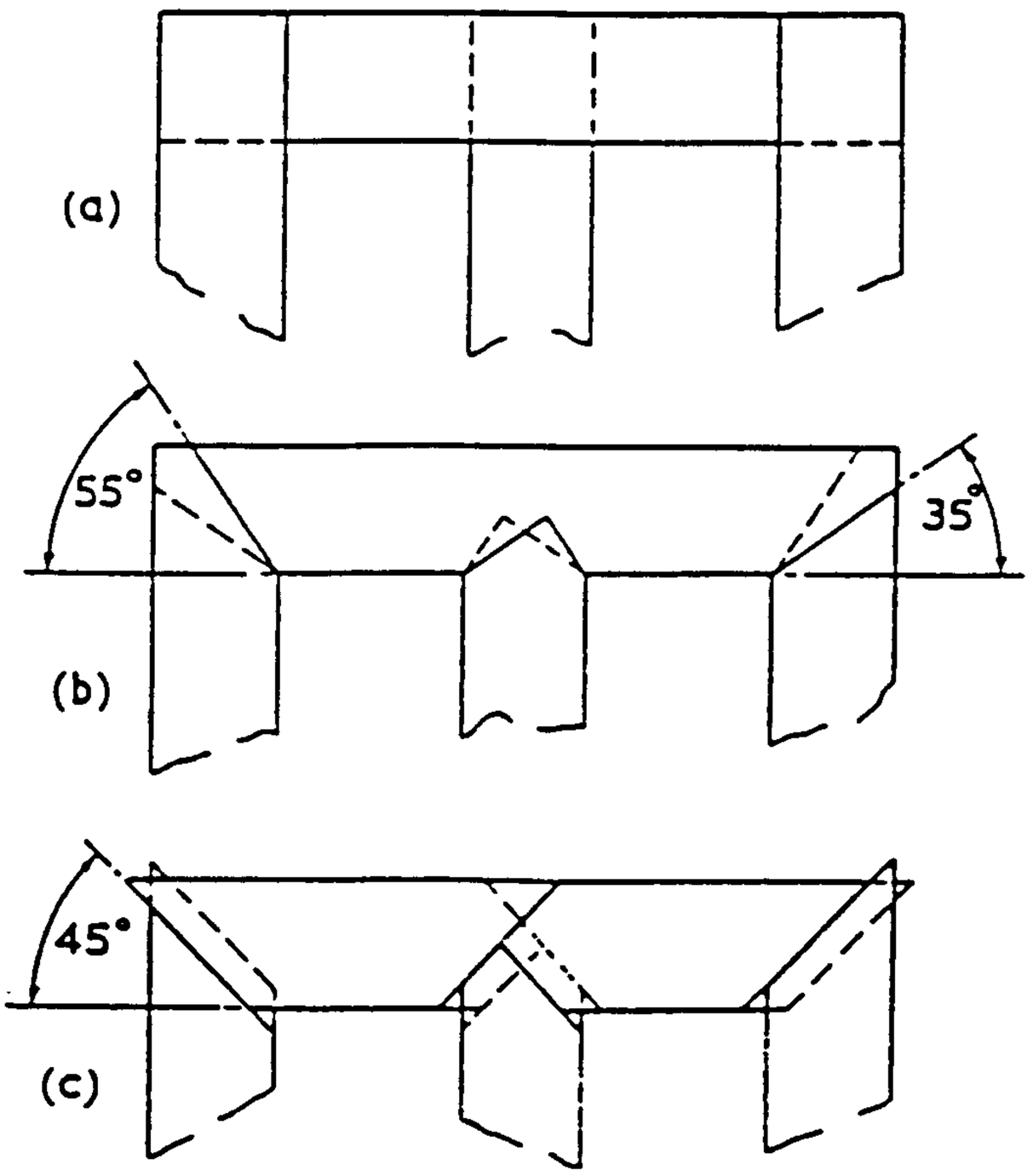

Fig. 3.4 Forms of interleaved joint: (a) square; (b) 35°/55° mitre; (c) 45° mitre.

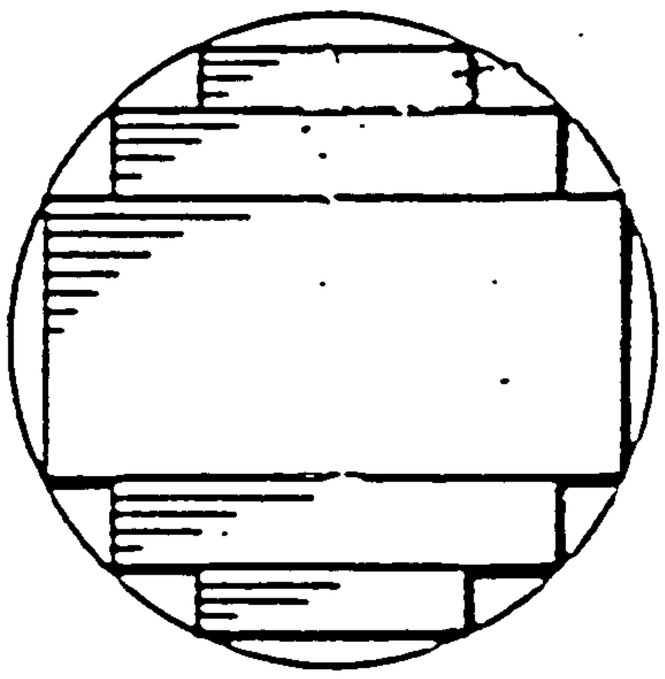

(a)

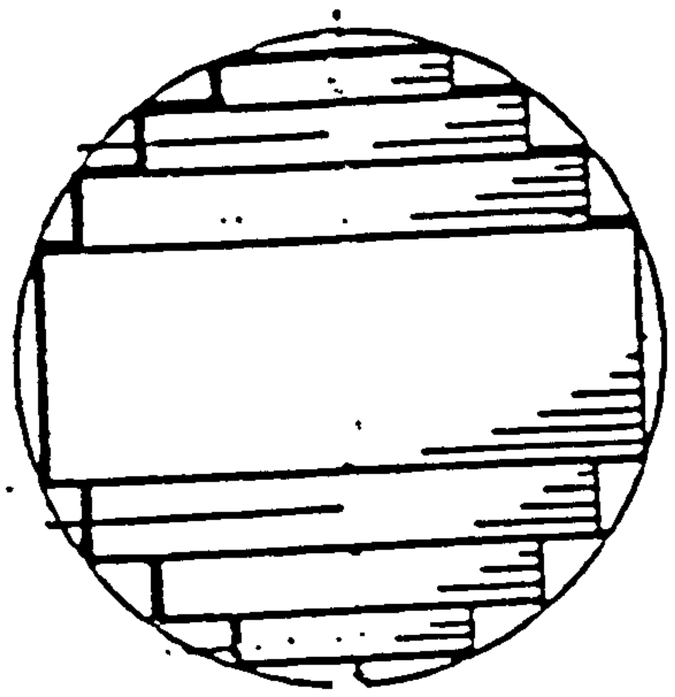

(b)

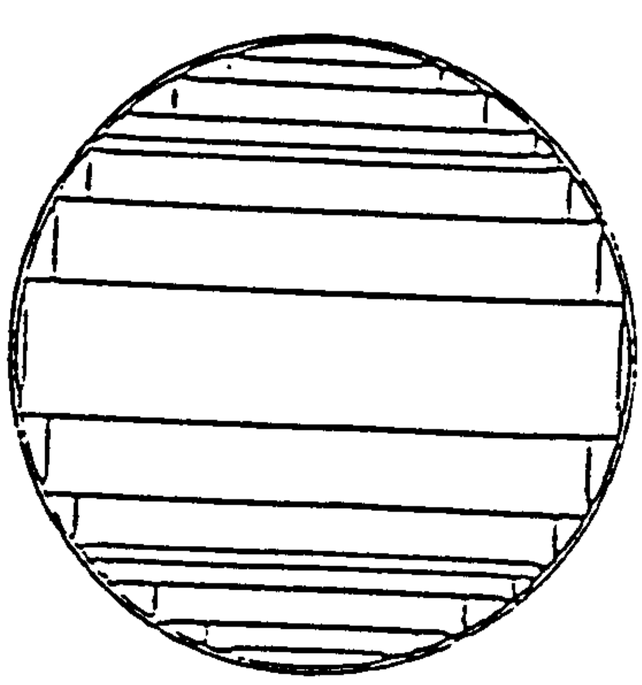

(c)

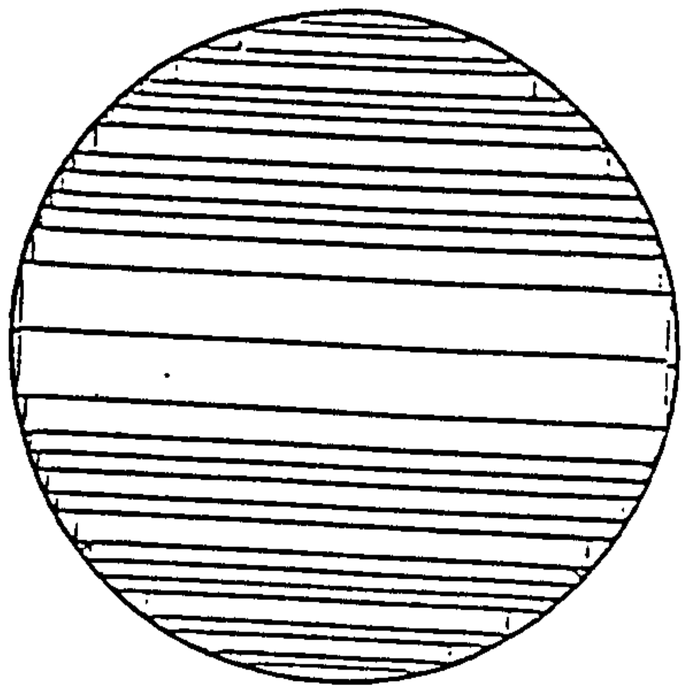

(d)

Fig. 3.5 Typical sections area of core type transformer limbs: (a) three steps; (b) four steps; (c) seven steps; (d) fourteen steps.

3.3. Transformer Windings

The basic material used as conductors for the transformer coils are limited to copper and aluminium in various forms, depending on the current and voltage requirements. Round wires and rectangular strips are commonly used but in recent years there has been an increased use of foil and sheets. Wires are generally suitable where the current is fairly low, as in high voltage-windings of distribution transformers. Strips, either in single form or groups in parallel are used, over a very wide current range from about 10A to the highest current level in the low-voltage winding of large power transformers. When the currents are not very large, foil or wire can replace the strip.

The wire or strip may be covered with a range of insulating materials such as synthetic enamel, silk, paper, or glass tape. The choice of the particular material is governed chiefly by the nature of the insulating fluid or impregnating substance which fills the space between the turns of the winding. The insulation of foil, especially at the edge, presents some problems, attempts have been made [11] to coat the foil with enamel insulation but interturn insulation is more common by using a thin paper or plastic during the manufacture of the coil.

Surrounding the windings and insulation of the majority

of power transformer is a liquid insulant. This serves the double purpose of providing good insulation between the winding, core and tank parts and for removing the heat resulting from the losses. The most common such material is oil. A more recent development is the use of gases, of which sulphur hexafluoride (SF6) is the most common. Under pressure this gas has very good electric strength and also good cooling properties.

CHAPTER 4

Transformer Core Losses

4.1 Core Loss

It is usual to divide the energy losses incurred in a power or distribution transformer into two group, (1) the copper losses of the windings commonly termed the load losses and (2) the iron losses of the core commonly termed the no load losses.

To enable a transformer to have a high efficiency these losses must be kept to a minimum. For power frequency applications, the use of more iron to reduce B and more copper to reduce resistance, reduces the losses incurred using existing conventional materials.

The losses in mains frequency power transformers are of great importance with respect to the cost of the energy wasted. The ratings of transformers designed for frequencies well in excess of mains frequency are much smaller and the cost of the energy losses are not so significant in terms of energy cost. The losses in high frequency transformers are more likely to be of concern with respect to the temperature rise exceeding the limitations of the core material and the insulation.

The losses in the magnetic circuit are divided into

two types, (1) hysteresis loss in core laminations, (2) eddy current loss in core laminations.

4.2 Hysteresis Loss in Core

If the magnetic force applied to a ferromagnetic specimen is increased to saturation and then reduced again to zero, the return B-H curve does not retrace the initial curve but lies above it [12]. This effect is called hysteresis and a typical characteristic is given in Fig.4.1 The value of B when H is zero, is called the residual flux density OR (or remanant flux density, B_r). To demagnetize the specimen completely, it is necessary to apply a negative magnetizing force represented by OC, this is called the coercive force, H_c. If the magnetizing force is increased in this reverse direction, saturation in the opposite direction is similarly obtained, (point D in Fig.4.1). If, finally, the magnetizing force is gradually reduced to zero, reversed, and increased to its maximum value in the original direction, the curve DEFA will be traced out. The complete curve forms a closed loop called a hysteresis loop.

The hysteresis loop can be regarded as a magnetic indicator or diagram. During each cycle, an amount of energy represented by the area enclosed by the loop is absorbed. Consider a toroid core of mean circumference, l metres, and cross-sectional area, A square metres. A coil of N turns is uniformly wound over the toroid. If the instantaneous value

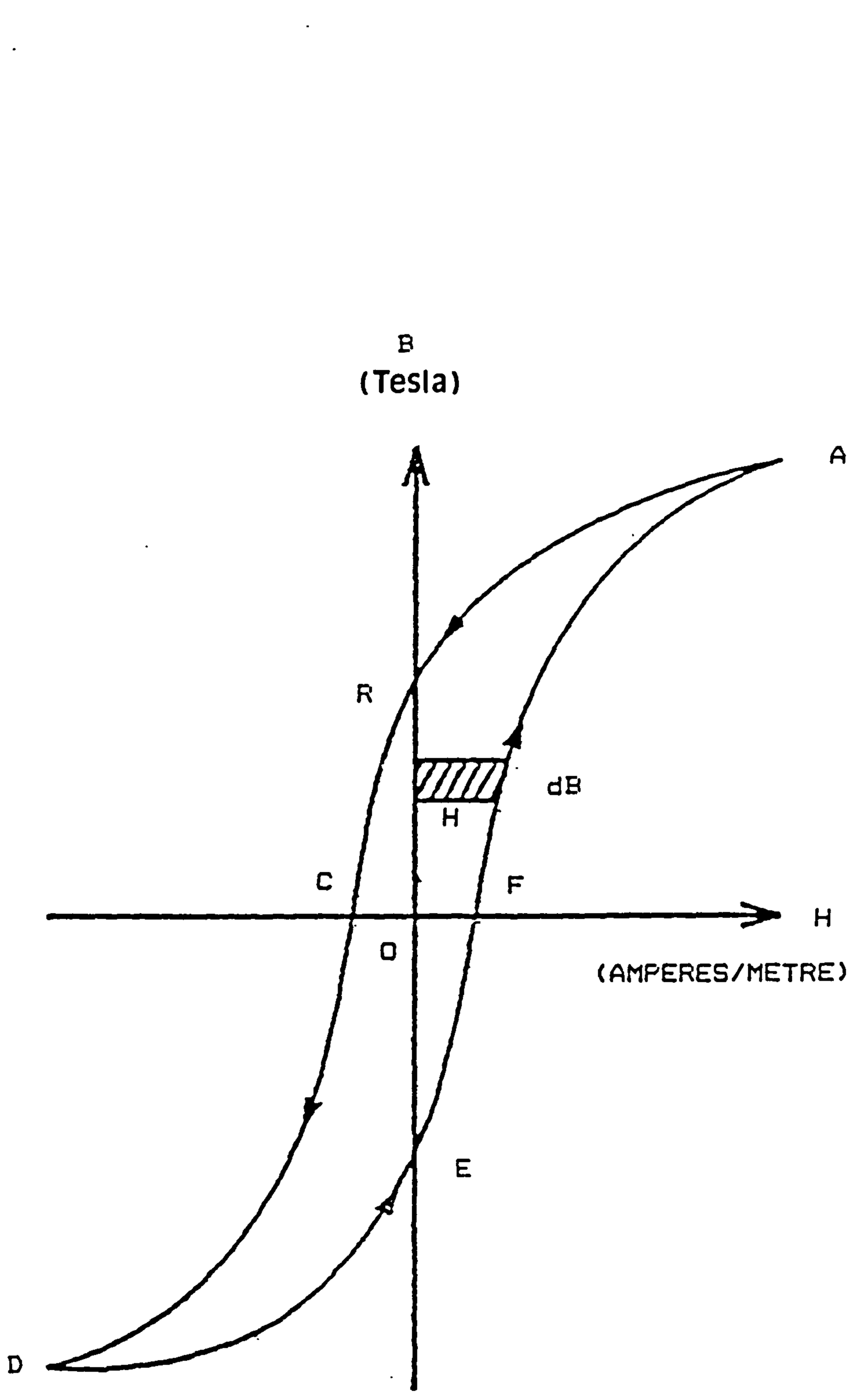

Fig. 4.1 Hysteresis loop of a typical ferromagnetic substance.

of the magnetizing current is i amperes, then the magnetizing force H is given by equation.

$$H = \frac{Ni}{l} \quad \left(\frac{ampere\ turn}{metre}\right) \tag{4.1}$$

If the value of the induction at the instant considered is B, then the induced voltage, e in the coil is given by the rate of change of flux linkages according to equation (4.2)

$$e = \frac{Nd\phi}{dt} = \frac{NAdB}{dt} \quad (volt) \tag{4.2}$$

The current i flowing at that instant will be opposed by this induced voltage and therefore power will have to be expended in order to maintain the increase in current. This required power is given by equation (4.3).

$$Power\ at\ any\ instant = ei = \frac{lAHdB}{dt} \quad (Watts) \tag{4.3}$$

$$Work\ done\ in\ time\ dt = \frac{lAHdBdt}{dt} \quad (joules)$$

$$= lAHdB \quad (joules) \tag{4.4}$$

$$Total\ work\ done\ for\ one\ cycle = lA\int HdB\ (joules) \tag{4.5}$$

It can be seen from Fig.4.1 that HdB is the area of an element of the B-H curve (shown shaded) and therefore, ∫HdB (for an entire cycle) is the area enclosed by loop. The volume of the toroid is 1A.

$$\frac{work\ done}{metre^3} = area\ of\ loop \quad (\frac{joules}{metre3}) \tag{4.6}$$

For the common steels employed in the construction of electrical transformers and machines an approximate relation for the loop area is given by

$$Area\ of\ loop = kB_m^n \tag{4.7}$$

where k is a constant, B_m is the peak flux density and n is an empirically determined constant is in the range of 1.6-2.0. If the material is carried through f cycles of magnetization per second, then the energy dissipated per second in hysteresis loss is directly proportional to f. Therefore, for the entire core, the power dissipated in hysteresis loss is given by

$$P_h = K_h f B_m^n \quad (\frac{W}{kg}) \tag{4.8}$$

where K_h is a constant determined by the nature of the ferromagnetic material and dimensions of the core [13].

4.3 Eddy Current Loss

A time-changing magnetic field in a conducting solid, either ferromagnetic or non-ferromagnetic, produces an induced voltage round closed paths that encircle the lines of magnetic flux. Circulating currents produced in the conductor by these voltages are known as eddy currents and the resulting heat losses are undesirable. In an effort to minimize these losses in transformers, the core material is made up of thin sheets, or laminations. These laminations are insulated from one another and placed parallel to the flux path.

The eddy current losses can be calculated, using classical theory. Consider with reference to Fig.4.2 a volume element of a lamination of thickness, d metres, and length 1 metre and depth of 1 metre. The field flux density B is varying sinusoidally in the direction shown where $B=B_m \sin\omega t$. The field flux ϕ through the area bounded by the shaded differential element is $2xB_m \sin\omega t$. The voltage induced by the pulsating flux is given by

$$e = \frac{d\phi}{dt} \tag{4.9}$$

$$e = \frac{d}{dt}(2xB_m \sin\omega t) \tag{4.10}$$

RMS voltage

$$E = \frac{2\pi f}{\sqrt{2}}(2xB_m) \quad (volt) \tag{4.11}$$

The current in the strips dx, flowing up one side and down on the other side, is given by

$$I = \frac{E}{\frac{2\rho}{dx}} = \frac{Edx}{2\rho} \tag{4.12}$$

where ρ is the electrical resistivity of the lamination material in Ohm-metre. Let the power dissipated in the differential element, dx, be P_{dx}, then

$$P_{dx} = EI = \frac{(4\pi^2 f^2 B_m^2 x^2 dx)}{\rho} \tag{4.13}$$

The power, P dissipated in the lamination is:

$$P = \int_0^{\frac{d}{2}} P_{dx} dx = \frac{4\pi^2 f^2 B_m^2}{\rho} \int_0^{\frac{d}{2}} x^2 dx \tag{4.14}$$

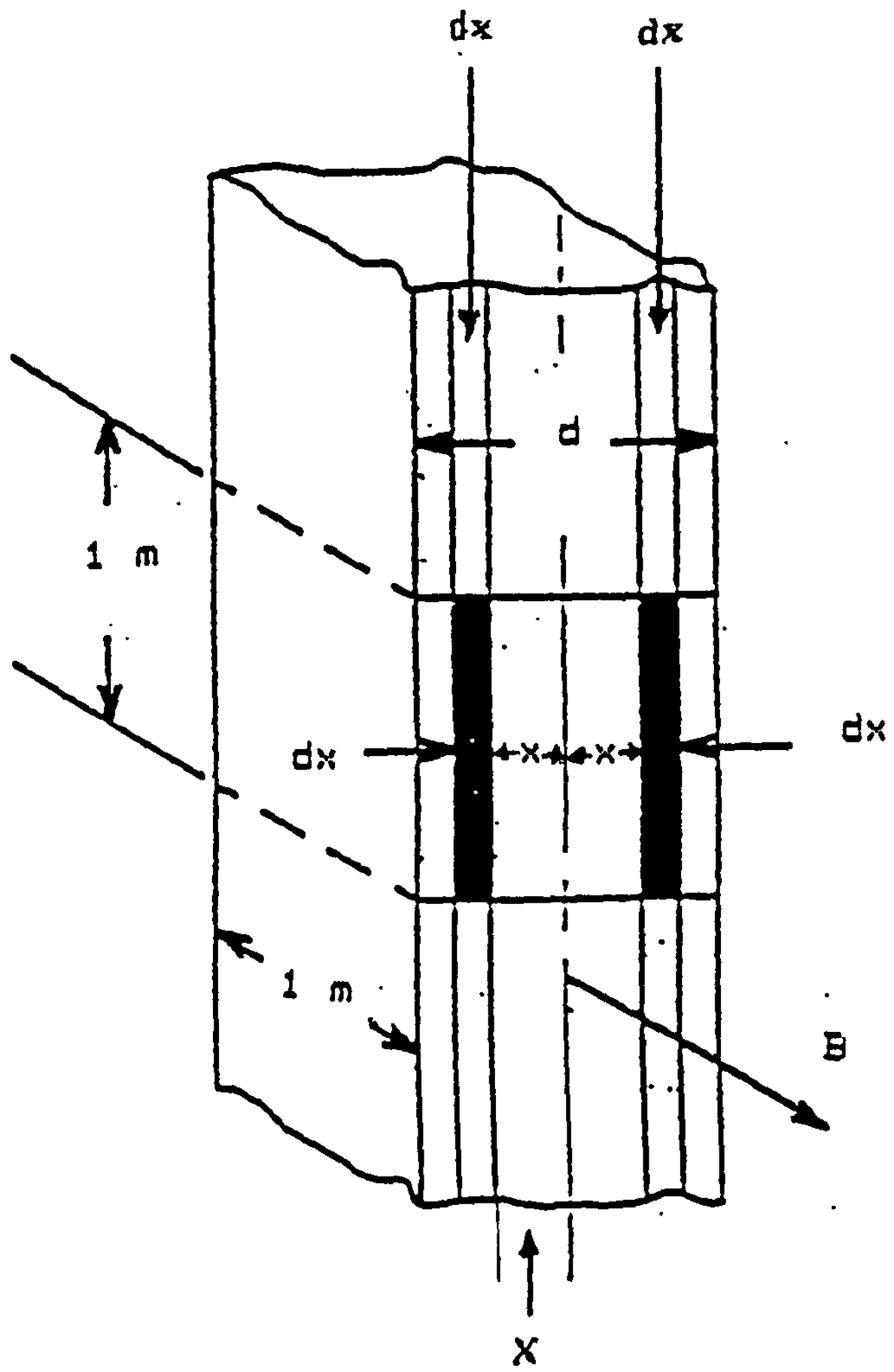

Fig. 4.2 Calculation of eddy current loss

or

$$P = \frac{\pi^2 f^2 B_m^2 d^3}{6\rho} \quad (Watts) \tag{4.15}$$

and since the volume of the element considered is d in metre^3 the eddy current loss per unit volume, P_{ec}.

$$P_{ec} = \frac{(\pi f B_m d)^2}{6\rho} \quad (\frac{watts}{metre^3}) \tag{4.16}$$

It is noted that the eddy current loss is proportional to the square of the thickness, d, of the laminations. In electrical machines the eddy current losses are minimized by the use of laminated material having high resistivity. Silicon steel has a resistivity several times greater than ordinary sheet steel. The resistivity of the new amorphous alloys are approximately three times those of silicon steel. The total expected core loss may thus be determined for a given volume and maximum flux density at any frequency by the equations (4.21)

$$P_{hy} = k_h B_m^n f \quad (\frac{W}{m^3}) \tag{4.17}$$

$$P_{edd} = k_e B_m^2 f^2 d^2 \quad (\frac{W}{m^3}) \tag{4.18}$$

Total expected core loss

$$P = P_{hys} + P_{eddy} \qquad (4.19)$$

or

$$P = k_h B_m^n f + \frac{(k_e B_m^2 f^2 d^2)}{1} \qquad (4.20)$$

Total expected core loss per cycle

$$\frac{P}{f} = K_h' + K_e' f \qquad (4.21)$$

where hysteresis loss/cycle $K_h' = K_h B_m^n$ and the eddy current loss/cycle $K_e' = (k_e B_m^n f^2 d^2)$. A plot of the component losses for each cycle are shown in Fig.4.3. However the total loss/cycle as measured on test exceeds the total loss/cycle calculated according to equation (4.21). The difference between the measured and the calculated total loss/cycle values is termed the anomalous loss.

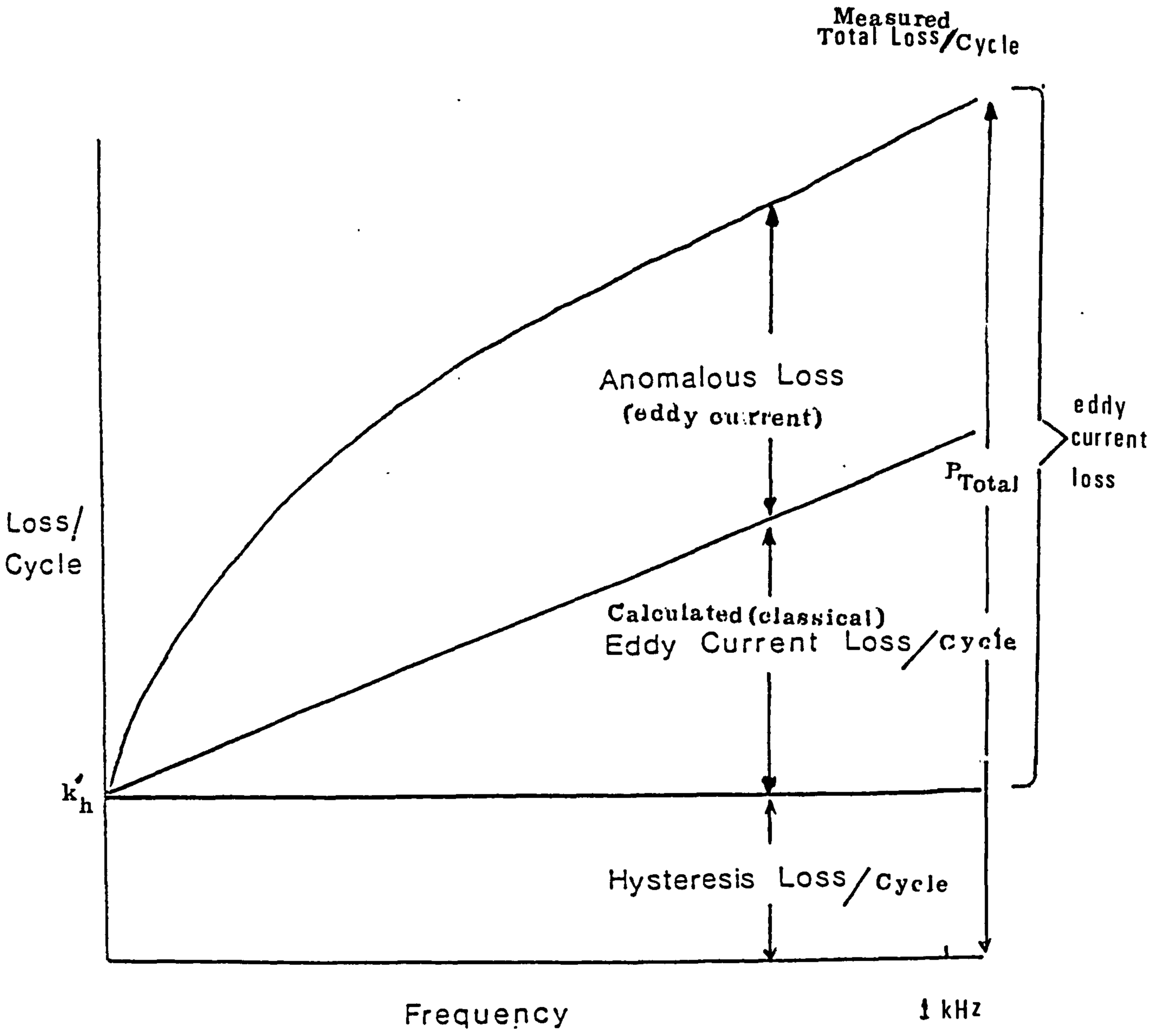

Fig. 4.3 Separation of core loss components

4.3.1 Anomalous Loss

In recent years the anomalous loss has received much attention since it can be responsible for as much as 50% of the total loss in silicon-iron at power frequencies [14]. It is to be noted that the classical eddy-current loss is calculated assuming that the material is homogenous and has constant permeability and the flux penetrates fully into the laminations. In order to determine the methods to reduce these losses, it has become customary to separate the total measured losses into hysteresis and eddy current components. The total loss per cycle plotted against frequency is shown in Fig.4.3 This is obtained by measuring the power loss over the frequency range of 20 Hz to 1000 Hz and extrapolating the characteristic to zero frequency. The classical eddy-current loss is calculated from equation (4.16). The sum of the extraploted hysteresis loss and the calculated classical eddy-current loss is significantly less than the measured losses. The difference between the measured total loss and the sum of the estimated hysteresis and eddy-current losses is termed the "anomalous" loss. An anomaly factor, η, is defined according to equation (4.22) to express this anomalous loss.

$$\eta = 1 + \frac{Anomalous\ eddy\ current\ loss}{Classical\ eddy\ current\ loss} \qquad (4.22)$$

The anomalous loss is treated as being an excess eddy current loss. The origin of this excess eddy-current loss has been attributed to many causes [15]. The principal cause in grain-oriented silicon-iron is the existence of domain walls [16], and about 75% of the loss has this origin.

4.4 The effect of Applied Stress on Power Loss

Grain-oriented silicon-iron is well known to be stress sensitive, whereby applied stresses have a marked effect on the materials magnetic properties. Stresses are induced in the transformer core laminations by the localized stresses produced by the bolts or clamps holding the core together and by depressions and waves in the lamination being removed during clamping. A further cause of stresses is the temperature variation throughout the core.

Silicon-iron laminations as produced are not flat and Wilkins and Thompson [17] have reported that waves with an amplitude of 3 mm per metre are common. When the material is compressed, in the construction of a transformer core, stresses of 2 MPa are produced. Another production defect is the saucer-like depression often found in the sheet and the same investigators have shown that one of these defects of diameter 12 cm and approximately 1 mm depression gives rise to a stress of 7 MPa when flattened.

The build up of a transformer core involves the bolting together of stacks of laminations. The manufacturer's aim is to achieve a stress perpendicular to the laminations of at least 3 MPa in order to maintain a tight core. However, Walker and co-investigators [18] have found that as a transformer ages it settles down and the stresses are reduced so that in order to maintain a stress of 3 MPa after several years use, an initial stress of up to five times this magnitude must be applied. Thickness variation in a stack of laminations will result in bending which induces a further stress.

All these contributions when summated can result in a stress of approximately 7 MPa (1000 psi)in the rolling direction. This has been confirmed by Banks and Rawlinson [19] using strain gauges mounted in different directions on the silicon-iron laminations.

The aforementioned stresses have a marked effect on the domain structure of silicon-iron. Compressive stresses applied on the rolling direction tend to induce the formation of domain patterns perpendicular to the [100] direction ([100] indicates the edge-direction lying in the x-axis for cubic crystals). The 90° domain walls produced will increase both the static hysteresis and anomalous loss components. The graph of power loss against stress shown a large positive gradient for increasing applied compressive stress, see Fig. 4.4. Investigations of Brown, Holt and Thompson [20] on 46

grade silicon-iron at 1.5 T peak induction showed that an approximate 30% increase in power loss was obtained under the application of a compressive stress of 3 MPa in the rolling direction.

Domain studies by Houze [21] have shown that tensile stresses in the rolling direction of up to 45 MPa remove the secondary domain structure such as spike and transverse domains which serve to reduce the magnetostatic energy and furthermore the 180° domain structure. Houze [22] had earlier postulated that this should lead to improved 180° domain wall mobility, thereby reducing the power loss. A large decrease in losses when a tension of approximately 15 MPa was applied along the 'easy' axis of single crystals of silicon-iron were found by Yamamoto and Nozawa [23]. The effect was much smaller when the orientation of crystals was less perfect, indeed in commercial materials particularly with normal grain size the application of a tensile stress actually increased the power loss. From this observation it will be clear that in evaluating a material for potential use in power transformers an investigation into its magnetic properties under conditions of applied stress is necessary.

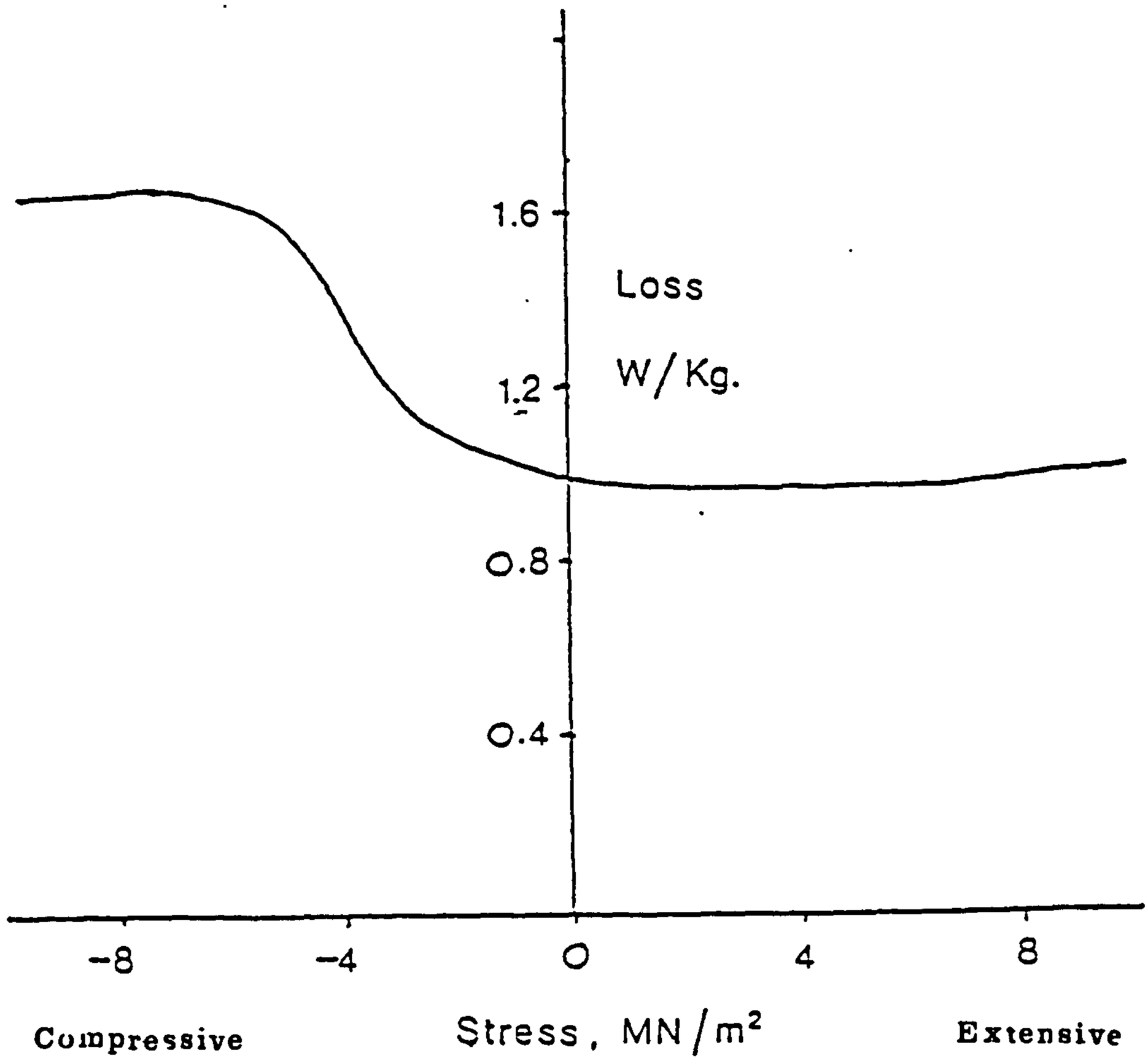

Fig. 4.4 A graph of power loss against stress in 3.25 % Si-Fe

CHAPTER 5

Transformer Core Material

5.1 Core Material

5.1.1 History of Transformer Core Material

The cores of modern power transformers still retain the same essential features developed over a hundred years ago when the first power transformers came into existence. The first transformer used mild steel for the magnetic circuit, the core loss in these transformers at a core flux density of 1.5T, 50 Hz was approximately 8 W/kg. With the development in core material, the core loss in modern transformers is now less than one tenth of the core loss in the past. The search for new core material with higher permeability and lower loss began very early, there are several distinct stages in the developments.

The first developments were associated with the addition of silicon. Barrent, et al. [24] discovered the beneficial results of adding silicon to low carbon steels. Hadfield [25] found that iron alloyed with silicon raised the maximum permeability, reduced the area of the hysteresis loop and eliminated the effect of magnetic ageing. Gumlich [26] investigated the advantage of iron alloyed with silicon because of its raised electrical resistivity, this led to the production of silicon-iron on a commercial scale which started in the U.S. and in the U.K. in 1905 and 1906 respectively. The addition of silicon to iron, at the same

time depressed the saturation magnetization and introduced difficulties with mechanical properties, but nevertheless the advantages of this alloy were quickly recognized and hot rolled silicon-iron took over from carbon steel in a short time. Between 1900 and 1930 the quality of the hot rolled silicon-iron improved with the power loss being reduced to 2.2 W/kg at 50 Hz and a core flux density 1.5 T. The second major breakthrough came in 1934, when Goss [27] invented the process which was characterized by two stage cold rolling with intermediate gauge annealing. This process was modified and further developed by Armco steel on a commercial scale. Although the degree of preferred orientation in the original material produced by Goss was about 40%, it was improved by adopting a batch type high temperature anneal which reduced the power loss to around 1.1 W/kg (at 50 Hz, 1.5 T). Subsequent general improvement in manufacturing techniques achieved a power loss of 0.9 W/kg by 1960. Since then no significant change has been seen in grain-oriented silicon-iron produced by this conventional process.

The appearance of grain-oriented silicon-iron with higher permeability, named HIB, marked another great step forward in the reduction in power loss as shown in Fig. 5.1 [28]. The invention was by Taguchi and Sakakura [29] in 1965 and in 1968 the new product was commercialized by Nippon Steel Corporation [30, 31]. The high permeability grain-oriented silicon-iron (hereafter HIB) achieved a reduction in

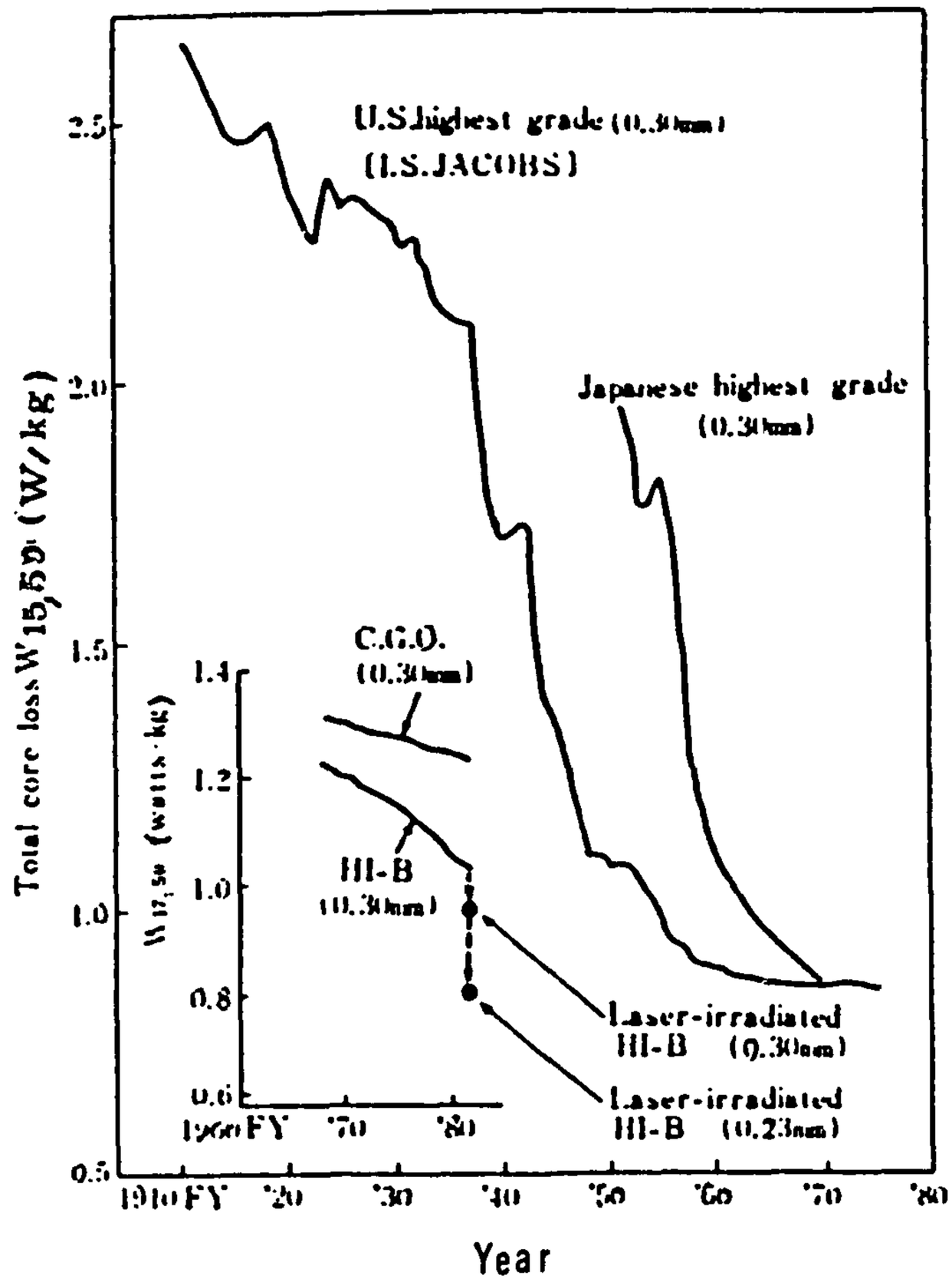

Fig. 5.1 Historical improvement in power loss of silicon-iron [28].

core loss of 15% compared with the grain-oriented 3% silicon iron [32] thanks to its almost perfectly oriented crystalline texture. Since the introduction of HIB, similar kinds of high permeability silicon-iron have been developed by other steel producers. In 1973 Kawasaki Steel corporation announced RG-H [33] and began commercial production in 1974. Also in 1973 TERNI-CSM developed Terni-μ [34] and in 1975 Allegheny Ludlum steel Corporation and General Electric Co. introduced Bron steel [35]. Another great reduction in power loss of core material was developed by the refinement of magnetic domains in grain-oriented silicon-iron [36]. Over sixty years ago the reduction in power loss by scratching the surface of electrical steel was reported by Hayes and Wolford [37]. However it had not been put into practice until Kuroki et al. [38] found that it could be obtained by a very small strain similar to that introduced by a ball-point pen, rather than a sharp scratch. The initial method was not successful because of the fact that the effect of the scratch could not be maintained when the scratched samples were stacked. Nozawa et al. [39] explained that the improvement in power loss due to scratching was attributed to the reduction in domain wall spacing. With the successful application of a laser irradiation system developed by Nippon Steel Corporation [40], in 1982, laser scratched high permeability grain-oriented silicon-iron (ZDKH) became commercially available. Together with reduced thickness and improved texture, a lower power loss of 0.6 W/kg at 1.5 T, 50 Hz (0.8W/kg at 1.7 T, 50Hz) was achieved [41].

5.1.2 Conventional grain-oriented silicon-iron (CGO)

Goss invented the Cold rolled grain-oriented silicon-iron, which was developed by Armco Steel, it is the most important commercial soft magnetic material. It is called conventional grain-oriented silicon-iron (CGO) or sometimes called oriented silicon steel or electrical steels [42] in contrast to high permeability grain-oriented silicon-iron. In the electrical engineering industry, particulary in the production of transformers, the CGO material is used in large quantities. The material has a (110)[001] texture, i.e. it is made up of the grains whose (110) planes lie at right angles to rolling of the sheet direction with their [001] planes parallel to the rolling direction as shown in Fig.5.2. Thus the crystalline texture of conventional grain-oriented silicon-iron (CGO) material is often referred as "Cube-on-edge" or "Goss" texture.

The most significant magnetic characteristic of grain-oriented silicon-iron is its magnetic anisotropy. Silicon-iron is made up of crystals of body-centred cubic lattice form, with the assist direction of magnetization along any one of the cube edge directions, which in terms of Miller indices are the <100> directions. The hardest direction of magnetization is a <111> direction, which in the plane of the sheet lies at approximately 55° to the rolling direction. Magnetic anisotropy of grain-oriented silicon-iron depends on the degree of orientation alignment of the crystalline

texture. This is indicated by the flux density induced at a field strength of 1000 At/m (B_{10} is the flux density produced at a field strength of 1000 At/m) [43].

After the discovery of the process by Goss in 1934, a gradual improvement in manufacturing techniques took place and a power loss of 0.9 W/kg at 1.5 T, 50 Hz was achieved by 1960. Since then no significant change has been seen in the process for CGO material. The recent improvement in the power loss of CGO material was mainly due to a reduction in lamination thickness. The thickness of CGO lamination used in transformer core ranges from 0.35 mm to 0.20 mm, more recently even 0.18 mm (7mil) is being employed in the U.S. for distribution transformers. In Europe 0.28 mm thick CGO (28M4) is the principal core material with a typical power loss of 0.8 W/kg at 1.5 T, 50 Hz and 1.2 W/kg at 1.7 T, 50Hz.

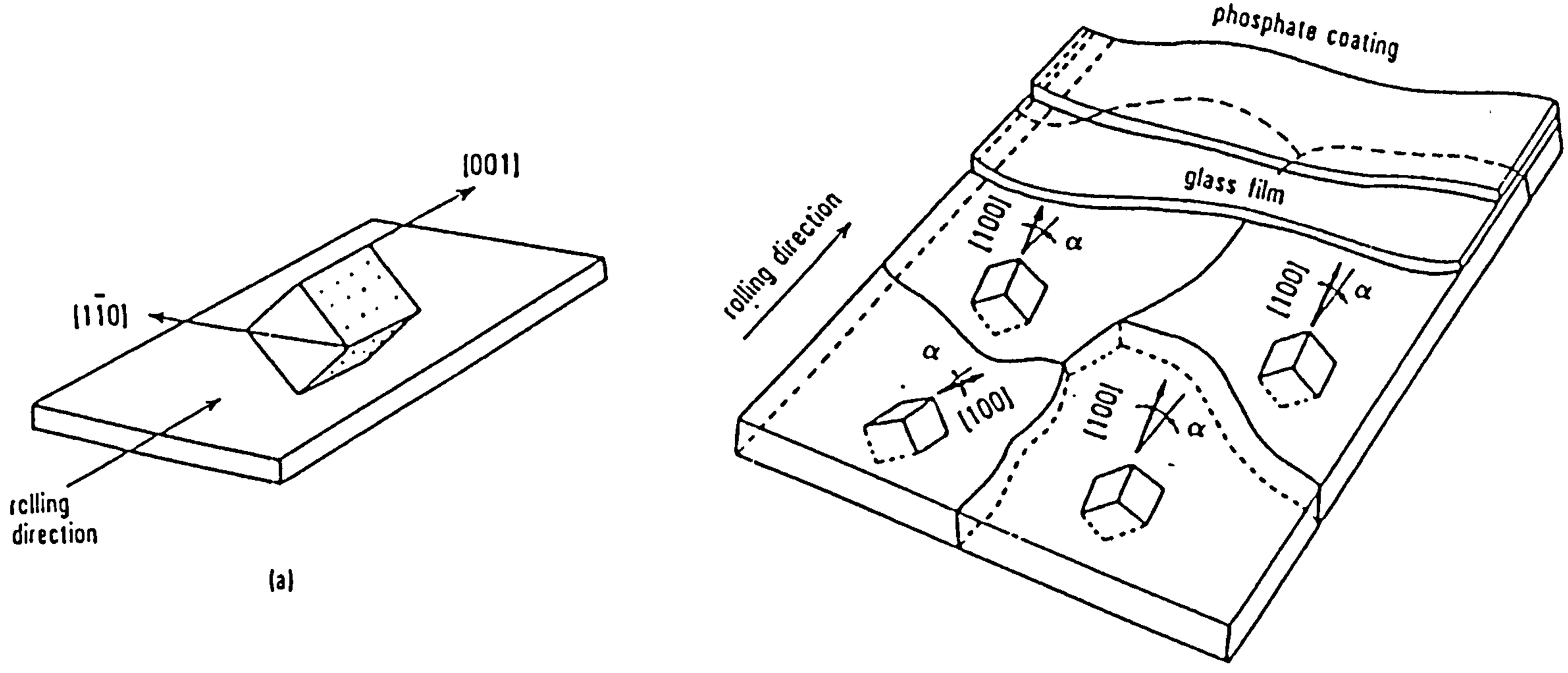

Fig. 5.2 Schematic diagram of (a) Goss oriented texture and (b) CGO material.

5.1.3 High permeability grain-oriented silicon-iron (HIB)

In 1968 high permeability grain-oriented silicon-iron (HIB) was produced by Nippon Steel Corporation and the same type of electrical steel was developed by some other steel producers. These materials have a higher degree of grain orientation achieved by adding a new grain growth inhibitor (aluminium nitride in the case of HIB) in addition to the conventional inhibitor (manganese sulphide). Fig.5.3 shows typical (100) pole figures of HiB and CGO materials [44]. The average deviation of the [001] axis from the rolling direction in CGO material is 7° and 75% of the grains are within a range of deviation of 10° [45]. The corresponding average deviation in HiB material is 3° and almost all the grains are within 10° deviation. This highly oriented crystalline texture gives rise to high permeability and the typical B_{10} value of HiB material is 1.92 T or more. The improvement in power loss of more than 15% was achieved mainly due to reduced hysteresis loss.

The higher degree of grain orientation of HiB material, at the same time, resulted in larger grain size. The typical grain size of HiB is ASTM No. 3 (X1) (10-15mm) whereas that of the CGO is ASTM No. 7 (X1) (3-5mm). Large grain size causes wider domain wall spacing, which in turn leads to a higher eddy current loss. Littmann [43] found the effect of grain size on power loss and pointed out that the optimum grain diameter would be around 1mm. However the detrimental

effect of large grains was overcome to a certain extent by tensile stress as shown in Fig.5.4 [44]. The progress in crystalline texture of the HiB material, together with the stress coating, also achieved a reduction in magnetostriction [46]. Consequently, the noise of transformers assembled from the HiB was decreased by 4-5 db compared with that of conventional transformers. Fig.5.5 shows the improved performances of full size transformers assembled from HiB material [46]. They are shown in comparison with transformers of identical geometry assembled from CGO material.

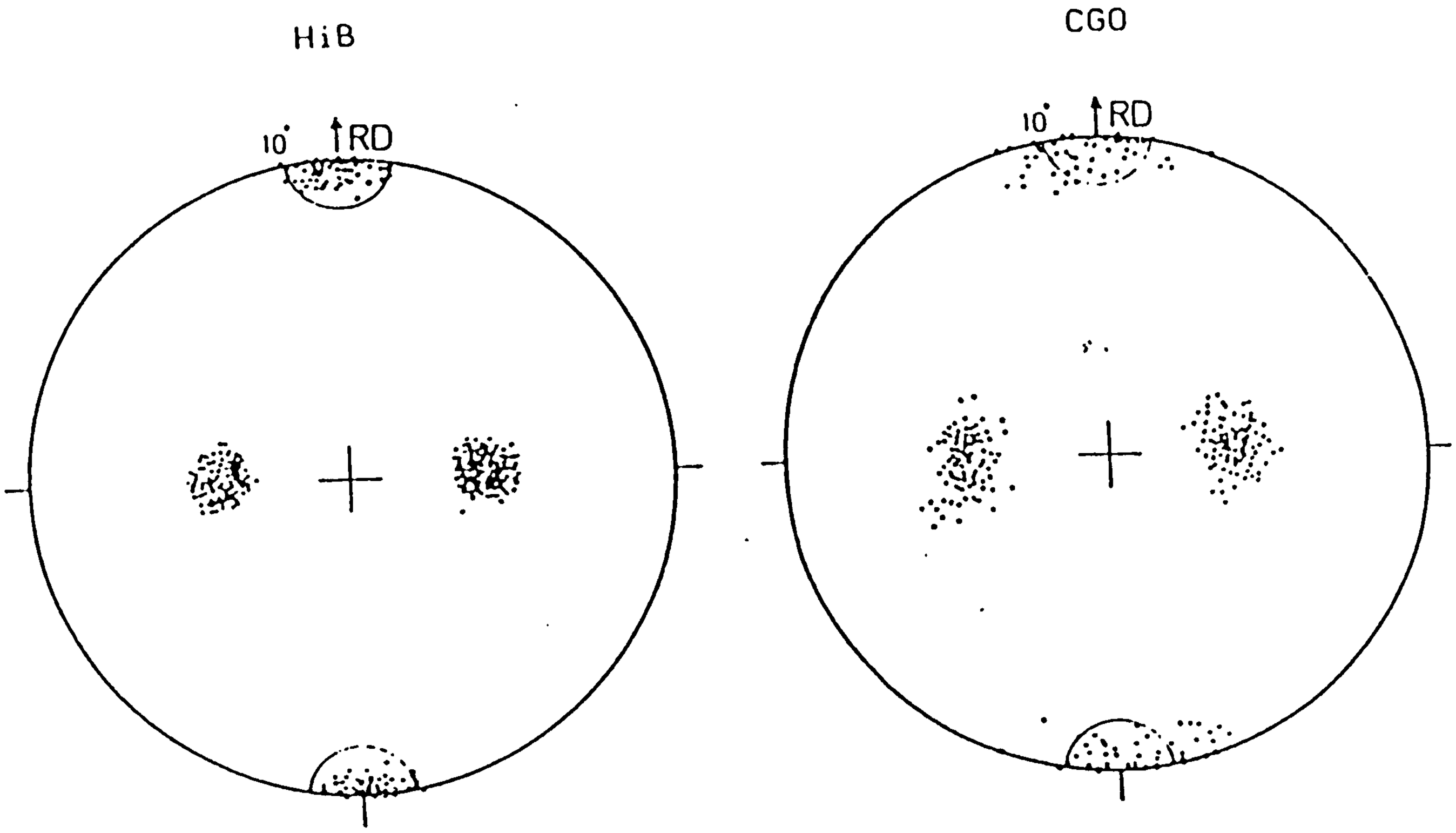

Fig. **5.3** (100) pole figure illustrative of grain oriented of HIB and CGO [**44**].

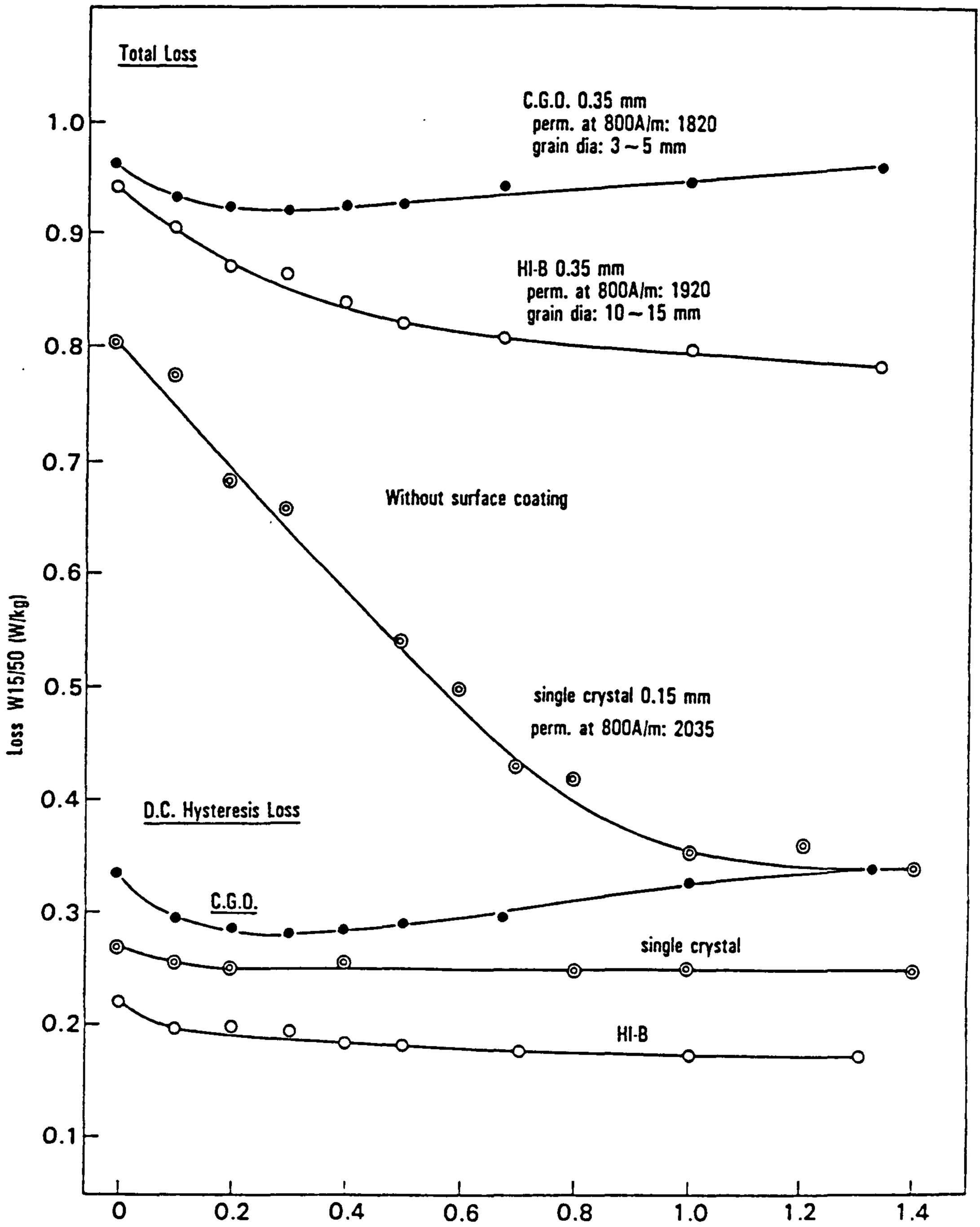

Fig. 5.4 Effect of tensile stress on power loss of CGO and HIB material [44].

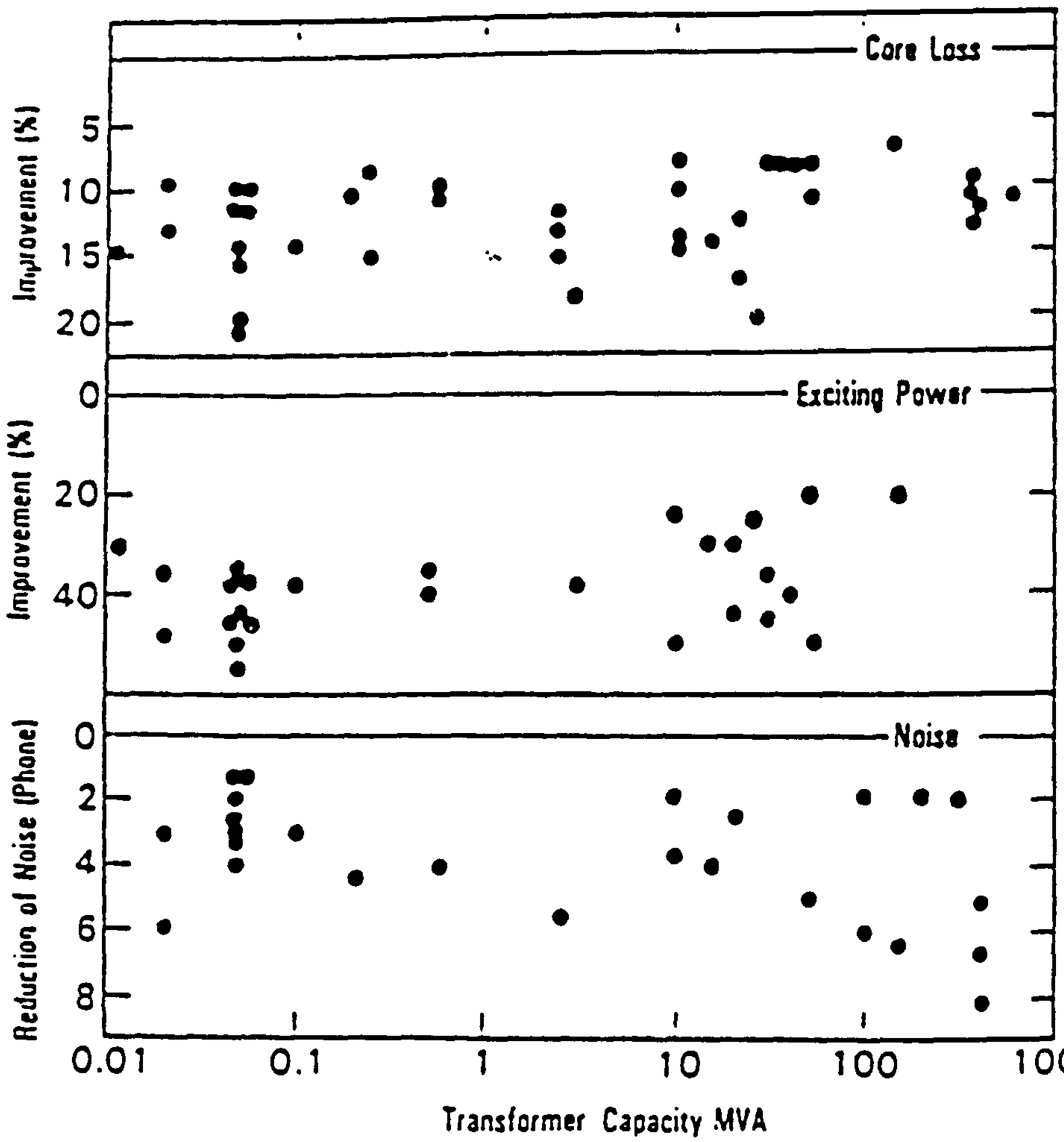

Fig. 5.5 Improved performance of transformers assembled from HIB material in comparison with those assembled from CGO material [**46**].

5.1.4 Laser scribed high permeability grain-oriented silicon-iron (ZDKH)

The domain refinement method was developed as a new measure for further reduction in power loss of HIB material. It was found that the domain refinement due to the introduction of a small regular strain on the surface of silicon-iron brought about a significant reduction in power loss. The improvement in power loss is attributed to the reduction in domain wall spacing resulting from the formation of supplementary domains caused by either mechanical scribing [39] or laser irradiation [47]. The laser beam pulse, focused through the optical lens system, is emitted onto the surface of the steel. The laser beam is scanned in the transverse direction of the steel and the irradiated spots form parallel dotted lines at intervals of several mm.

The power loss obtained by laser scribing ranges between 0.05 W/kg and 0.15 W/kg at 1.7 T, 50 Hz. The improvement depends on the thickness of the material and the degree of orientation. Ichijima et al.[41] found that the thicker the sheet and the higher the permeability, the larger is the reduction which results.

In addition to the domain refinement by the laser beam pulse as mentioned above, there are some alternative techniques which have been suggested. Mechanical scribing with a ball-point pen [38] was the first successful attempt

to reduce the power loss. It was extended to an improved method employing a ball bearing [48], however because of the low productivity it was replaced by the laser scribing. A domain control technique named "spark ablation" was developed, making use of high voltage electrical discharge [49]. An improvement in core loss of the order of 10% was achieved by the spark ablation. Krause et al. [50] suggested a method employing a continuous CO_2 laser. It was claimed that the reduction in the power loss of 9% was achievable at 1.7 T without any coating damage. Von Holle and Schoen [51] investigated the domain refinement by a continuous-wave Nd:YAG laser. The average reduction in power loss measured both in single strip and experimental cores was 9 % in the flux density range of between 1.0 T and 1.8 T.

5.2 Amorphous Materials

Amorphous metal alloys were known more than twenty five years ago, the term amorphous generally meaning not crystalline on any significant scale or random atomic structure but, with short range atomic ordering. Amorphous alloy is sometimes called metal glass. There are a variety of techniques that can be used in the production of amorphous but they are all involve the rapid solidifying of the alloying constructions from the gas or liquid phase, so quickly that atoms are frozen in their liquid configuration. The magnetic properties of amorphous alloys appear to have advantages over those of existing magnetic materials, the

property of greatest potential significance to electrical engineers is their low power loss. Amorphous alloys have unique properties which result from their non-crystalline structure, these are discussed in chapter 7. The following sections deal with the production of amorphous material.

5.2.1 Production of Amorphous Material

Amorphous material alloys are of the basic composition $(TM)_{80}\ M_{20}$, where (TM) represents one or more of the transition metals, Iron (Fe), Cobalt (Co) and Nickel (Ni), and M represents one or more of the metalloid or glass-former elements, Phosphorous (P), Boron (B), Carbon (C) or Silicon (Si). These alloys may be made by several methods, e.g. electrodeposition, chemical deposition, or vapour deposition, including ion sputtering. The preferred method of manufacture though is rapid cooling from the melt because it is faster, applicable to a wider range of composition, probably gives materials of greater uniformity and is adaptable to large scale production [52].

To obtain the amorphous phase by any of the liquid quenching techniques, the alloy must cool through the melting temperature to the glass transition temperature, without crystallizing. The factors controlling the glass transition temperature and crystallization are both structural and kinetic. The structural factors are concerned with atomic arrangement, bonding and atomic size effects. These factors

tend to have limited predictive value, and kinetic factors tend to be dominant [52]. The kinetic factors studied by Turnbull [53] and by Spaepen and Turnbull [54] are the nucleation and crystal growth rate and diffusion rates compared to the cooling rate. The alloy must have a high resistance to homogeneous nucleation of crystals and the glass transition temperature must occur at temperatures not too far below the liquidus. Thus a low eutectic temperature compared to the melting point of the metallic element coupled with a metal-rich eutectic composition favours the formation of the amorphous phase. The majority of the present interest in amorphous magnetic metals is concerned with their preparation by direct solidification from the melt. The interest in this method stems from the wide variety of alloys that can be made as well as from the potential lower cost of preparation. Since the pioneering work of Duwez et al.[55], a number of devices have been reported for obtaining the necessary high quenching rates and for producing continuous filaments. These devices are described in the following sections.

5.2.2 The Gun Technique

Fig.5.6 shows schematically, the gun technique developed by Duwez and Willens [56]. A small quantity, up to 100mg of the metal or alloy is melted in a graphite crucible with an orifice of about 1mm diameter at the bottom. The melt does not fall through the orifice because of high surface tension.

The molten metal, ejected by means of a shock wave, passes through the orifice and spreads onto a copper substrate in the form of thin foils (up to 15μm in thickness). The substrate can be maintained at low temperatures. The shock wave is generated by the rupture of a thin myler diaphragm, located between the high and low-pressure chambers, by means of an inert gas at high pressure. The product is an irregular thin foil, porous in nature and with varying cross-sectional area. The thickness of the foils varies and owing to their uneven cross-section it is difficult to measure their properties.

5.2.3 Piston-and-Anvil and Double Piston Technique

Pietrokowsky [57] developed this technique and utilizes the concept of catching a molten droplet between a stationary anvil and fast moving piston. During its fall the molten droplet cuts a beam of light, triggering the piston motion. A number of variations of this device with differences in either the melting technique or the process of releasing the piston have been developed over the years, based on this simple design. Fig.5.7 shows, a two piston device using magnetic yokes to close the piston and anvil developed by Cahn et al.[58]. The final product obtained in all the above cases is a foil of almost uniform thickness suited for both physical and mechanical property investigation. The thickness can be as large as 100μm, i.e. approximately ten times that obtained in the "gun" technique, but the cooling rate is

considerably reduced. Although, since the extraction of heat is from both surfaces of the foil, the overall cooling rate in this technique is still of the order of 10^5 °C/s.

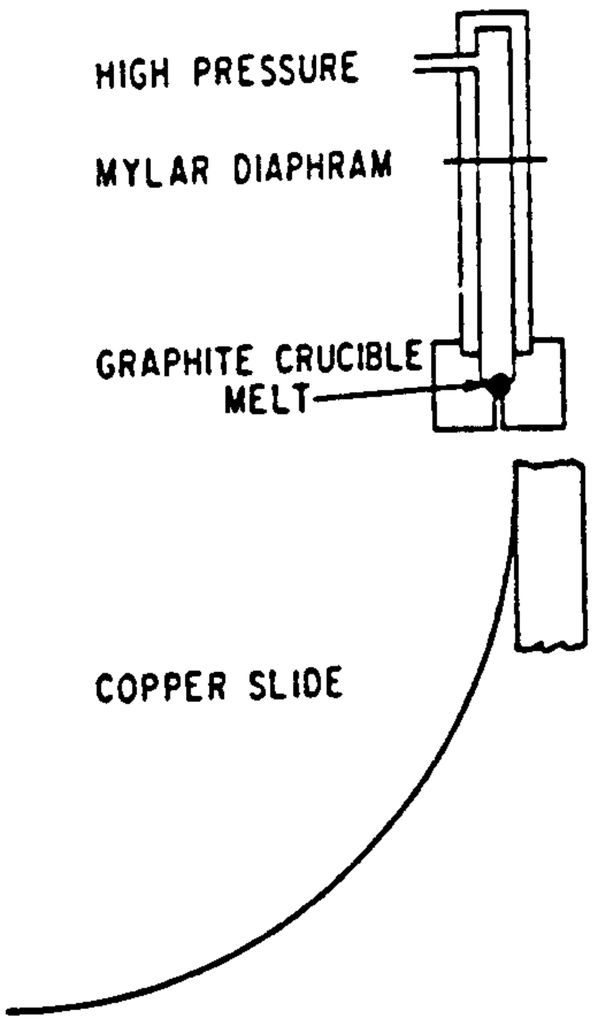

Fig. 5.6 Apparatus for splat cooling by the gun technique, due to Duwez and Willens [56].

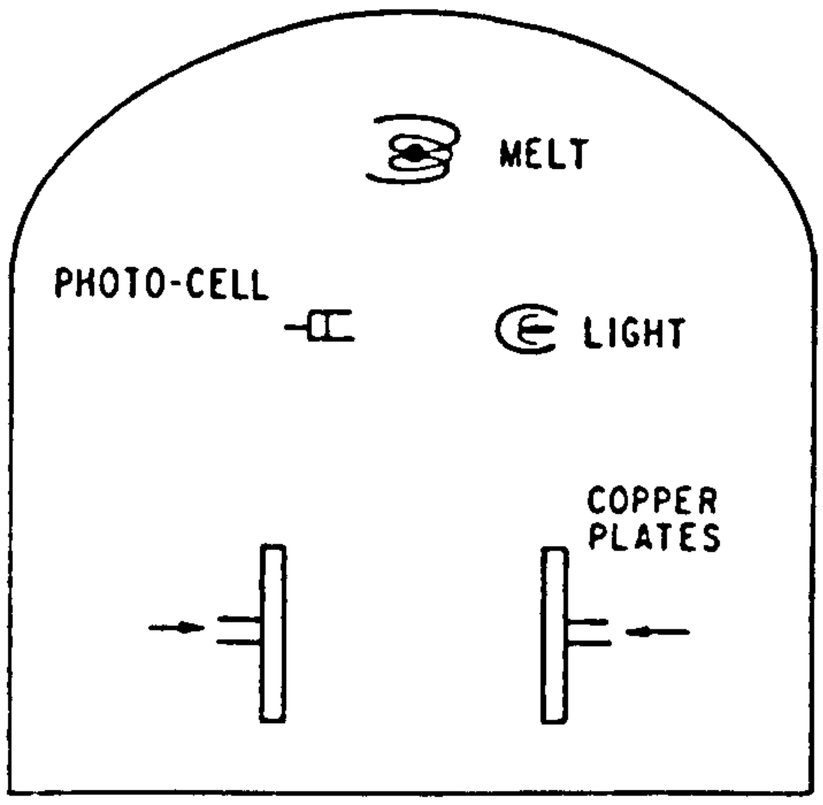

Fig. 5.7 Apparatus used for the two-piston technique, due to Cahn et al [58].

5.2.4 Centrifuge and Rotary Splat Quencher Technique

This technique was developed by Kumar and Sinha [59] who built a simple apparatus to solidify a melt rapidly into foils, by melting the material in a graphite crucible with a 0.6mm diameter hole near the top, and then centrifuging the melt in the crucible. The centrifugal force thus developed ejects the metal onto a copper drum surrounding the crucible. Since the foils or flakes formed are quite thick, the cooling rates are expected to be at least two or three orders of magnitude less than those obtained by the "gun" technique. In the rotary splat quencher described by Cahn et al.[58], a levitated melted drop falls onto a pair of rapidly rotating vanes in vacuo. The vanes atomize the drop and project it against a surrounding copper cylinder.

5.2.5 Torsion Catapult Technique

This is a technique based on a spring-loaded catapult device developed by Roberge and Herman [60]. In this technique the alloy is melted in a crucible placed at the end of a torsion bar and then catapulted against a cold copper substrate. During its motion, the torsion bar is abruptly stopped when it strikes a shock absorber while the melt continues to travel at a high speed until it strikes the cold conducting substrate. With this device, bulk foil specimens were obtained solidified at quenching rates comparable with those of the piston-and-anvil technique. The greatest

advantage of this method is that foils, without any porosity, with an average thickness of 40 to 60μm and suitable for physical and mechanical tests can be obtained. In contrast to the piston-and-anvil technique, foils obtained by the catapult technique are free from the effects of plastic deformation. In spite of the continuity of the foils, the thickness along their entire length tends to be irregular. In all of the techniques described so far, the size and amount of the product is limited. Since very fast cooling rates have to be realized, the thickness of the foils will of necessity, have to be small. However, there are no restrictions as regards to the length or the width of the sample. Methods of obtaining rapidly quenched foils in large quantities are described in the following sections.

5.2.6 Plasma-Jet Spray Technique

This technique was developed by Moss et al.[61], with quenching rates of the order of 10^7 °C/s. The material was produced continuously at the rate of a few grams per minute. Both reactive and refractory metals can be quenched since there is no container problem. In this method, fine powder of the alloy is injected into a high-temperature plasma and the molten droplets impinge at a high velocity onto a cooled copper substrate. Although the products of this technique have been used for the measurement of mechanical properties, the fact that they are only 89% dense suggest that the mechanical properties may not be truly representative of the

behaviour of the material.

5.2.7 Filamentary Casting Technique

Pond and Maddin [62] developed the filamentary casting technique, this technique of casting produces flat filaments with a thickness of 5 to 50μm. As shown in Fig. 5.8, in this technique the molten alloy is forced through a sapphire orifice from a graphite mould and allowed to strike the interior of a spinning drum. A pneumatic cage raises the mould slowly so that the impinging melt does not hit the previously solidified ribbon. Chen and Miller [63] developed a variation of this technique. As shown in Fig.5.9, in this technique the molten alloy was ejected into a pair of rapidly rotating steel rollers, held together under pressure. The alloy solidifies while passing through the rollers. The cooling rate is estimated to be 10^5 °C/s. A similar technique, with rolls covered with a hard chrome surface rotating at a high speed has been investigated by Babic et al [64]. A variation of this technique is now in commercial use [65]. In this technique the melt is ejected onto the outside of a drum as shown in Fig. 5.10. A small ingot of the correct composition is melted in a quartz tube by resistive or high frequency heating. On the application of argon gas under pressure to the tube, the melt is ejected through an orifice in the end of the tube onto a rotating copper drum where it is instantly quenched. The solidified melt is formed into a ribbon by the rotation of the drum and the finished ribbon

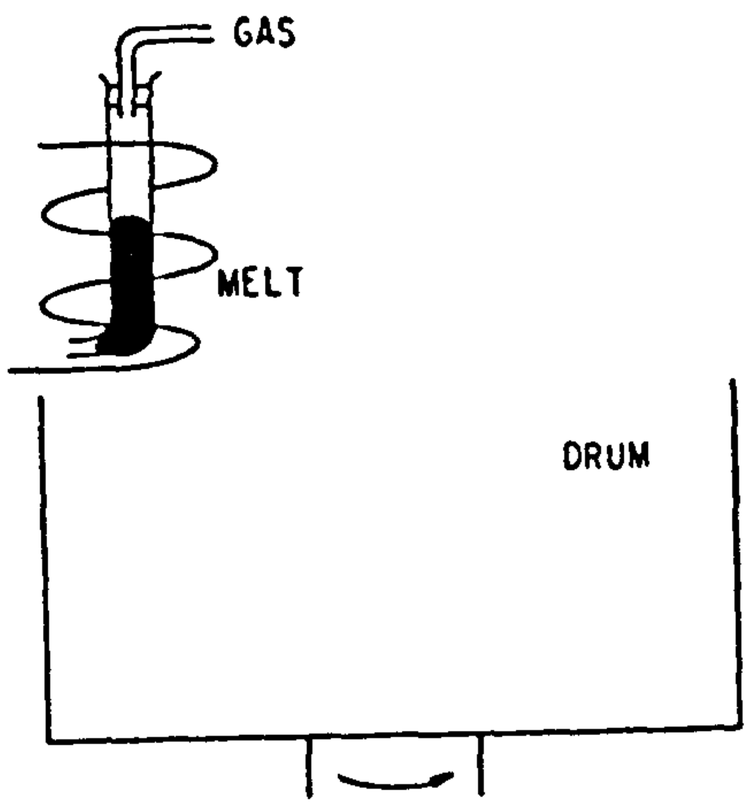

Fig. 5.8 Apparatus used for continuous casting of ribbon, due to Pond and Maddin [62].

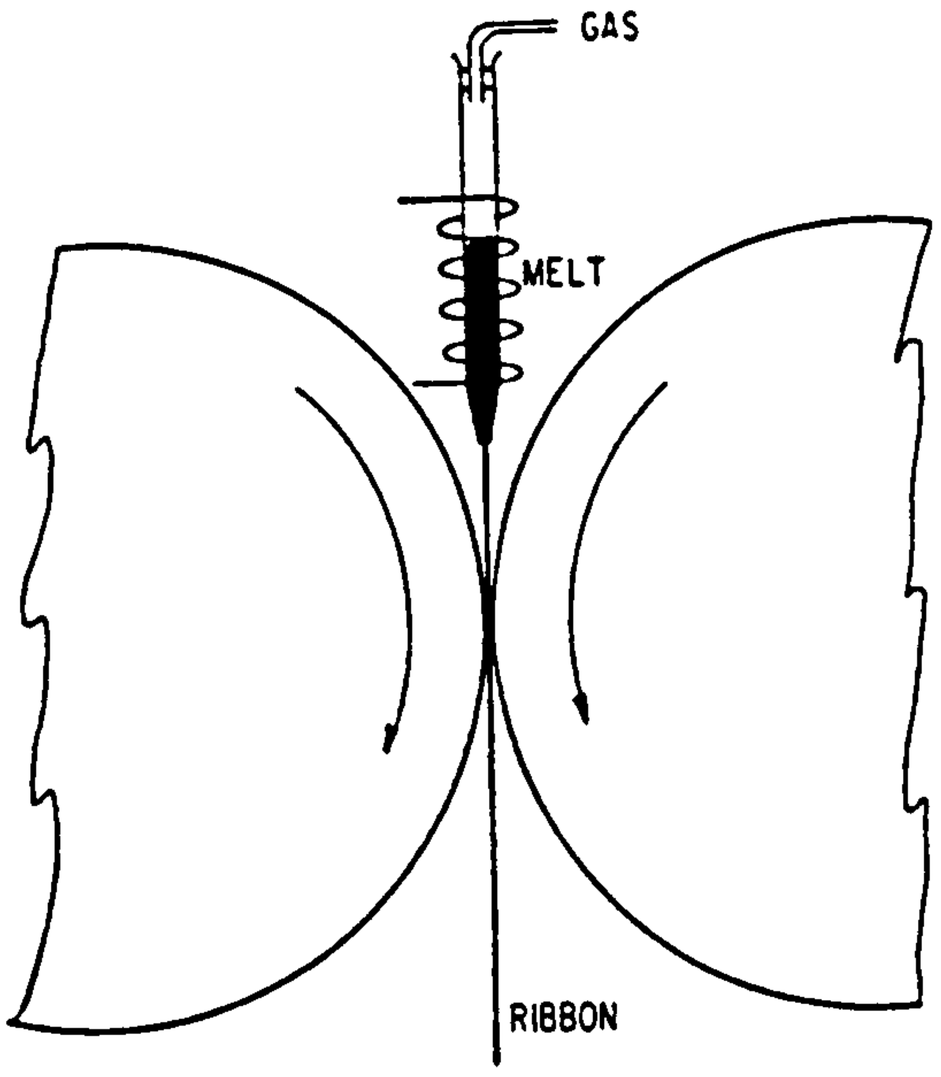

Fig. 5.9 Double roller casting of ribbons, due to Babic [64].

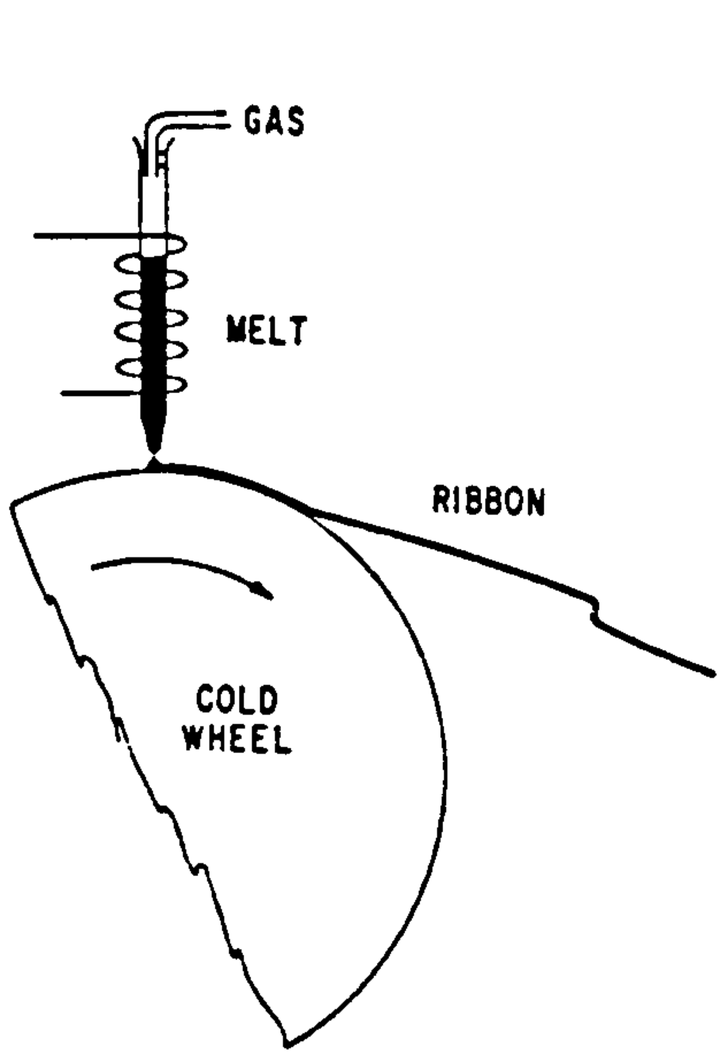

Fig. 5.10 Single roll casting of ribbon, due to Liebermann [65].

may be collected after it has left the drum. The crucial factors of the operation are the melt temperature, gas pressure, length and diameter of the orifice and the speed of the surface of the drum. The angle at which the ejected melt impinges on the drum [65] is also important. This kind of device has been used, with a varying degree of success, in many laboratories to produce alloys of many different, but basically similar, compositions. Liebermann and Graham [65] have demonstrated that the gas pressure must be in the range 28-70kPa with an orifice diameter of from 340 to 480μm and the surface drum speed in the range 20 to 40 m/s. Ribbons were initially made 1 to 2mm wide and 25 to 50μm thick with lengths varying from a few metres up to kilometres. A typical production speed was approximately 2 km/min of ribbon.

The drum-quenched technique produces in air a ribbon that is cooled from one side only. Hence the surface which is in contact with the drum is macroscopically flat but contains elongated dimples caused by trapped air bubbles. The upper surface is macroscopically smooth and shiny but curved, therefore the two surfaces are not parallel. Consequently if the ribbons are stacked to form a toroid or core, it is difficult to achieve a packing factor as high as 90%. The profile and quality of the ribbon can be improved by operating the quenching apparatus under vacuum conditions [66]. This study also showed that it is possible to make ribbons of 7mm width using a single-orifice system under vacuum conditions.

A wider ribbon may be made by using a single rectangular orifice or two rows of simple jets with the second row arranged so that its jets fill up the gaps left by the first row. Using this methods 5cm wide ribbons are at present commercially available, however for use in power transformers materials of at least 15cm wide will be required. It has been reported that ribbon approximately 17-20cm wide has successfully been produced [67]. This production technique is the most suitable and efficient method in terms of large scale manufacture and from an economic of point view. The announcement by Allied Signal Inc. that Metglas products will build a 60,000 ton per year production plant using drum quenching system shows the importance of this method [68]. Although there seems to be a possibility that the quality of many parameters of the ribbon will be improved with more research and development, it cannot be foreseen that the thickness of the ribbon can be increased. This limitation is due to the high cooling rate required, typically 10^5 or 10^6 °C/s, from the melting point to the glass transition temperature that is necessary to achieve a truly amorphous condition, i.e. an assembly of dense random-packed spheres, rather than a micro-crystalline structure.

5.2.8 Melt Extraction Technique

There are two melt extraction systems capable of producing amorphous ribbons in a continuous method. Maringer and Mobley [69] developed a crucible melt extraction

technique and the pendant drop melt extraction technique was developed by Maringer et al [70]. Fig.5.11 shows a diagram of the crucible melt technique. The edge of the rapidly rotating disk contacts the clean surface of a molten metal alloy. As the periphery passes through the liquid metal, some metal solidifies, adheres to the disk and is brought out of the liquid. As a result of thermal contraction and centrifugal force, the metal, now in the form of a ribbon, is thrown free after residing on the disk for a period of time. By varying the disk geometry, contact depth, speed, temperature of the melt and other parameters, a variety of ribbon geometries may be made. By introducing notches on the wheel, short ribbons can be produced directly. Care must be exercised to keep the surface free of slag and other impurities by operating under an inert gas or in vacuum. The pendant drop melt extraction method is shown in Fig.5.12 and is a very similar technique. The molten drop is supported by its own surface tension on the end of a rod of the same material. The great advantage of this technique is the elimination of orifices and crucible and their attendant problems. This technique, because of its simplicity, is readily run in a vacuum system using an electron beam for heating.

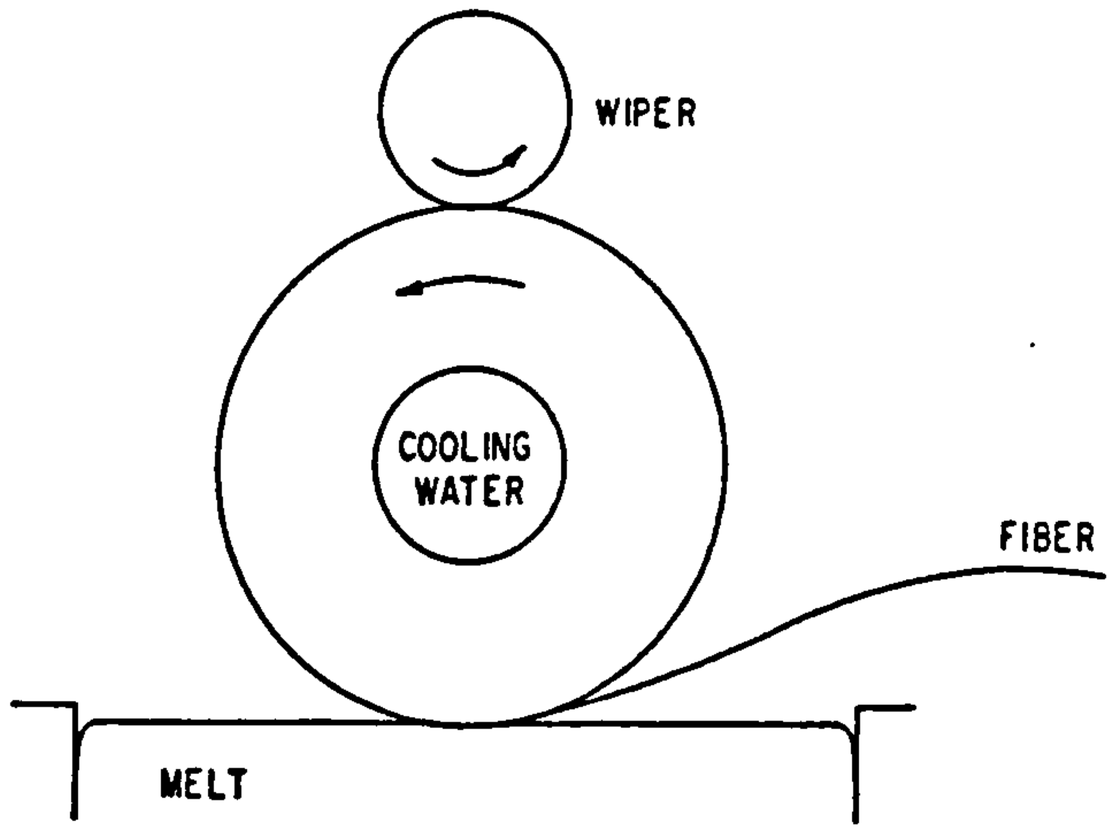

Fig. 5.11 Crucible melt extraction, due to Maringer and Mobley [69].

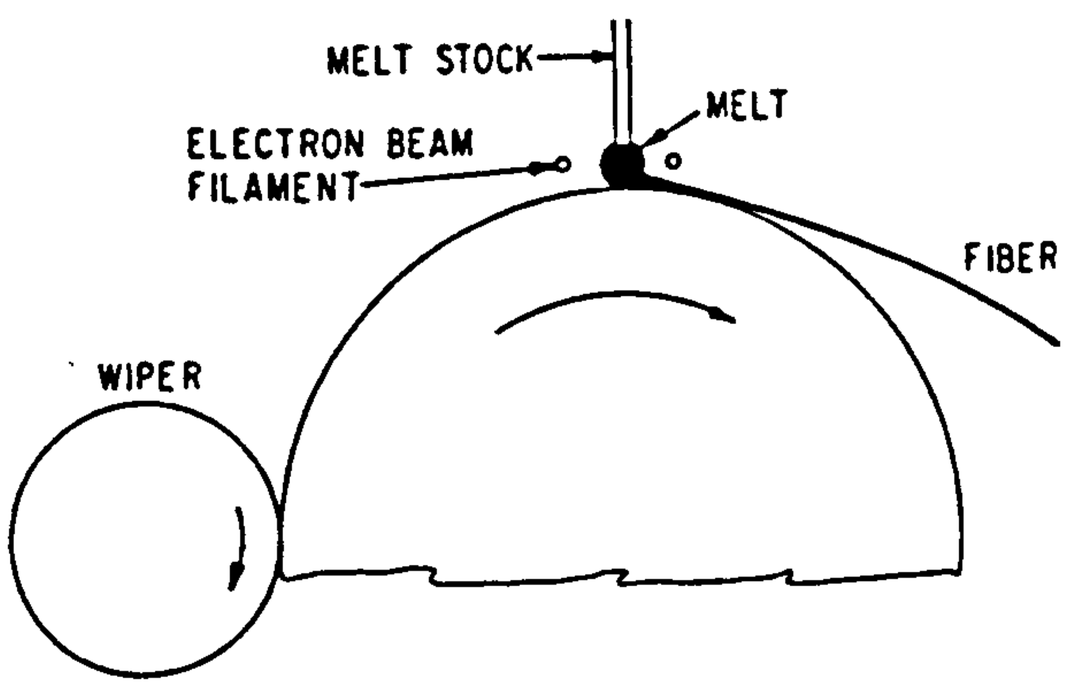

Fig. 5.12 Pendant drop melt extraction, due to Maringer et al [70].

CHAPTER 6

Application of Amorphous Material

6.1 Introduction

It was considered appropriate to investigate the various applications which have already employed amorphous metal. Such experience could then be utilized and put to use in the design and construction of the transformer core which is the subject of the current research. The applications may be divided into two categories, power devices and electronic devices.

6.1.1 Power Devices

For many years the driving force for the use of amorphous alloys was the saving of energy in power system distribution transformers [72,73,74]. A decade of progress in the development has highlighted the complexity involved in the commercial introduction of amorphous alloys [71]. The arguments in favour of the use of amorphous alloys are low losses and therefore low operating costs, the major disadvantages are lower saturation flux density and very small ribbon thickness when compared with silicon iron [75]. Luborsky has reported [73] that 0.5% of the total electric power generated is lost as iron losses in distribution transformers. Hence, if the core loss could be reduced by a

factor of say 3 by replacing silicon-iron by amorphous alloys, approximately $300 million could be saved annually in the U.S.A. and about £20 million a year in the U.K.[73,76]. The costs of building transformers using Metglas 2605 ribbon material have been compared with those for transformers made from 3.2% silicon-iron. Fig.6.1 shows the results obtained according to the Luborsky report [73]. It assumes that the material cost for Metglas 2605 will be 1.5 times that for the silicon-iron. It can be seen that the use of amorphous ribbon materials would increase the overall cost of the transformer by 127% of its present level [73], but the energy saving during operation would recover this extra cost many times during the life of the transformer.The measured performance of small amorphous cored transformers has been reported by several workers [77,78]. Recently Allied Corporation constructed a large metallic glass transformer weighing 102 kilograms [79]. This utility-scale three phase toroidal transformer was tested at output powers up to 30kW. These tests showed that the transformer is more efficient than a comparable commercial dry-type unit of the same rating. At its rated power, the total power loss was less than 60% of that of the commercial unit as shown in Fig. 6.2. It is significant that the 87.5% and 21% reductions in core and copper losses respectively were achieved with only a 15% increase in total weight, despite the 20% reduction in saturation induction that resulted from the replacement of silicon iron by ferromagnetic amorphous material. It should

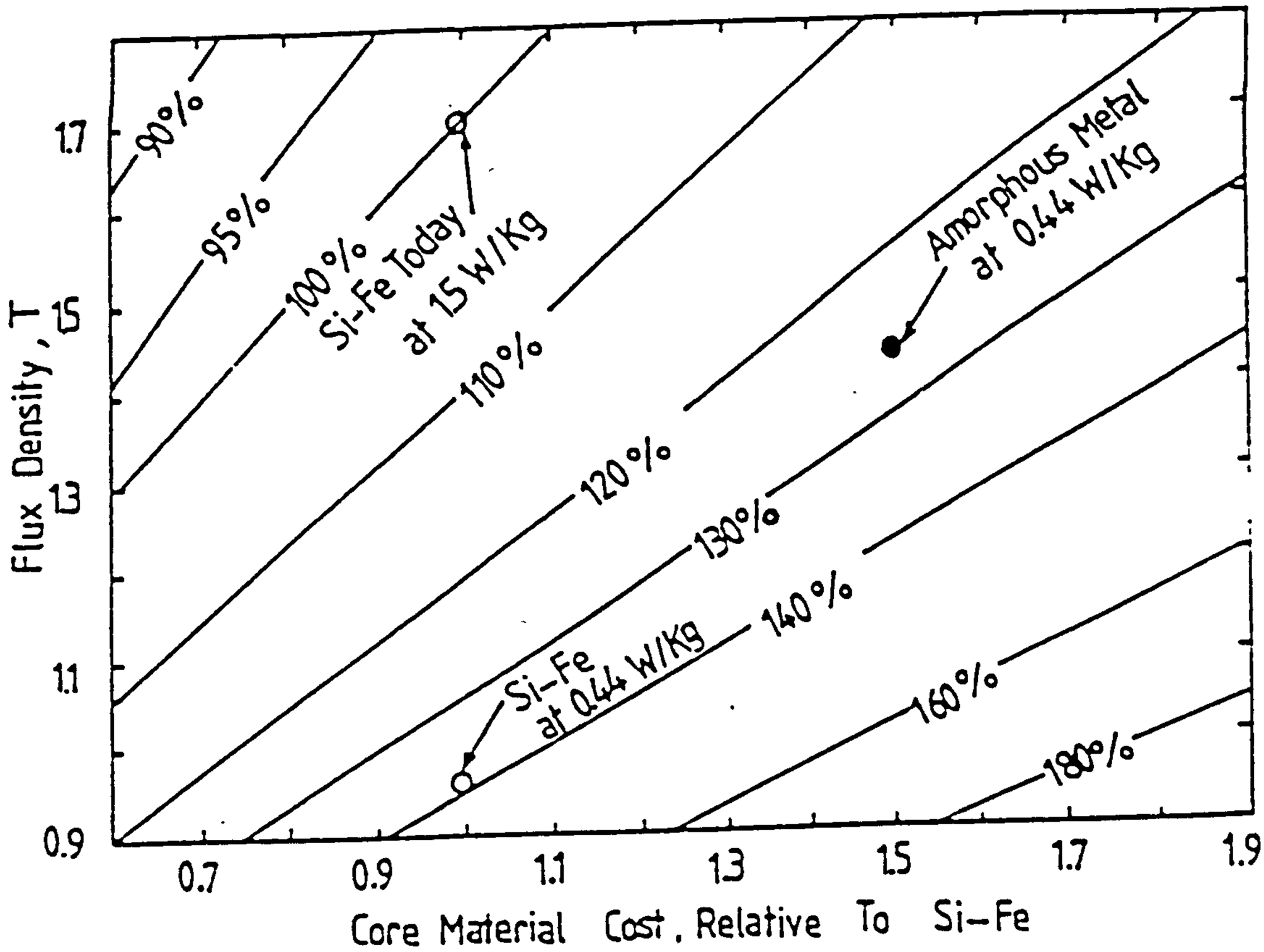

Fig. **6.1** Comparison of costs of transformer made from amorphous FeB and conventional Fe 3.2% silicon, due to Luborsky [**73**].

	Commercial (dry-type)	Metallic Glass
Core Loss, W	112	14
Exciting Current, A	25	0.12
Copper Energy Loss at 15 KVA, W	210	166
Operating Temperature, °C	100	70

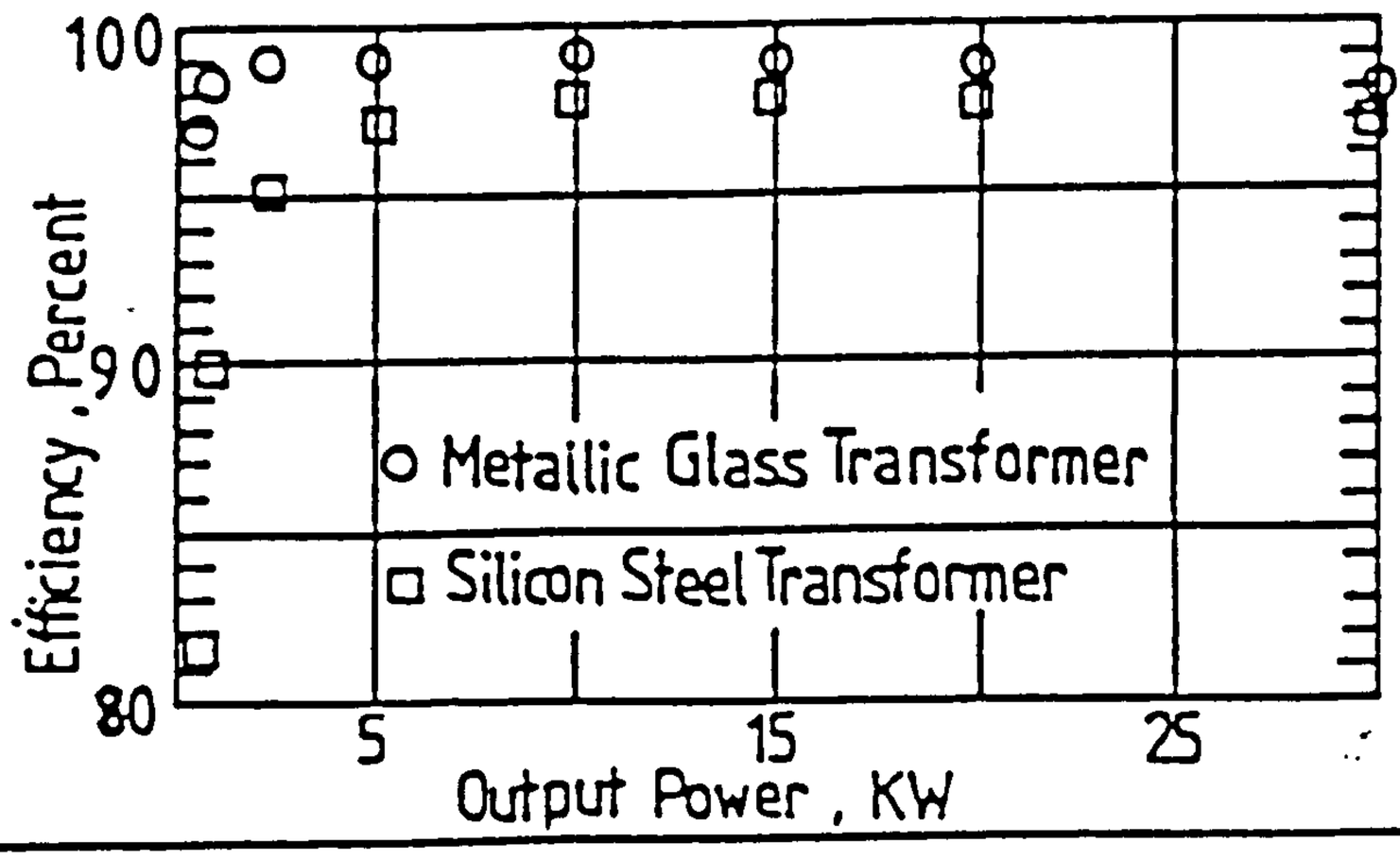

Fig. 6.2 Comparison of metallic glass and conventional 15 kVA transformers [79].

be noted that in recent times, because of the premium on power loss, transformers designers are decreasing the operating flux level of the core material in order to decrease the losses in conventional silicon-iron transformers [80]. Consequently, the difference between the operating flux of amorphous alloy cores and silicon-iron is decreasing. The very thin thickness (ribbon thickness 2605-S2, 25 μm) of the amorphous material which is a characteristic is not likely to change drastically, being about one-tenth of conventional electrical sheet steel. This has two independent disadvantages [75] firstly, the number of sheets required for a given device is increased by a factor of at least ten with an obvious increase in handling and assembly cost. This deficiency is less serious if a wound-core construction is used and may be alleviated if stacks of ten or more amorphous sheets can be handled like conventional laminations. Secondly, as lamination thickness decreases, the stacking factor decreases. This effect is particularly severe if the laminations are not of uniform thickness and a stacking factor of 0.9 has only been obtained with difficulty under laboratory conditions. It is possible however that the high electrical resistivity and small sheet thickness of the amorphous alloys may remove the need to provide an electrical insulation coating between layers, such insulation if used would further reduce the stacking factor.

6.1.2 Amorphous Materials in Machines

Amorphous alloys offer a soft magnetic material with lower losses than conventional silicon-iron to be used in low frequency devices such as transformer and machine cores. Progress has been made in this area not only in Europe and USA [81-86], but also in Eastern Europe [87-90], China and India [91]. The use of amorphous ribbons in the stator of an a.c. motor or in the rotor of a d.c. type would permit a significant reduction in magnetic losses. In contrast with transformers, where the magnetic field is in the same direction and only the polarity of the field vector changes, in a.c. stators or d.c. rotors the orientation of the magnetic field varies continuously. In a d.c. rotor, for instance, the flux paths undergo a 360° re-orientation for each field pair during each revolution. The use of amorphous ribbon materials would permit the required flux re-orientation to occur more readily than in conventional steels. A laminated stator core, of a 1/3 horse power motor, using amorphous alloy was recently made by General Electric [92]. Power measurements taken show that the core losses are less than one fifth those of similar silicon-iron stator. The use of amorphous alloys in motors will require the solution of some difficult manufacturing problems, such as the difficulty of fabricating electrical machines from laminations of a very thin and very hard material. Designers in General Electric [93] are working on the concept of helical casting of ribbon for motor stators which eliminates

the necessity for punching laminations and resolves these difficulties.

Finally, there are good reasons to believe that the use of amorphous alloys in power devices could be commercially advantageous, although it is clear that much engineering ingenuity and manufacturing investment will be required to exploit fully the advantages of amorphous alloys.

6.1.3 Wound Type Core Distribution Transformers

Amorphous metals became commercially available in the 1970's and as economic evaluation of the core losses grew in importance, several manufacturers began to investigate the feasibility of building amorphous core transformers. In the USA, General Electric Company had its first 75kVA amorphous transformer installed in April 1982. The initial amorphous transformer core designed by GEC in the USA is shown Fig.6.3. The primary and secondary coils were continuously wound using a gear driven split arbour assembled around the centre core leg. It has now been in service for over six years and continues to operate with the same low core loss and exciting current levels when first built. A summary of the test results at rated excitation measured at periodic intervals during the past six years is shown in Table 6.1, [94].

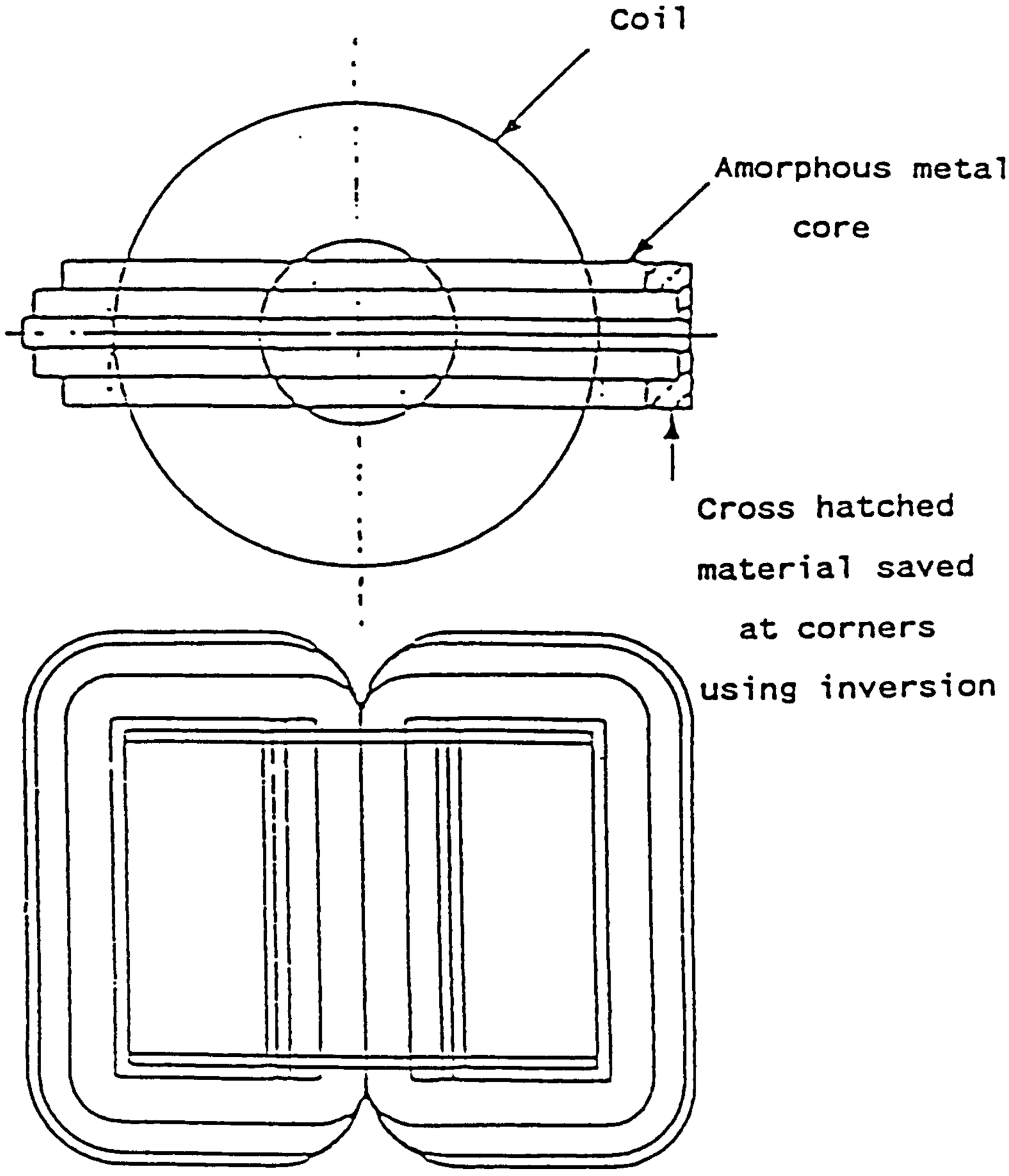

Fig. 6.3 The initial amorphous cored transformer designed by GEC in the USA, formed with two cruciform type wound cores the coils are continuously wound onto the centre leg.

TEST-DATE	CORE-LOSS,(W)	EXCITING-CURRENT,(A)
31/3/82	34.9	0.80
29/6/82	34.7	0.84
26/4/83	34.8	0.73
29/9/83	34.8	0.79
12/4/84	35.2	0.73
28/8/84	34.1	0.79
40/4/86	35.4	0.75
20/5/86	35.1	0.80
90/6/87	34.7	0.81

Table **6.1** Summary during five years in service of a 75 kVA amorphous transformer [**94**].

In 1983, the Electrical Power Research Institute (EPRI) in USA initiated a programme to accelerate the development of amorphous cores through the building of a pilot manufacturing facility and extensive field testing of the transformers. Costs were shared in this development programme between General Electric and the Empire State Electric Energy Research Corporation. A thousand pole-mounted single-phase wound core distribution transformers with 25kVA rating were made in 1985 [95] and shipped to 90 EPRI member utilities for a two year field trial. The transformers have been monitored and to date the core losses have remained stable. There has been no failures attributable to the amorphous metal core. Only five of the 1000 demonstration units have been returned for reasons such as lightening strikes, falling from a utility pole and being subjected to three times rated load [92]. The typical performance of these 1000 transformers is compared with silicon-iron transformers in Table 6.2. [94].

The transformer cores were built using amorphous material developed and produced by Allied Signal Inc. Metglas products with sponsorship from the EPRI. The thin amorphous ribbon material lends itself most readily to the production of wound loop single phase cores, onto which the turns are wound by purpose built machinery. In 1986 the success of the initial research programme led General Electric Company to announce the commercial availability of 25kVA and 50kVA single-phase distribution transformers. The company is

	Amorphous	Silicon-Iron
Core loss (W)	15.4	57
Load Loss (W)	328	314
Exciting current (%)	0.14	0.36
Impedance (%)	2.45	2.45
Audible Noise (db)	33	40
Temperature Rise ($^{\circ}$C)	48	57
Weight (kg)	200	184.5

Table **6.2** Comparison of characteristic of a 25 kVA amorphous transformer to an equivalent silicon-iron transformer [**94**].

now offering single-phase transformers from 75kVA to 500kVA in any standard combination of primary and secondary voltage. General Electric has now sold 1000 units of various sizes, other manufacturers making amorphous core transformers include Westinghouse Electric, McGraw-Edison, and Kuhlman.

Now that the first transformers have been commercialized, the task remains to make them competitive in a large segment of the market. From a manufacturing standpoint, this will require introducing a higher degree of automation to the assembly process. Part of the problem is the larger amount of material handling involved in making the new transformers. Most efforts made in this area have been carried out in the USA, by Allied Corporation (recently renamed Allied Signal Inc. Metglas Products). Some three-phase amorphous core units have been produced in the USA, although the main demand is for small single phase distribution transformers in the USA (and Japan). The majority of the units produced to date use toroidal or wound cores. The wound core can be formed by winding continuous strips through pre-formed coils using special machinery thereby eliminating joints and making a continuous path for flux.

6.1.4 First Prototype Amorphous Transformer Core Development in the UK

A development project has been undertaken by General Electric Company in the UK. The object of the project was to

build transformers which could be used on the UK supply system to gain service experience. Two transformers were assembled, one to assess the manufacturing difficulties and the second for field trials. At the beginning of the project amorphous metal was available only as 25μm thick ribbon and this limited the choice of design options. The design was for a single-phase oil cooled, pole-mounted, distribution transformer of 16kVA rating, having a voltage ratio of 11000/250V the core was of the wound type with windings on both legs.

Two cores were manufactured by the Allied Corporation using Metglas 2605S-2 and delivered to GEC in the annealed condition. The cores were wound in six step cruciform construction, the limbs were fitted with cast epoxy sleeves to enhance mechanical strength. Both transformers were manufactured by winding the turns through the core using a removable and rotatable former fitted around the core limbs. Each leg winding consisted of an L.V. coil and H.V. coil, the H.V. being wound directly onto the L.V.with suitable insulation. Loss measurements were taken on both cores and Fig.6.4 shows the loss as a function of flux density in the cores. Core No.1 was bound with a polyester adhesive material, whereas the core No.2 was bound with cotton tape and coated with an elastomeric resin. Due to the different stresses applied, different losses were measured. The difference between these two measurements are shown in the curves (b) and (c) of figure 6.4. In the same figure curves

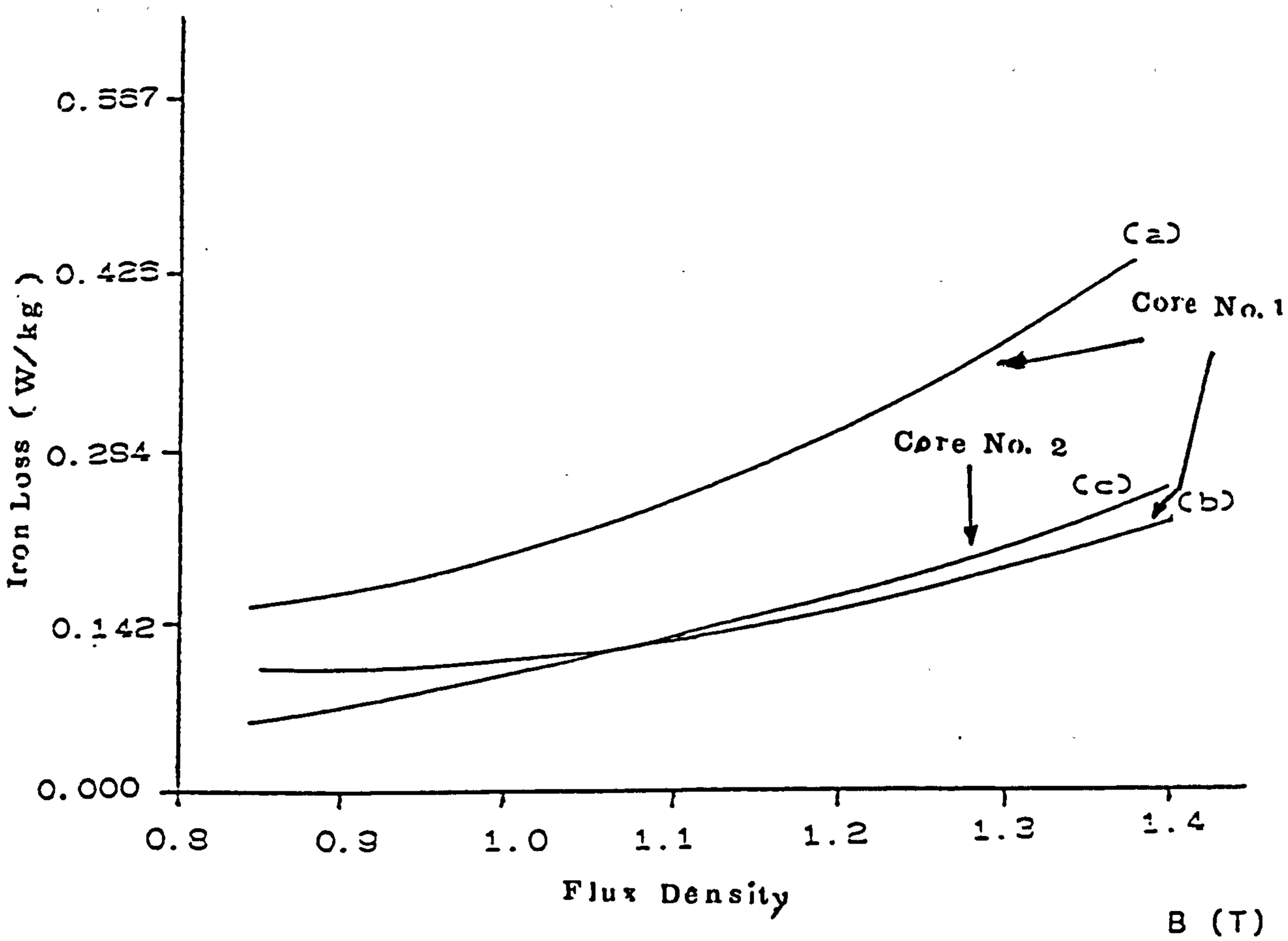

Fig. 6.4 Power loss against flux density for the single-phase core assembled from Metglas 2605-S2 by GEC in the UK; (a) and (b) core No.1 and (c) core No.2.

(b) and (a) show the difference between the measured loss before and after assembly of core no.1, respectively. The cores were mechanically unstable and the brittle nature of the material resulted in particles of metal becoming detached. It was essential to prevent metallic particles entering the winding or insulating oil. One of the transformers was put into service in October 1984 and is subject to periodic inspection and loss measurement [96,97].

6.1.5 Commercial Production

The favourable results of the assessment in the EPRI project, plus the progress of suitable manufacturing processes, led General Electric in early 1986 to continue manufacturing and selling amorphous transformers commercially. A 50kVA amorphous core transformer was introduced for general sale in mid 1986, followed later by a 75kVA and 100kVA rating and more recently 3-phase, 150, 300 and 500kVA. Table 6.3 shows the commercial availability of amorphous distributions transformers from GE company as of August 1988. With 10,000 units produced to date and the volume doubling every year, GE has clearly established a leadership. It is expected that continued development will provide a full range of 1-phase and 3-phase transformer for distribution purposes. The companies, EPRI, Allied and GE are optimistic about the future of amorphous and are making major investments. Allied has plans to invest in a 60,000 ton metal

Type	kVA	Amorphous					Silicon-iron				
		Core loss (W)	Wind. loss (W)	Exc. curr. (%)	Imp. (%)	Wt. (lb)	Core loss (W)	Wind. loss (W)	Exc. curr. (%)	Imp. (%)	Wt. (lb)
Single phase	10	12	102	.31	1.6	318	29	111	.6	1.8	300
	15	16	141	.27	1.9	422	41	143	.7	1.9	321
	25	18	330	.15	2.5	441	57	314	.36	2.5	406
	50	29	455	.13	2.7	719	87	462	.23	3.2	709
	75	37	715	.09	3.3	994	122	715	.38	3.0	821
	100	49	944	.09	3.0	1131	162	933	.21	2.6	961
Three phase	75	45	925	.14	4.0	2030	142	956	.31	4.1	2000
	150	80	1397	.10	3.9	2870	216	1429	.24	3.5	2900
	300	165	1847	.10	3.9	4360	412	2428	.14	5.1	3600
	500	230	3282	.09	4.8	6090	610	3589	.18	4.6	4900

Table **6.3** Performance comparison of General Electric amorphous metal units with grain-oriented silicon-iron units [**98**].

casting facility [98]. In addition, EPRI, ESEERCO and GE have entered into the third phase of the amorphous project to mechanize the core making process and GE is making significant investment in manufacturing processes and facilities to scale up production [76].

6.2 Electronic Devices

There is a rapidly growing interest in the application of metallic glasses in special transformers and inductor coils for use in electronic circuits [99-101]. Appropriate choice of composition and subsequent heat treatment of ribbon enable the properties of these device to be tailored to meet widely differing requirements. In most of electronic devices, the amount of magnetic material used in each device is small. Thus the cost of the material is normally an insignificant fraction of the total cost of the device. In these types of applications, the performance characteristics dominate and therefore expensive alloying additions are permissible.

6.2.1 Magnetic Shielding

Mendelsoh et al [102] have investigated the use of amorphous alloys for shielding. The combination of high permeability and high yield strength allows amorphous alloys to be used in flexible magnetic shields [102,103]. Large sheets were made by a simple weaving process and then coated with a polymer. The properties of the cylindrical shields

made from these woven fabrics were measured at 60Hz and compared to an equal weight shield wrapped from polycrystalline 80% Ni 20% Fe foil neither shield was annealed. The shielding ratios of the woven amorphous material which is a measure of the shields effectiveness is higher when compared with the polycrystalline foils. The woven amorphous material, however, has the advantage of flexibility without changing the shielding performance because it is less sensitive to mechanical strain. The first commercial product utilizing amorphous alloy for magnetic shielding was Metshield offered by Allied Corporation [103].

6.2.2 Cable Shielding

Several choices are available to eliminate the magnetic field pick-up of cables, for example thin walled convoluted tubing or braided sheaths of high permeability alloys. Amorphous alloys with zero magnetostriction are materials uniquely suitable for this application because they can be braided or woven practically without loss of material permeability. The shielding factor as a function of frequency for cables with 8 mm O.D. measured in a constant a.c. field of 1 A/cm is shown in Fig. 6.5. Boll and Warlimont [104] here, compare a cable braid made by continuous helical winding of 3 mm x 0.03 mm strip of crystalline Permalloy and of Co base amorphous material [105,106].

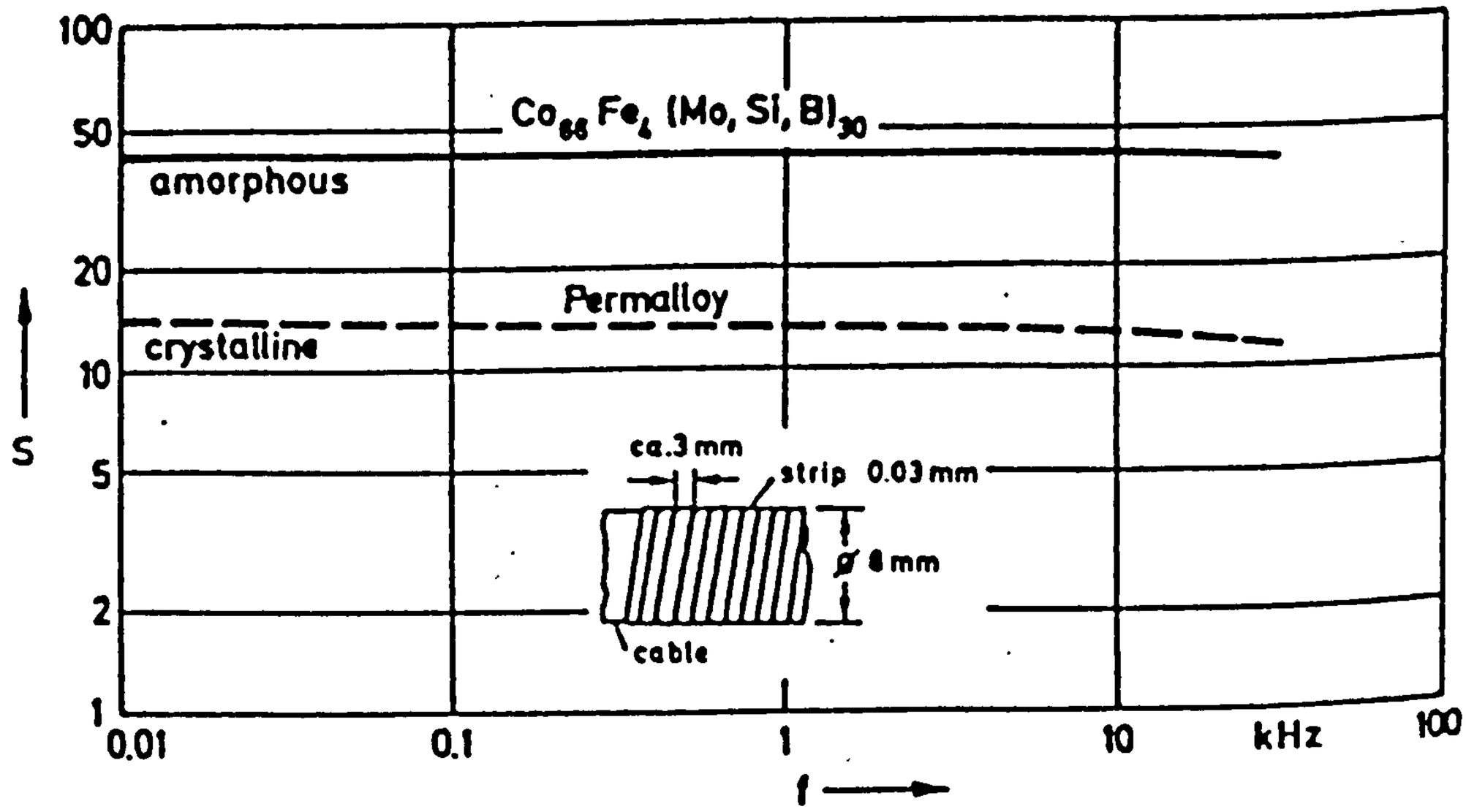

Fig. **6.5** Shielding factor S as a function of frequency f of thin cable braids, due to Boll and Warlimont [**104**].

6.2.3 Delay Lines

The high magnetostriction, the large magnetomechanical coupling factor and the low magnetic anisotropy of Fe-rich and Fe-Ni based metallic glasses make these materials attractive for application in variable delay lines and in tunable surface acoustic wave components. The use of amorphous alloys in acoustical delay was first reported by Azai et al [107]. Delay lines are important components in radar, computer and other signal processing equipment. Their quality is determined by their magnetomechanical and ΔE behaviour, where ΔE is the change in Young's modulus E with applied field H. The ΔE effect is extremely large in a variety of amorphous alloys tested for delay lines. Shirae et al [108] investigated another potential application of amorphous alloys by their use in a transversal filter which are essentially delay lines and make use of magnetostrictive waves in amorphous ribbons. They are frequently used in communications and telephone lines.

6.2.4 Magnetic Heads

Alloys with low magnetostriction and high permeability have been used as cores in recording heads by several researcher [109-112]. The zero magnetostriction high cobalt amorphous alloys are preferred for these applications. Materials for magnetic heads based on the principle of induction require high initial permeability, adequate

saturation, high electrical resistivity, high mechanical hardness and wear resistance. Zero magnetostriction is also desirable. The unique combination of magnetic and mechanical properties of some amorphous alloys makes these materials attractive for magnetic heads. The long reliable operation of tape recorders, recording with low distortion with high coercivity tapes and high-frequency response are the potential advantages of the new material group. The application of Fe-Co-Si-B based amorphous materials for magnetic heads with a saturation flux density of 0.95T [113] and even more up to 1.3T [114] and an initial permeability of 20,000 at 1kHz were reported.

CHAPTER 7

Transformer Core Design, Manufacture and Test

7.1 General Design Considerations

A design exercise was carried out initially to compare for a given transformer rating the transformer core parameters when using silicon-iron and amorphous metal for the core material. Following this exercise a design for an amorphous cored transformer was finalised, the core dimension being tailored essentially to meet a 3-kHz 20-kVA rating, several cores for this size of transformer were built and tested. In addition a silicon-iron uncut core was purchased so that a direct comparison could be made of the electrical and magnetic properties.

7.1.1 Design Comparison Silicon Iron v Amorphous Metal Core

The advantages of an amorphous metal core compared with a silicon-iron core for a medium frequency power transformer are illustrated by the parameters listed in Table 7.1. These were obtained following a design exercise for a 20 kVA, 800/600 V transformer, design No.1 for operation at 1-kHz and design No.2 for 3-kHz. The designs were produced for the flux densities shown, the number of turns on each of the foil type windings being appropriate to the flux density specified. The

Description	Amorphous Metal 2605-S2		Silicon Iron	
	Design No.1	Design No.2	Design No.1	Design No.2
Type	Air cooled	Air cooled	Air cooled	Air cooled
Phase	Single	Single	Single	Single
Frequency (kHz)	1	3	1	3
Rating (kVA)	20	20	20	20
HV Winding (V)	800	800	800	800
LV Winding (V)	600	600	600	600
Flux Density(T)	1.4	1.4	1	0.4
Volt/Turn (V)	7.5	22.2	11	26.7
Total No. turn*	107	36	72	30
Total No. turn+	80	28	54	23
Weight (kg)	6.8	4.34	14	25
Spec.Loss(W/kg)	8	35	23	19
Core Loss (W)	82	228.0	322	475
Thickness (mm)	0.025	0.025	0.05	0.05
Overall Core Dimension (mm)	328x146	186x146	320x178	275x227.5
Window Dimension (mm)	248x66	106x66	193x51	97x49.5
Cross Section Area (mm)	40x40	40x40	50x50	60x60

* High voltage + Low voltage

Table 7.1 Comparison of transformer design using cores of silicon iron and Metglas 2605-S2.

transformer core design also took into account assumed typical impedance values. Building factors of 1.5 and 1.0 and space factors of 0.75 and 0.88 were assumed in the amorphous and silicon-iron designs respectively.

The design for the silicon iron cored transformer has been based on current practice with regard to the core material and the flux densities used at the frequencies specified. A number of different amorphous metal alloys were available of which the iron based alloys appear to be the most suitable for frequencies in the band 1 to 3-kHz. A considerable amount of information was available for the amorphous metal alloys produced by Allied Signal under the trade name of Metglas. For this comparison the characteristics of the Metglas alloy 2605S-2 have been used. The maximum flux density value of 1.4 T was chosen following inspection of the data provided by the manufacturer although 1.4 T at 3-kHz may be optimistic. The higher flux density possible with the amorphous metal produces a significant reduction in core weight compared with silicon iron. Another point to be noted in the comparison was the further reduction in core weight achieved at 3-kHz in the amorphous metal design, a similar reduction was not possible with silicon-iron due to the reduced flux density necessary at 3-kHz. The increase in core loss at 3-kHz may however be unacceptable using 2605-S2 and other amorphous metal alloys, for example 2605S-3A, may be more suitable (see later comparison of table 7.2)

7.1.2 Choice of Amorphous Core Material and Type of Construction

The characteristics of amorphous metal alloys vary according to the composition of the alloy, i.e. iron based, nickel iron based and cobalt alloys are available. The iron based alloys are best suited to frequencies in the range 50-Hz to 200-kHz [115]. In addition to the ribbon form, a strip material called powercore* is available, similar to conventional steel laminations. As the name implies, powercore strip is intended for use in built up cores of power frequency transformers as a substitute for silicon iron laminations. The powercore strip comprises 6 layers of ribbon loosely bonded together, the losses associated with the strip are greater than for the equivalent quantity of material in ribbon form. The larger losses associated with powercore strip when used at frequencies in the range 1-kHz to 3-kHz preclude its use and only the ribbon form of amorphous metal has been considered. The use of ribbon material dictates that the core will be of the wound type. Of the iron based alloys produce by Metglas both 2605S-2 and 2605S-3A appear to be suitable and another design comparison was made for a 20 kVA transformer using these alloys, the results are given in Table 7.2.

* Powercore is a trade name used by Allied Signal Inc.

Description	Amorphous 2605-S2		Amorphous 2605-S3A	
Type	Air cooled	Air cooled	Air cooled	Air cooled
Phase	Single	Single	Single	Single
Frequency (kHz)	1	3	1	3
Rating (kVA)	20	20	20	20
HV (V)	800	800	800	800
LV (V)	600	600	600	600
Flux Density (T)	1.0	1.0	1.0	1.0
Volt/Turn (V)	5.3	16	5.3	16
Total No.turn*	150	50	150	50
Total No.turn+	112	38	112	38
Weight (kg)	8.3	4.8	8.43	4.87
Spec.Loss (W/kg)	5.2	25.0	3.0	10.0
Core Loss (W)	65.0	180.0	38.0	73.0
Thickness (mm)	0.025	0.025	0.0175	0.0175
Overall Core Dimension (mm)	416.6x146	213x146	416.6x146	213x146
Window Dimension $(mm)^2$	336.6x66	133x66	336.6x66	133x66
Cross Section Area $(mm)^2$	40x40	40x40	40x40	40x40

* High voltage + Low voltage

Table 7.2 Comparison of transformer design using Metglas 2605-S2 and 2605-S3A.

The predicted core losses for 2605S-2 may be acceptable at 1.4-T, 1-kHz but not at 1.4-T, 3-kHz (see table 7.1), a reduced flux density of 1-T was therefore used in the comparison for Table 7.2. The lower losses of 2605S-3A appear to be advantageous but the material is approximately 30% more expensive. The deciding criteria will be the temperature rise of the core, the maximum continuous service temperature must not exceed 150°C.

It was decided initially to concentrate the research mainly on the cheaper Metglas 2605-S2. Enough material was purchased to make several cores in the 4-6 kg weight range, sufficient to evaluate the consistency of the results. Only a small quantity of Metglas 2605-S3A was purchased, sufficient for one core of about 5 kg in weight. The assembly of this latter core would only be attempted once experience had been gained with the cheaper 2605-S2 material.

The main reason for choosing 2605-S2, apart from price may be summarized as follows:

a) the losses with this material were likely to be acceptable at 1.4 T at 1-kHz and possibly at 1.0 T at 3kHz.

b) during the early stages of core manufacture, a certain amount of wastage was likely to occur until the winding techniques were perfected.

c) The thinner 2605S-3A ribbon was likely to prove more difficult to wind. The ribbon thicknesses of Metglas 2605-S2 and 2605-S3A were 0.025 mm and 0.0175 mm respectively. The

space factor would be inferior for 2605-S3A due to the larger number of turns required. Wound cores using silicon iron are usually cut (C-cores) to allow the separately assembled windings to be placed on the limbs. The mating surfaces are preferably ground flat to minimise the air gap and its effect on the magnetic circuit. To implement a similar assembly method for amorphous ribbon will be difficult to achieve without special cutting facilities. Even with such facilities the stress introduced during manufacture and the clamping of the finished transformer core were likely to have detrimental effects on the magnetic characteristics. Hence the decision was made to use uncut wound cores with the windings assembled directly onto the limbs. It was foreseen that methods for coil winding directly onto an uncut core could easily be developed.

7.1.3 Transformer Core Dimensions

The dimensions of the amorphous cores to be manufactured were based on the design for a 20-kVA, 800/600 V transformer, operating at a flux density of 1-T and 3-kHz. A core building factor of 1.5 and a core space factor of 0.75 were assumed in the design see Table 7.2 for 2605-S2. The ribbon material was only available in a limited number of widths, 50 mm wide being nearest to the ideal requirement for a square core cross section. The core dimensions were modified from those given in table 7.2 as follows:

Cross section area = 50 x 32 (mm^2)

Window dimensions = 125 x 65 (mm^2)

7.2 Transformer Core Manufacture and Annealing

7.2.1 Core Winding

Transformers using amorphous metal for the core can have the core losses reduced by as much as 60-70% compared with transformers made with the best grain-oriented electrical steel. Achieving this low loss in the transformer will require careful attention to material handling, core winding, annealing and core support. The amorphous metal alloy was susceptible to bending stress which can in turn increases core loss.

The core shape chosen was a simple rectangular core with the windings intended to be wound onto both limbs through the core window. The mandrel on which the ribbon was to be wound to form the core must take into account whether the core will be self supporting or not during the annealing process. A self supporting core would have the mandrel removed before annealing, in this case a collapsible mandrel would be required. However a simpler non collapsible mandrel was chosen which would be left in place during the annealing process. It was considered beneficial to support the core during annealing, despite the likely expansion of the mandrel affecting the inner turns of the ribbon, these turns could be removed after annealing. The mandrel was thus made from mild steel strip to the dimensions of the core window. Two removable side plates were fitted and a centrally located axle on which the mandrel was rotated. Fig. 7.1 shows the main features of the mandrel assembly. The mandrel was

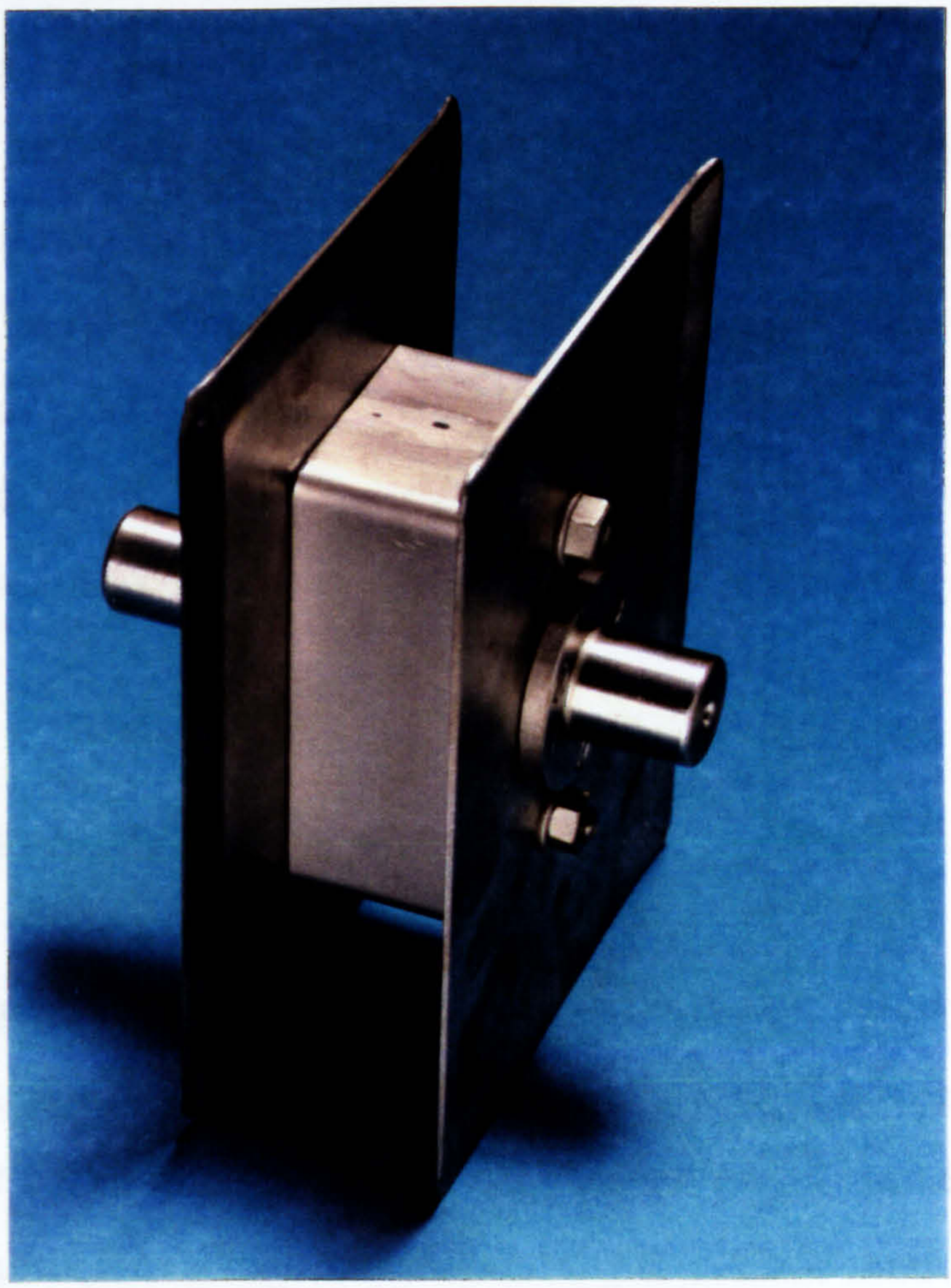

Fig. 7.1 Construction of mandrel around which the ribbon is wound to form the transformer core.

mounted in a lathe and rotated to draw off the ribbon from a pay off spool. The pay off spool had an adjustable friction brake to tension the ribbon during winding onto the mandrel. The winding tension used was approximately 1 kg. The arrangement of the lathe and pay off spool is shown in Fig. 7.2. The system was found to operate satisfactorily after adjustments were made to the mandrel alignment and ribbon tension. After winding the ribbon, the side plates and axle were removed before the annealing process commenced. A total of three cores were wound using 2605-S2 and one using 2605-S3A.

7.2.2 Purpose of Core Annealing

The magnetic properties of amorphous alloys such as METGLAS alloy 2605-S2 and 2605-S3A may be optimised by annealing. The reason for annealing was to minimize the level of stress caused during casting of the ribbon and in the core winding processes. The combination of temperature and time chosen for the annealing cycle was such that it would relieve the stresses as far as possible without causing crystallization of the amorphous alloy. A magnetic field applied during the annealing cycle was used primarily for inducing uniaxial anisotropy (domain alignment) in the ribbon.

H H Liebermann [116] investigations showed that the stresses in amorphous alloys caused by the rapid quench casting process could be removed at an anneal temperature as

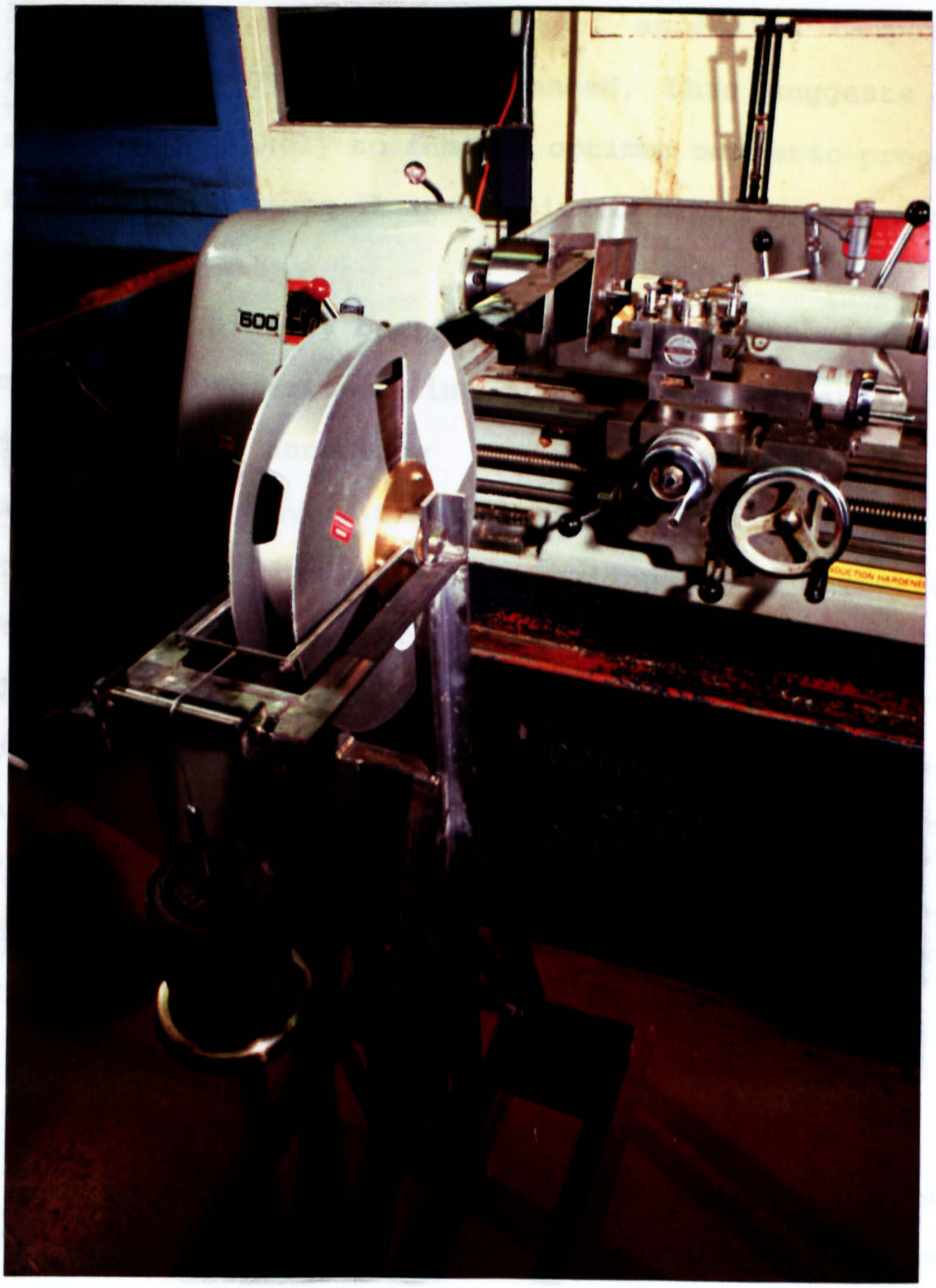

Fig. 7.2 Winding ribbon onto lathe mounted mandrel from pay off spool.

low as 310°C. Since the use of annealing temperature in excess of 310°C were recommended, this suggests that the stress most likely to inhibit optimum magnetic properties in finished cores was that associated with ribbon winding.

As has already been stated, METGLAS alloys possess good magnetic properties in the as-cast state. In some applications annealing may be inappropriate, however annealing improves the magnetic performance and optimal results were obtained by annealing in a magnetic field. Ribbons which have been annealed were found to be less flexible than in the as-cast state and they also tend to retain their annealed shape. The main features of the annealing procedure suggested by Metglas are given in the following section.

7.2.3 General Conditions of Annealing Process

7.2.3.1 Preparation of Cores Prior to Annealing

The cores when formed into their final shapes should avoid excessive stressing of the material. The use of any organic materials which would oxidize during annealing should be avoided. All wire, adhesives or tapes must be capable of withstanding the annealing temperature without distorting or outgassing. The thermal expansion of any supporting structures for example the mandrel must be minimal. The wire used to provide the magnetic field must be insulated with a suitable material.

7.2.3.2 Annealing Atmosphere

An inert atmosphere, free from oxidizing agents, should be used, for example argon, nitrogen or helium. A vacuum would also be acceptable but may cause problems due to a lack of convective heat transfer [117]. In our case nitrogen was used during the annealing process in the laboratory furnace.

7.2.3.3 Temperature Cycle

The core was placed in the inert gas filled furnace and the magnetic field applied. The core was brought up to its soak temperature and maintained at that temperature for the required soak time and then cooled. The inert atmosphere and magnetizing field were maintained throughout the cycle. The temperature cycles recommended for use vary depending upon the desired magnetic properties, most cycles used a soak temperature below 450°C [118,119]. The temperature of the core was of most importance during annealing rather than the temperature of the furnace. For large cores, multiple thermocouples would be necessary to monitor the core temperature during the heat-up, soak and cool-down periods. Two thermocouples were used in our case, inserted inside the core in different positions to measure the temperature.

7.2.3.4 Handling After Annealing

One of the prime objectives of annealing was to relieve mechanical stresses, therefore annealing of the cores can only be done after forming and not before. Even after annealing, stress can be induced in the core by mechanically abusing it and care must be taken to avoid this. The ribbons were more brittle after annealing and rough handling can cause damage. Proper annealing will result in cores with excellent magnetic properties.

7.2.3.5 Application of Magnetic Field During Annealing Process

The magnetic field used during annealing was applied in the direction in which the core would be magnetized during normal use. Once the ampere-turns required to generate the magnetizing field were determined, a suitable number of turns and the d.c. current were selected. Experiments have shown that most benefit from annealing would be obtained with a d.c. field applied of 800 AT/m [120]. The magnetic field used during the annealing process induces uniaxial anisotropy (domain alignment). To fully develop this anneal induced anisotropy, the core material should approach magnetic saturation during the annealing process. It is noteworthy that using a magnetic field greater than the minimum value required to saturate the core material has no beneficial or detrimental effect on the resultant magnetic properties. The

following equation (7.1) may be used to determine the ampere-turn requirement for a given core and field strength,

$$I\,N = H\,D \qquad (At) \qquad (7.1)$$

Where:

I = d.c. current (A).

D = mean path length (m).

N = number of turns.

H = magnetic field (At/m).

The magnetic field was applied by winding the core with a suitable wire size selected to minimize its resistance and any noticeable localized heat dissipation. Bare copper wire was used insulated with ceramic beads to prevent shorting between turns and between the turns and the core.

7.2.4 Annealing Process Under Laboratory Condition

Fig. 7.3 shows the annealing test apparatus set up in the laboratory. The annealing cycle recommended by Allied Corporation and other researchers for amorphous Metglas 2605-S2 was as follows [116,117,121]:

(i) heat up from ambient to the soak temperature with a temperature rise rate of between 1-10°C per minute.

(ii) hold at the soak temperature, specified as between 340-

410°C for 2 hours.

(iii) cool with the temperature decreasing at a rate of 1-10°C per minute.

The magnetic field should be maintained throughout the annealing cycle.

From the information available, the soak temperature to be used for Metglas 2605-S3A was not clear, for example Nathasigh and Liebarmann [116] suggested that for optimum magnetic properties the soak temperature should be just above or below the Curie temperature which for the alloy 2605-S3A was 358°C. The soak temperature recommended by Metglas was however 430°C. It was decided therefore to initially use a soak temperature of 310°C, i.e. below the Curie temperature and then after the performing the electrical tests to repeat the anneal at a soak temperature of 385°C, now above the Curie temperature.

The heat up rate for Metglas 2605-S3A was similar to 2605-S2, the soak time was for three and a half hours and the cooling rate 5°C per minute. Fig. 7.4 to 7.6 show the temperatures recorded during the annealing of three different Metglas 2605-S2 cores. The soak temperatures recorded were in the range 365-371°C and the soak times approximately two hours. The heating up rate was between 1-5°C per minute and the cooling down rate was 1°C per minute. The cooling down rate could be influenced by the rate of flow of nitrogen gas

fed into the furnace. Fig. 7.7 and 7.8 show the annealing cycles for Metglas 2605-S3A for soak temperature of 310°C and 385°C respectively. The core temperatures were recorded using two thermocouples inserted in the core between the ribbon in different positions. The slight differences in the annealing cycle for 2605-S2 produced negligible effect on the core loss and exciting VA per kg measured on the three cores assembled.

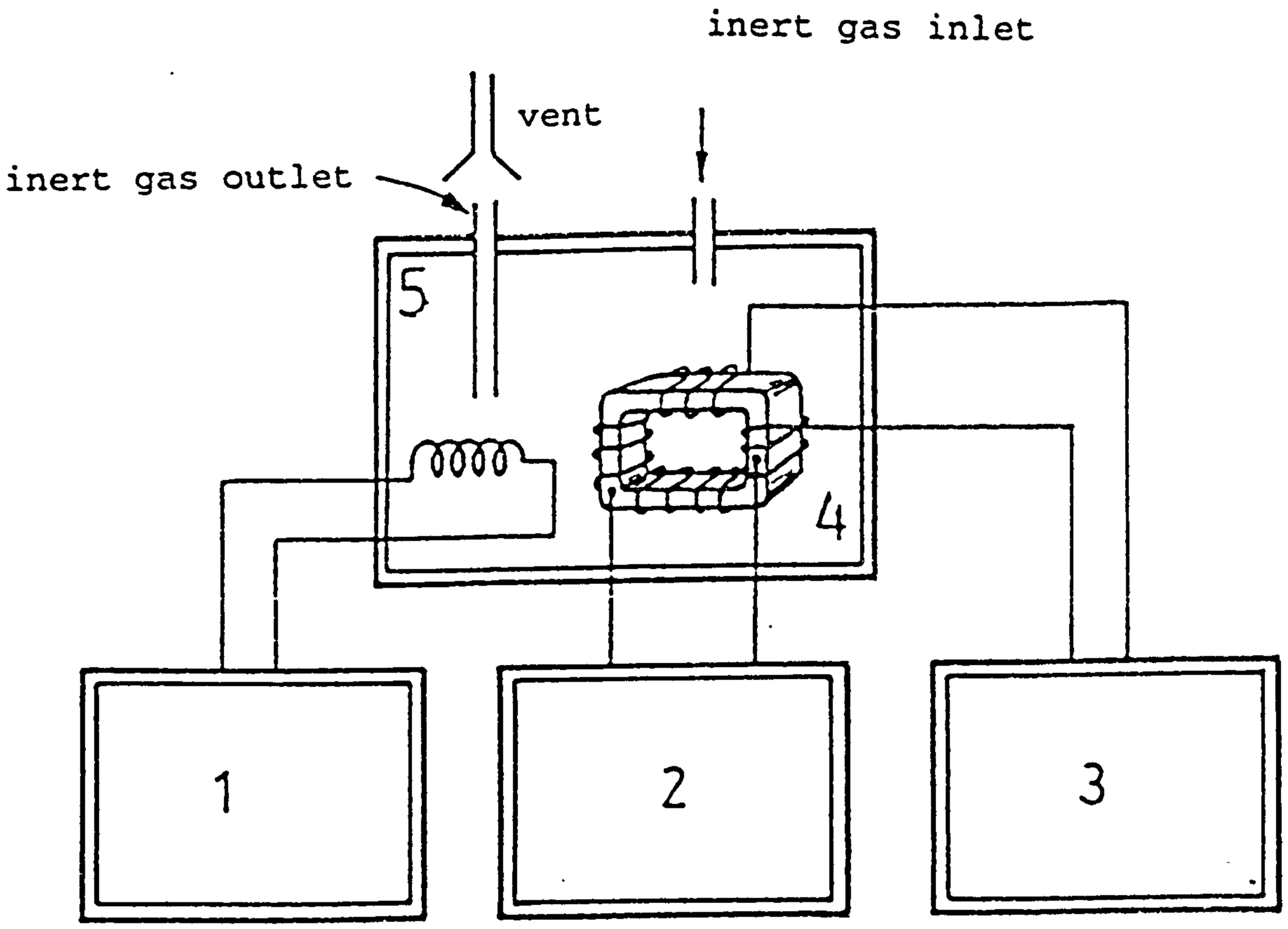

1-Temperature control unit

2-Temperature measurement unit

3-D.C.current source

4-Transformer core

5-Inert gas furnace

Fig. 7.3 Annealing apparatus of amorphous material

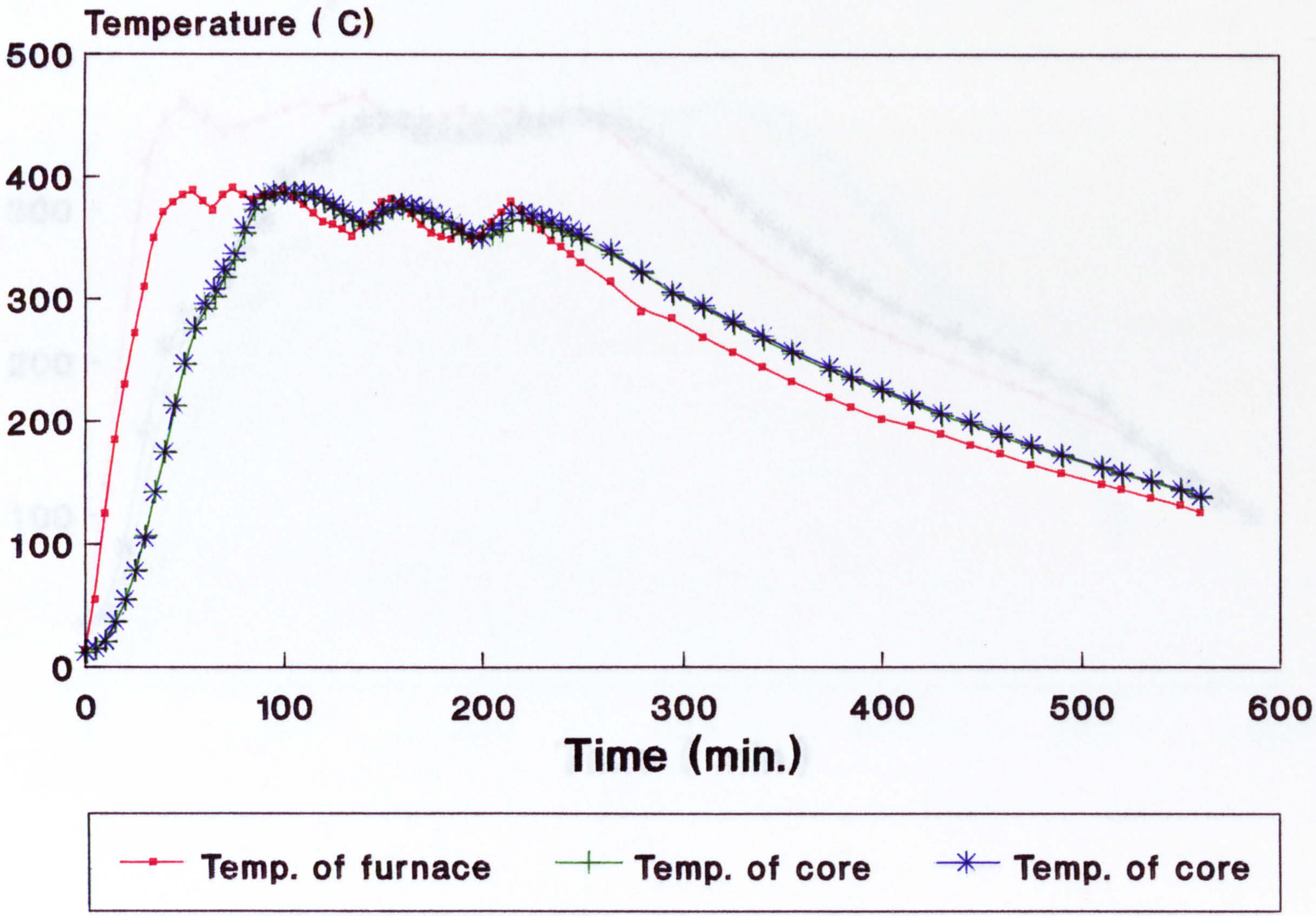

Fig. 7.4 Annealing cycle of amorphous core No.1, 2605-S2.

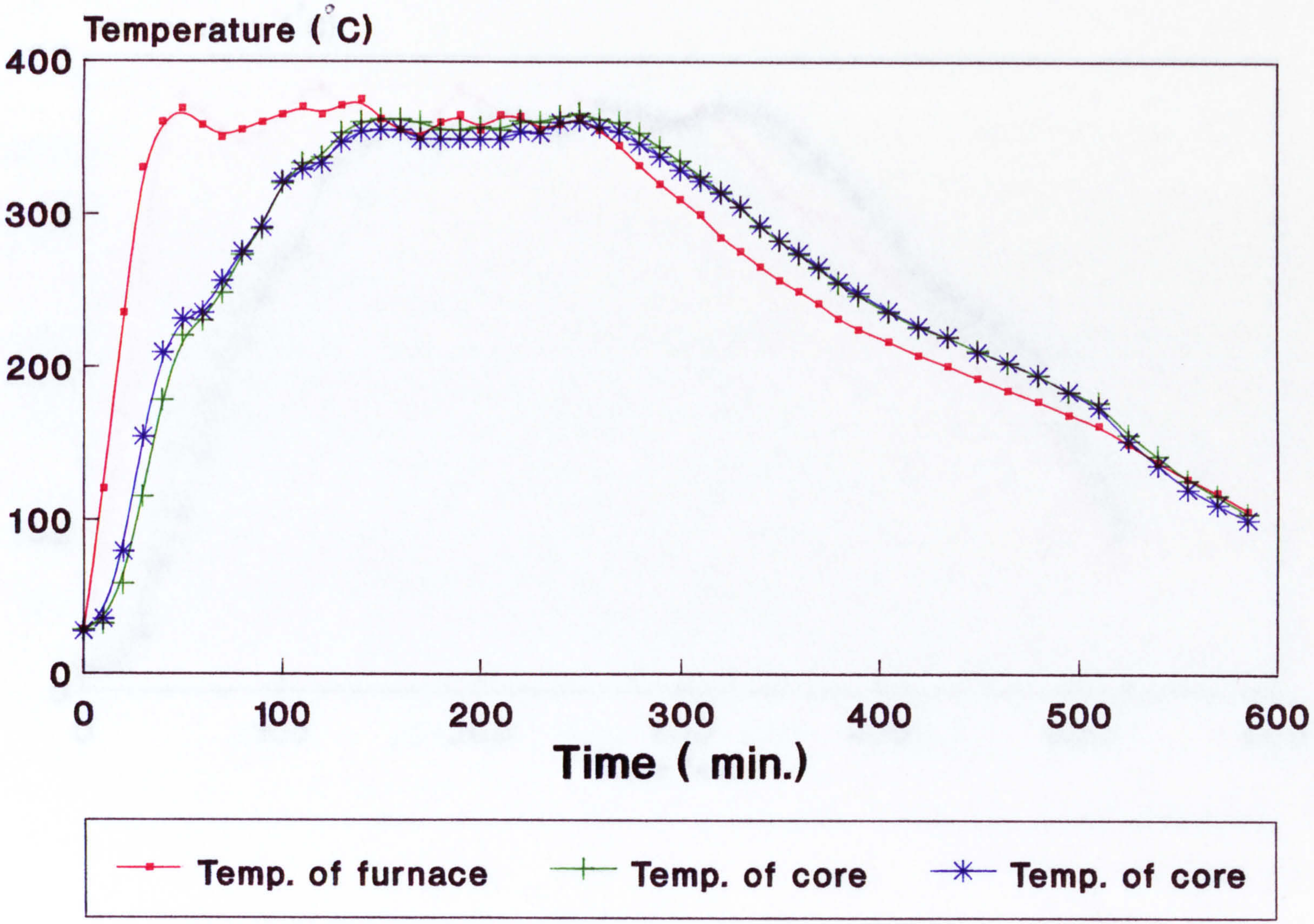

Fig. 7.5 Annealing cycle of Metglas 2605-S2 core no.2.

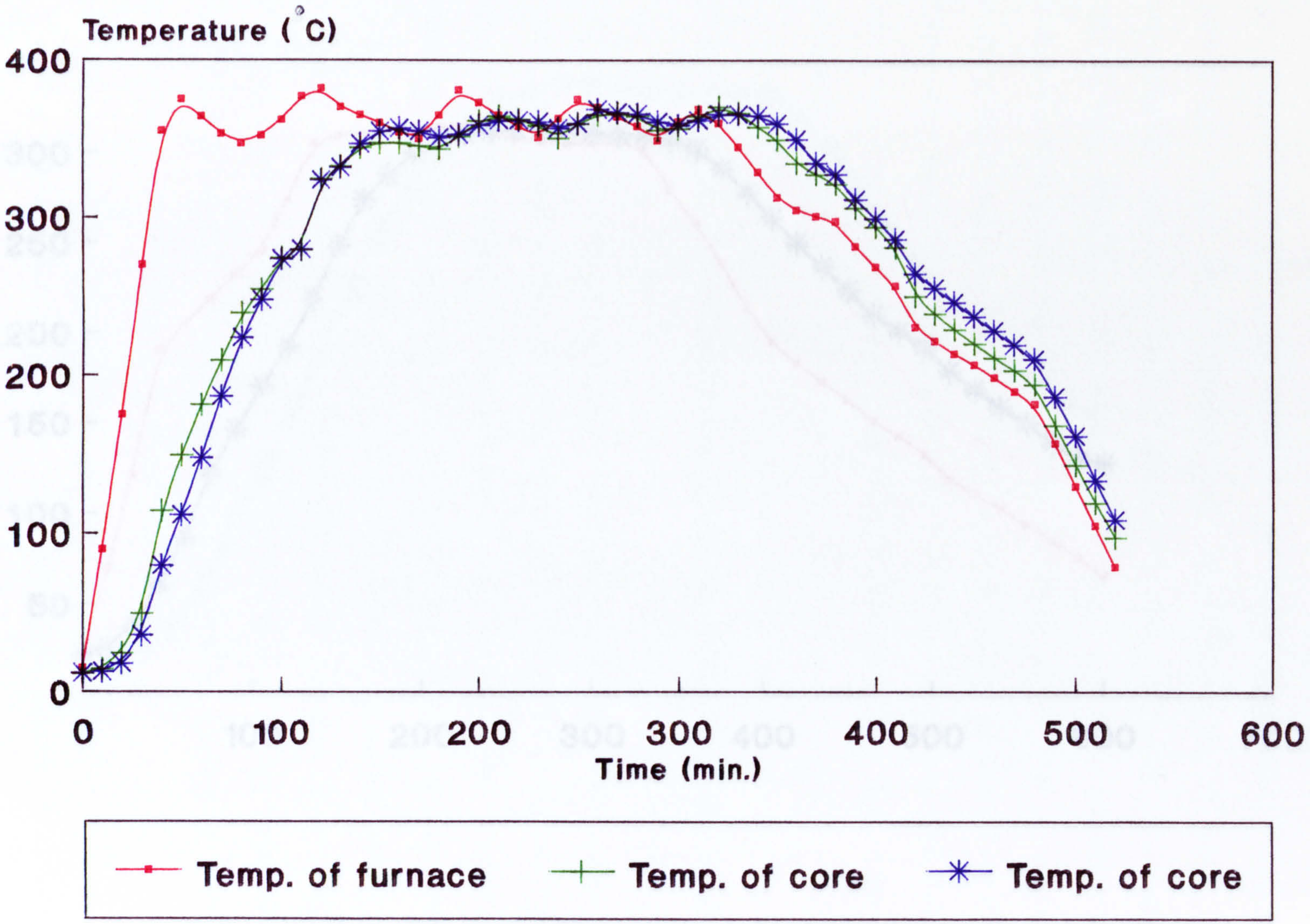

Fig. 7.6 Annealing cycle of Metglas 2605-S2 core no.3.

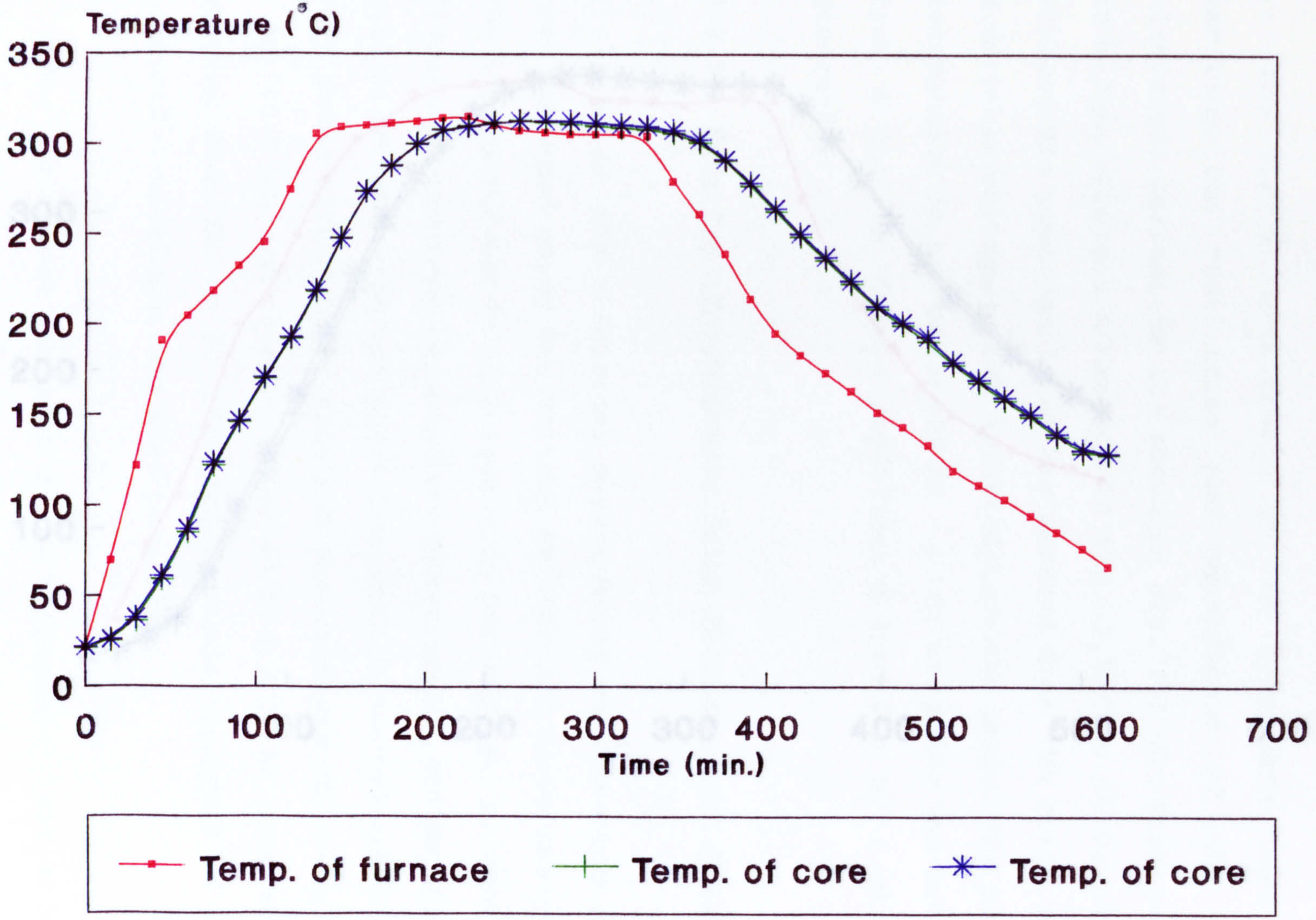

Fig. 7.7 Annealing cycle of Metglas 2605S-3A core no.4.

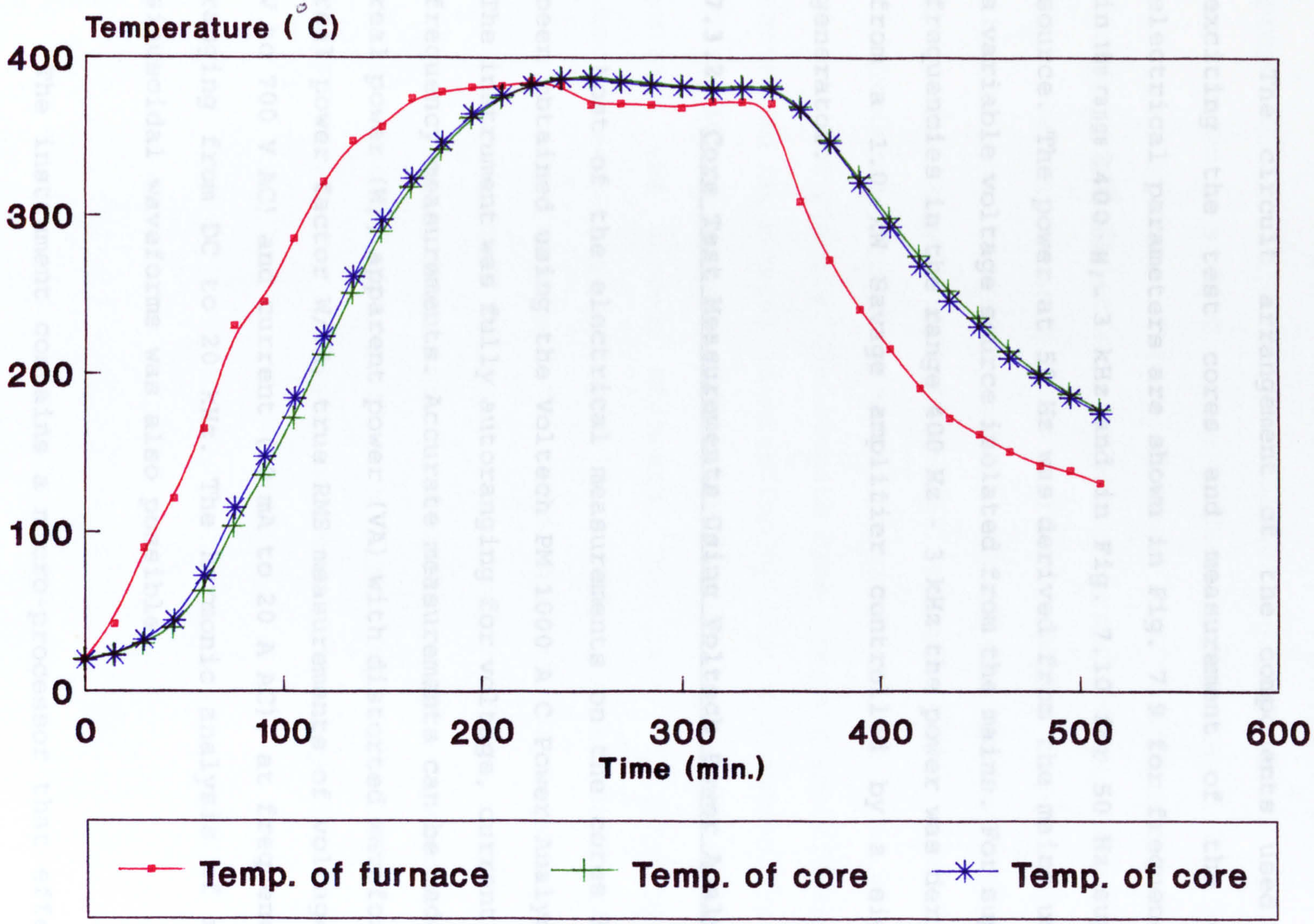

Fig. 7.8 Reannealing cycle of Metglas 2605S-3A core no.4.

7.3 Transformer Core Tests

7.3.1 Test Circuit Apparatus

The circuit arrangement of the components used for exciting the test cores and measurement of the core electrical parameters are shown in Fig. 7.9 for frequencies in the range 400 Hz - 3 kHz and in Fig. 7.10 for 50 Hz supply source. The power at 50 Hz was derived from the mains using a variable voltage source isolated from the mains. For supply frequencies in the range 400 Hz - 3 kHz the power was derived from a 1.0 kW Savage amplifier controlled by a signal generator.

7.3.2 Core Test Measurements Using Voltech Power Analyser

Most of the electrical measurements on the cores have been obtained using the Voltech PM 1000 A C Power Analyser. The instrument was fully autoranging for voltage, current and frequency measurements. Accurate measurements can be made of real power (W), apparent power (VA) with distorted waveforms, real power factor W/VA, true RMS measurements of voltage (2 V to 700 V AC) and current (20 mA to 20 A AC), at frequencies ranging from DC to 20 kHz. The harmonic analysis of non-sinusoidal waveforms was also possible.

The instrument contains a micro-processor that effects measurements by sampling and digitizing the voltage and current waveforms and then computes the required measurement

in its processor. Fig. 7.11 shows in block diagram form the main functional components of the instrument. For the voltage measurement an input attenuator (8MΩ impedance) generates a proportional low level voltage signal. For current measurements a 25mΩ current shunt generates a low level voltage signal. These signals are buffered by the differential amplifiers (1) which permit the inputs to float with respect to each other and with respect to ground. The signals from the differential amplifiers are amplified by programmable-gain amplifiers (2), the gain being selected by the processor according to the magnitude of the input voltage and current signals. The outputs from the gain amplifiers are converted to digital information by fast A-D converters (3) which effect simultaneous scanning of the signals on the voltage and current channels. The rate of scanning is controlled by the processor (4) depending on the frequency of the voltage signals. The digital data captured by the processor is used to compute the value of the measurement selected by the keyboard (5), and the result is presented on the 4 1/2 digit LED display (6). The full specification of the PM 1000 power analyser is given in the appendix I.

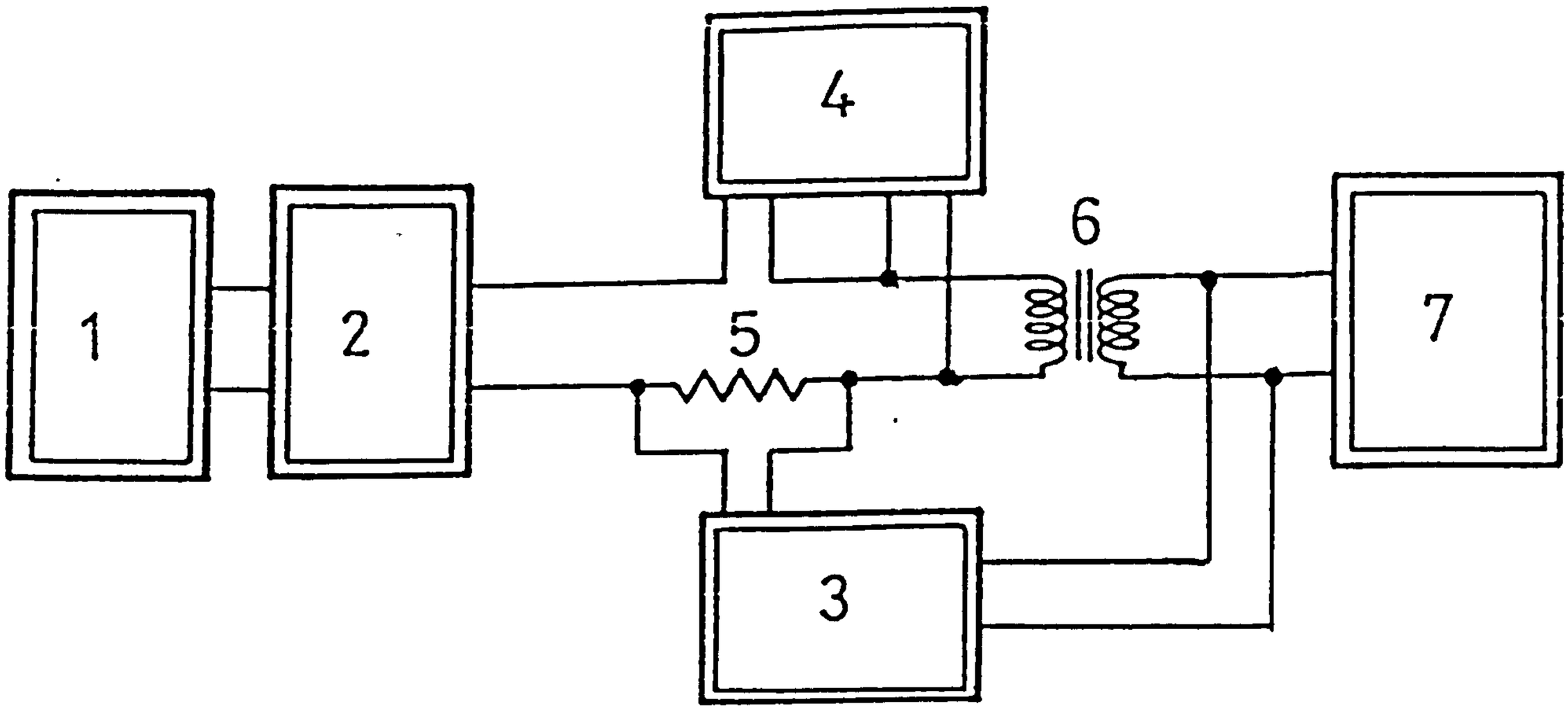

1 - Advance signal generator

2 - Savage amplifier (1.0 kW)

3 - Telequipment oscilloscope DM64

4 - Voltech PM1000 AC power analyser

5 - Current waveform monitoring resistor 2 Ω

6 - Transformer core under test

7 - Avometer model DA116

Fig.7.9 Schematic diagram of the circuit used to measure total loss and exciting power of single phase transformer at 400-3000 Hz.

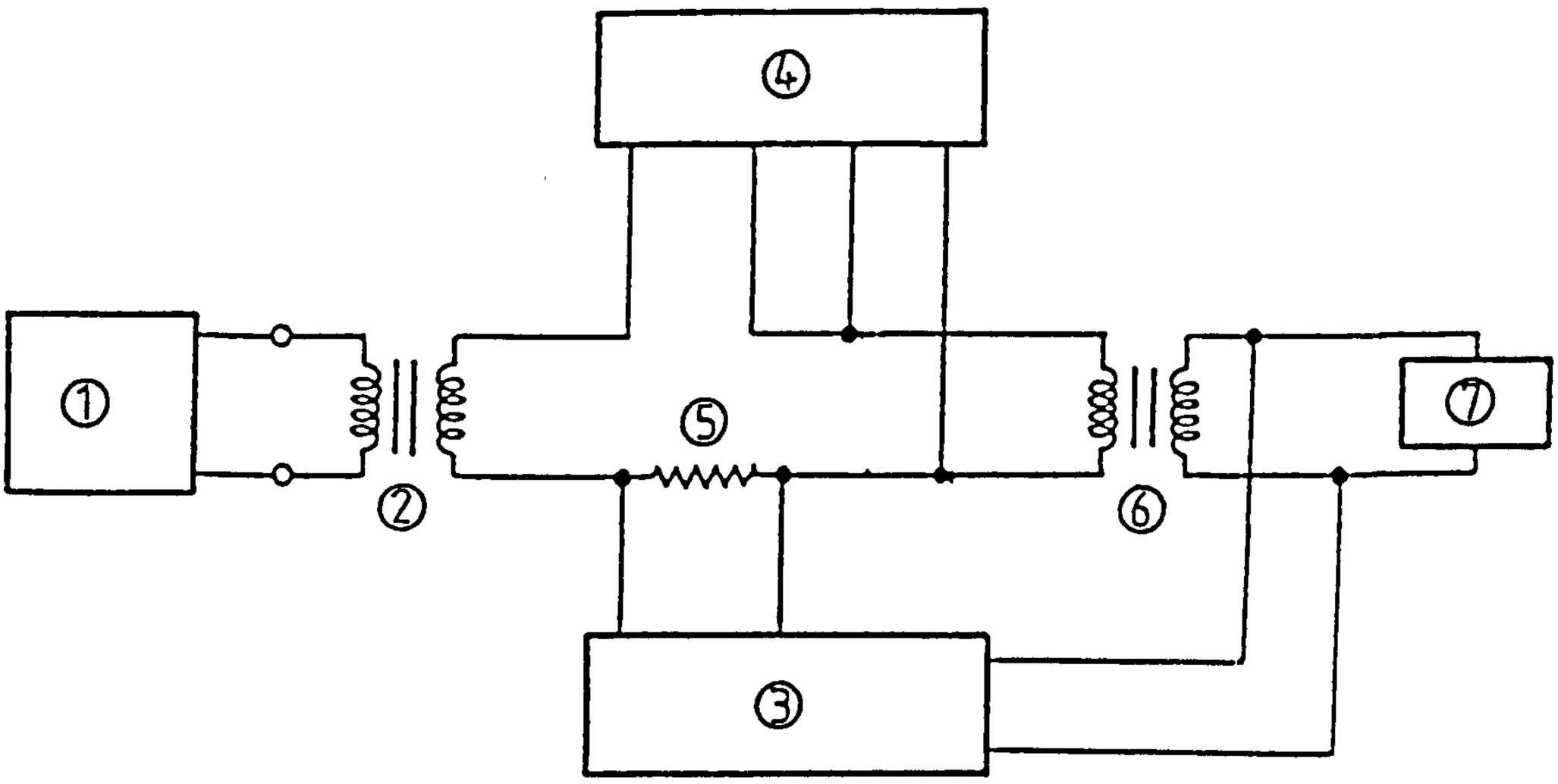

1 - Variac

2 - Isolation transformer

3 - Telequipment oscilloscope DM64

4 - Voltech PM1000 AC power analyser

5 - Current waveform monitoring resistor 2 Ω

6 - Transformer core under test

7 - Avometer model DA116

Fig. 7.10 Schematic diagram of the circuit used to measure total loss and exciting power of a single phase transformer at 50 Hz.

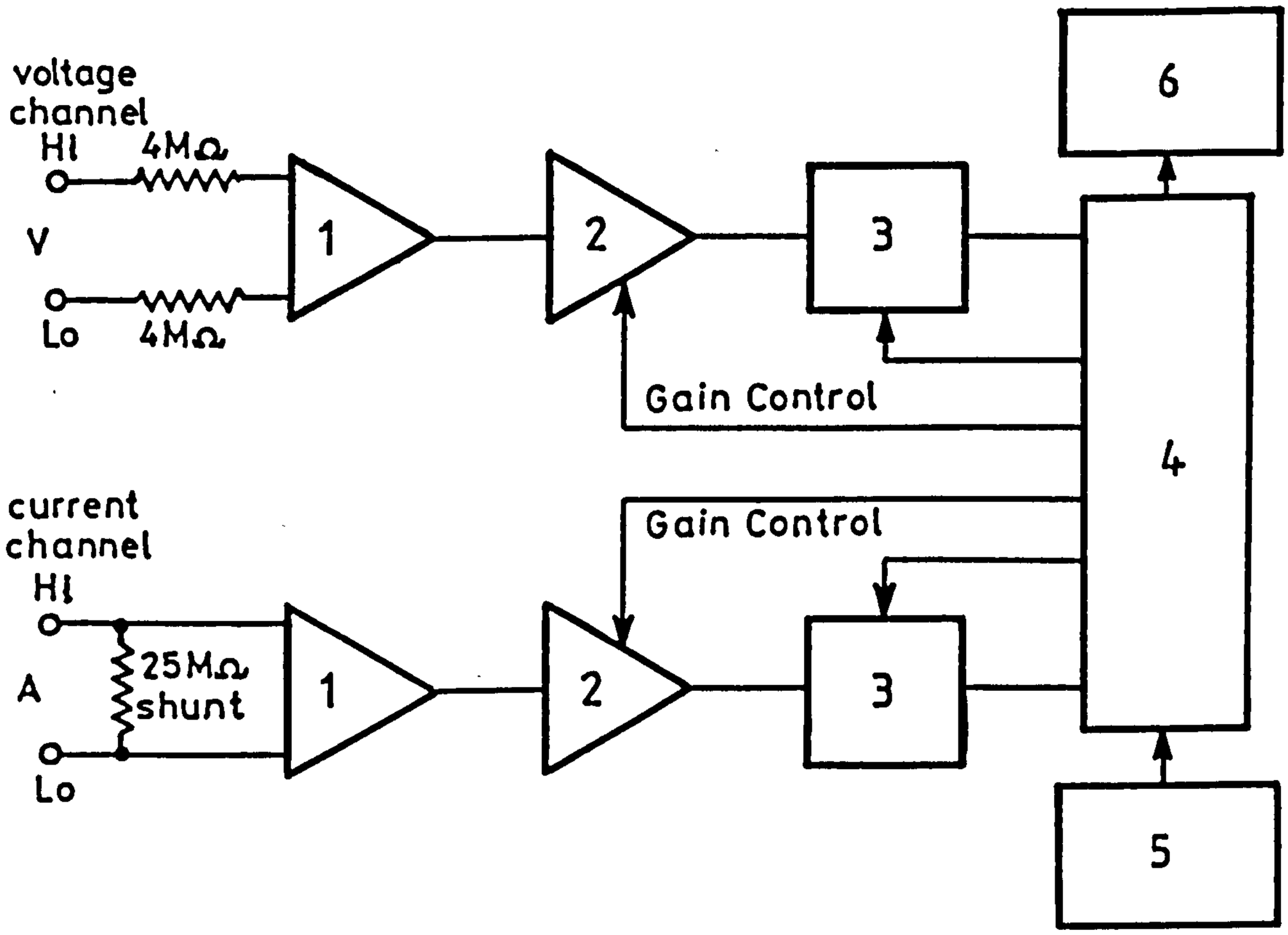

1 - Differential input

2 - Gain amplifier

3 - A-D converter

4 - Processor

5 - Keyboard

6 - L.E.D display

Fig. 7.11 Schematic functional arrangement of PM 1000.

7.3.3 Primary and Secondary Windings for Test Cores

The test cores were wound with a primary and secondary winding. The number of primary turns was determined essentially by the requirements of the flux density range to be covered and the voltage range available from the supply source at each frequency. The purpose of the secondary winding was to monitor the core flux density value and its waveshape by a measurement of the secondary induced voltage.

The cross section area A for each of the cores were separately calculated in the following way to minimize the error.

$$E.C.S.A. = \frac{(Wt.C)}{(M.P.C)\,x\,(M.D)} \qquad (7.2)$$

where:

E.C.S.A. = effective cross section area (m^2)

Wt.C. = weight of core (kg)

M.P.C. = mean path of core (m)

M.D. = metal density (kg/m^3)

The number of primary turns was calculated from the induced voltage equation:

$$E_{rms} = 4FfB_{max}AN_1 \quad (volts) \qquad (7.3)$$

where

A = effective cross section area of the core material, (E.C.S.A) (m^2)

E_{rms} = the voltage induce in the windings (V)

F = the form factor, (which for sinusoidal input F=1.11 and for square wave, F=1)

N_1 = the number of primary turns

f = the supply voltage frequency (Hz)

To cater for a maximum core flux density of 1.2 T at 2 and 3 kHz a primary winding of 10 turns was wound onto the core. The secondary winding was also wound with 10 turns. For use at frequencies of 50, 400, 1000 Hz, a primary coil winding of 20 turns was used. The Voltech PM 1000 was connected as shown in Fig. 7.9 and 7.10 to measure the primary winding supply voltage, current, core loss and exciting power (VA). The secondary winding induced voltage was measured using an Avometer and the waveform displayed on storage type oscilloscope together with the primary winding current waveform (the oscilloscope earth lead in the primary circuit was connected to the winding terminal). A comparison of the primary and secondary winding voltages on both the oscilloscope and Avometer revealed a negligible difference. The primary winding resistance measured on dc were 0.118 Ω and 0.059 Ω for 20 and 10 turns respectively, the power loss in this resistance has been assumed to be negligible in comparison with the core losses (for example core loss and copper loss at 1.0 T, 50 Hz were 0.47 W and 1.02 x 10^{-3} W respectively, at 1.0 T, 3 kHz were 129.7 W and 40 x 10^{-3} W respectively).

7.4 Comparison of Core loss and Exciting Power of Metglas 2605-S2 with silicon-iron

The silicon-iron core used in the tests was an uncut wound type with the following specification:

Core lamination thickness	0.05 (mm)
Overall dimensions	256 x 150.2 (mm^2)
Cross section area	51.2 x 49.4 (mm^2)
Window dimension	154 x 50 (mm^2)

Three amorphous cores using 2605-S2 were assembled the test measurements (per kg) of each only differed by an insignificant amount, the results given are for core No.3 which weighed 5.9 kg. Tables A.2 to A.6 list the test results for silicon-iron and Table A.7 to A.11 the results for Metglas 2605-S2 (see appenxix II). A comparison of the core losses and exciting power are illustrated graphically in Fig. 7.12 to 7.16 for each the of the frequencies of 50 Hz, 400 Hz, 1kHz, 2kHz and 3kHz. As expected the per kg losses and exciting VA are considerably less for Metglas 2605-S2, for example Table 7.3 compares the core loss and exciting VA at 1-T for each of the test frequencies.

The results may be used to identify the flux density for a given core loss at each of the various operating frequencies. Table 7.4 provides such a comparison of operating flux density for both materials for core losses of

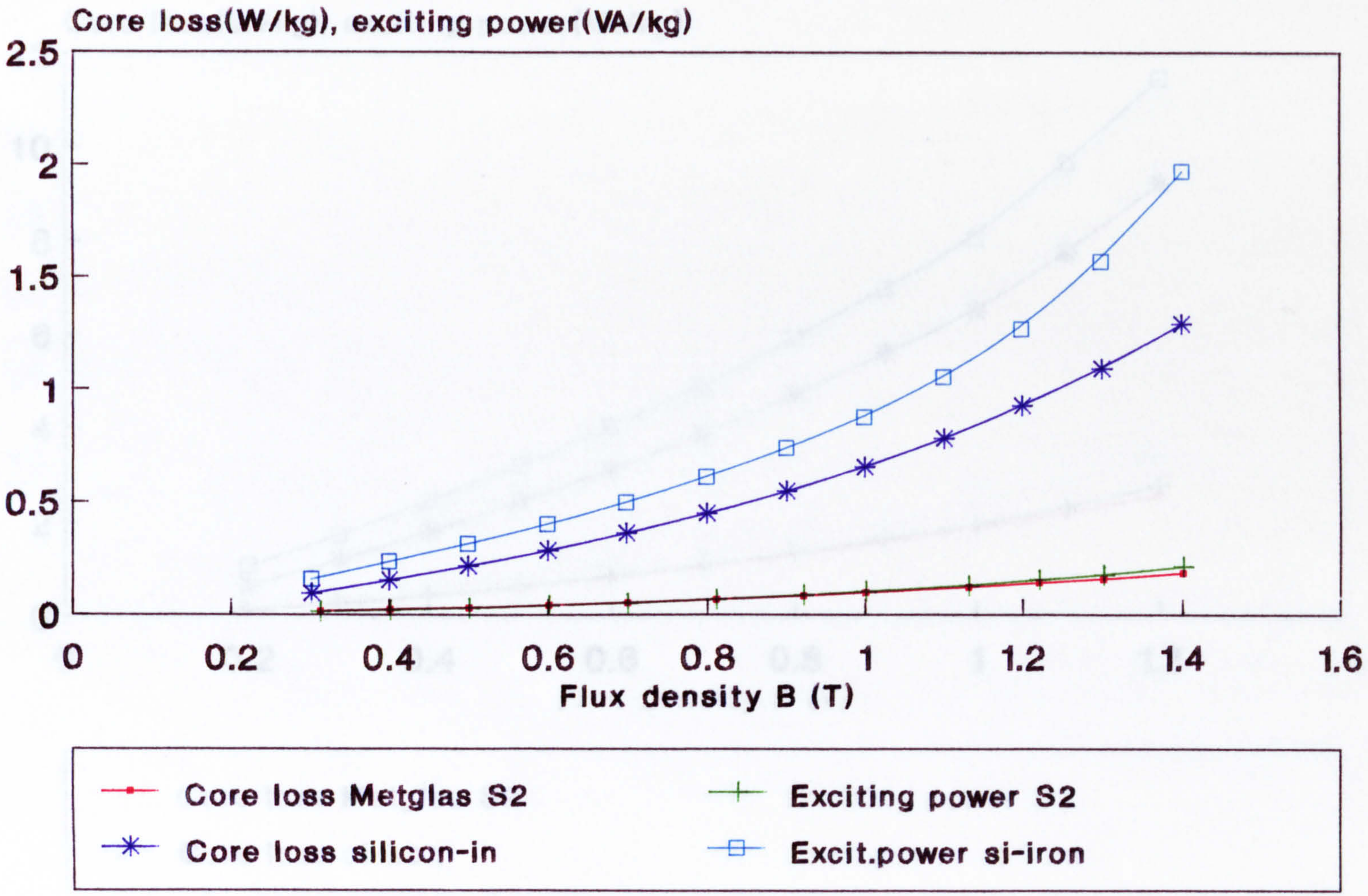

Fig. 7.12 Comparison of core loss and exciting power silicon iron with Metglas 2605-S2 at various flux density 50 Hz.

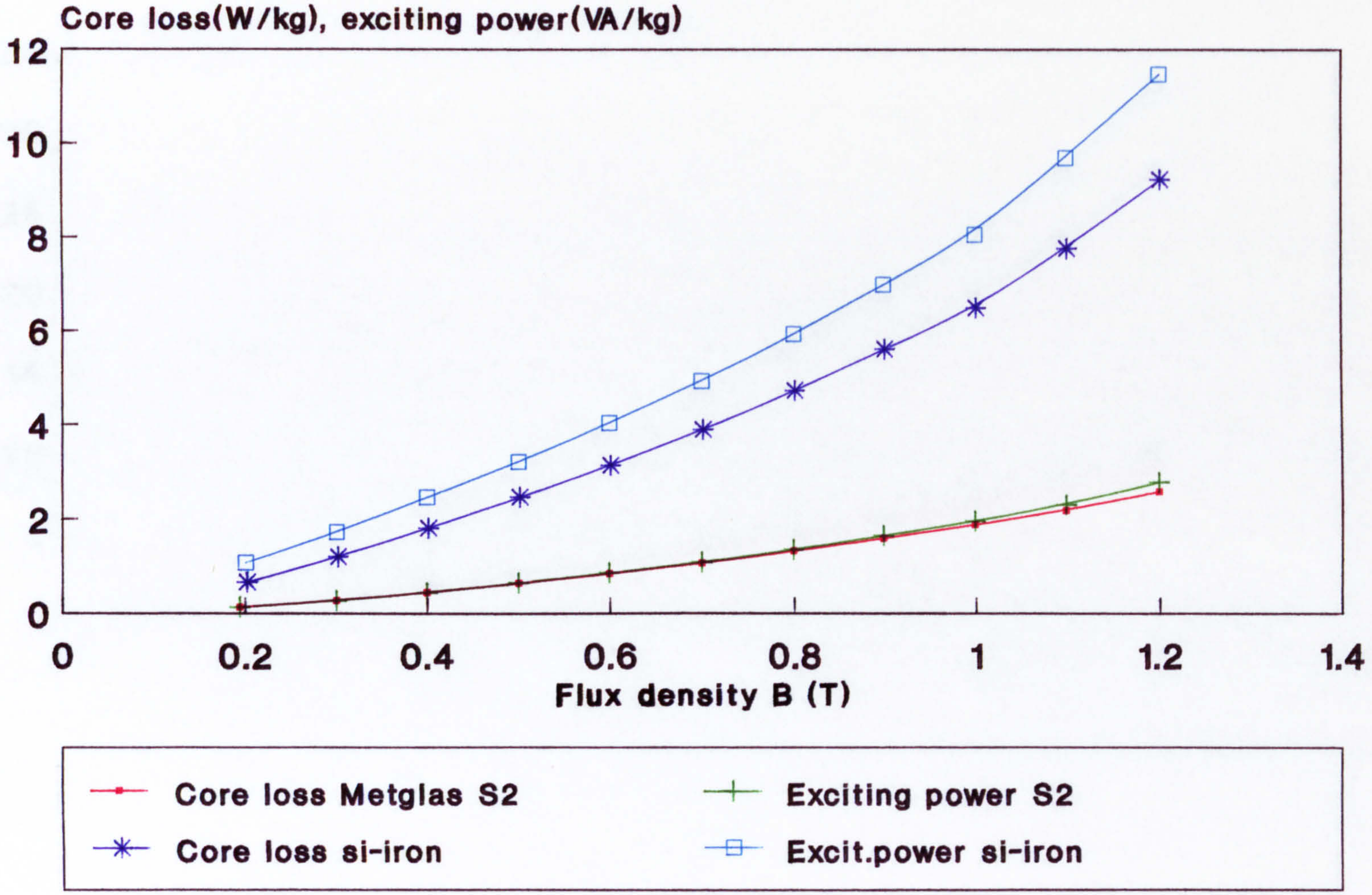

Fig. 7.13 Comparison of core loss and exciting power silicon-iron with Metglas 2605-S2 at various flux density 400 Hz.

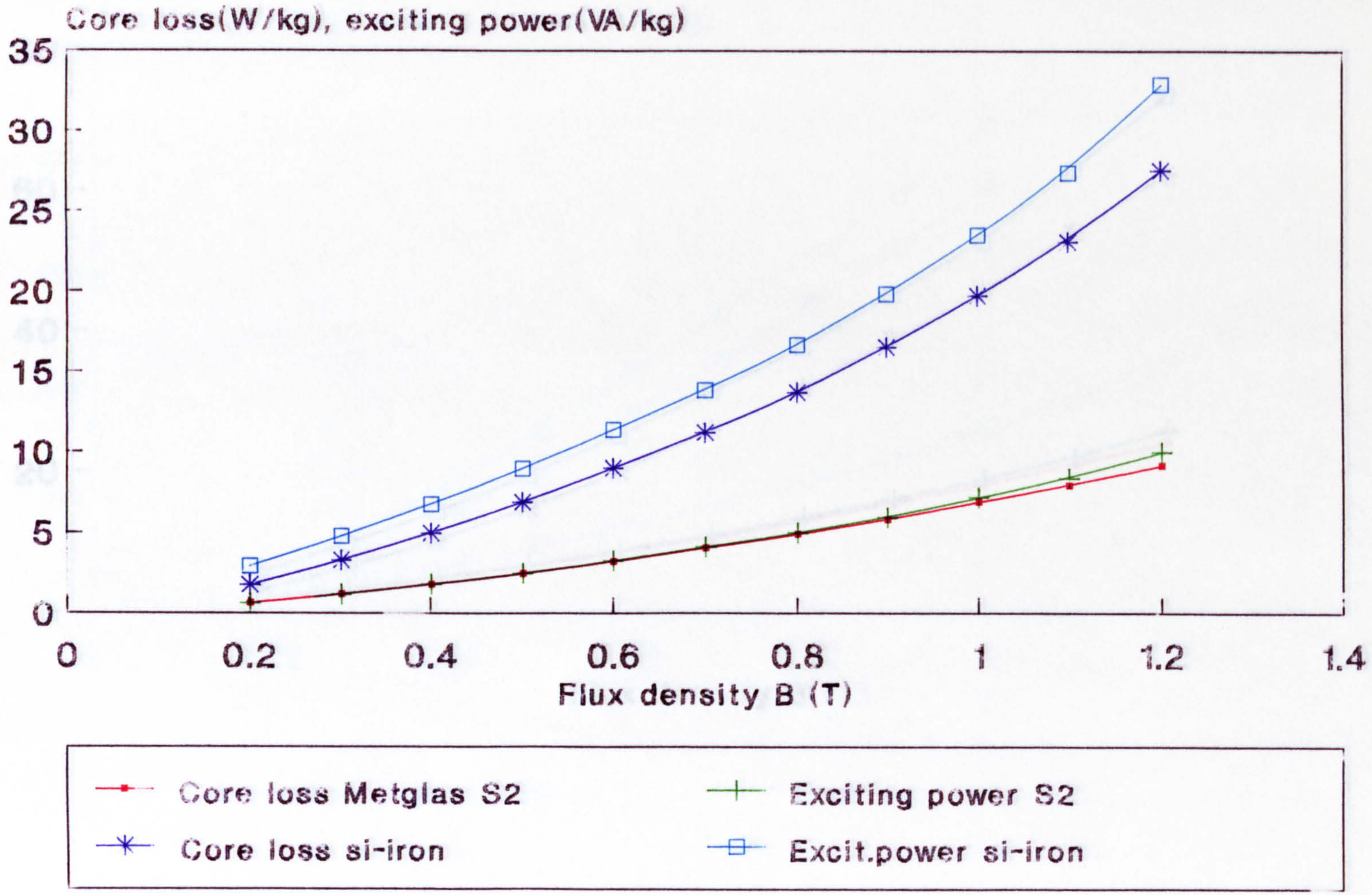

Fig. 7.14 Comparison of core loss and exciting power silicon-iron with Metglas 2605-S2 at various flux density 1000 Hz.

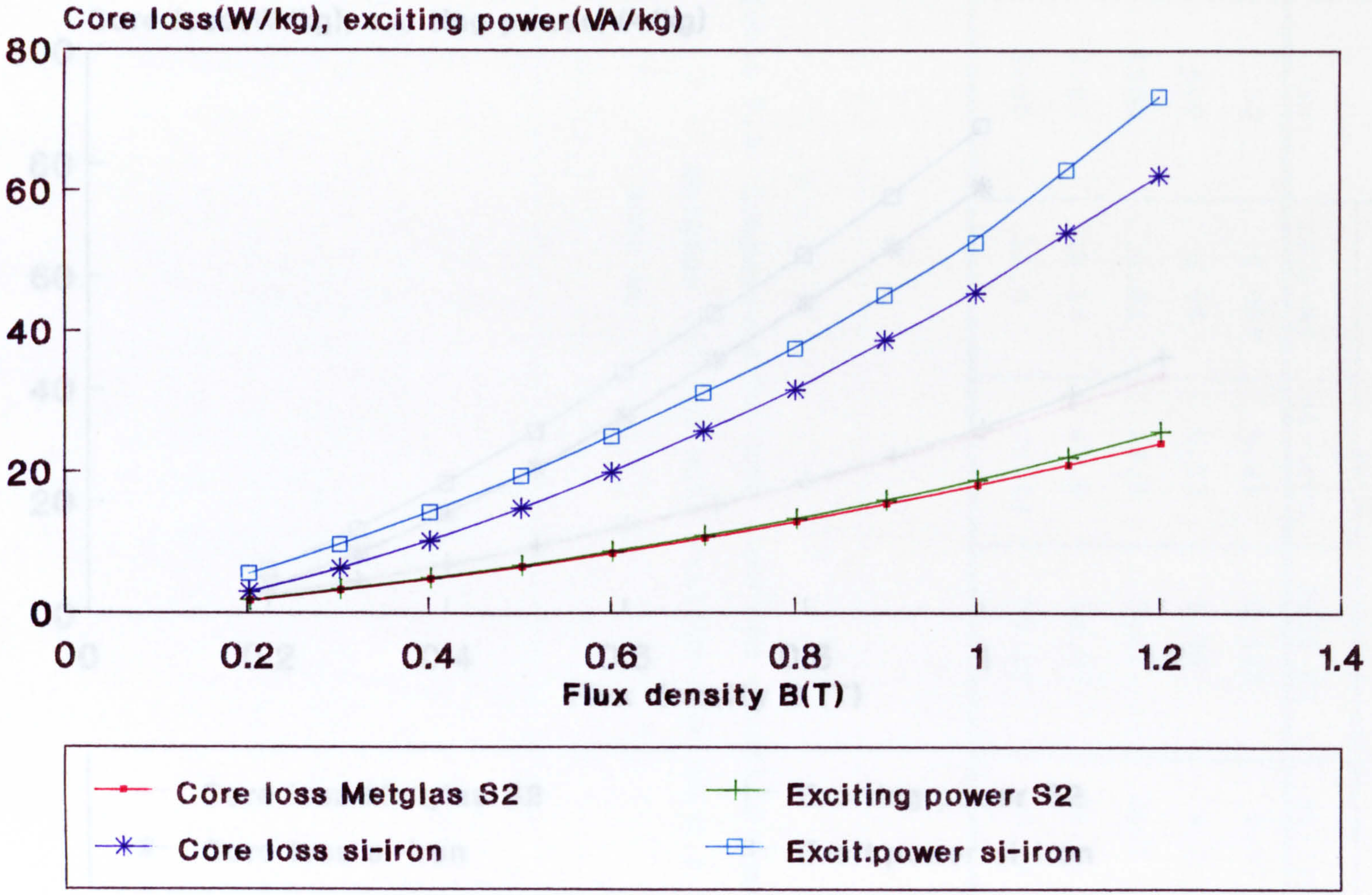

Fig. 7.15 Comparison of core loss and exciting power silocon-iron with Metglas 2605-S2 at various flux density 2000 Hz.

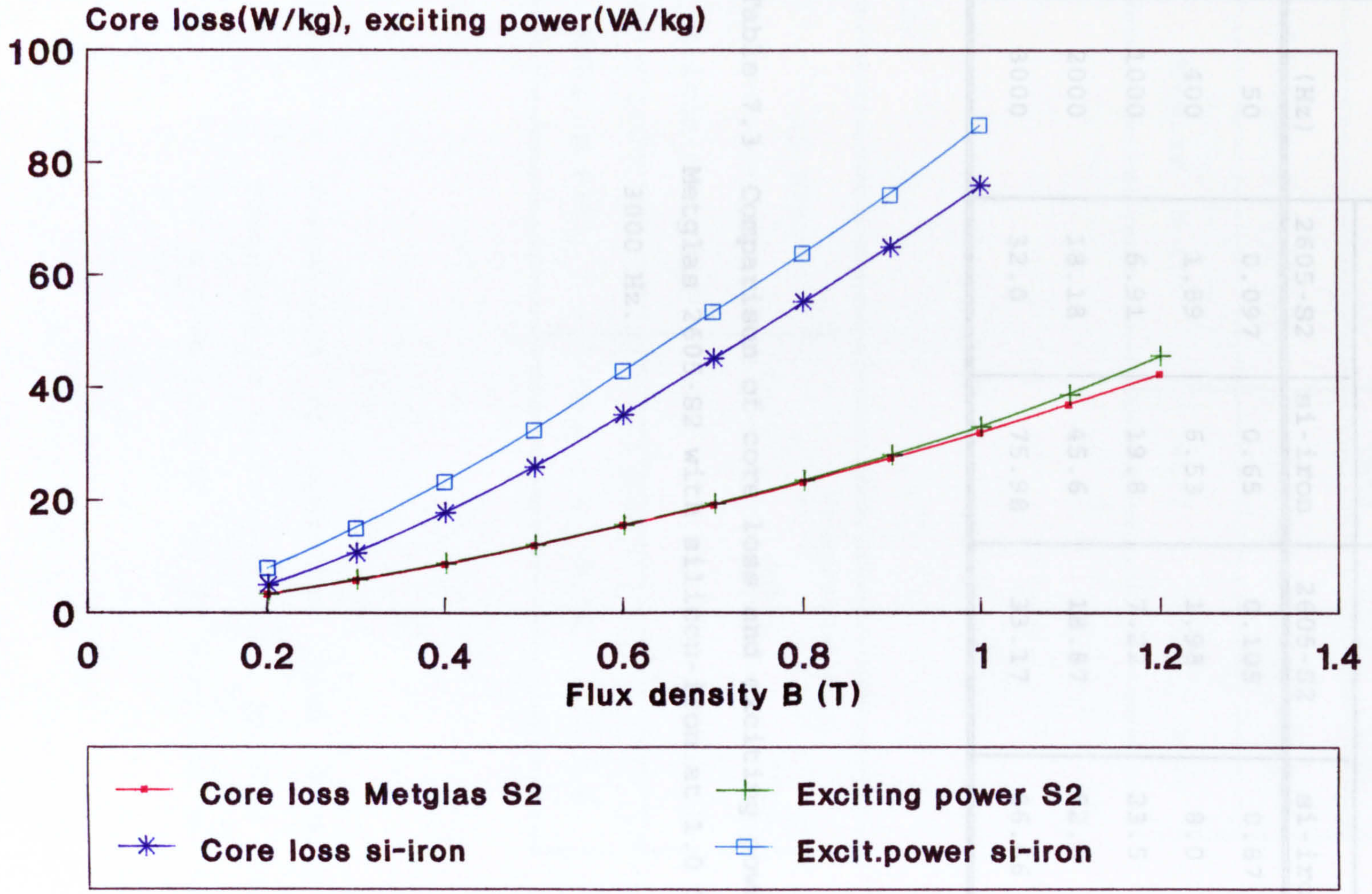

Fig. 7.16 Comparison of core loss and exciting power silicon-iron with Metglas 2605-S2 at various flux density 3000 Hz.

Frequency	Core loss (W/kg)		Exciting power(VA/kg)	
(Hz)	2605-S2	si-iron	2605-S2	si-iron
50	0.097	0.65	0.105	0.87
400	1.89	6.53	1.98	8.0
1000	6.91	19.8	7.22	23.5
2000	18.18	45.6	18.87	52.6
3000	32.0	75.98	33.17	86.66

Table 7.3 Comparison of core loss and exciting power of Metglas 2605-S2 with silicon-iron at 1.0 T, 50-3000 Hz.

(a)

20 W/kg	Frequency (Hz)		
	1000	2000	3000
Silicon-iron B (T)	1.0	0.6	0.44
Metglas B (T)	>1.2	1.0	0.74

(b)

15 W/kg	Frequency (Hz)		
	1000	2000	3000
Silicon-iron B(T)	0.84	0.5	0.35
Metglas B(T)	>1.2	0.86	0.6

Table 7.4 Comparison of operating flux density and frequency of silicon-iron and Metglas 2605-S2 for a core loss of (a) 20 W/kg and (b) 15 W/kg.

(a) 20 W/kg and (b) 15 W/kg at 1, 2 and 3kHz.The results clearly illustrate the greater operating flux densities possible when using Metglas 2605-S2.

7.5 Comparison of Core Loss Results Metglas 2605-S3A with 2605-S2

A quantity of Metglas alloy 2605-S3A was purchesed towards the end of the project to evaluate its characteristics and suitability. This alloy has already been referred to in section 7.1.2 where a design comparison was made with Metglas alloy 2605-S2. One major difference between the alloys was the ribbon thickness, 2605-S2 = 0.025 mm,2605-S3A = 0.0175 mm thick.

A core was wound using 2605-S3A with similar dimension used previously for 2605-S2, the core was then annealed and tested. Fig. 7.17 shows the core loss results for amorphous Metglas 2605-S3A material at different flux densities for frequencies of 50-3000 Hz. Fig. 7.18 to 7.20 compares the losses of both types of amorphous material at different flux density at frequency of 50-3000 Hz. Core loss of amorphous Metglas 2605-S3A at 50, 400, 1000, 2000 and 3000 Hz was 34, 31, 24, 21 and 20% lower than 2605-S2 respectively.

The measured loss of 2605-S3A were higher than expected, particularly at 3-kHz, it was considered likely that the annealing cycle followed was not the optimum one for low

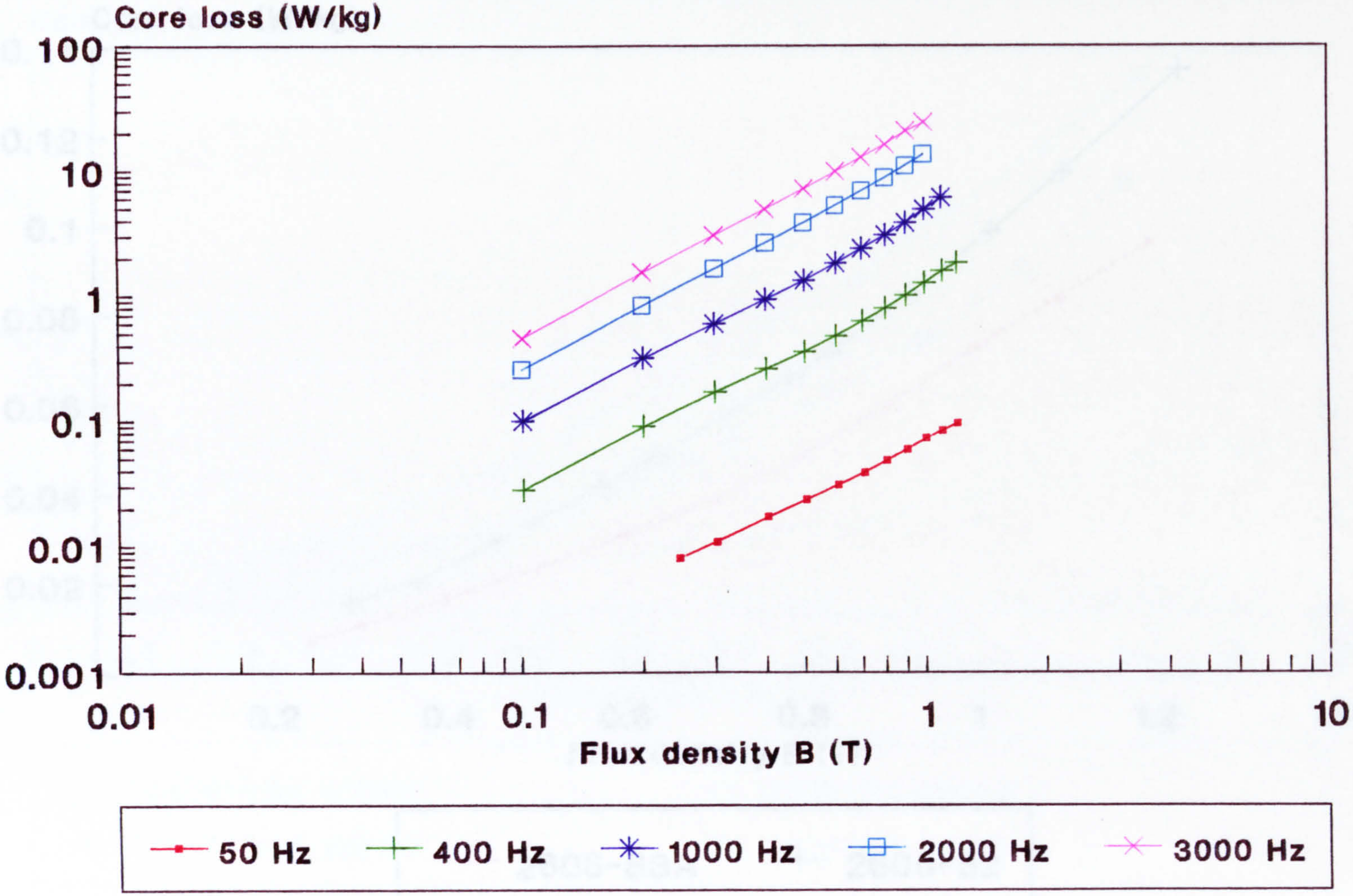

Fig. 7.17 Core loss of amorphous 2606-S3A at 50, 400, 1000, 2000 and 3000Hz at different flux density core No.4.

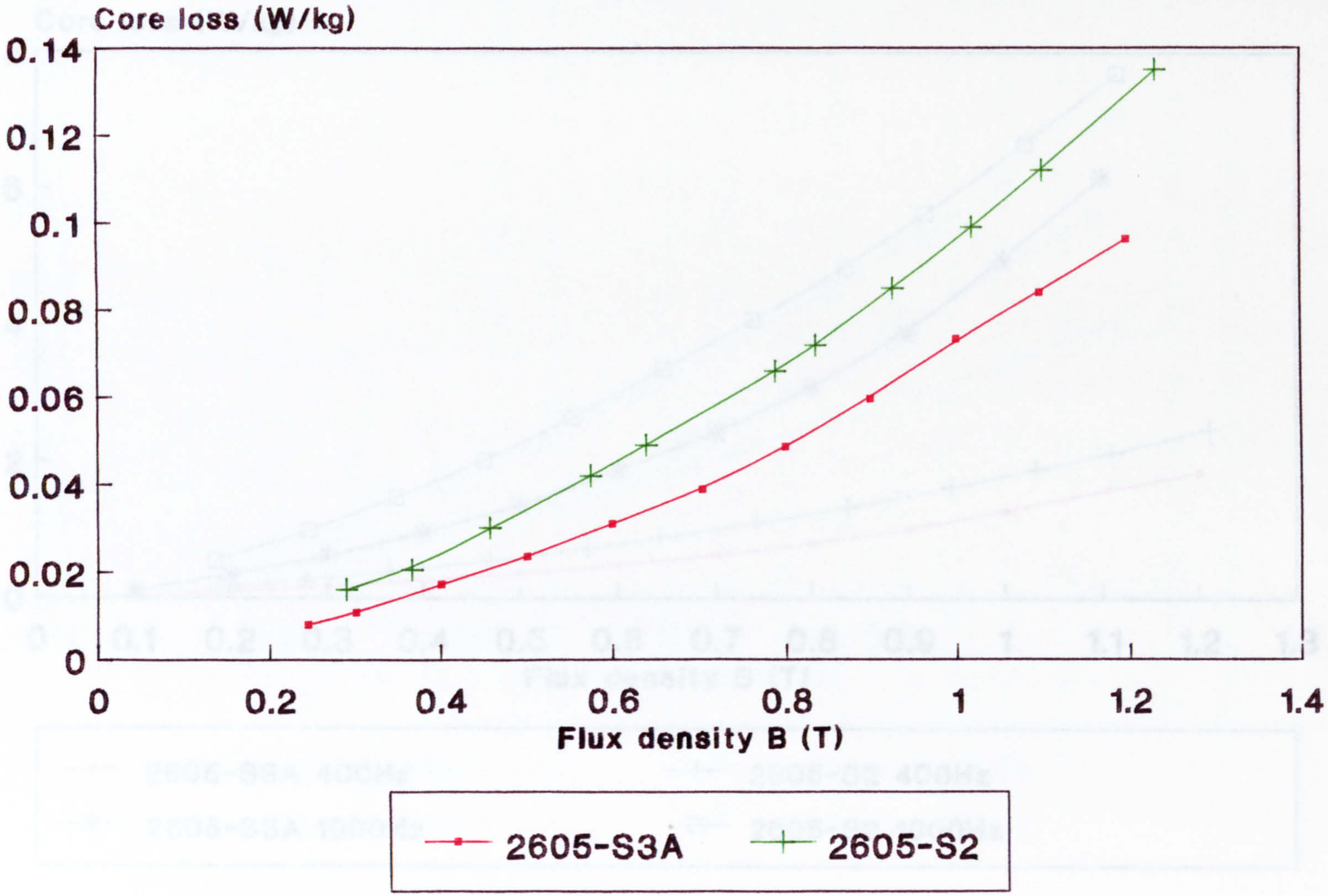

Fig. 7.18 Comparison of core loss of amorphous 2605-S2 with 2605-S3A at 50Hz, different flux density.

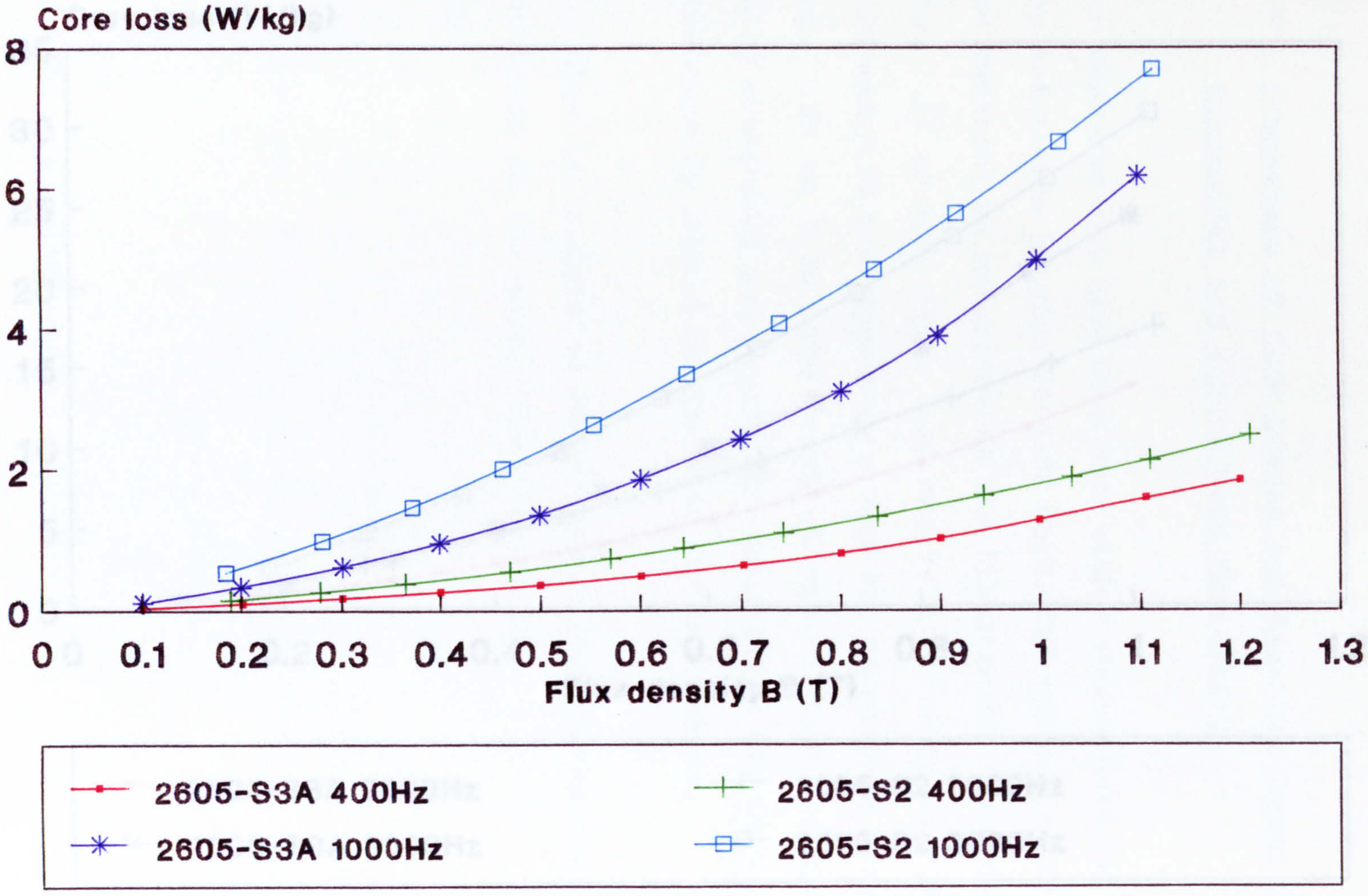

Fig. 7.19 Comparison of core loss of amorphous 2605-S2 with 2605-S3A at 400 and 1000Hz at different flux density.

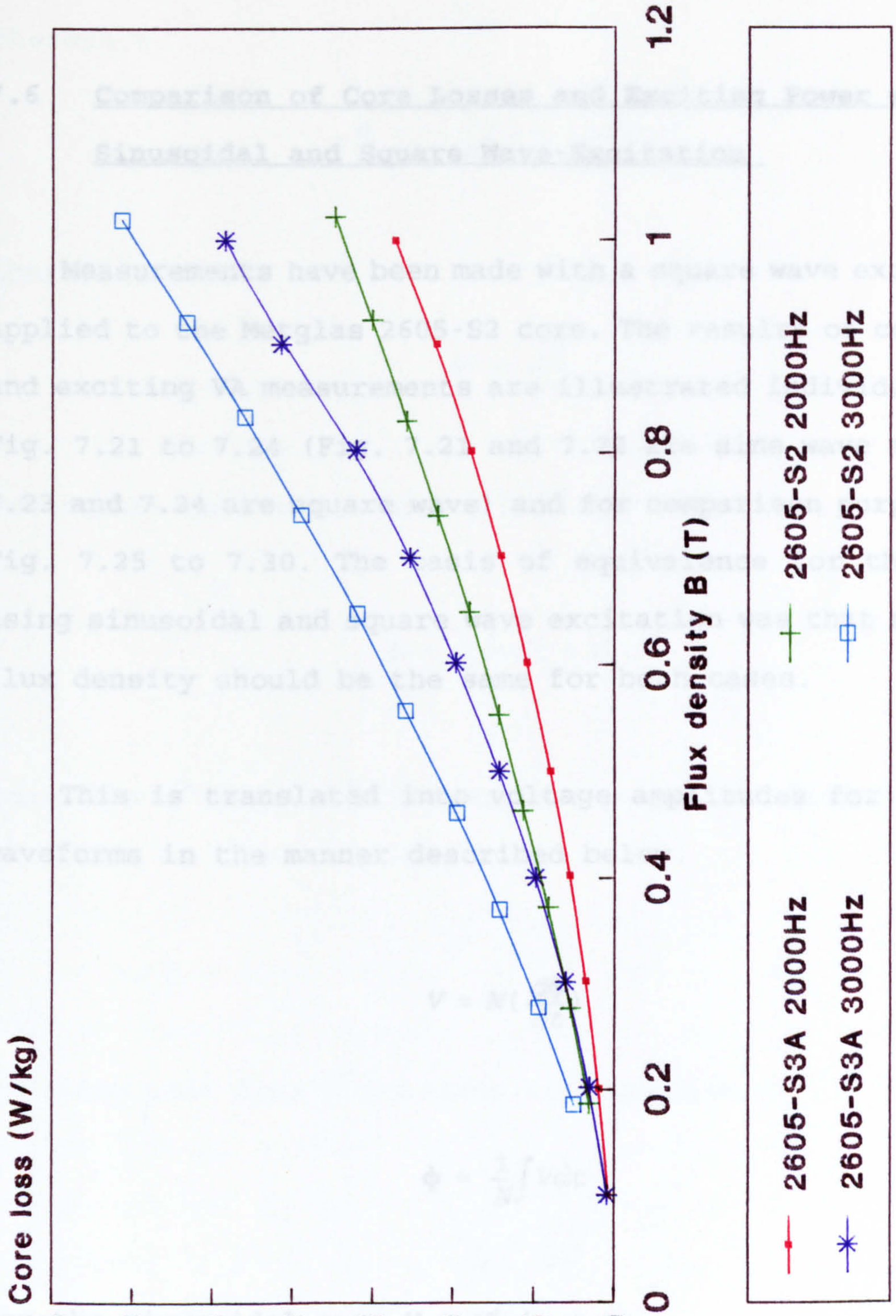

Fig. 7.20 Comparsion of core loss of amorphous 2605-S2 with 2605-S3A at 2000 and 3000Hz at different flux density.

loss. The information obtained from Allied Signal regarding the annealing of 2605-S3A was vague, such information being of a proprietary nature.

7.6 Comparison of Core Losses and Exciting Power with Sinusoidal and Square Wave-Excitation

Measurements have been made with a square wave excitation applied to the Metglas 2605-S2 core. The results of core loss and exciting VA measurements are illustrated individually in Fig. 7.21 to 7.24 (Fig. 7.21 and 7.22 are sine wave and Fig. 7.23 and 7.24 are square wave) and for comparison purposes in Fig. 7.25 to 7.30. The basis of equivalence for the tests using sinusoidal and square wave excitation was that the peak flux density should be the same for both cases.

This is translated into voltage amplitudes for the two waveforms in the manner described below.

$$V = N\left(\frac{d\phi}{dt}\right) \qquad (7.4)$$

$$\phi = \frac{1}{N}\int V dt \qquad (7.5)$$

For the sinusoidal case $V = V^{*}\sin\omega t$

where

V^* is the peak sinusoidal voltage, ω is the angular frequency, N the number of winding turns

Therefore

$$\phi = -\left(\frac{1}{N}\right)\left(\frac{V^*}{\omega}\right)\cos\omega t \qquad (7.6)$$

therefore

$$\phi^* = \frac{V^*}{\omega N} \qquad (7.7)$$

For square wave v = V in any half cycle

$$\phi = \frac{1}{N}\int v dt = \frac{V}{N}t \qquad (7.8)$$

Peak flux ϕ^* where t = T/4 where T is the waveform period

$$\phi^* = \frac{V}{N}\frac{T}{4} \qquad (7.9)$$

Equating peak flux ϕ^* for sine and square wave

$$\frac{V^*}{\omega N} = \frac{VT}{4N} \qquad (7.10)$$

with $\omega = 2\pi f$ and $T = 1/f$

then

$$\frac{V^*}{2\pi fN} = \frac{V}{4fN} \qquad (7.11)$$

or

$$V^* = \frac{\pi V}{2} \qquad (7.12)$$

but V^* (sine wave peak) $= \sqrt{2}\ V_{rms}$

where V_{rms} = rms value of sinewave voltage.

substituting $\sqrt{2}\ V_{rms} = (\pi/2)\ V$

or

$$V_{rms} = \frac{\pi V}{2\sqrt{2}} = 1.11\ V \qquad (7.13)$$

Hence for the same peak flux or flux density conditions, the rms value of the sinewave voltage is 1.11 times the amplitude of the square wave voltage. In the case of the square wave voltage, the flux waveform is triangular. The fundamental component of the triangular flux waveform produced by the square voltage is about 80% of the sinewave flux produced by the sinusoidal applied voltage. The higher order harmonic amplitudes of a triangular waveform decrease with the square of the order $(1/n^2)$. Hence slightly lower losses would be expected with square wave excitation.

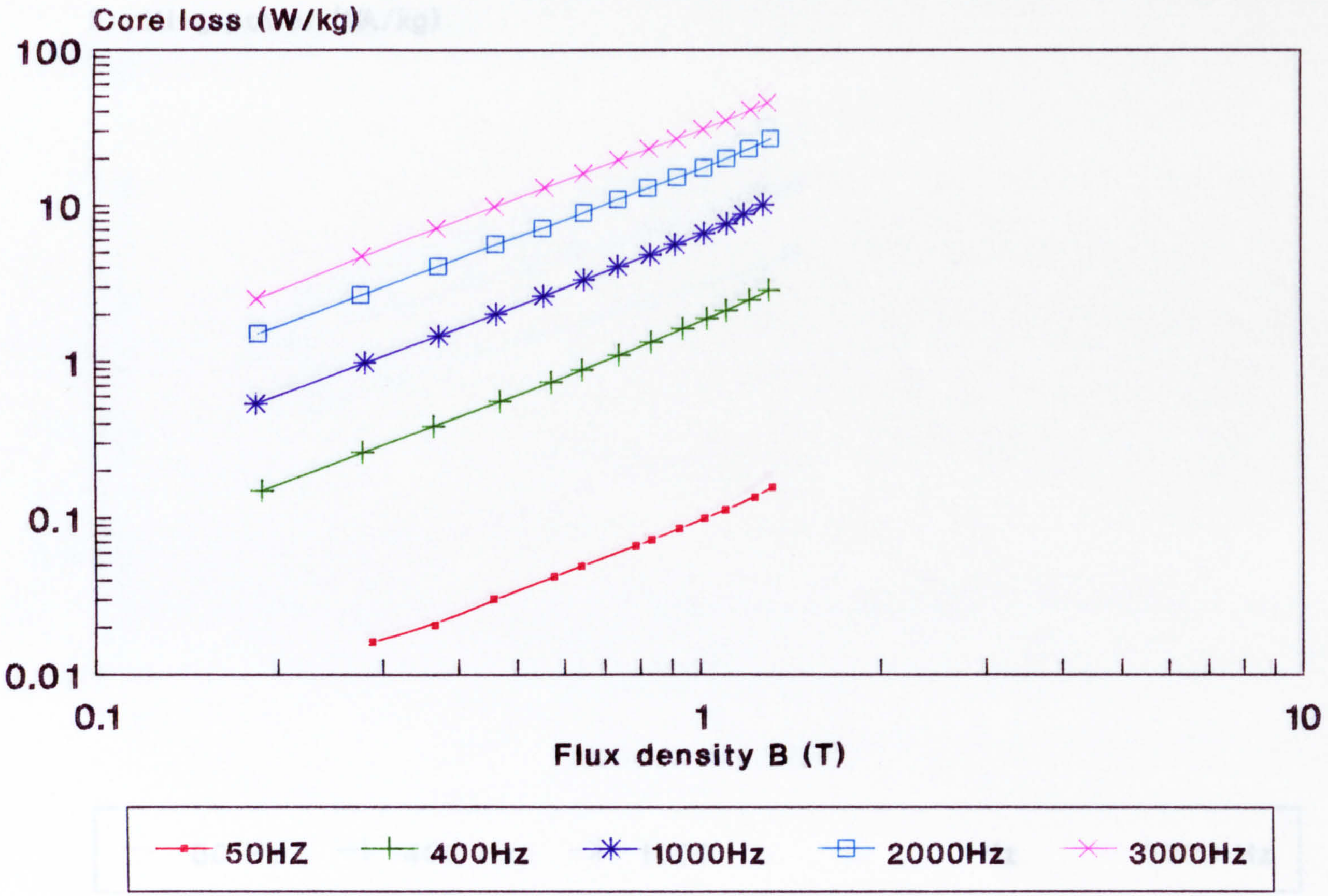

Fig. 7.21 Core loss of Metglas 2605-S2 at 50, 400, 1000, 2000 and 3000Hz at different flux density sine wave core No.2.

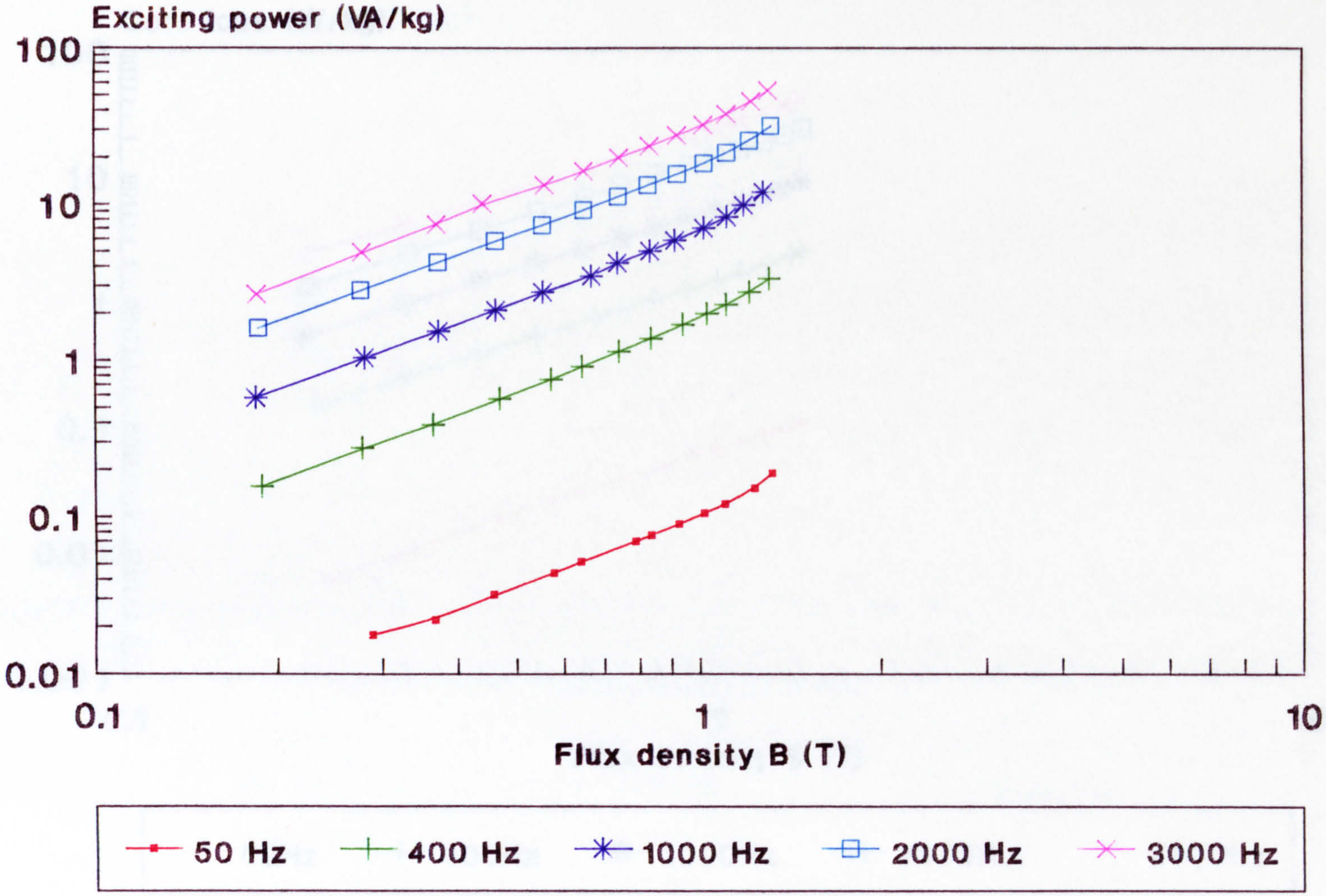

Fig. 7.22 Exciting power of Metglas 2605-S2 at 50, 400, 1000, 2000 and 3000 Hz at different flux density sine wave core No.2.

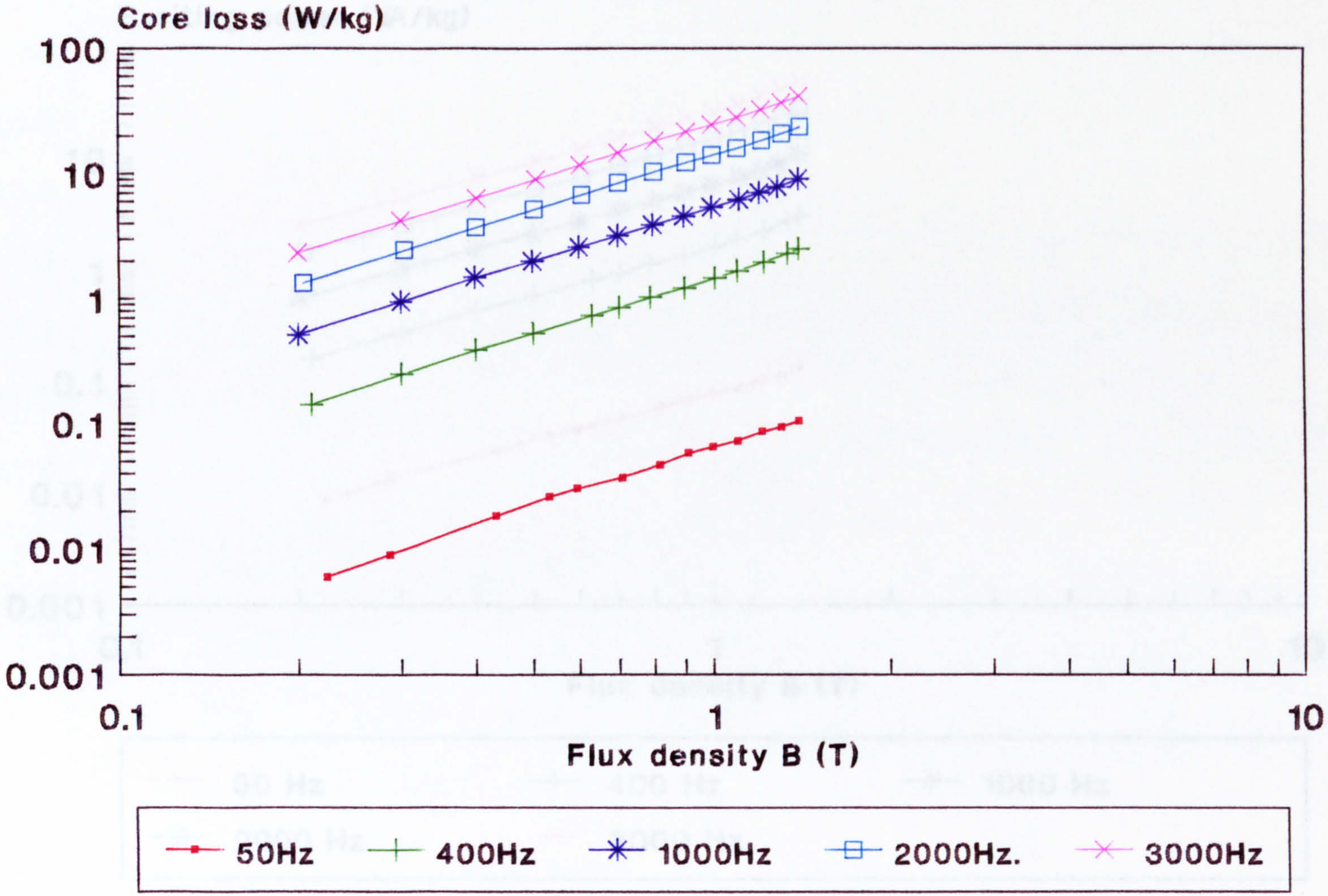

Fig. 7.23 Core loss of Metglas 2605-S2 at 50, 400, 1000, 2000 and 3000 Hz at different flux density square wave core No.2.

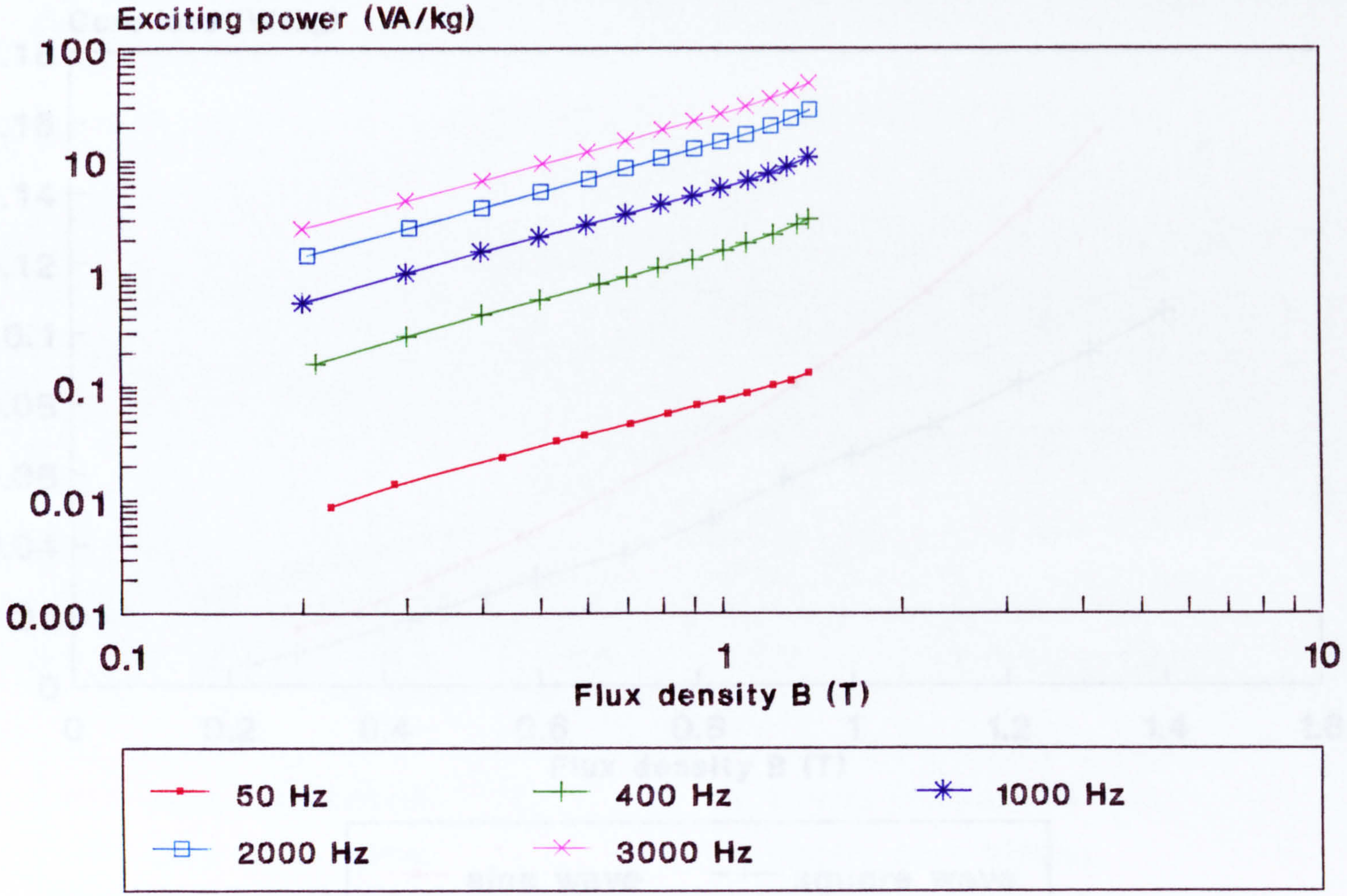

Fig. 7.24 Exciting power of Metglas 2605-S2 at 50, 400, 1000, 2000 and 3000 Hz at different flux density square wave core No.2.

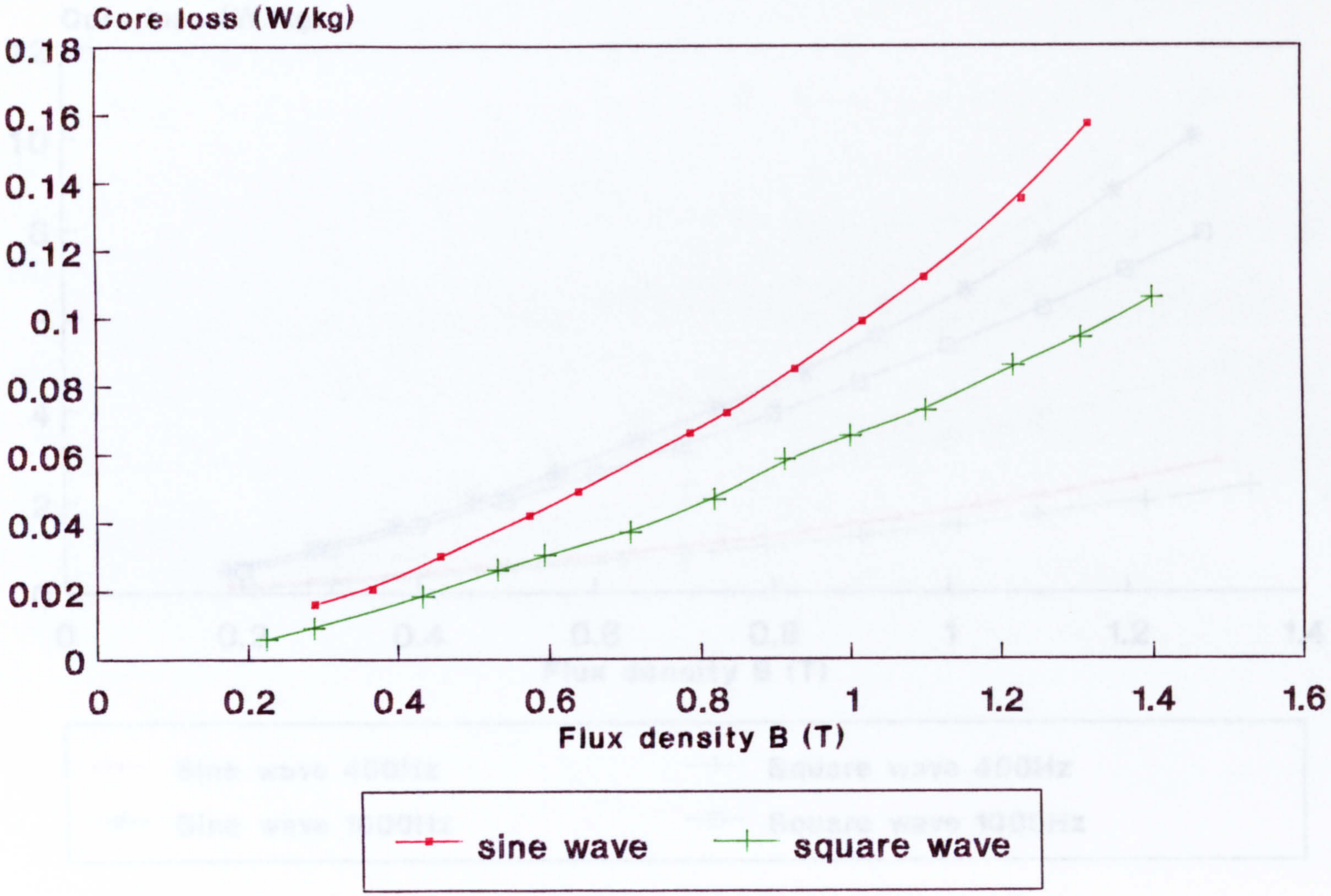

Fig. 7.25 Comparison of core loss of Metglas 2605S2 at 50Hz at different flux density sine wave and square wave core No.2.

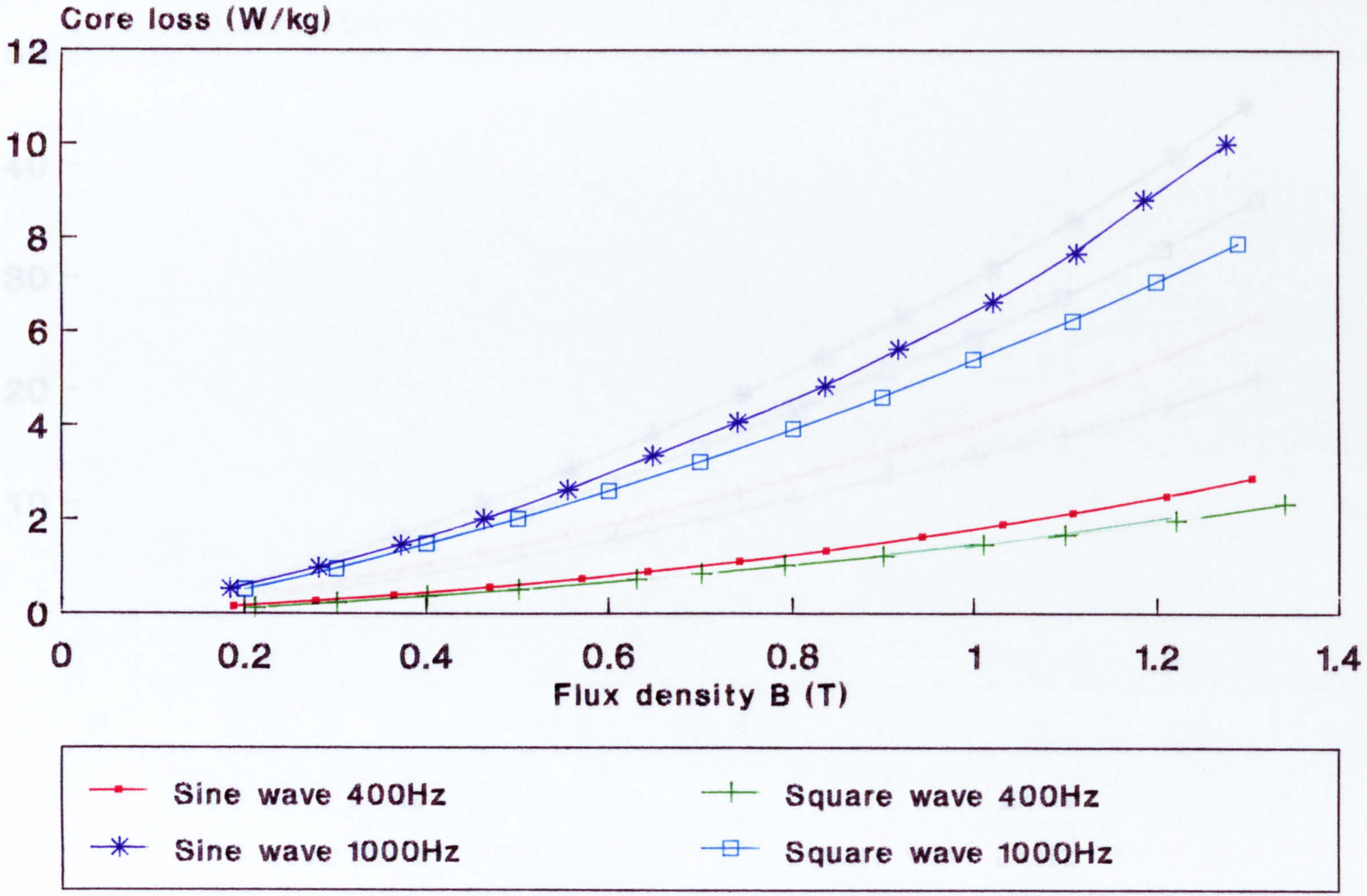

Fig. 7.26 Comparison of core loss Metglas 2605-S2 at 400 and 1000 Hz at different flux density sine and square wave core no.2.

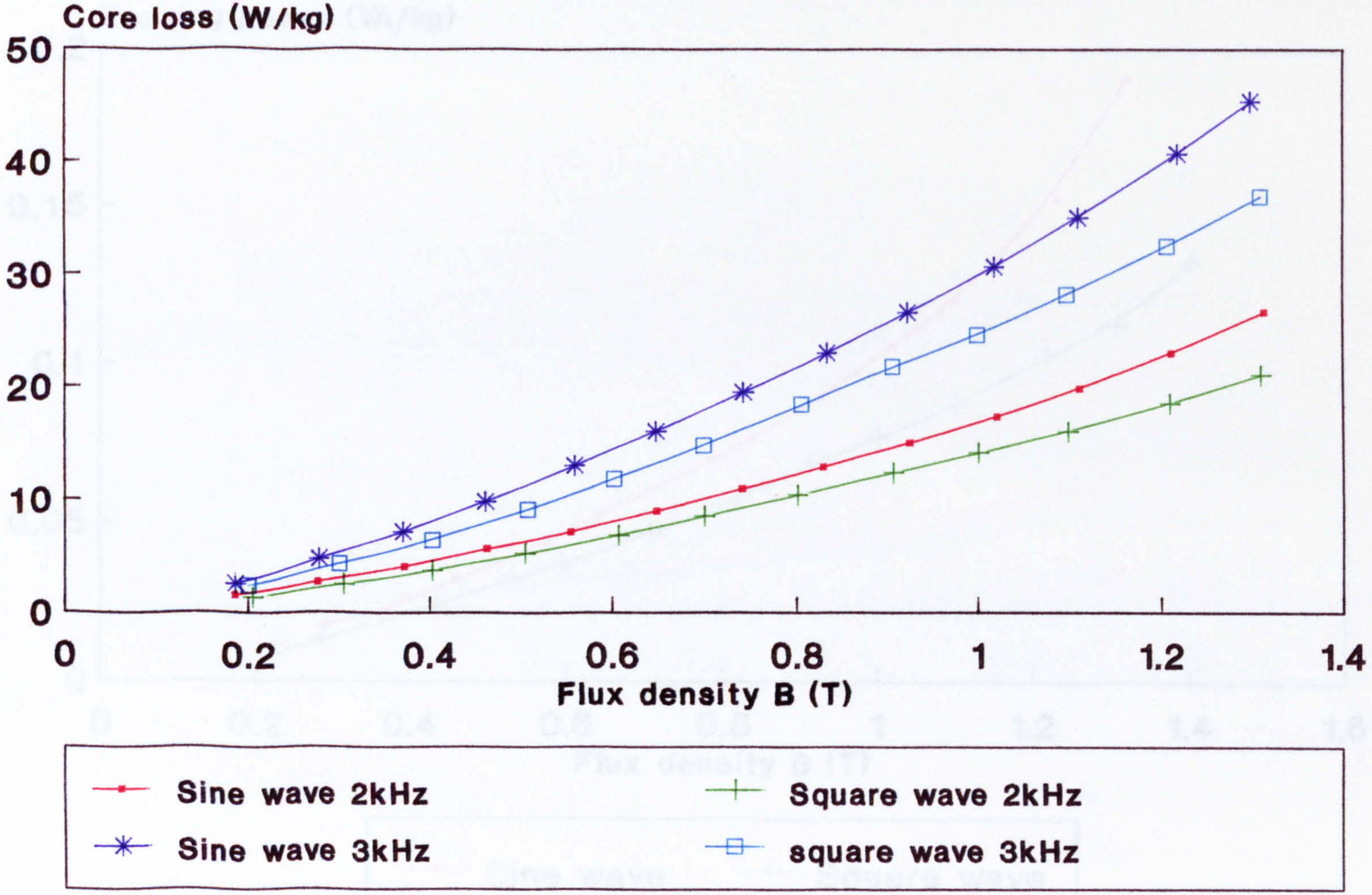

Fig. 7.27 Comparison of core loss of Metglas 2605-S2 at 2 and 3kHz, different flux density sine and square wave core no.2.

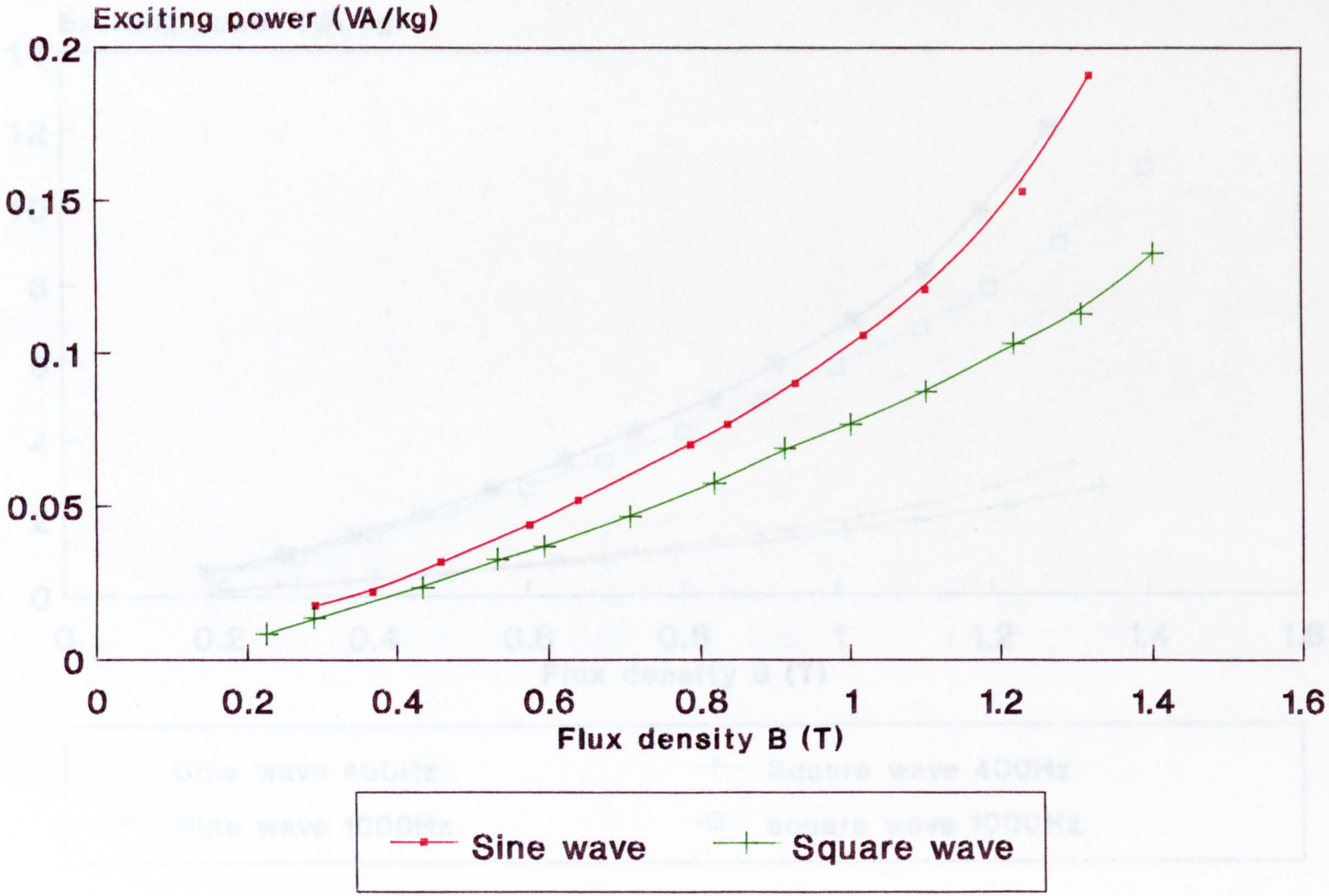

Fig. 7.28 Comparison of exciting power of Metglas 2605-S2 at 50 Hz, different flux density sine and square wave core No.2.

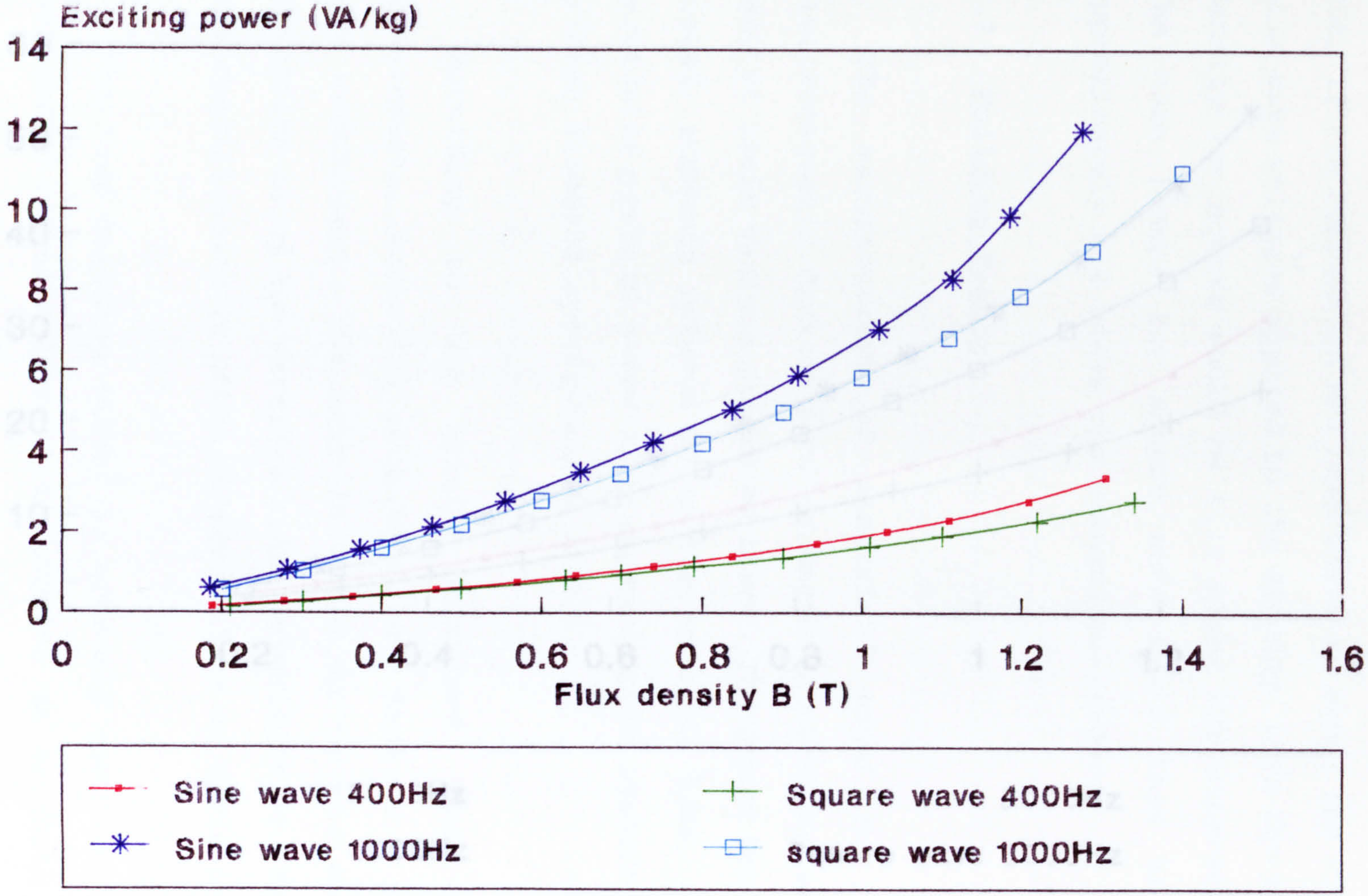

Fig. 7.29 Comparison of exciting power of Metglas 2605-S2 at 400 and 1000Hz,different flux density sine and square wave core no.2.

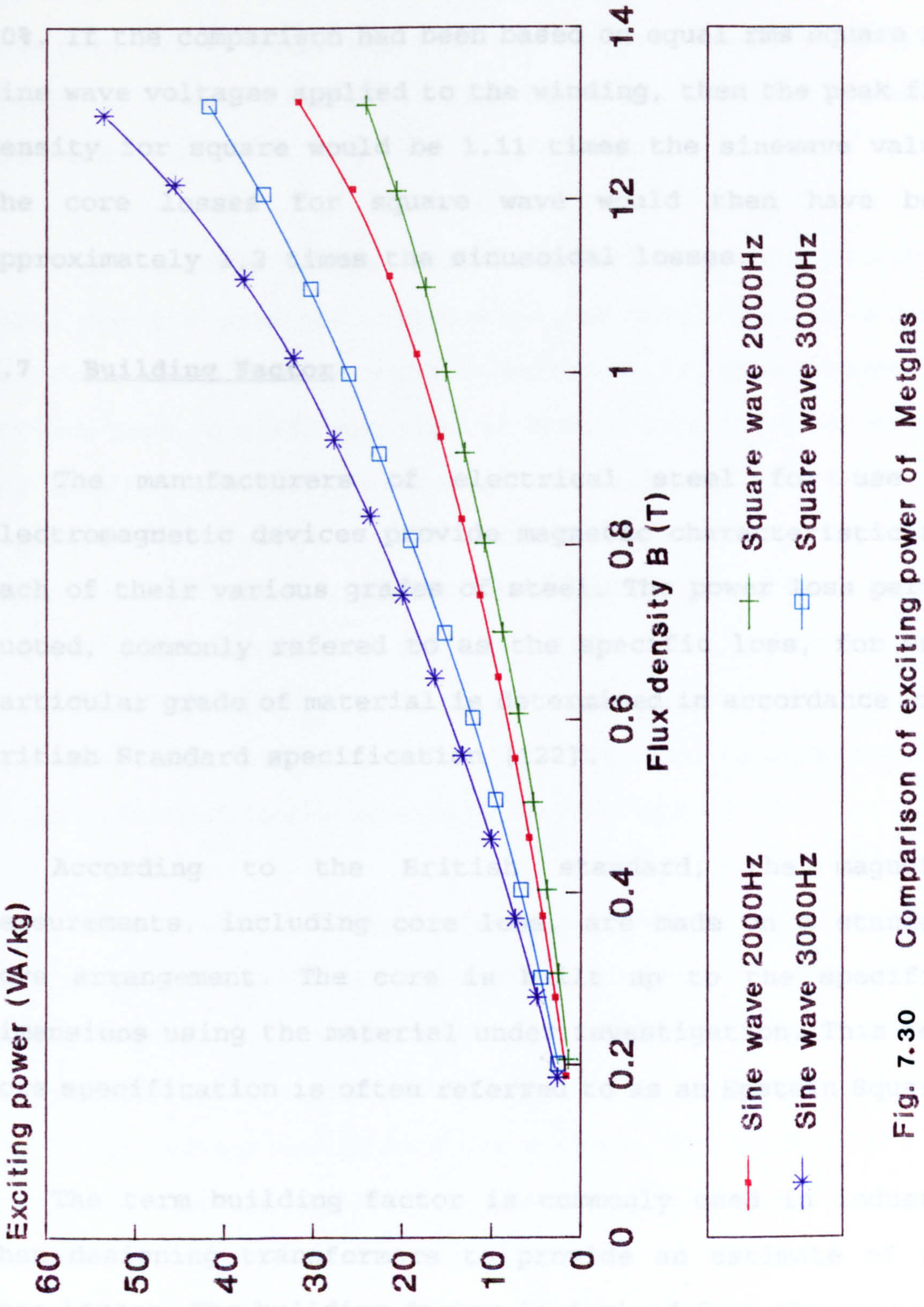

Fig. 7.30 Comparison of exciting power of Metglas 2605S2 at 2000 and 3000Hz different flux density sine and square wave core no.2.

A comparison of the test results for sinewave and square wave voltages produces a corresponding difference in the losses namely the square wave losses are reduced by about 20%. If the comparison had been based on equal rms square and sine wave voltages applied to the winding, then the peak flux density for square would be 1.11 times the sinewave value. The core losses for square wave would then have been approximately 1.2 times the sinusoidal losses.

7.7 Building Factor

The manufacturers of electrical steel for use in electromagnetic devices provide magnetic characteristic for each of their various grades of steel. The power loss per kg quoted, commonly refered to as the specific loss, for each particular grade of material is determined in accordance with British Standard specification [122].

According to the British standard, the magnetic measurements, including core loss, are made on a standard core arrangement. The core is built up to the specified dimensions using the material under investigation. This test core specification is often referred to as an Epstein Square.

The term building factor is commonly used in industry when designing transformers to provide an estimate of the core losses. The building factor is derived from the ratio of actual core losses measured on a completed transformer core

and the core losses for the same core weight estimated using the losses as derived by the British standard method. Based on experience, manufacturers are able to accurately predict the core losses using building factors previously obtained on built up or wound cores of which there are many variations in construction.

In the case of the amorphous metals, the manufacturers also provide loss characteristics for their various alloys. However since the amorphous material is manufactured in ribbon form, a different type of common core has been adopted by Metglas for the measurement of what may be termed the specific loss. This common core is made in the form of a toroid constructed of ribbon wound hand tight onto a ceramic bobbin and secured with polyimide tape. The ribbon width is either 25 or 50 mm, the mean magnetic path length is 13 cm and the weight of 30 grams [117]. The core is annealed with a longitudinal field applied in the ribbon direction.

The building factor for the amorphous alloys may therefore be calculated from the loss measurements made on the assembled wound cores and the loss as predicted using the manufacturers specific loss. Fig. 7.31 to 7.33 show the building factors calculated for a range flux density for the two amorphous alloys and the wound silicon-iron core at supply frequencies of 1 kHz, 2kHz and 3 kHz respectively. Fig. 7.34 shows the comparison of the building factor at 1 T for Metglas 2605-S2 with 2605-S3A at 1, 2 and 3 kHz.

In the case of the wound uncut silicon-iron core, at 2 and 3 kHz the building factor decreased from just over one to 0.74 as the operating flux density level was increased from 0.3 to 1.0 T. At 1 kHz the building factor ranged from 1.3 to 0.9 over the same flux density range. For the amorphous alloy 2605-S2, the building factor at 1 kHz remained almost constant at about 1.3. At 2 and 3 KHz, the building factor decreased slightly from about 1.7 at 0.3 T to 1.3 at 1.0 T. The results for the amorphous alloy 2605-S3A gave building factors which varied more widely between each frequency, 2.3 to 2.5 at 3 kHz, 2.0 to 2.3 at 2 KHz and 1.5 to 1.8 at 1 kHz.

The building factor of less than 1 for the silicon-iron illustrates the effectiveness of the uncut wound type of core in minimising core loss. The Epstein square core arrangement will incur greater losses particularly at the corners where the built up laminations overlap. For the two amorphous alloys the larger building factor associated with 2605-S3A may be attributed to:

(1) the smaller ribbon thickness of 2605-S3A will require more turns to be wound for a given weight of core

(2) the annealing treatment to which 2605-S3A was subjected is unlikely to have been the optimum.

For the amorphous alloy 2605-S2, a building factor in the range 1.3 to 1.6 (depending on flux density) will give a reliable prediction of the core losses to be expected in a wound type uncut core.

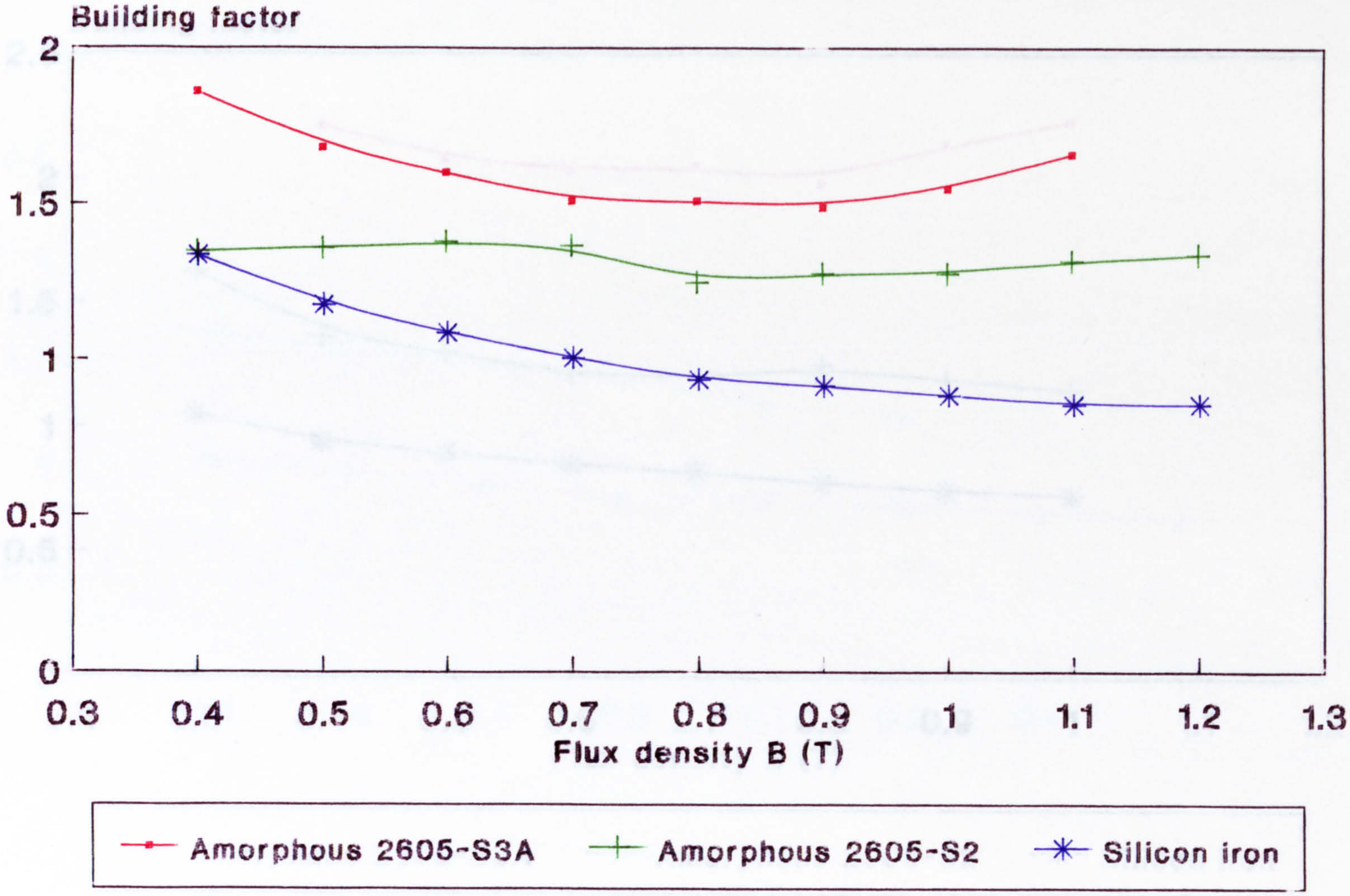

Fig. 7.31 Variation of biulding factor with flux density of amorphous cores compared with slicon-iron at 1000 Hz.

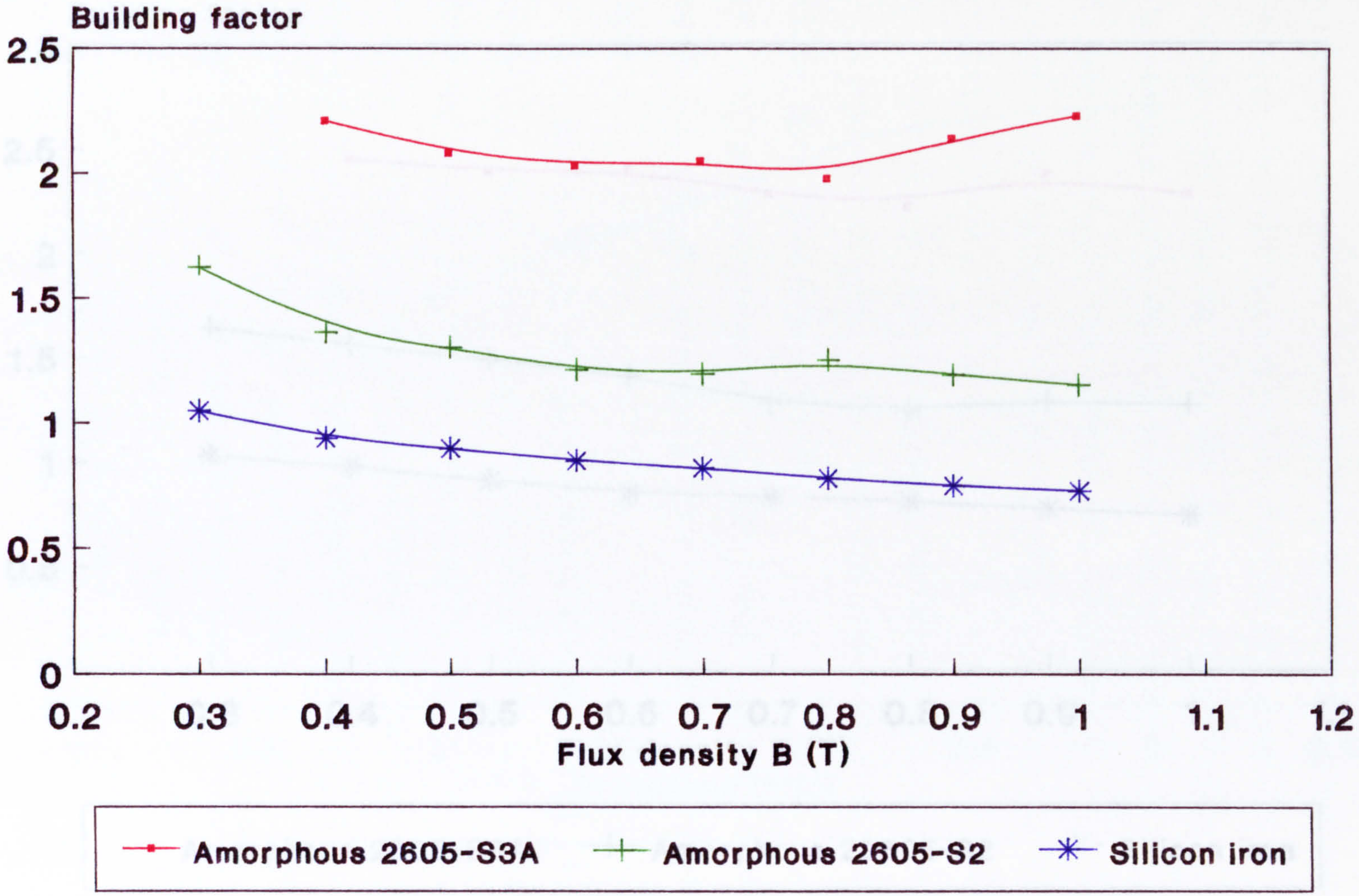

Fig. 7.32 Variation of building factor with flux density of amorphous cores compared with silicon steel core at 2000 Hz.

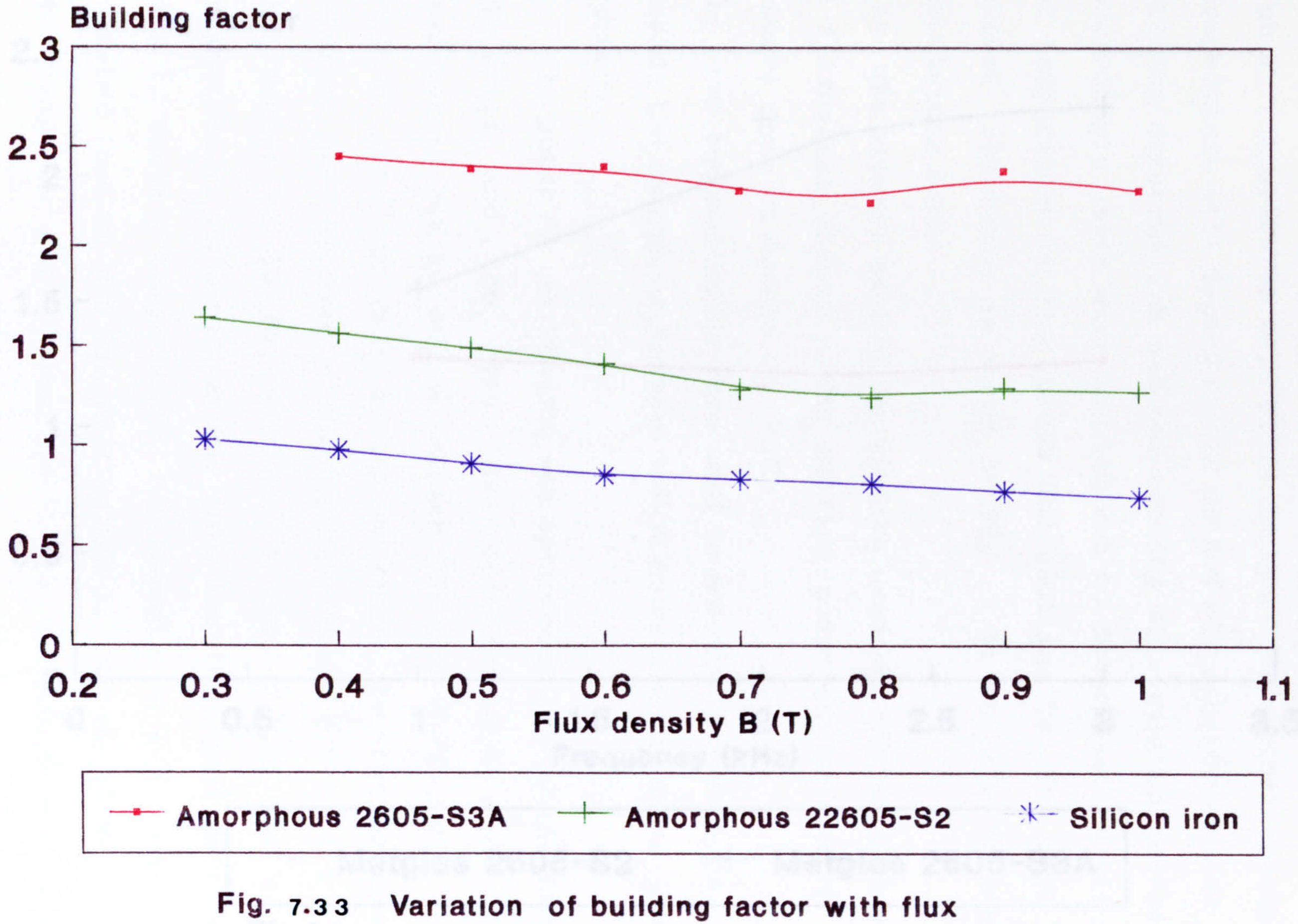

Fig. 7.33 Variation of building factor with flux density of amorphous cores compared with silicon steel at 3000 Hz.

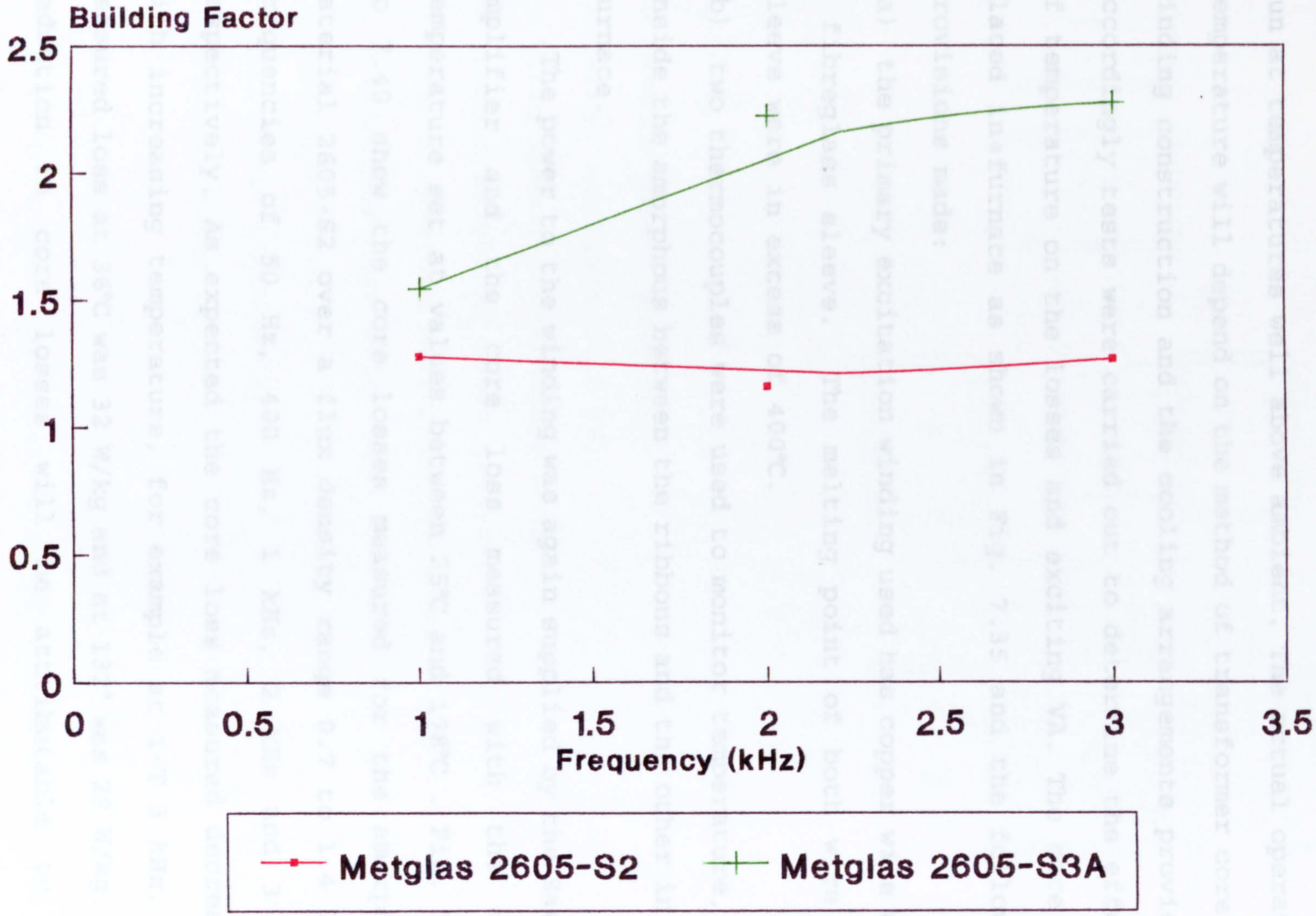

Fig. 7.3 4 Building factor of Metglas 2605-S2 and 2605-S3A at 1, 2 and 3 kHz 1-T.

7.8 Effect of Temperature on Core Losses

Under normal operating conditions the amorphous core will run at temperatures well above ambient. The actual operating temperature will depend on the method of transformer core and winding construction and the cooling arrangements provided. Accordingly tests were carried out to determine the effects of temperature on the losses and exciting VA. The core was placed in a furnace as shown in Fig. 7.35 and the following provisions made:

(a) the primary excitation winding used has copper wire with a fibreglass sleeve. The melting point of both wire and sleeve were in excess of 400°C.

(b) two thermocouples were used to monitor temperature, one inside the amorphous between the ribbons and the other in the furnace.

The power to the winding was again supplied by the Savage amplifier and the core loss measured with the core temperature set at values between 25°C and 178°C . Fig. 7.36 to 7.40 show the core losses measured for the amorphous material 2605-S2 over a flux density range 0.7 to 1.4 T at frequencies of 50 Hz, 400 Hz, 1 kHz, 2 kHz and 3 kHz respectively. As expected the core loss measured decreased with increasing temperature, for example at 1-T 3 kHz, the measured loss at 36°C was 32 W/kg and at 132° was 29 W/kg. The reduction in core losses will be attributable to the resistivity of the core material increasing with temperature and thereby reducing the eddy current losses.

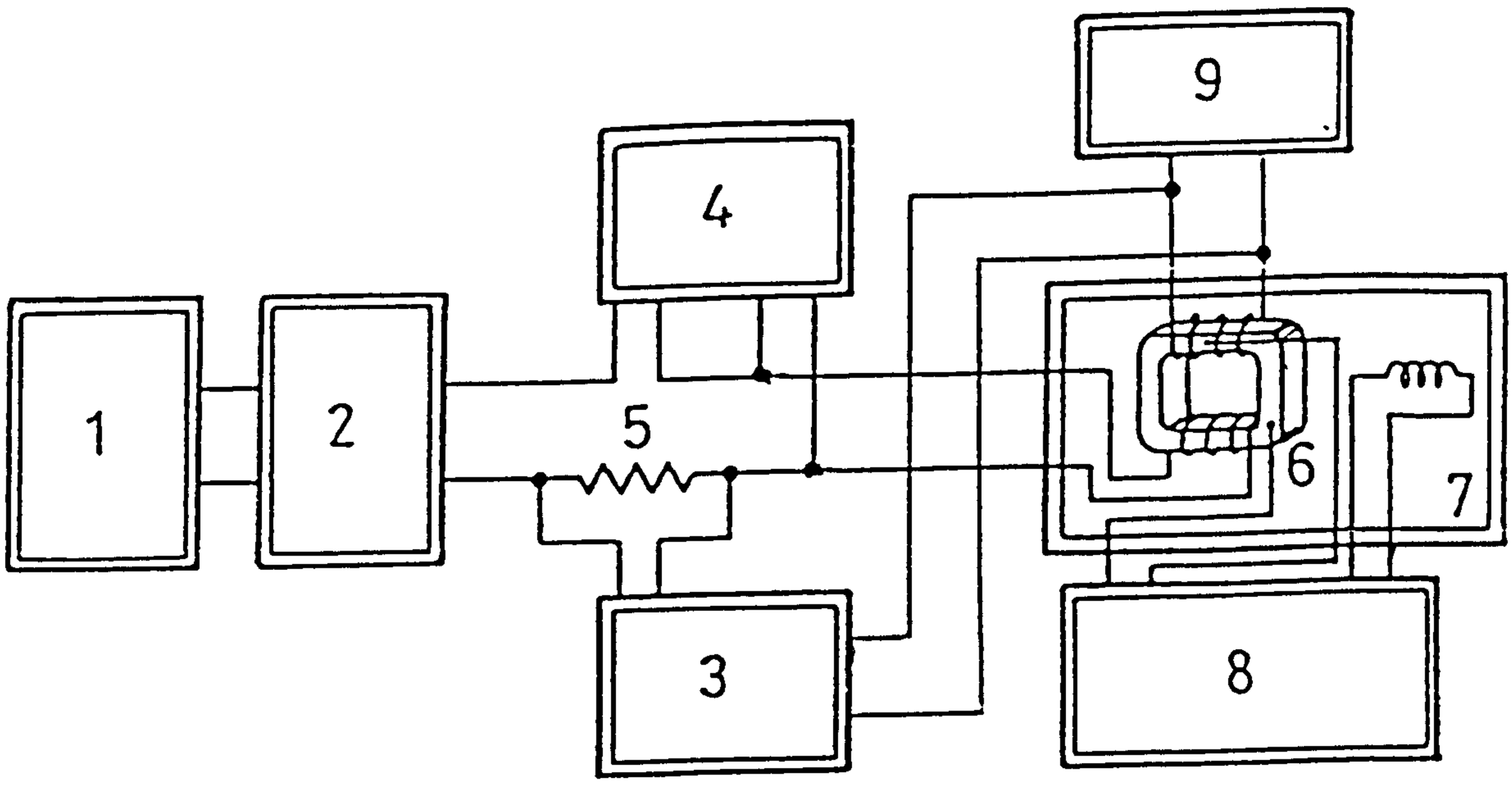

1 - Advance signal generator

2 - Savage amplifier (1.0 kW)

3 - Telequipment oscilloscope DM64

4 - Voltech PM1000 AC power analyser

5 - Current waveform monitoring resistor 2 Ω

6 - Transformer core under test

7 - Inert gas furnace

8 - Electronic thermometer

9 - Avometer model DA116

Fig.7.35 Core loss and exciting power measurement with applied temperature.

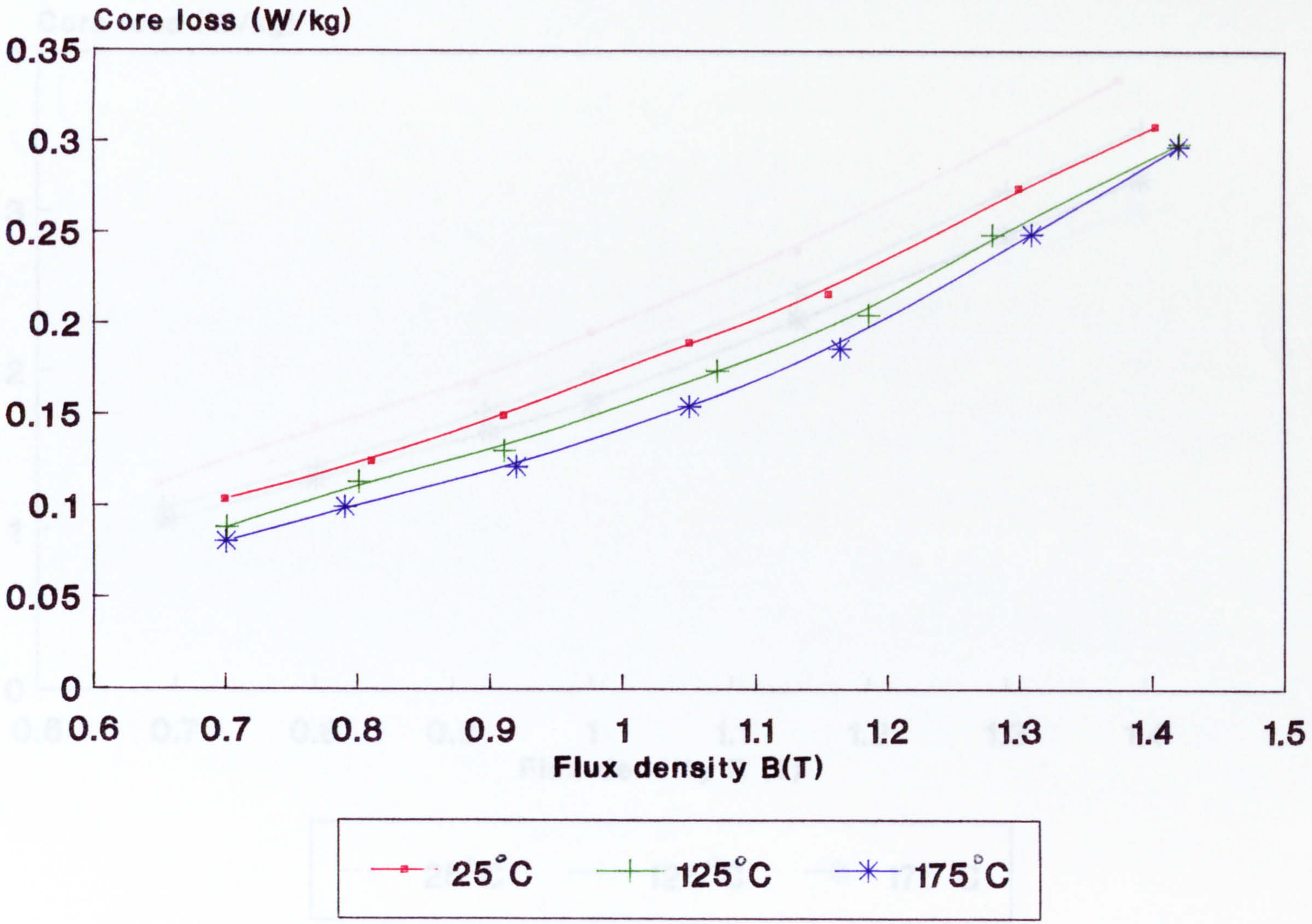

Fig. 7.36 Effect of temperature on core loss of Metglas 2605-S2 at 50 Hz core no.1.

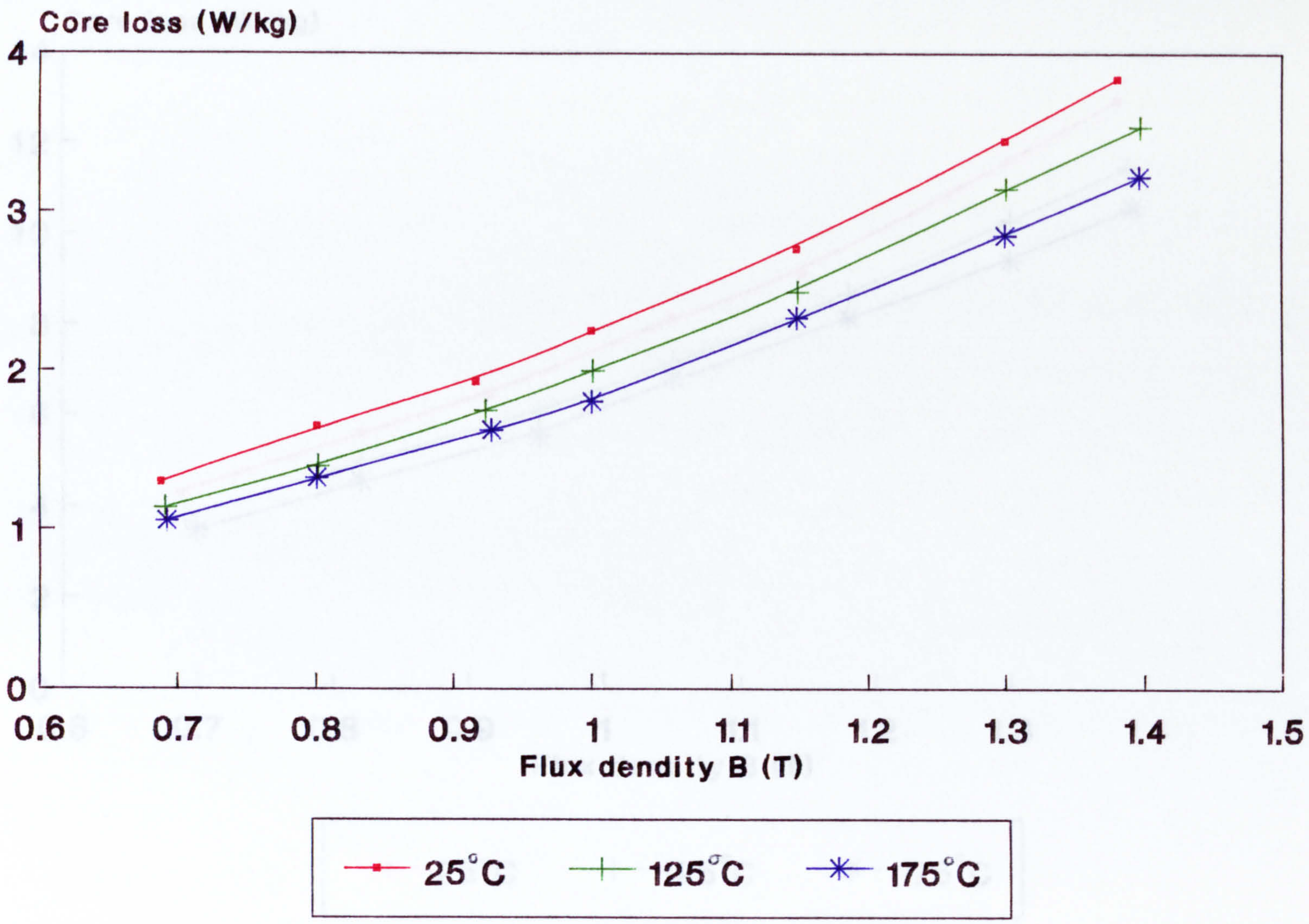

Fig. 7.37 Effect of temperature on core loss of Metglas 2605-S2 at 400 Hz core no.1.

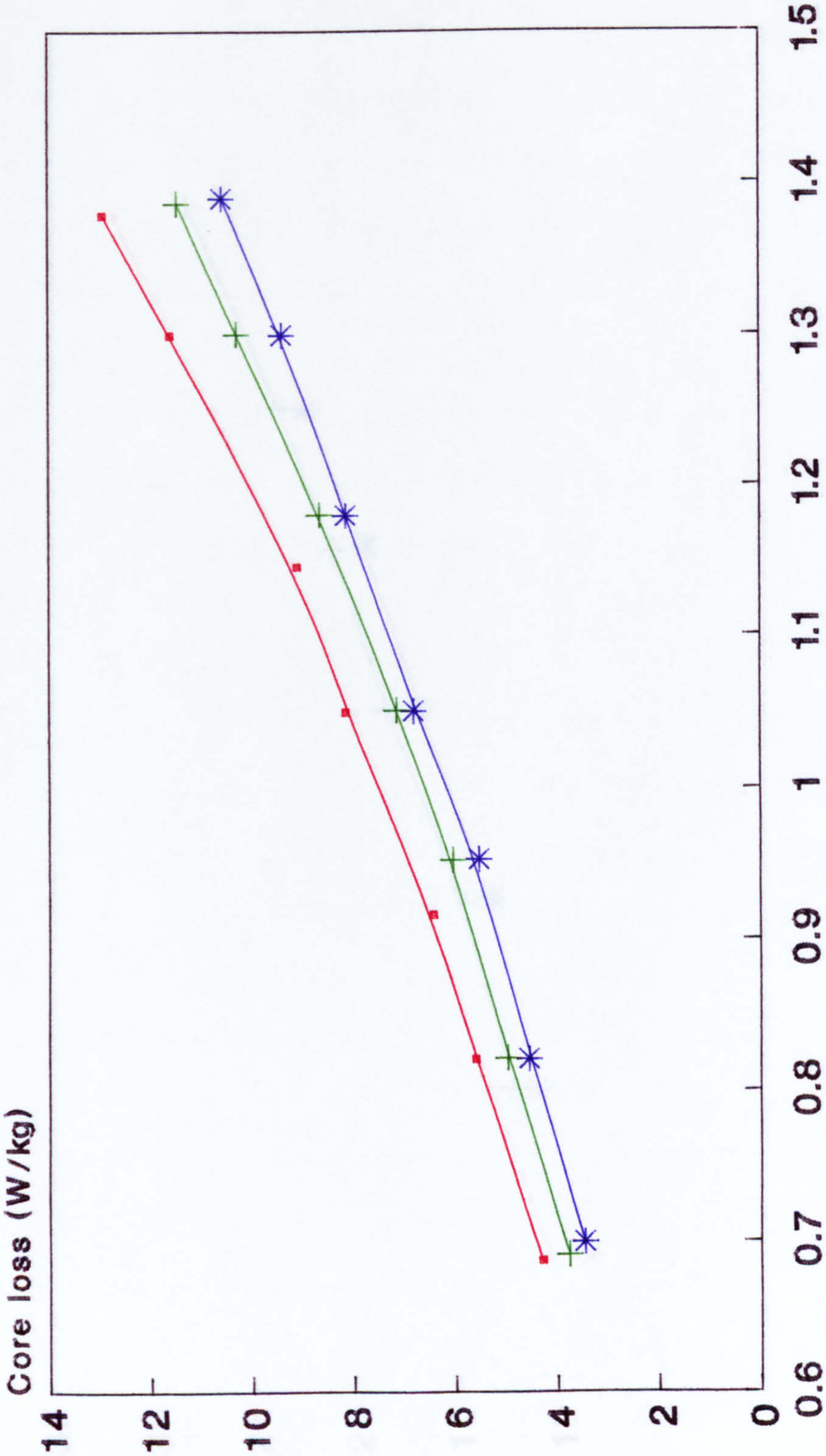

Fig. 7.38 Effect of temperature on core loss of Metglas 2605-S2 at 1000 Hz core no.1.

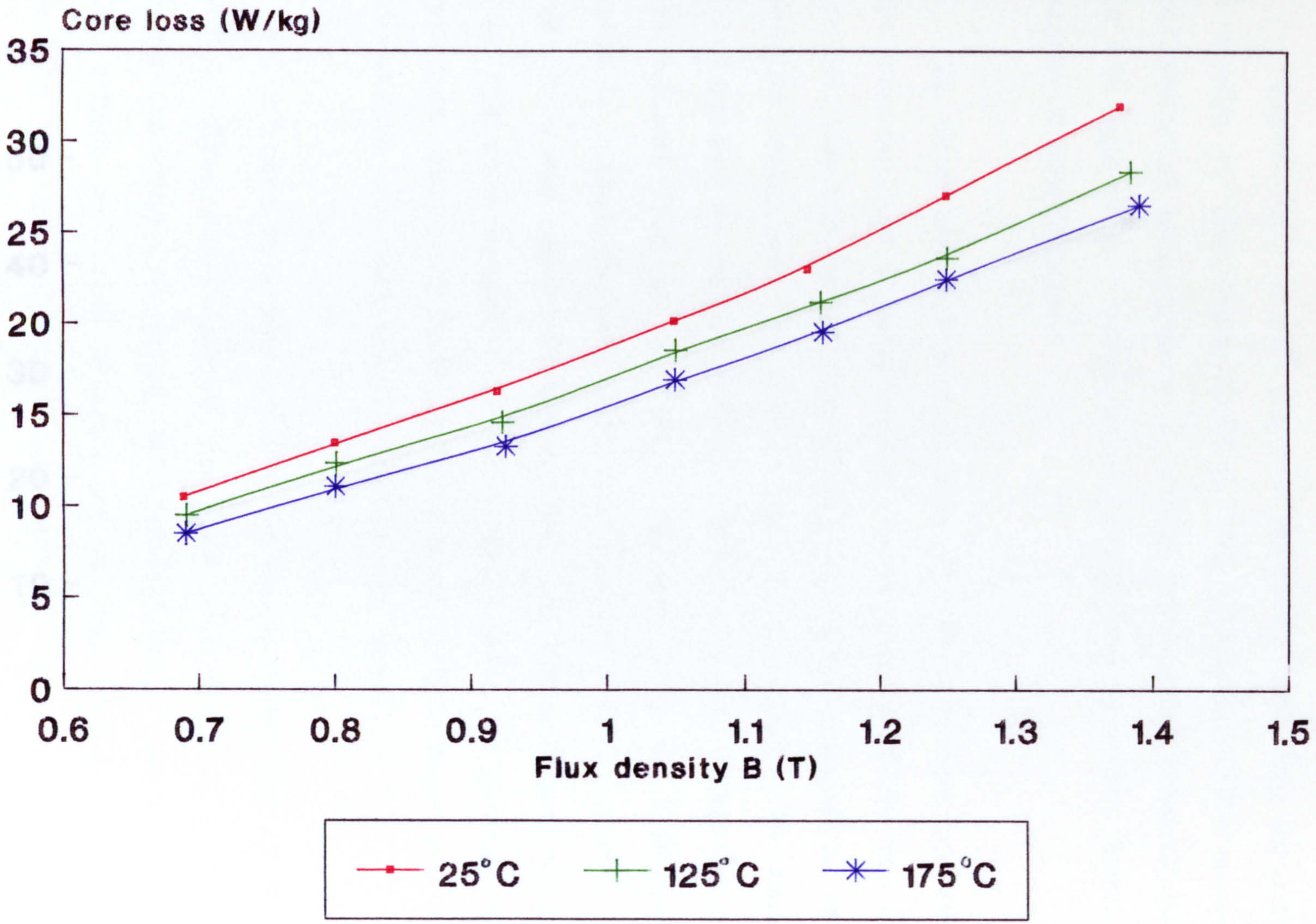

Fig. 7.39 Effect of temperature on core loss of Metglas 2605-S2 at 2000 Hz core no.1.

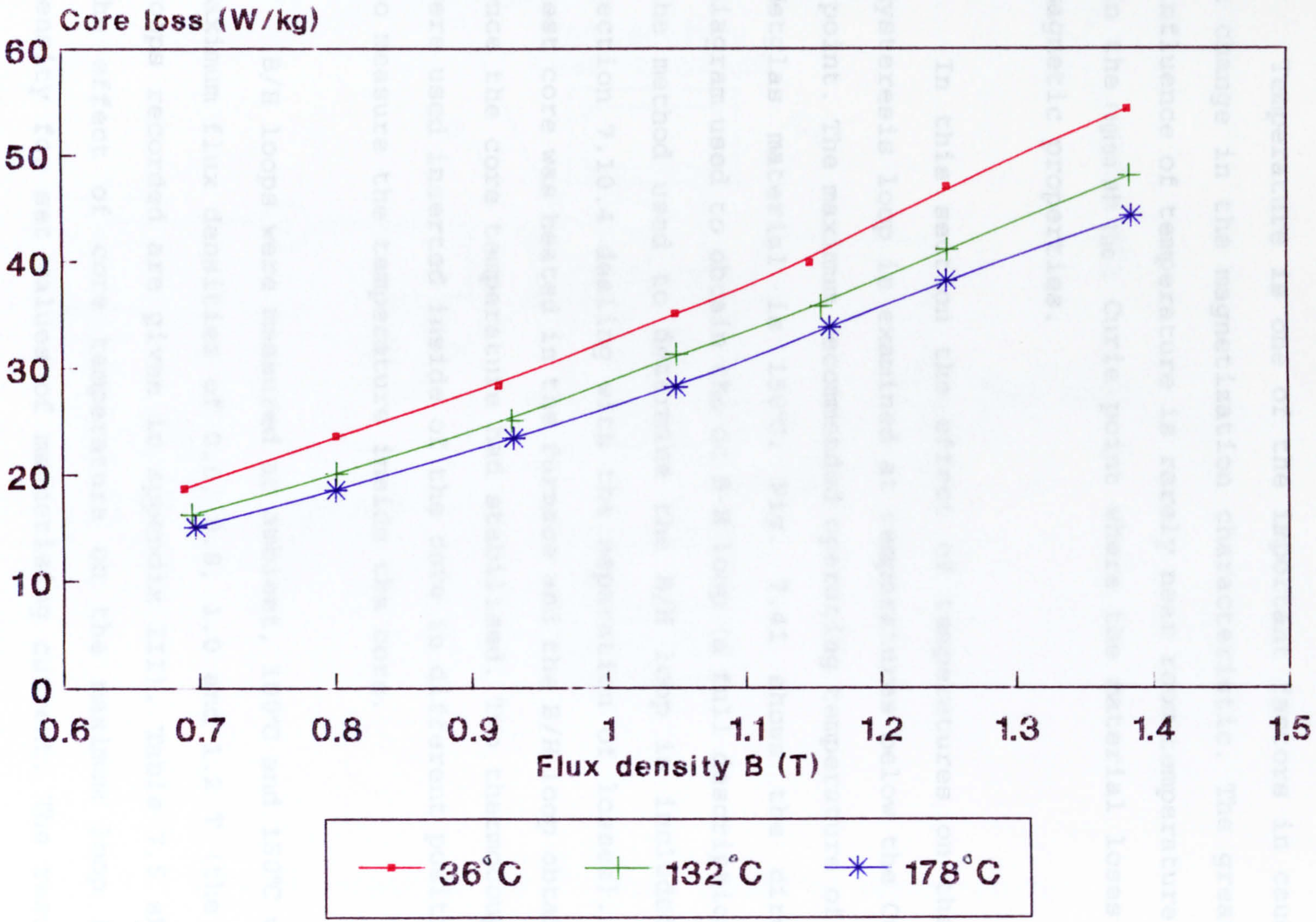

Fig. 7.40 Effect of temperature on core loss of Metglas 2605-S2 at 3000 Hz core no.1.

7.9 Effect of Temperature on Hysteresis Loop Metglas 2605-S2

Temperature is one of the important factors in causing a change in the magnetization characteristic. The greatest influence of temperature is rarely near room temperature but in the region of the Curie point where the material loses its magnetic properties.

In this section the effect of temperatures on the DC hysteresis loop is examined at temperatures below the Curie point. The maximum recommended operating temperature of the Metglas material is 150°C. Fig. 7.41 shows the circuit diagram used to obtain the dc B-H loop (a full description of the method used to determine the B/H loop is included in section 7.10.4 dealing with the separation of losses). The test core was heated in the furnace and the B/H loop obtained once the core temperature had stabilised. Two thermocouples were used inserted inside of the core in different positions to measure the temperature inside the core.

B/H loops were measured at ambient, 100°C and 150°C with maximum flux densities of 0.6, 0.8, 1.0 and 1.2 T (the B/H loops recorded are given in appendix III). Table 7.5 shown the effect of core temperature on the maximum loop flux density for set values of magnetising current. The results show that the loop area sligthly decreases with increase the core temperature.

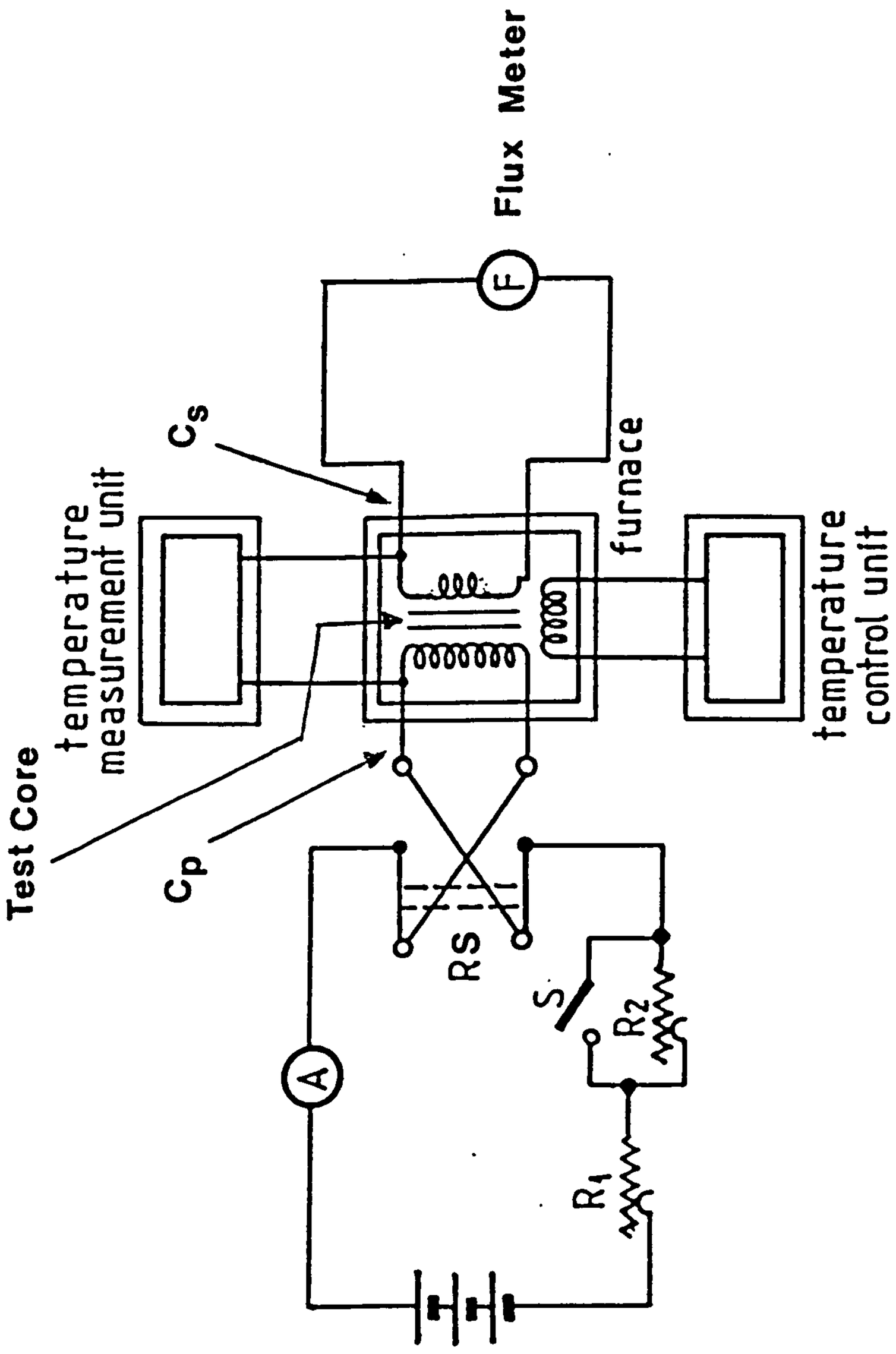

Fig. 7.41 Circuit diagram for finding effect of temperature on hysteresis loop.

	Maximum loop flux density			
B_{max} Ambient	0.6	0.8	1.0	1.2
B_{max} 100°C	0.58	0.78	0.97	1.15
B_{max} 150°C	0.56	0.74	0.92	1.06

Table 7.5 Effect of core temperature on the maximum loop flux density for set values of magnetising current.

If the same magnetising force used at ambient temperature to establish a particular value of B_{max} was maintained, an increase in core temperature results in a reduction of B_{max} and similarly the remanent flux density B_r. If the same peak flux densities had been maintained the magnetising current would need to be increased as core temperature increased.

7.10 Separation of Core Losses

7.10.1 Core Loss Components

The losses in transformer cores fall into the categories of hysteresis and eddy current loss. The eddy current loss is taken to include the classical eddy loss plus the additional anomalous eddy current loss. A brief description of these losses and their dependencies are given in chapter 4. For the core designed and tested it will be useful to determine the magnitudes of each component loss. The next section outlines some of the methods which may be used for their separation.

7.10.2 Separation of Losses

There are a number of ways to separate the hysteresis loss from the eddy current (future references to eddy current loss in this section will refer to the sum of the classical eddy current loss and the anomalous eddy current loss). For the purposes of this research absolute accuracy in the separation is not essential, only an indication of the

magnitude of the eddy current loss is required to assess whether interturn insulation of the ribbon is necessary.

The loss separation has been obtained by measurement of the B/H loop area. The hysteresis loop was found by exciting the core with DC current, so that virtually no eddy currents were generated to produce extra loss. As shown previously the net energy delivered to the material per unit volume will be equal to the area contained within the hysteresis loop for one traverse of that loop.

The ac hysteresis loss P_1 at any frequency f_o, core volume $V(m^3)$ and loop area $A_{BH}(Joule/m^3)$ for a particular maximum flux density, may then be calculated using :

$$P_1 = A_{BH} V f_o \qquad (7.14)$$

The eddy current loss component P_2 may now be obtained from the difference between the measured no-load losses P and the hysteresis loss as determined using hysteresis loop, P_1

$$P_2 = P - P_1 \qquad (7.15)$$

7.10.3 Determination of Hysteresis loop DC Method

The circuit used to measure the B/H loop is shown in Fig. 7.42. The core under test was wound with two coils. Coil C_p

was connected to the battery source via resistors R_1, R_2, switch S and the reversing switch RS. The resistance R_1 was used to adjust the maximum current value setting corresponding to the peak induction and R_2 to set an intermediate current level below the maximum. The other coil C_s was connected to a fluxmeter F which provides a measure of the flux change when the switch S or RS were operated to change the current in the coil P. Using the above arrangement B/H loops were obtained for Metglas 2605-S2 and 2605-S3A for peak flux densities of 0.6, 0.8, 1.0, 1.2-T. Using a Bitpad digitiser to obtain (x,y) co-ordinates of various points around the B/H loop . The area within the loop was calculated using a Fortran program (see appendix IV)

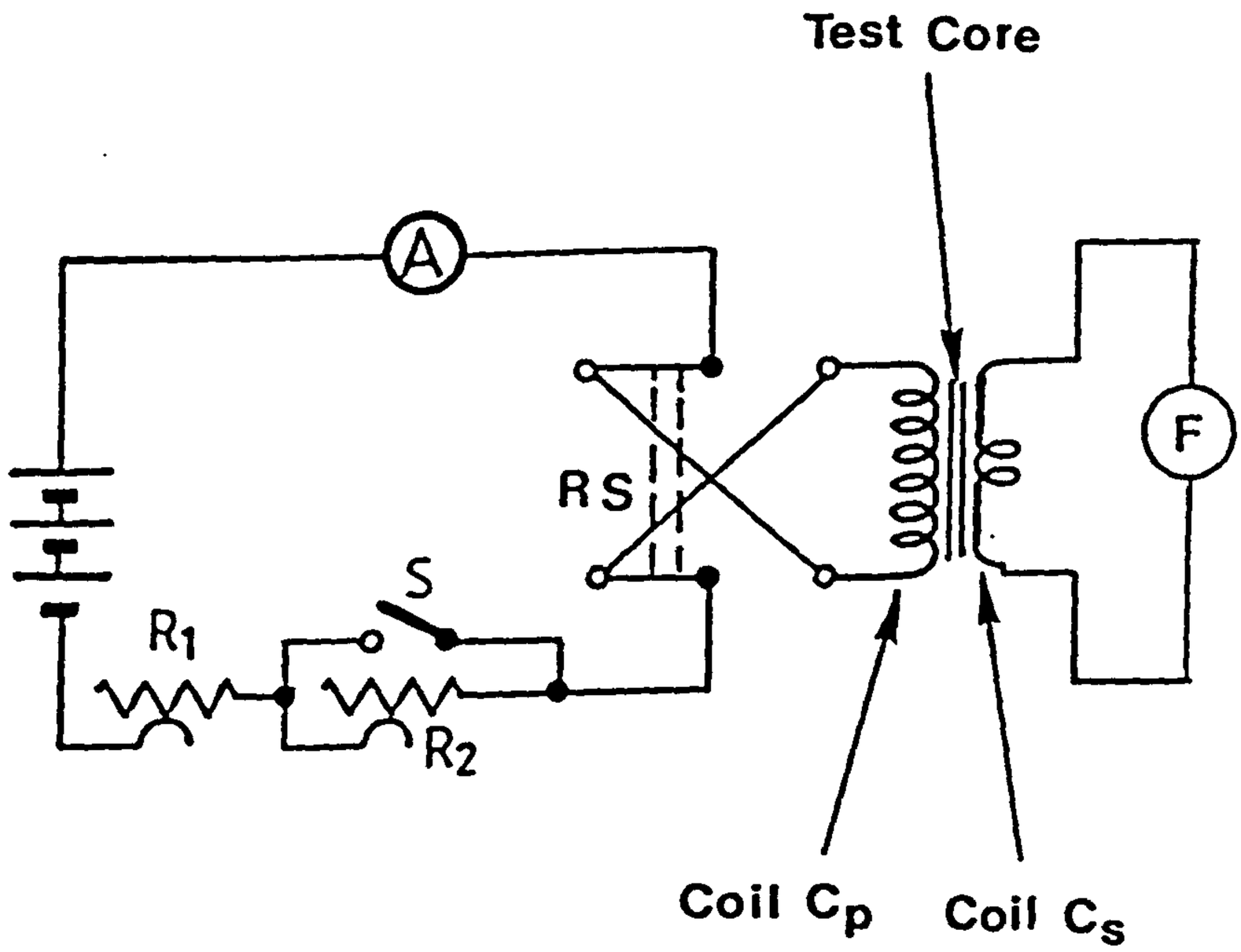

Fig.7.42 Circuit diagram for determination of hysteresis loop.

7.10.4 Oscilloscope Display of Hysteresis Loop [123]

The hysteresis loop can also be displayed on an oscilloscope, the trace is called Lissajous figure. With reference to the circuit diagram shown in Fig. 7.43 voltage V_y, which is proportional to the flux density B, is applied to the oscilloscope Y-plate and voltage V_x which is proportional to H, is applied to the X-plates. Again the core under test was wound with two coils, the primary C_p and secondary C_s winding. The magnetising current i_1 provides a voltage drop V_x across the resistor R_s proportional to the magnetising force H

$$V_x = i_1 R_s \tag{7.16}$$

$$Hl = i_1 N_1 \tag{7.17}$$

$$i_1 = \frac{Hl}{N_1} \tag{7.18}$$

Therefore

$$V_x = \frac{R_s lH}{N_1} \tag{7.19}$$

The secondary winding C_s induced voltage V_2 is proportional to the rate of change of the core flux. For the propose of the

B/H loop a voltage proportional to the flux or the flux density was needed. An integrating network consisting of R and C was employed to obtain a voltage V_y which was proportional to ϕ or B.

For the secondary winding of the transformer core:

$$V_y = \frac{1}{C}\int i_2 dt, \qquad i_2 = \frac{V_2}{R} \quad if \quad \frac{1}{\omega C} \ll R$$

$$V_y = \frac{1}{CR}\int V_2 dt \tag{7.20}$$

but

$$V_2 = N_2 \frac{d\phi}{dt} \tag{7.21}$$

so

$$V_y = \frac{N_2}{RC}\int \frac{d\phi}{dt} dt \tag{7.22}$$

$$V_y = \frac{N_2}{RC}\phi \tag{7.23}$$

The frequency of the supply voltage V_1 determines the speed of the tracing spot on the screen which at 50 Hz or above was fast enough for the human observer to have the impression of a static display. However the displayed loop

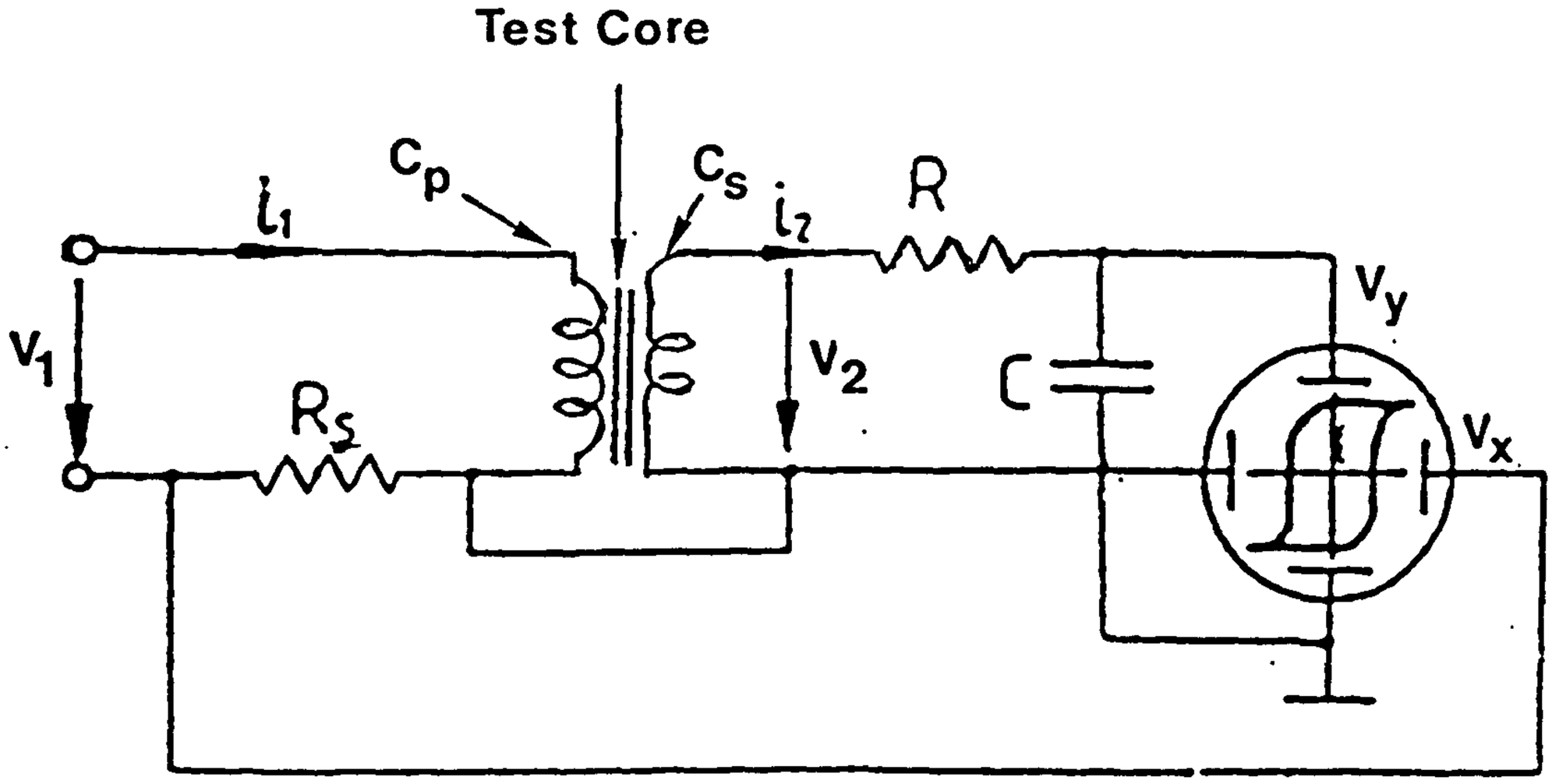

Fig. 7.43 Oscilloscope display of B/H loop.

will include not only a component current associated with the hysteresis loss but also a component of current associated with the eddy current loss. The accuracy of the displayed loop compared with the actual B/H loop will therefore depend on the magnitude of the eddy current loss. Since the eddy current loss depends on the square of the supply frequency, the loop accuracy will therefore deteriorate as the frequency increases.

The B/H loops obtained by this method were therefore only useful in a very limited way, in fact the change in loop shape with increasing frequency may be attributed to the increase of the eddy current loss. The oscillograms obtained at frequencies between 50-Hz and 3-kHz and peak flux densities between 1-T are shown in the appendix V.

7.10.5 Results of Core Loss Separation

The separation of core losses used the method outlined in section 7.10.2 by measurement of the total core loss when excited with a.c and a derived measurement of the hysteresis loss obtained from the d.c B/H loop. The losses at frequencies of 50, 400-Hz, 1, 2 and 3-kHz for a range of peak flux densities from 0.7 to 1.4 T are given in Fig. 7.44 to 7.48 for the alloy 2605-S2. Table 7.6 enables a comparison to be made of the hysteresis and eddy current loss sustained at 1-T for frequencies of 50-Hz to 3-kHz. The eddy current loss at 3-kHz for Metglas 2605-S2 does indicate a need to consider

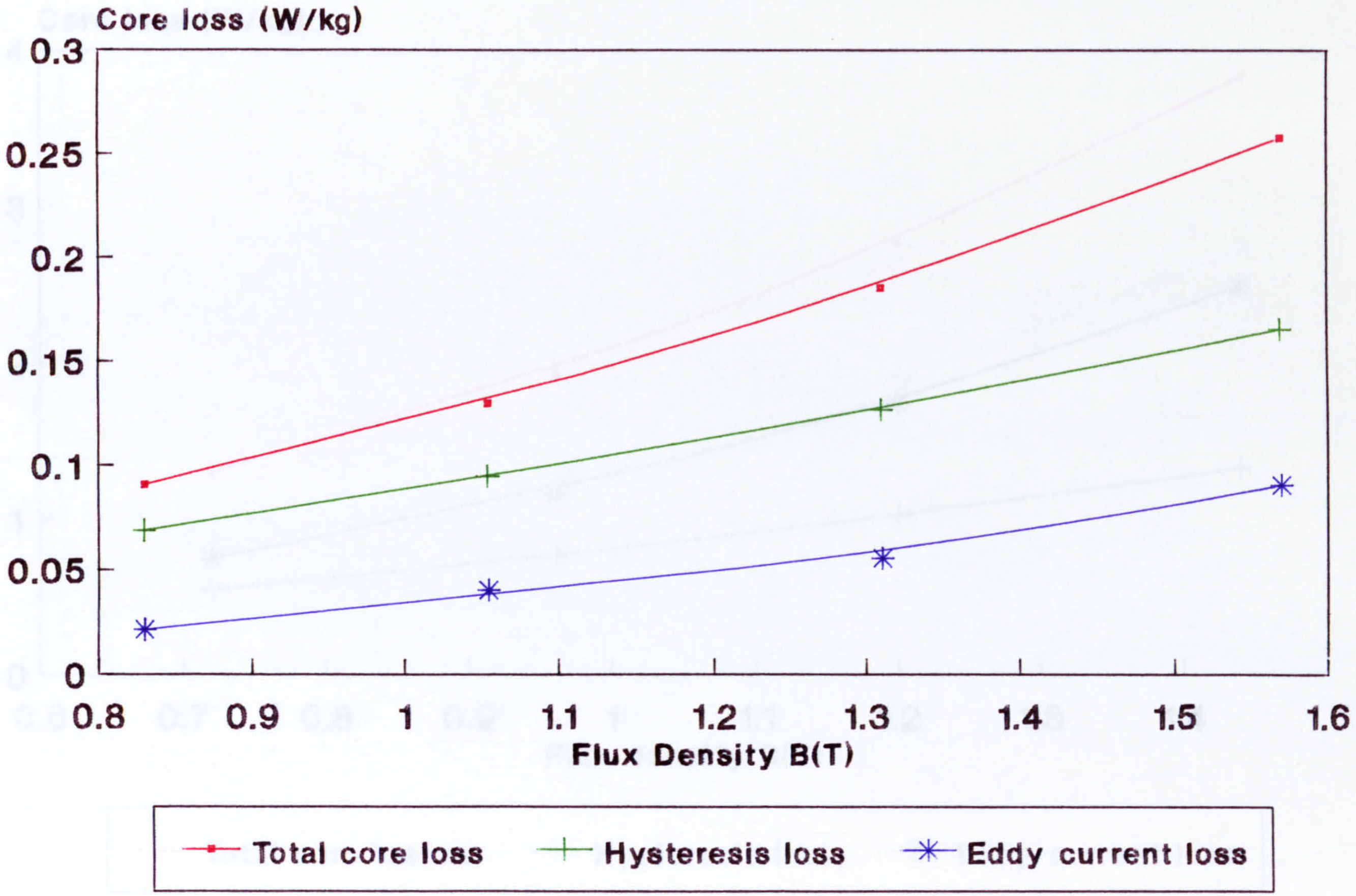

Fig. 7.44 Separation of core losses amorphous material 2605-S2 DC method (hysteresis loop)at 50 Hz core No.1

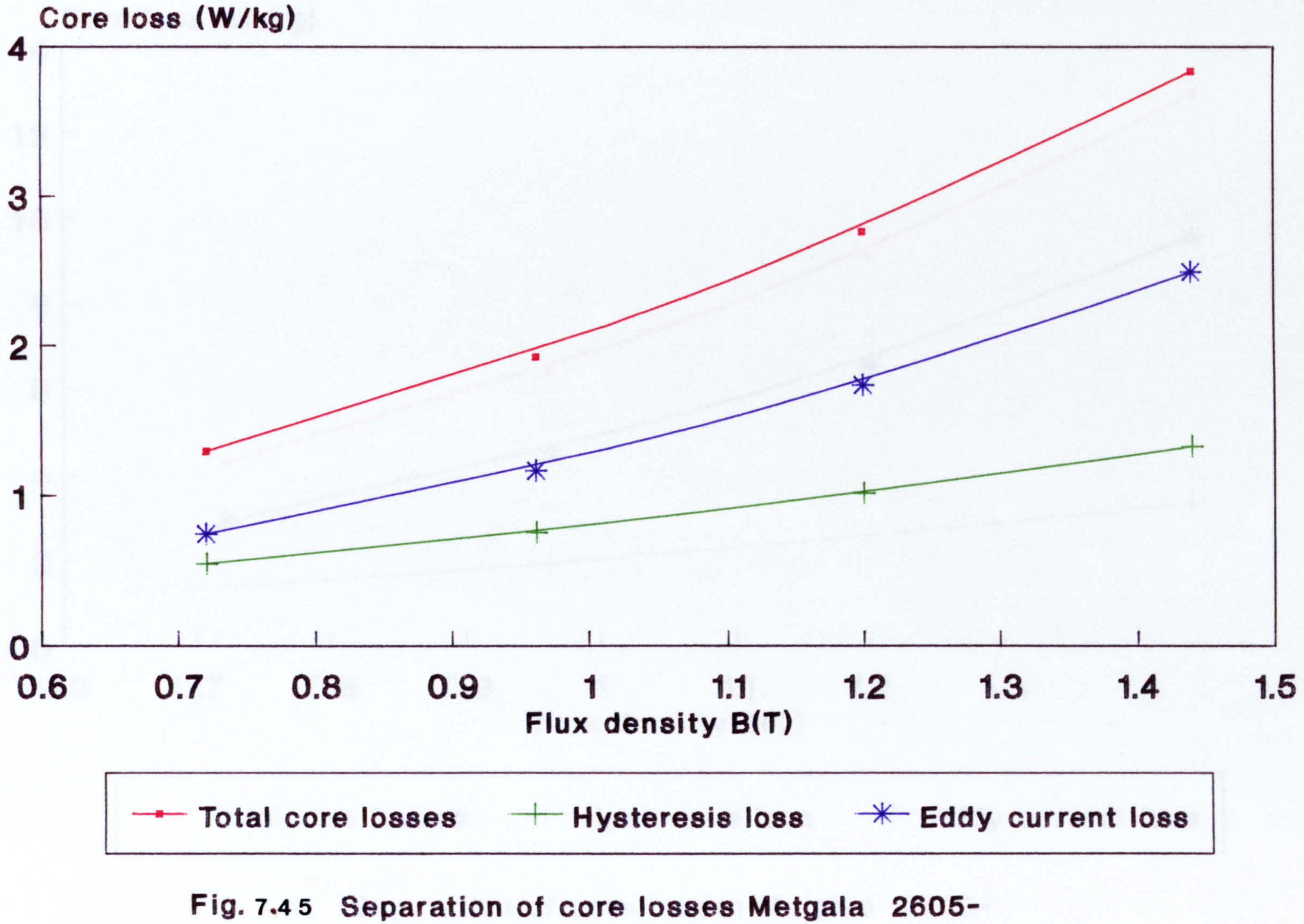

Fig. 7.45 Separation of core losses Metgala 2605-S2 DC method (hysteresis loop) at 400Hz core No.1.

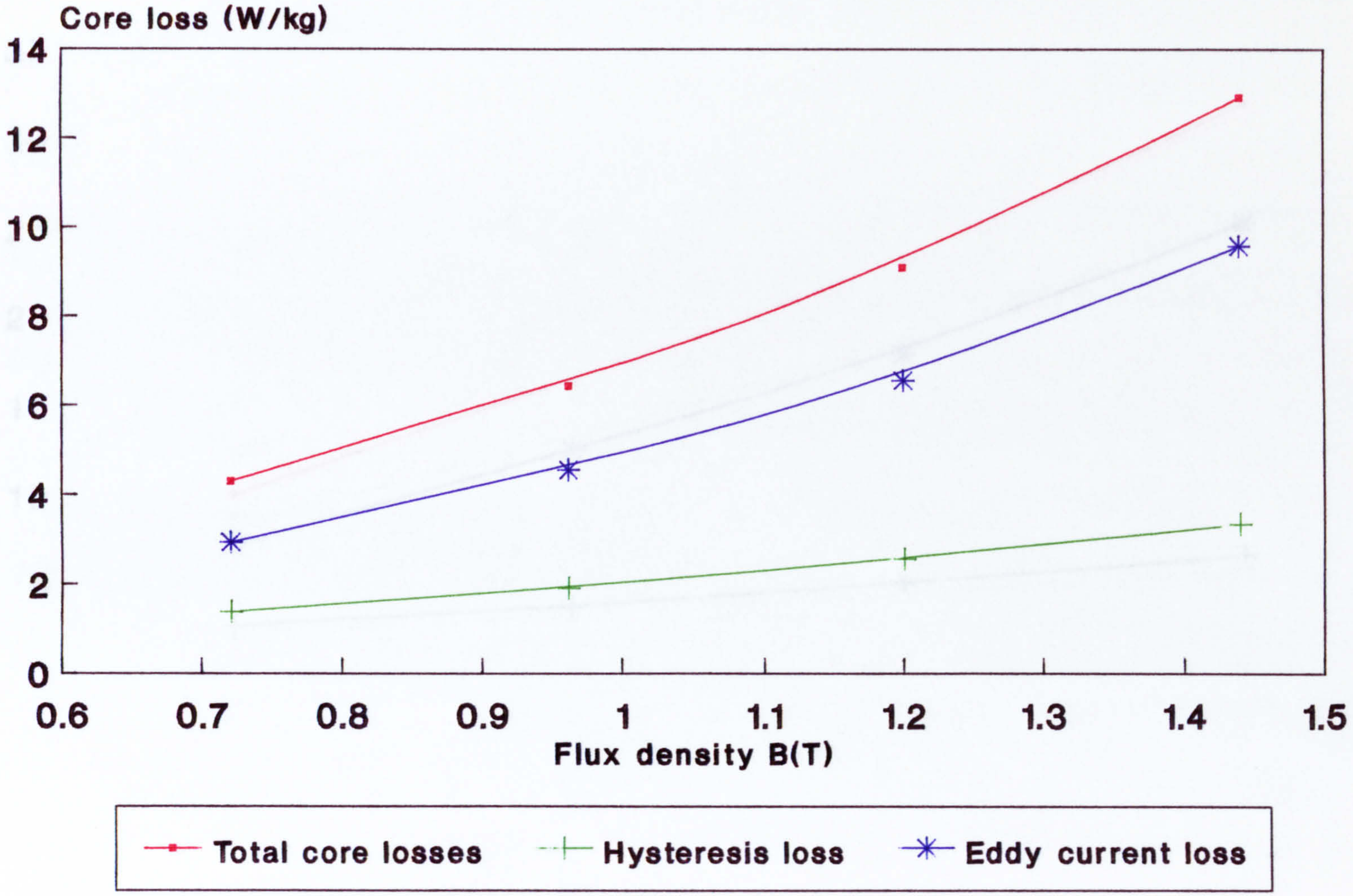

Fig. 7.46 Separation of core losses Metglas 2605-S2 DC method(Hysteresis loop) at 1000Hz core No.1.

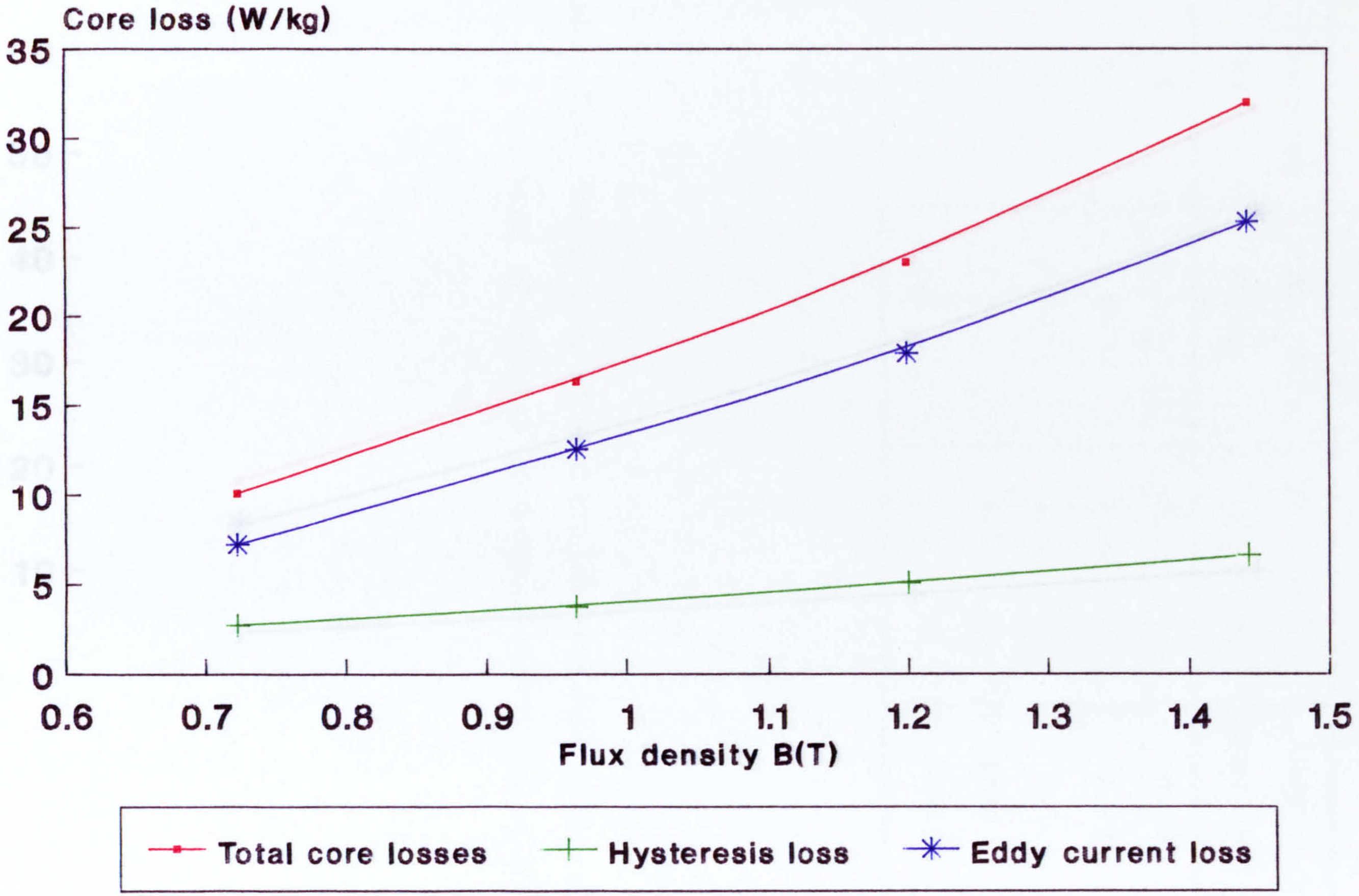

Fig. 7.47 Separation of core losses Metglas 2605-S2 DC method(Hysteresis loop) at 2000Hz core No.1.

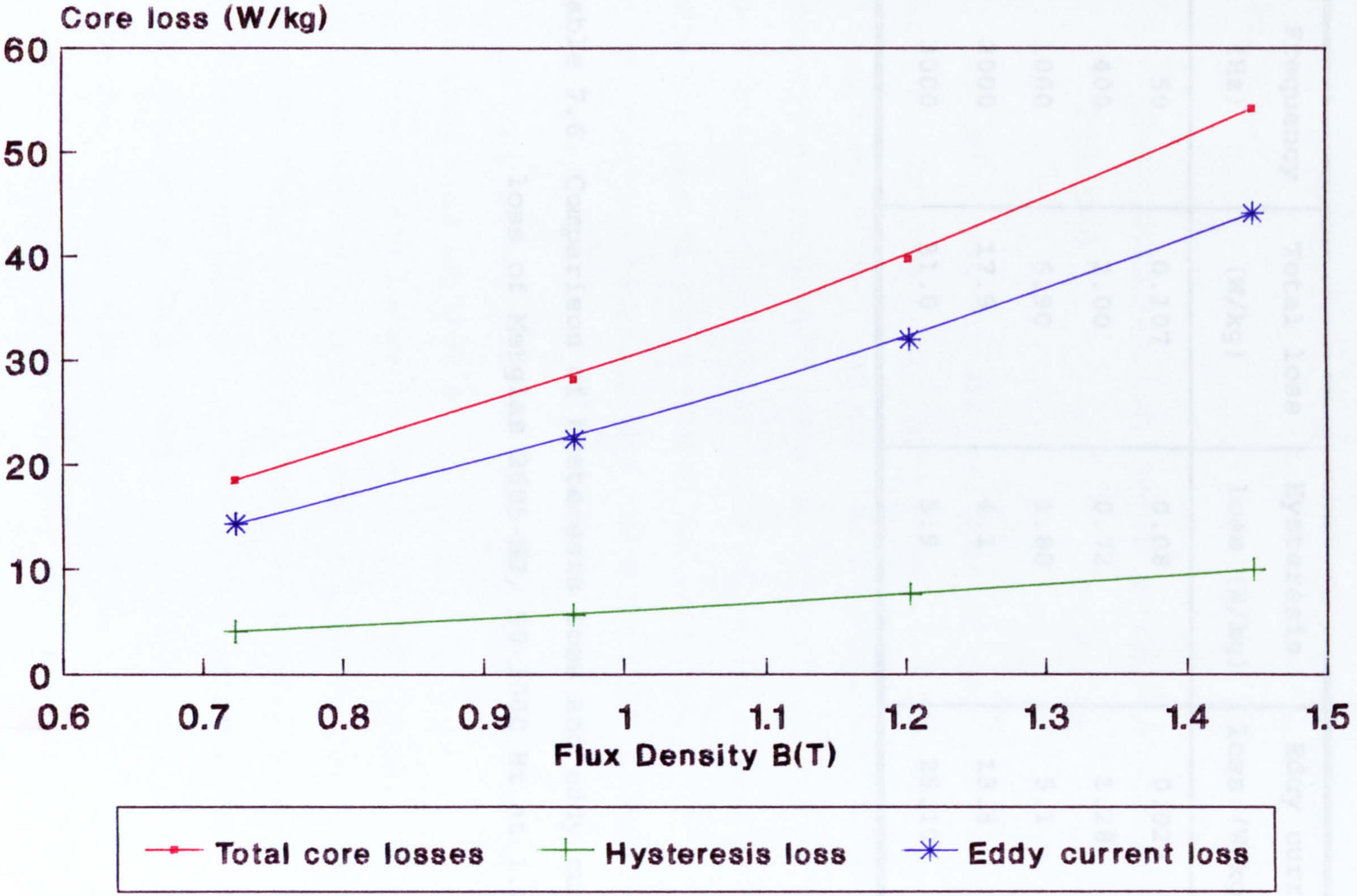

Fig. 7.48 Separation of core losses Metglas 2605-S2 DC method(Hysteresis loop) at 3000Hz core No.1.

Frequency (Hz)	Total loss (W/kg)	Hysteresis loss (W/kg)	Eddy current loss (W/kg)
50	0.107	0.08	0.027
400	2.00	0.72	1.28
1000	6.90	1.80	5.1
2000	17.9	4.1	13.8
3000	31.0	5.9	25.10

Table 7.6 Comparison of hysteresis loss and eddy current loss of Metglas 2605-S2, 50-3000 Hz at 1.0T.

the provision of insulation between the layers of ribbon. However provision of insulation between the layers of ribbon will seriously affect the core space factor, particularly so with a large number of turns of very thin ribbon making up the core.

7.11 Comparison the B/H Loop of Metglas 2605-S2 with 2605-S3A

The B/H loops for Metglas 2605-S2 and 2605-S3A measured using the dc loop method with a peak flux density of 1-T are illustrated in Fig. 7.49 and 7.50 respectively. The following comparison may be made from the loops:

a) at the peak flux density, the magnetising forces were 2.4 AT/m for 2605-S2 and 8.6 AT/m for 2605-S3A.

b) the coercive force was 0.94 AT/m for 2605-S2 and 1.48 AT/m for 2605-S3A

c) the loop area of the Metglas 2605-S3A is slightly greater than loop area of 2605-S2

According to the data provided by Allied Signal, the peak and the coercive magnetising force is greater for 2605-S2 than 2605-S3A. It is very likely that the annealing cycle used was not correct for the optimum conditions of small loop area and high saturation flux density. The B/H loop for 2605-S3A indicates that a peak saturation density of less than 1-T would be appropriate to minimise the magnetising current.

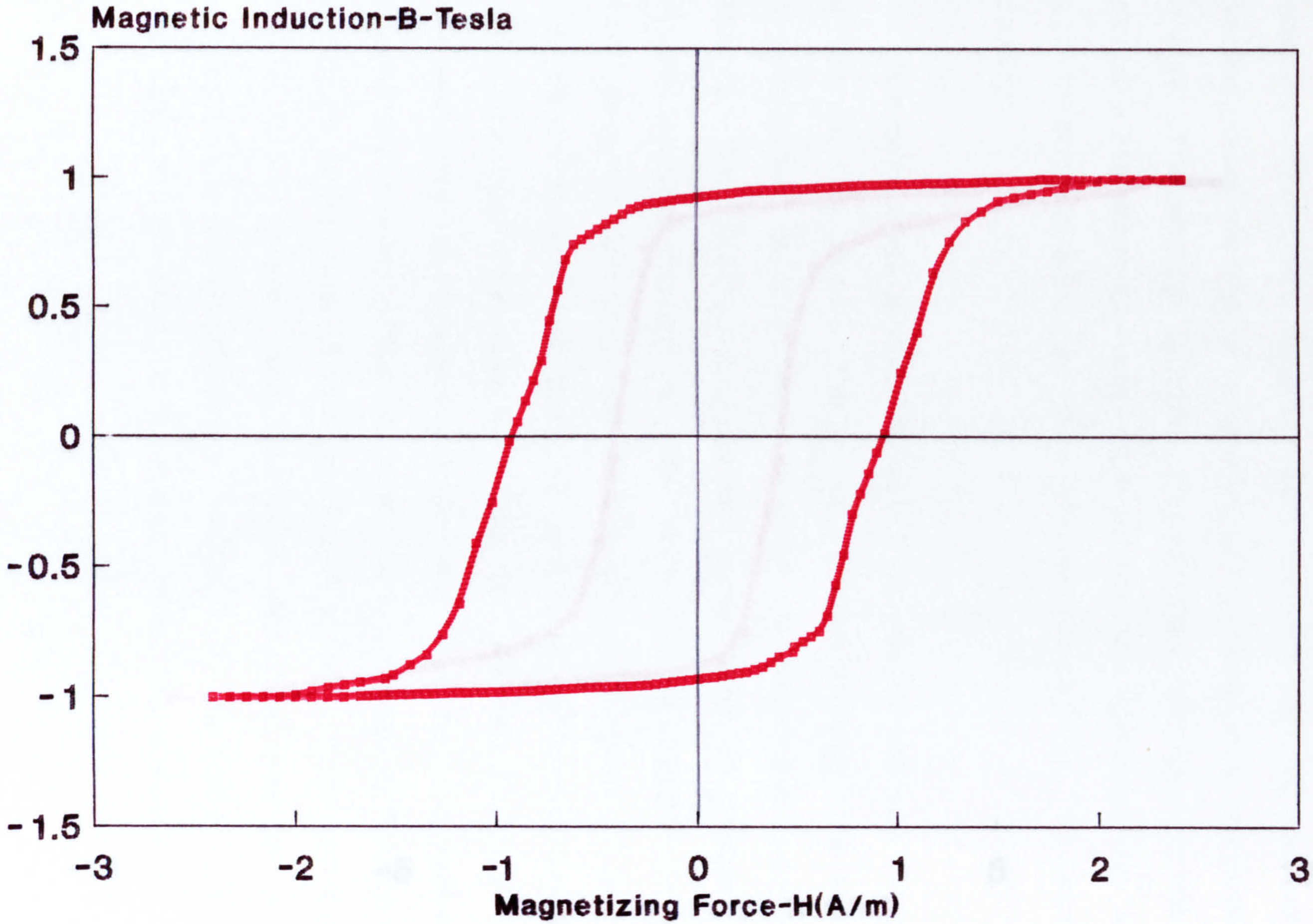

Fig. 7.49 B/H loop of Metglas 2605-S2 at flux density 1.0 T at ambient temperature.

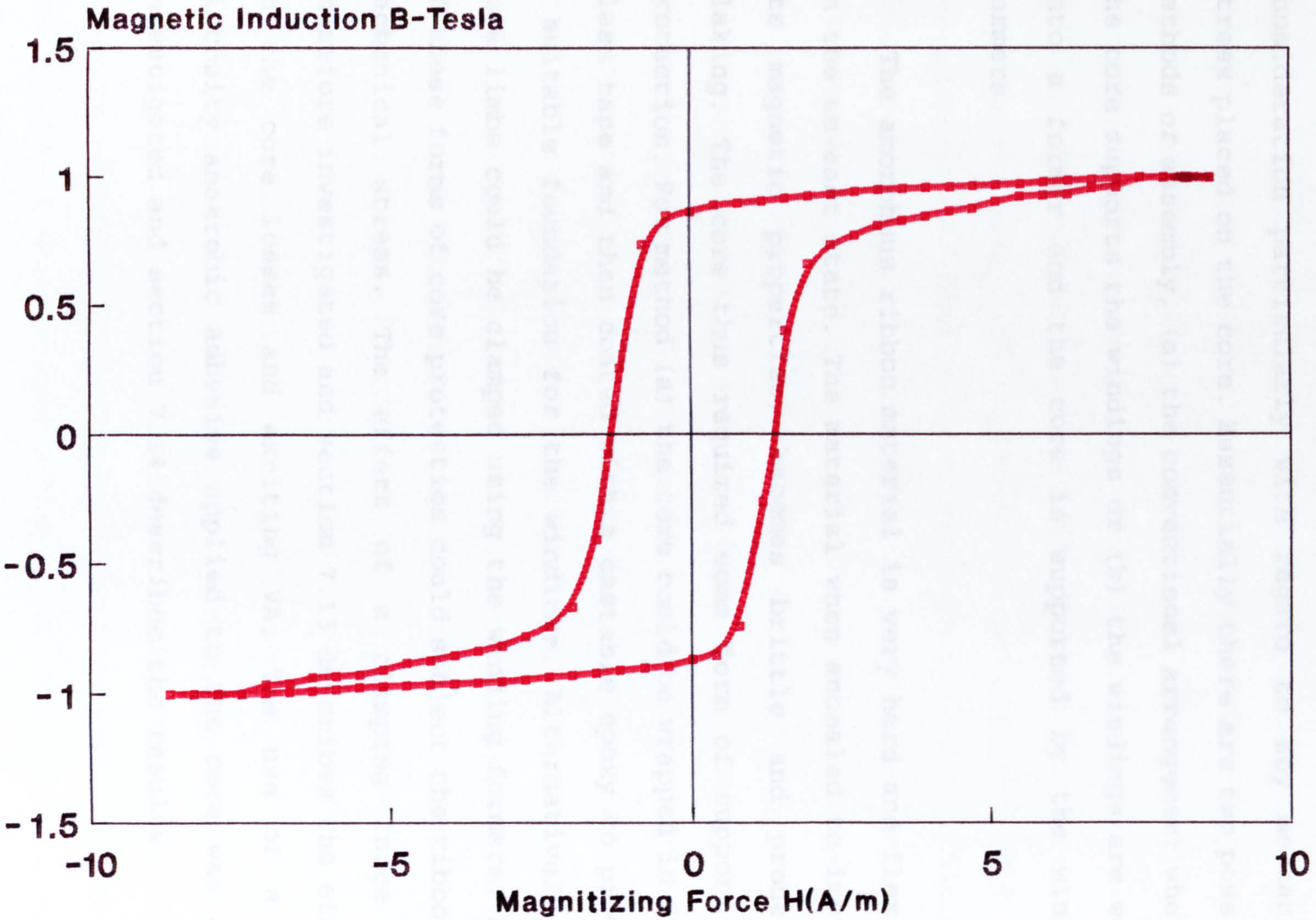

Fig. 7.50 B/H loop of Metglas 2605-S3A at ambient temperature flux density 1.0 T.

7.12 Core Protection Postanneal

The method of assembly of core and winding needs careful consideration particularly with regard to any mechanical stress placed on the core. Essentially there are two possible methods of assembly, (a) the conventional arrangement whereby the core supports the windings or (b) the windings are wound onto a former and the core is supported by the winding formers.

The amorphous ribbon material is very hard and flexible in the as-cast state. The material when annealed to improve its magnetic properties, becomes brittle and prone to flaking. The core thus required some form of support and protection. For method (a) the core could be wrapped in fibre glass tape and then coated with a castable epoxy to provide a suitable foundation for the windings. Alternatively the core limbs could be clamped using the winding formers. Both of these forms of core protection could subject the ribbon to mechanical stress. The effect of a clamping force was therefore investigated and section 7.13 describes the effect on the core losses and exciting VA. The use of a low viscosity anaerobic adhesive applied to the core was also investigated and section 7.14 describes the results.

7.13 Effect of Clamping Pressure on the Core Losses

After annealing, the core will need to be mechanically protected due to the brittle nature of the ribbon. Whatever the method used for core protection and coil support, some pressure will inevitably be applied to the core. Previous investigations (see chapter 4.4) have shown that the losses and exciting VA were subject to change when the ribbon material was subjected to mechanical stress. A simple test was therefore devised to apply pressure to the core limbs as shown in Fig. 7.51. The core rests on a table (not shown) and pressure was applied to both limbs by the hook and weights. The pressure applied was therefore similar to clamping the core limbs. The losses and exciting VA were measured using windings wound onto the core yokes. The core loss results for applied pressures of 0, 2.8 psi (19.3 kN/m^2) and 5.6 psi (38.6 kN/m^2) are given in appendix VI. It was is apparent from the results that the effect on core loss was almost negligible, the inaccuracies associated with the measurement would have been of the same order as the differences recorded.

The effect of the applied clamping pressure on the exciting VA was much more pronounced and the results are illustrated in Fig. 7.52 to 7.56 for flux densities in the range 0.2 to 1.4 T for frequencies of 50, 400-Hz, 1, 2 and 3-kHz. The increase was particularly noticeable at flux density levels above 0.8-T, for example at 1.4 - T, 1 - kHz, the

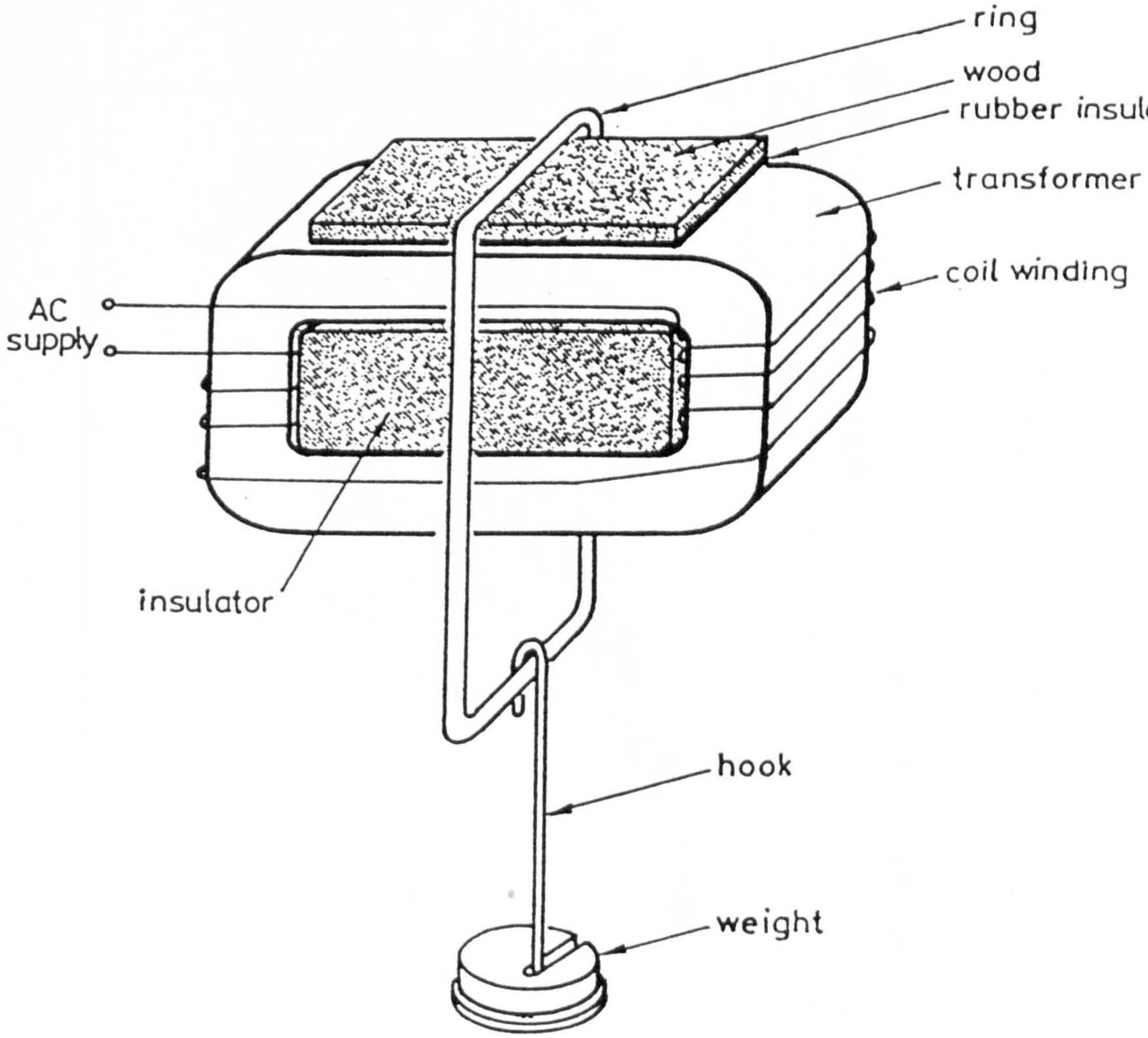

Fig. 7.51 Method of applying pressure to the core limbs.

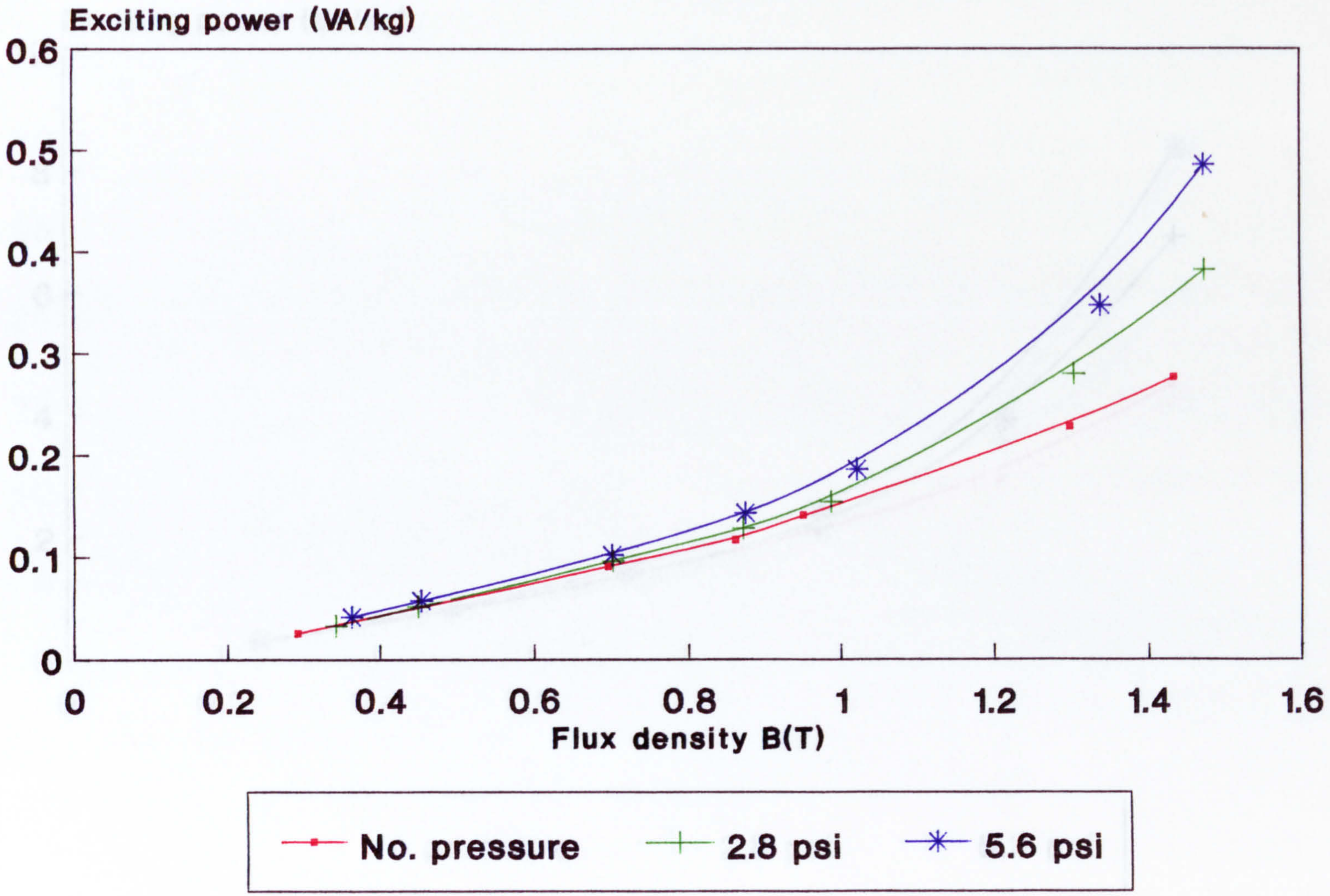

Fig. 7.52 Exciting power sensitivity of Metglas 2605-S2 with pressure 0, 2.8 and 5.6 psi at 50 Hz core No.1.

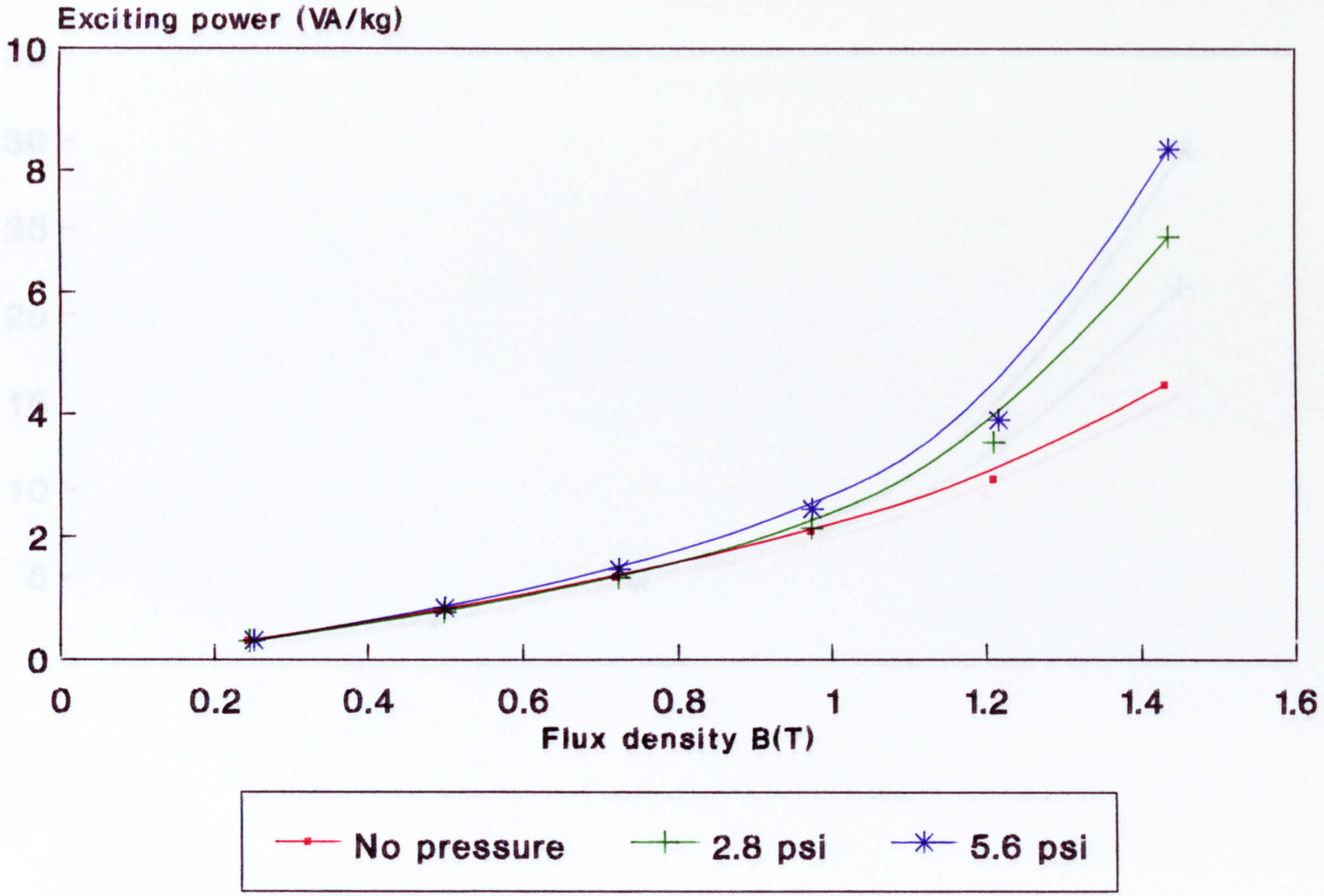

Fig. 7.53 Exciting power sensitivity of Metglas 2605-S2 with pressure 0, 2.8 and 5.6 at 400 Hz core No.1.

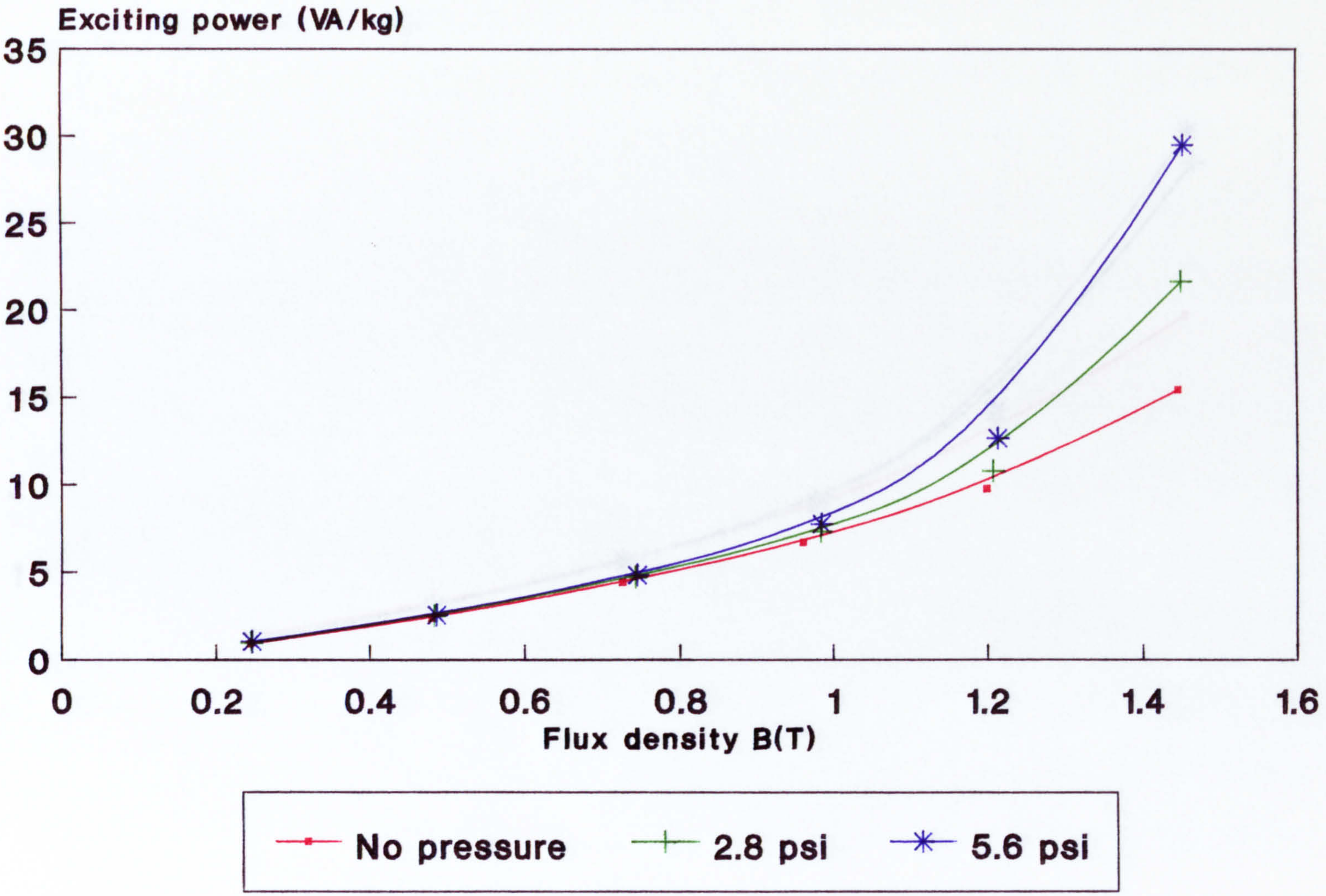

Fig. 7.54 Exciting power sensitivity of Metglas 2605-S2 with pressure 0, 2.8 and 5.6 psi at 1000 Hz core No.1.

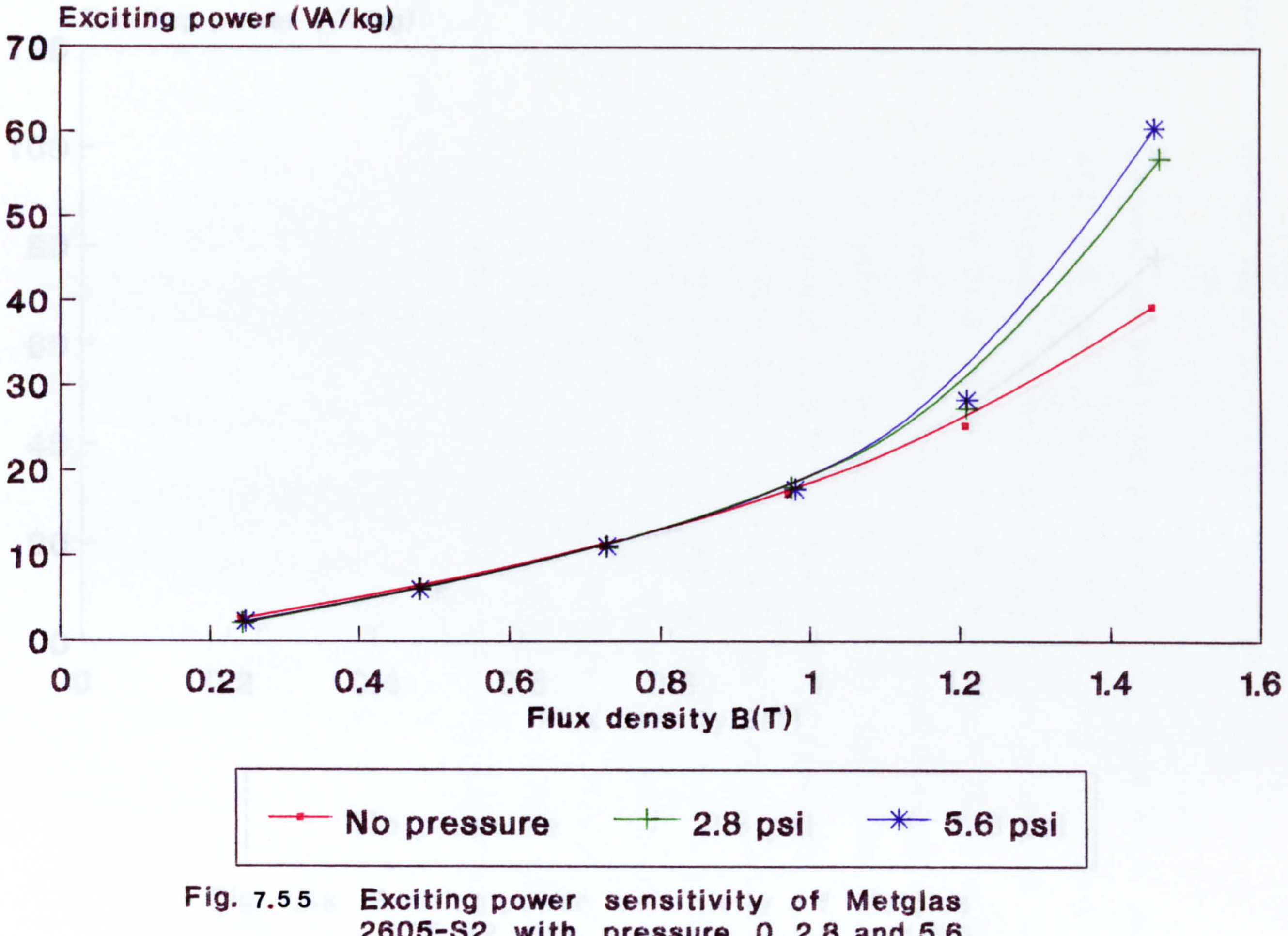

Fig. 7.55 Exciting power sensitivity of Metglas 2605-S2 with pressure 0, 2.8 and 5.6 psi at 2000 Hz core No.1.

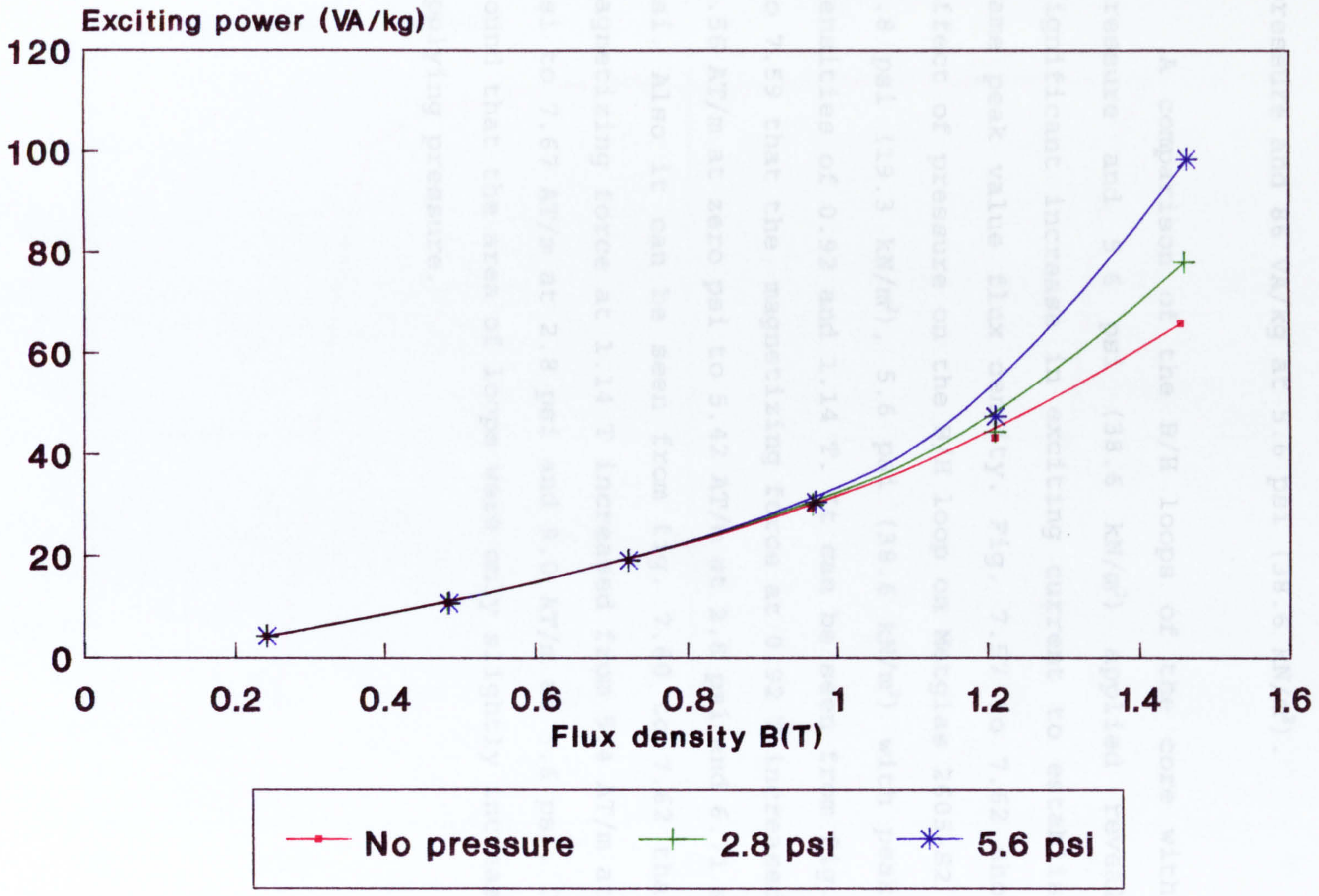

Fig. 7.56 Exciting power sensitivity o f Metglas 2605-S2 with pressure 0, 2.8 and 5.6 psi at 3000 Hz core No.1.

exciting VA measured was 13.8 VA/kg with zero pressure and 25.8 VA/kg with 5.6 psi(38.6 kN/m^2), the corresponding measurement at 1.4 - T, 3 kHz was 60.5 VA/kg with zero pressure and 86 VA/kg at 5.6 psi (38.6 kN/m^2).

A comparison of the B/H loops of the core with zero pressure and 5.6 psi (38.6 kN/m^2) applied revealed a significant increase in exciting current to establish the same peak value flux density. Fig. 7.57 to 7.62 show the effect of pressure on the B/H loop on Metglas 2605-S2 at 0, 2.8 psi (19.3 kN/m^2), 5.6 psi (38.6 kN/m^2) with peak flux densities of 0.92 and 1.14 T. It can be seen from fig. 7.57 to 7.59 that the magnetizing force at 0.92 T increased from 4.56 AT/m at zero psi to 5.42 AT/m at 2.8 psi and 6.71 at 5.6 psi. Also it can be seen from fig. 7.60 to 7.62 that the magnetizing force at 1.14 T increased from 5.4 AT/m at zero psi to 7.67 AT/m at 2.8 psi and 9.0 AT/m at 5.6 psi. It was found that the area of loops were only slightly increased by applying pressure.

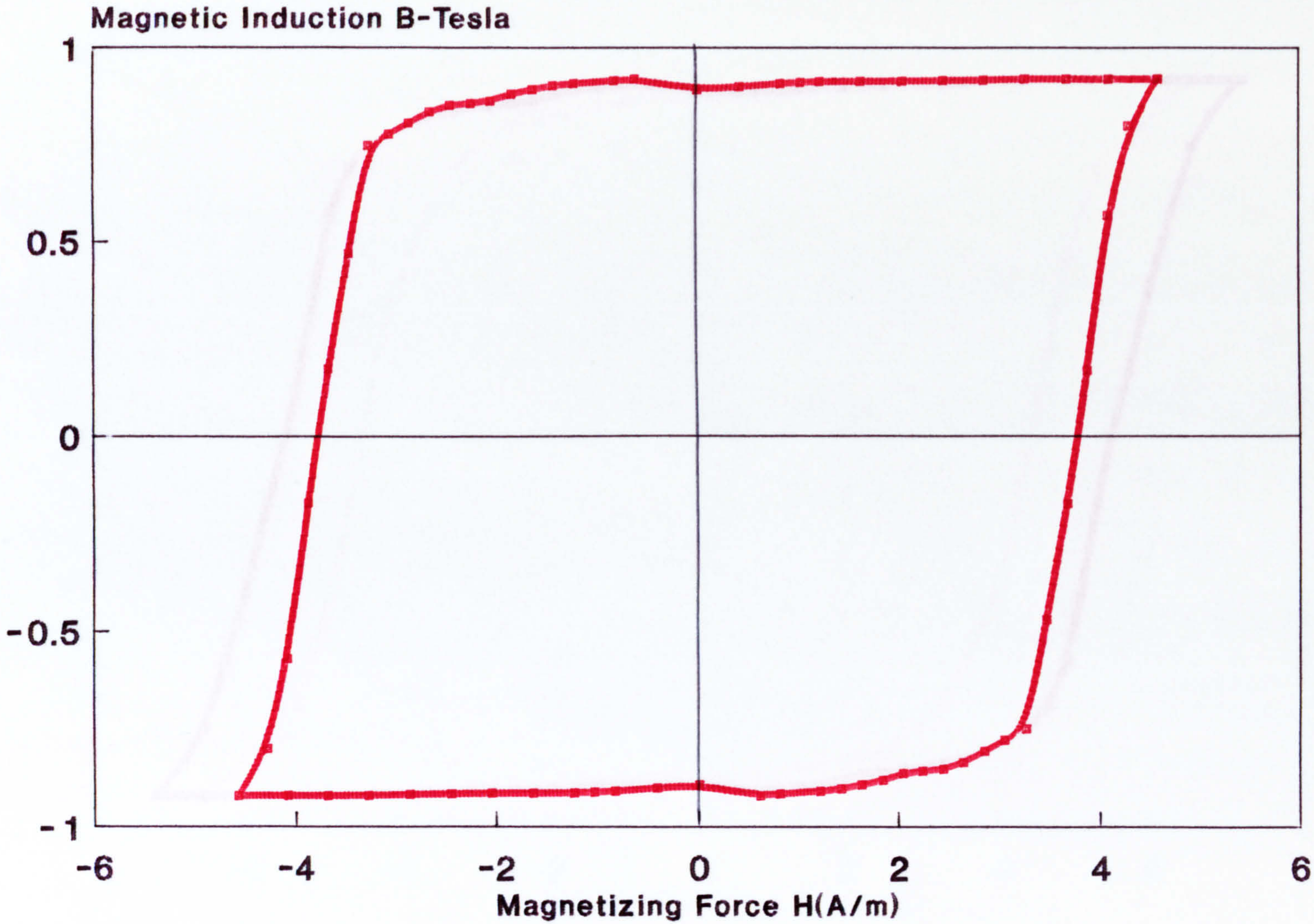

Fig. 7.57 B/H loop of Metglas 2605-S2 at flux density 0.92 T no pressure applied.

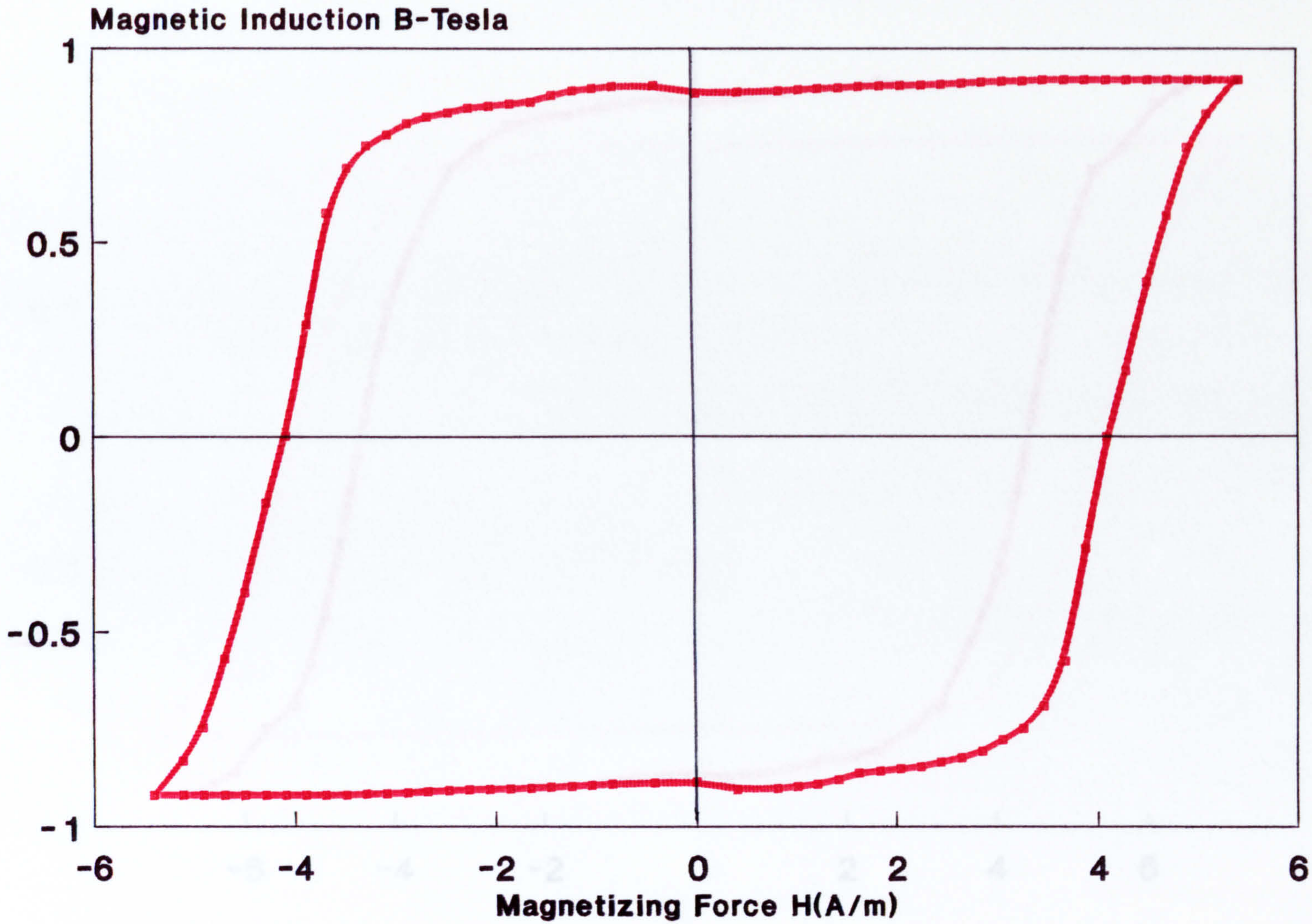

Fig. 7.58 B/H loop of Metglas 2605-S2 applied pressure 2.8 Psi(19.3 kN/m^2) 0.92 T.

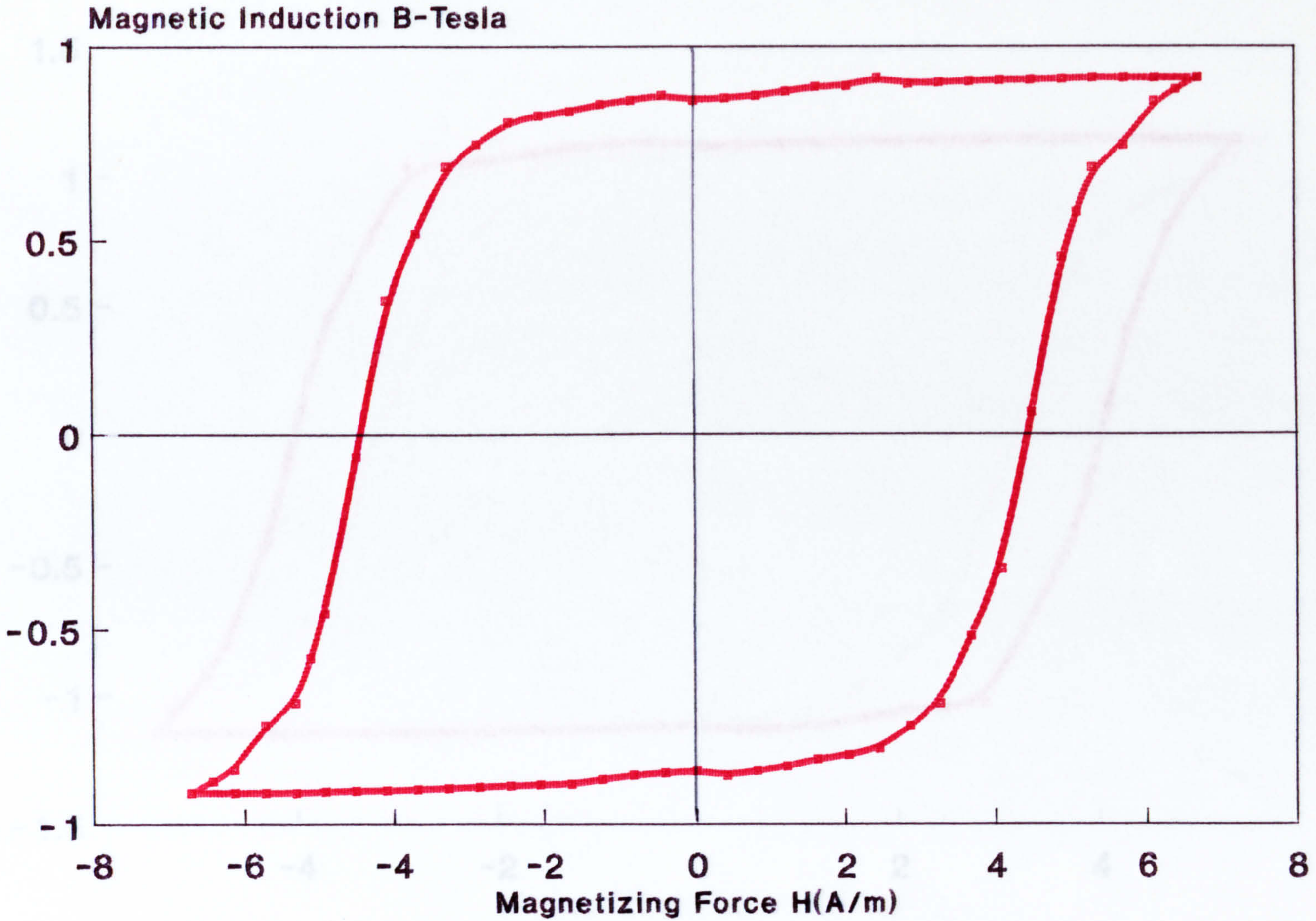

Fig. 7.59 B/H loop of Metglas 2605-S2 applied pressure 5.6 Psi(38.6 kN/m^2) 0.92 T.

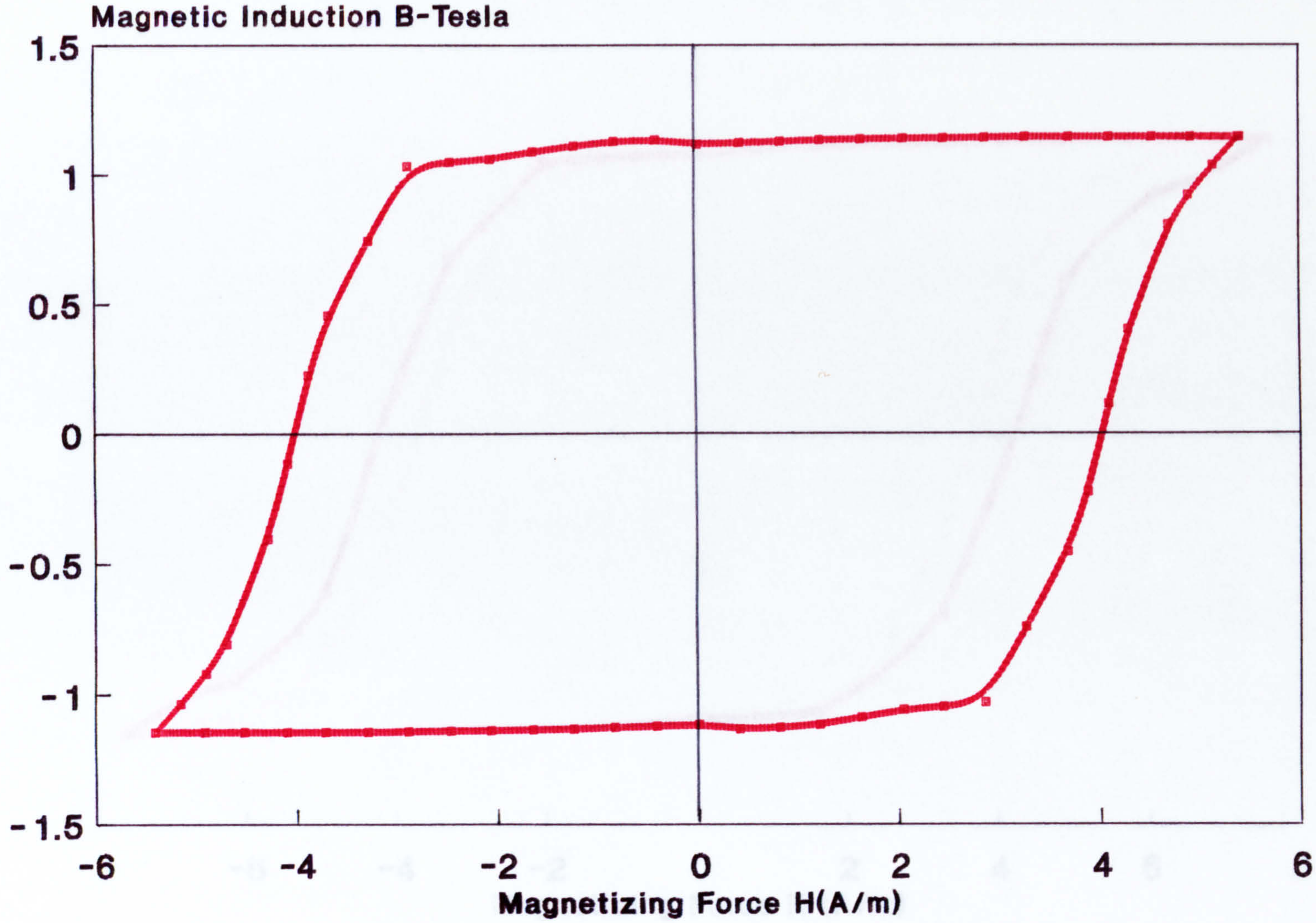

Fig. 7.60 B/H loop of Metglas 2605-S2 at flux density 1.14 T no pressure applied.

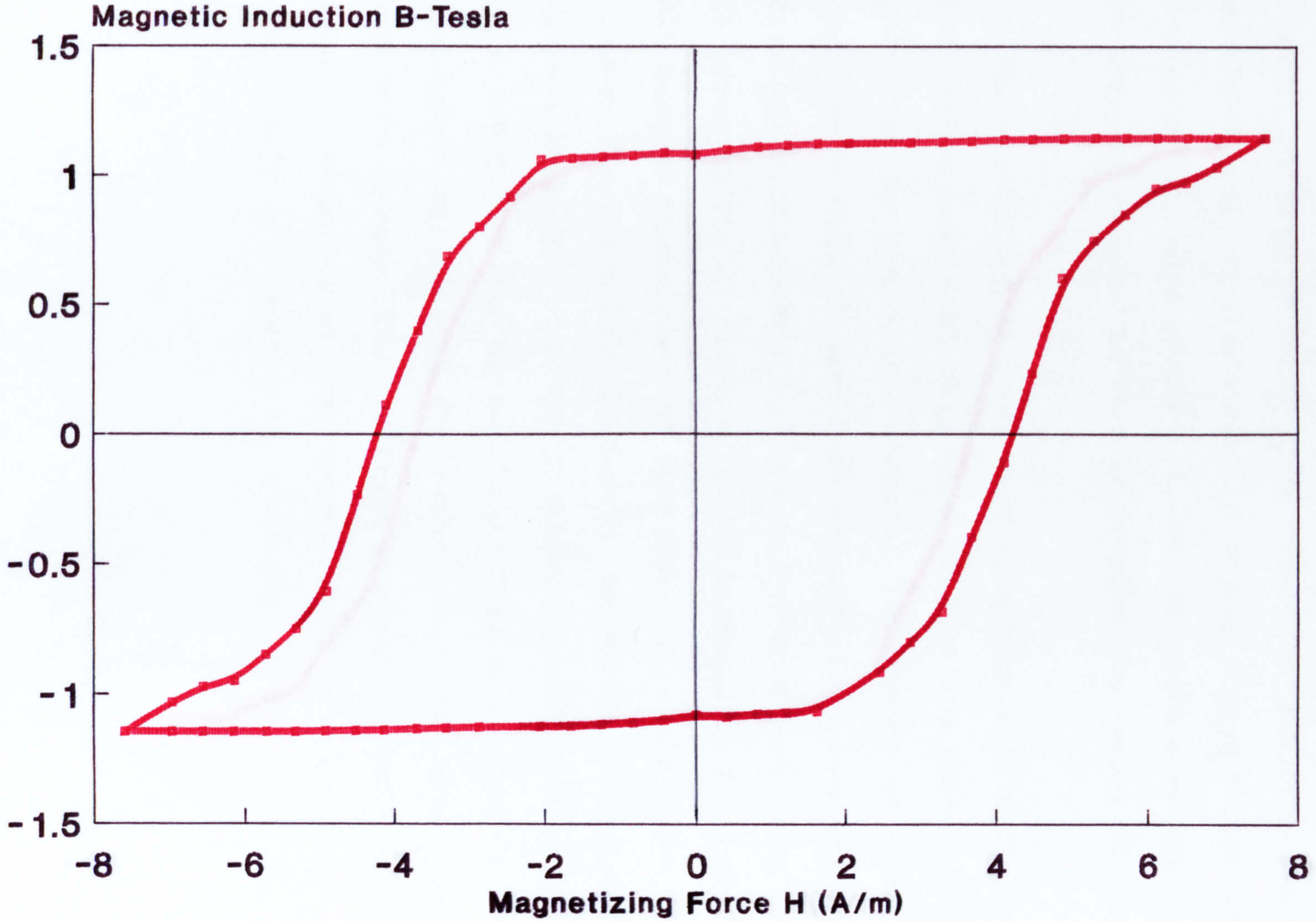

Fig. 7.61 B/H loop of Metglas 2605-S2 applied pressure 2.8 psi(19.3 kN/m^2) at 1.14 T.

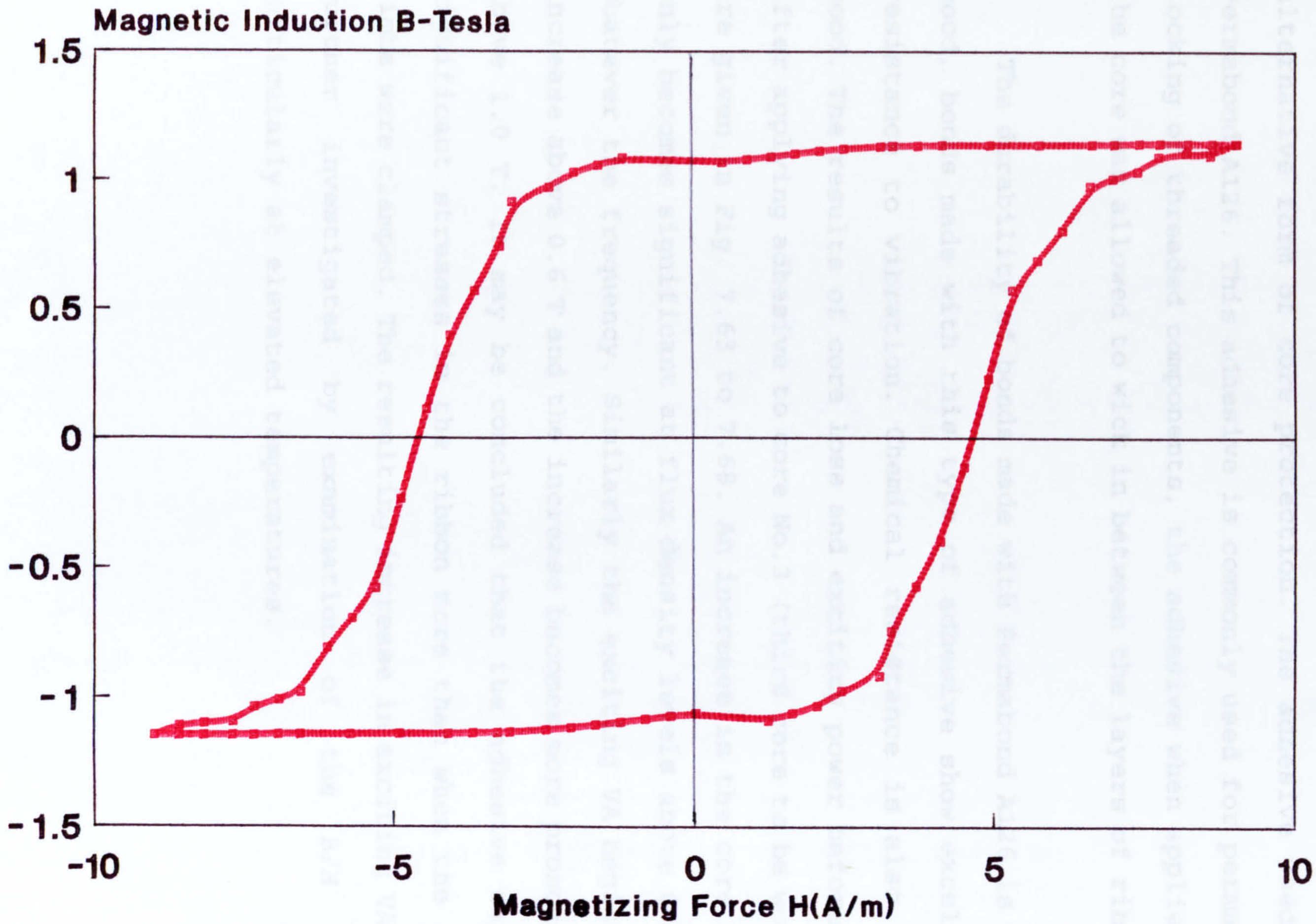

Fig. 7.62 B/H loop of Metglas 2605-S2 applied pressure 5.6 psi (38.6 kN/m^2) at 1.14 T.

7.14 Effect of Applying Adhesive to Core

The use of a low viscosity adhesive was tested as an alternative form of core protection. The adhesive used was Permabond A126. This adhesive is commonly used for permanent locking of threaded components, the adhesive when applied to the core was allowed to wick in between the layers of ribbon.

The durability of bonds made with Permabond A126 is very good, bonds made with this type of adhesive show excellent resistance to vibration. Chemical resistance is also very good. The results of core loss and exciting power before and after applying adhesive to core No.3 (third core to be wound) are given in Fig. 7.63 to 7.68. An increase in the core loss only becomes significant at flux density levels above 0.6 T, whatever the frequency. Similarly the exciting VA begins to increase above 0.6 T and the increase becomes more pronounced above 1.0 T. It may be concluded that the adhesive caused significant stresses in the ribbon more than when the core limbs were clamped. The resulting increase in exciting VA was further investigated by examination of the B/H loop particularly at elevated temperatures.

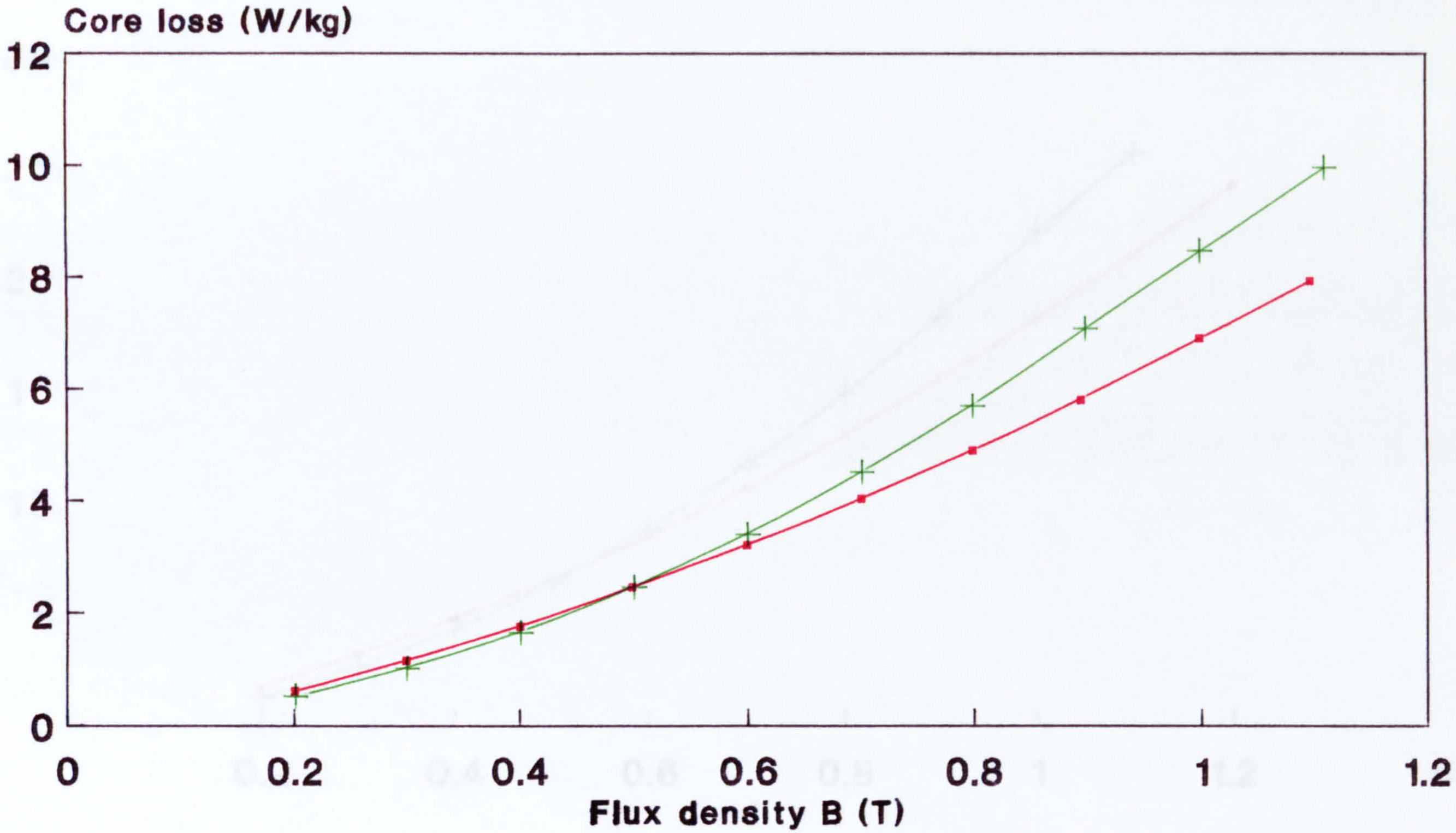

Fig. 7.63 Comparison of core loss Metglas 2605-S2 at 1 kHz different flux density without and with adhesive core No.3.

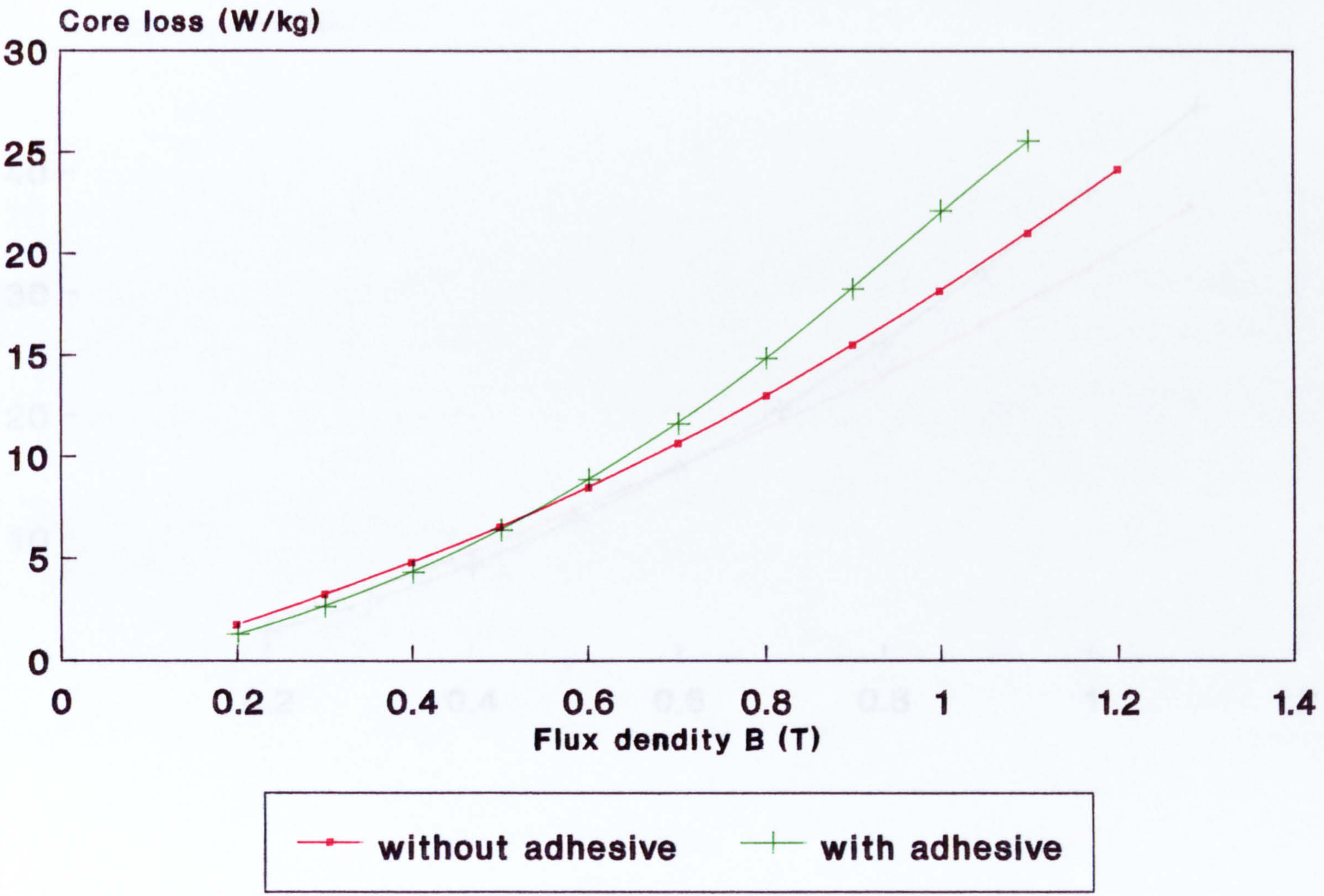

Fig. 7.64 Comparison of core loss Metglas 2605-S2 at 2-kHz different flux density without and with adhesive core No.3.

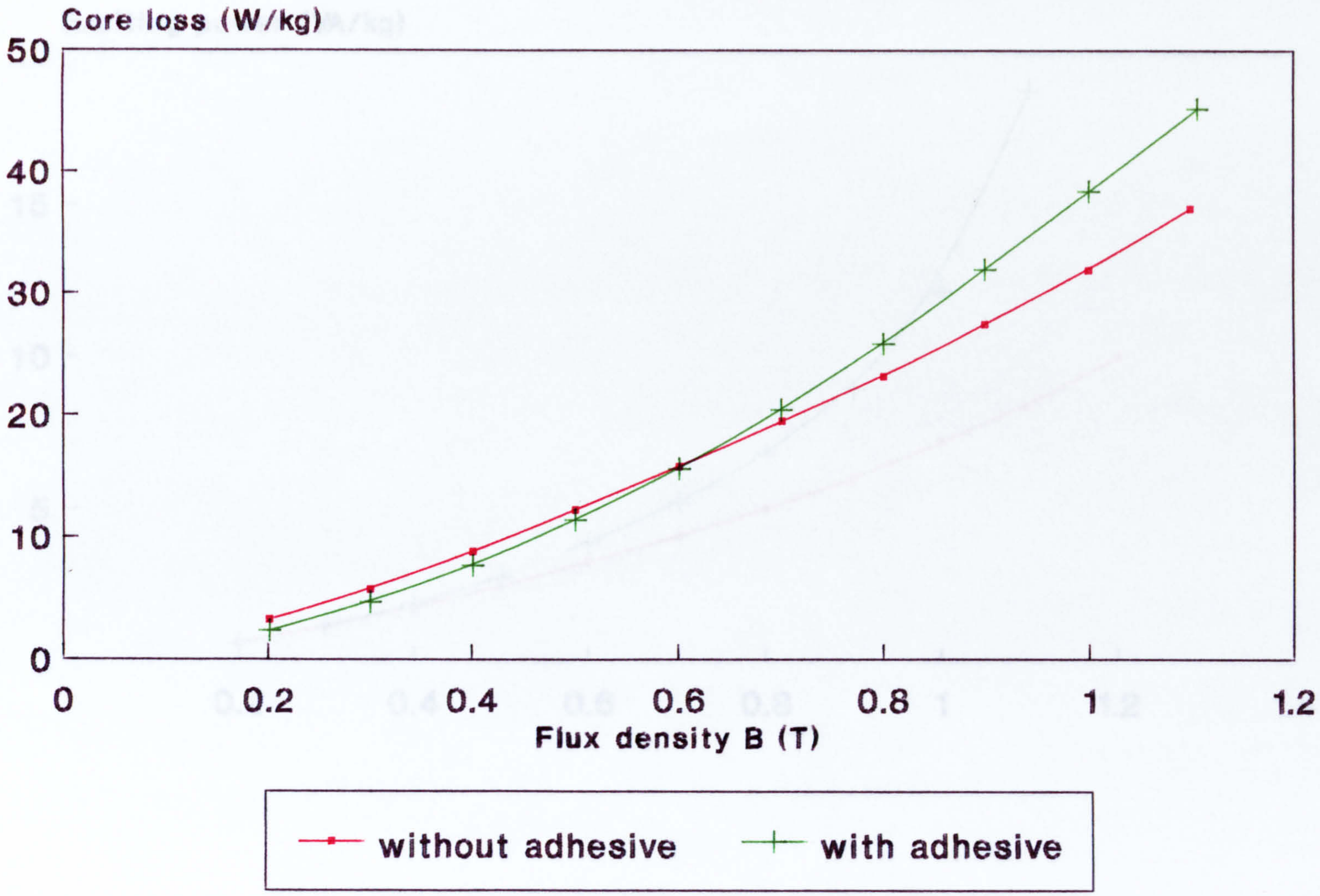

Fig. 7.65 Comparison of core loss Methlas 2605-S2 at 3-kHz different flux density without and with adhesive core No.3.

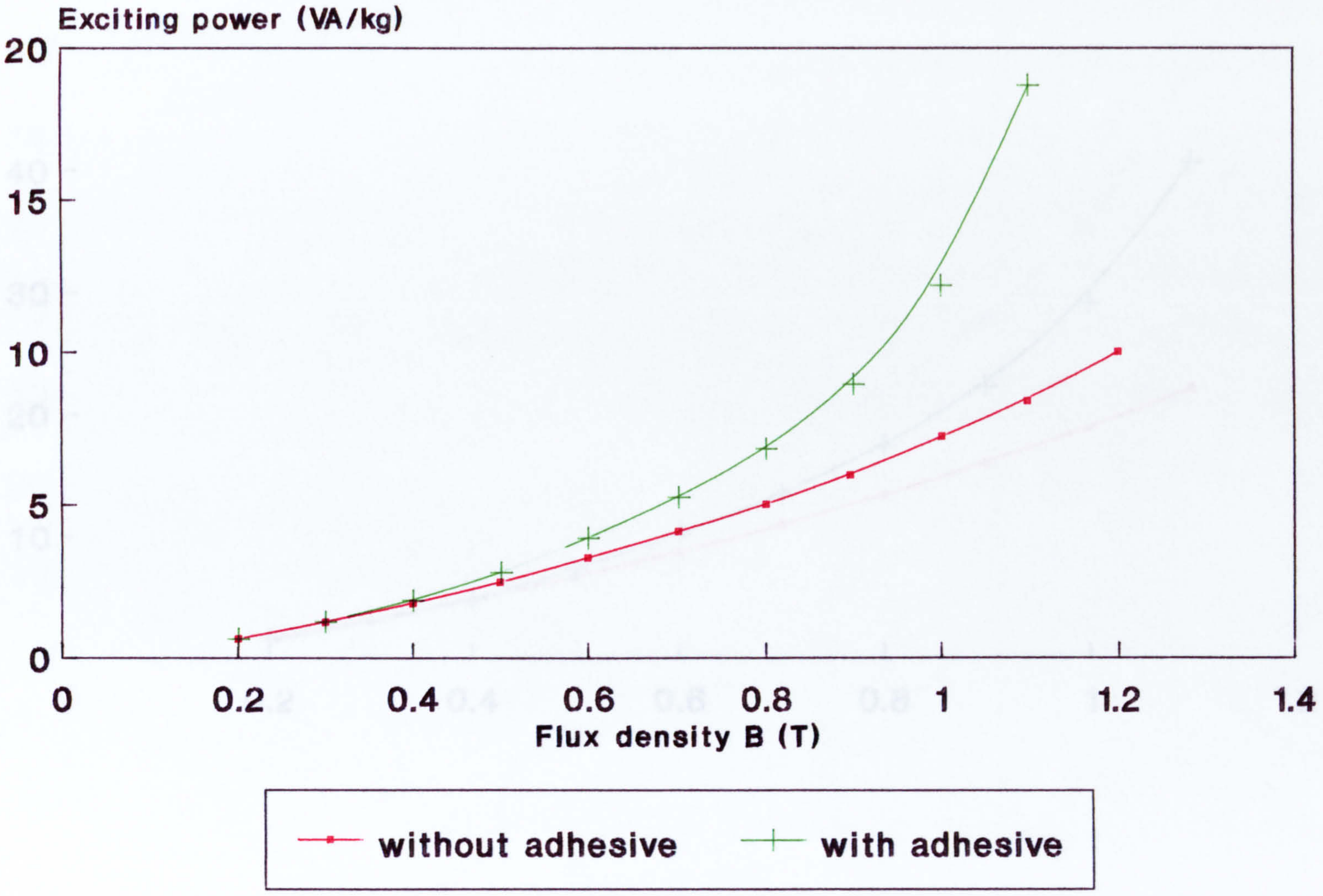

Fig. 7.66 Comparison of exciting power Metglas 2606-S2 at 1-kHZ different flux density without and with adhesive core core No.3

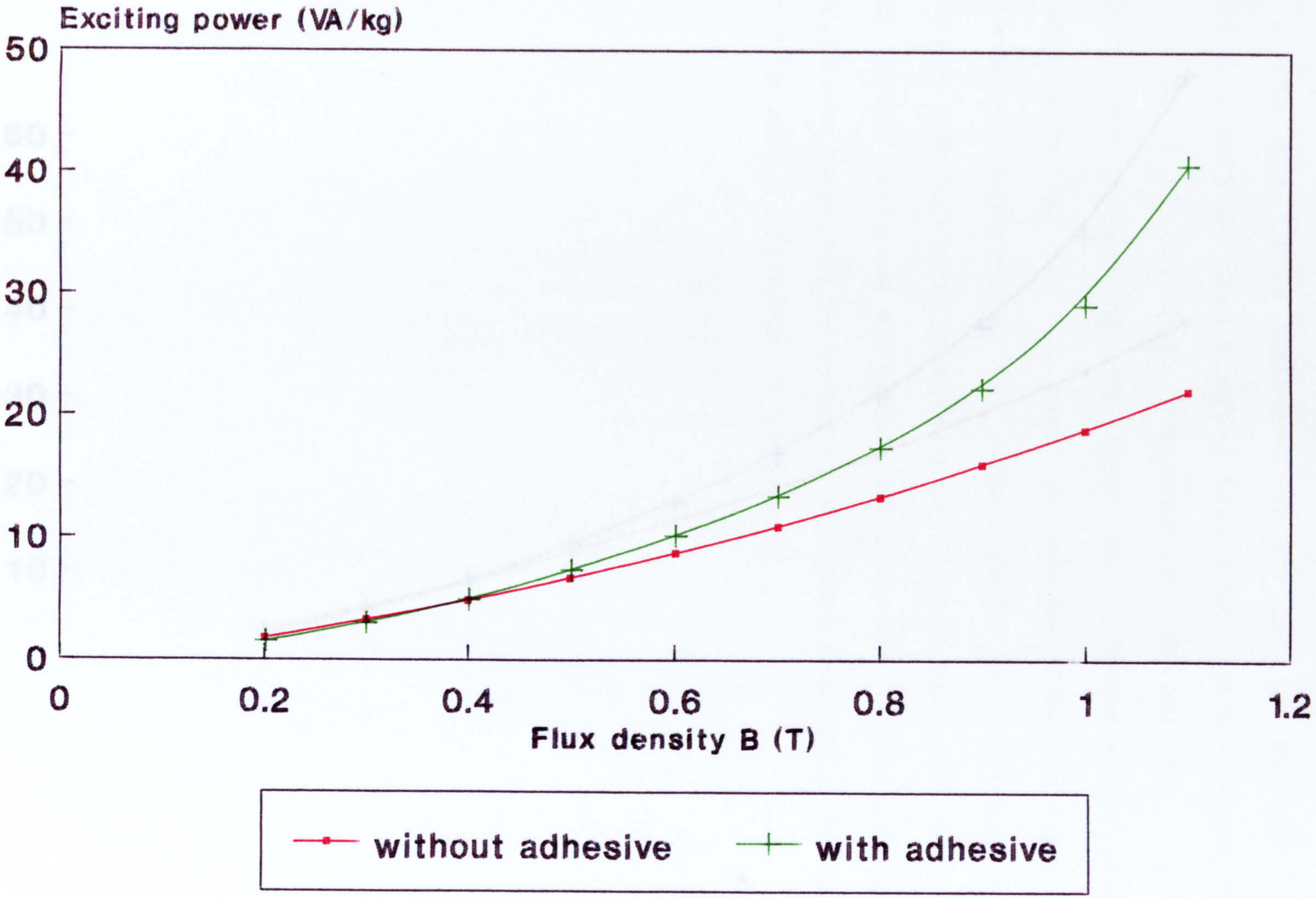

Fig. 7.67 Comparison of exciting power Metglas 2605-S2 at 2-kHz different flux density without and with adhesive core No.3.

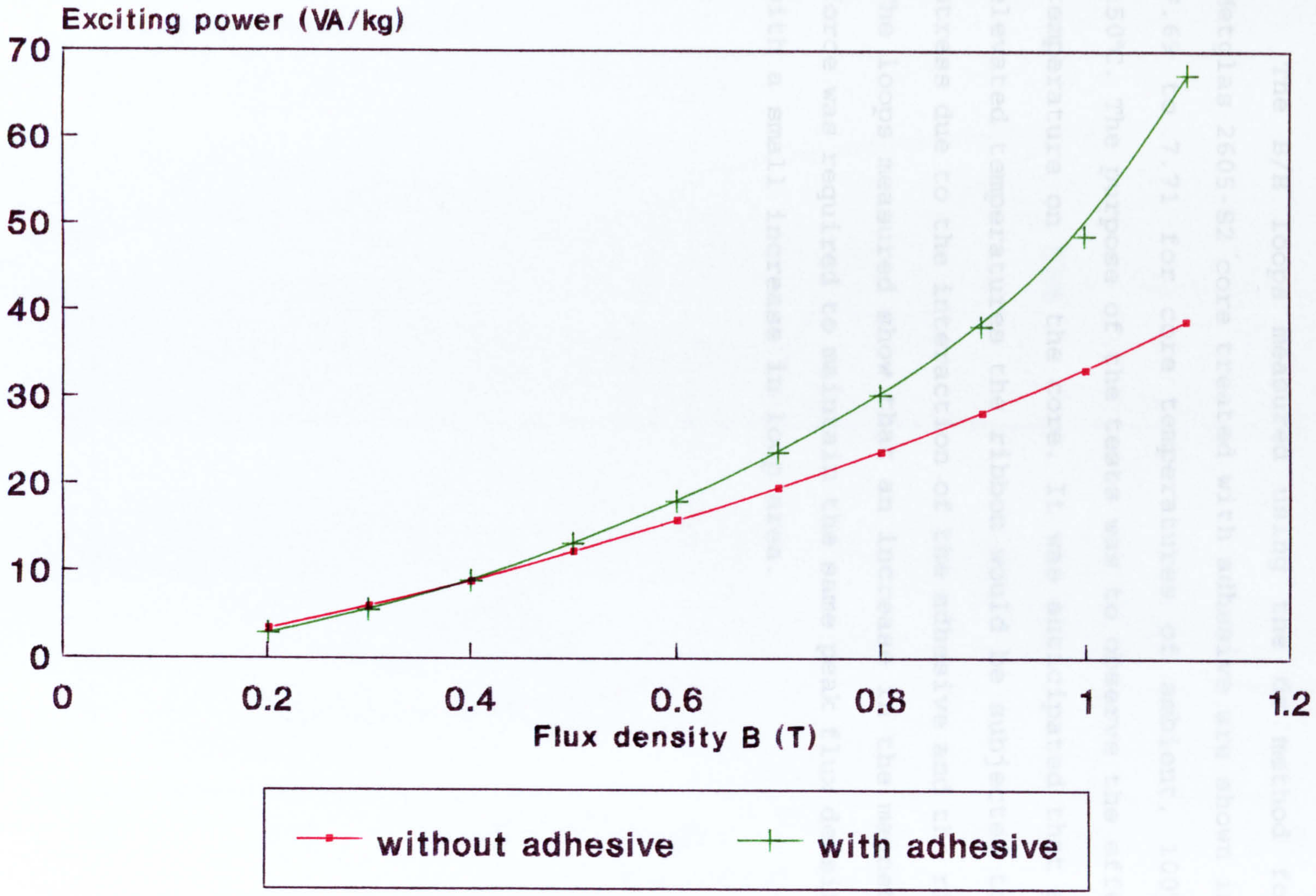

Fig. 7.68 Comparison of exciting power Metglas 2605-S2 at 3-kHz different flux density without and with adhesive core No.3.

7.14.1 Effect of Temperature on B/H Loop on Core Treated with Adhesive

The B/H loops measured using the dc method for the Metglas 2605-S2 core treated with adhesive are shown in Fig. 7.69 to 7.71 for core temperatures of ambient, 100°C and 150°C. The purpose of the tests was to observe the effect of temperature on the core. It was anticipated that at the elevated temperatures the ribbon would be subjected to more stress due to the interaction of the adhesive and the ribbon. The loops measured show that an increase in the magnetising force was required to maintain the same peak flux density and with a small increase in loop area.

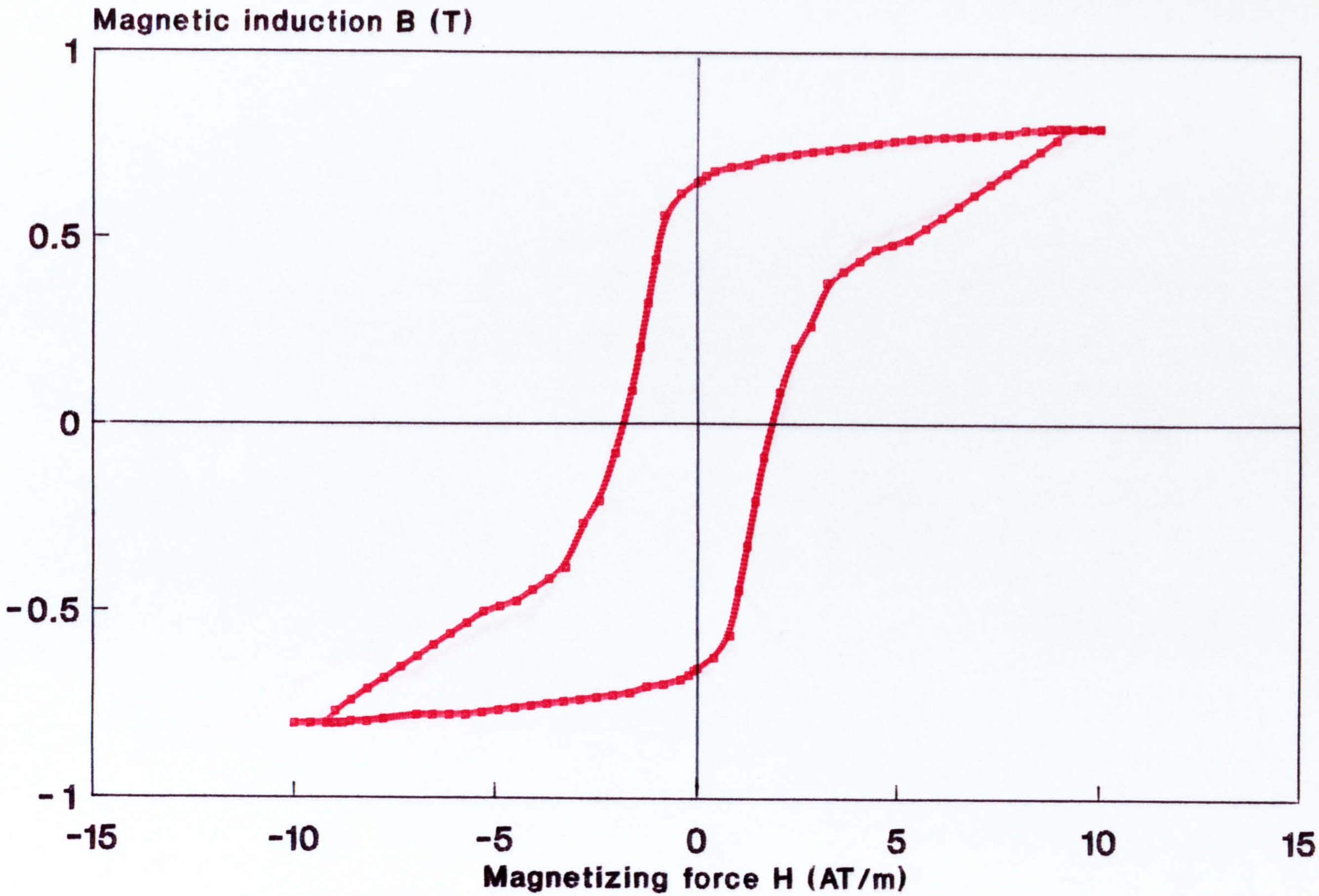

Fig. 7.69 Hysteresis loop of amorphous 2605-S2 core treated with adhesive at ambient temperature flux density 0.8 (T).

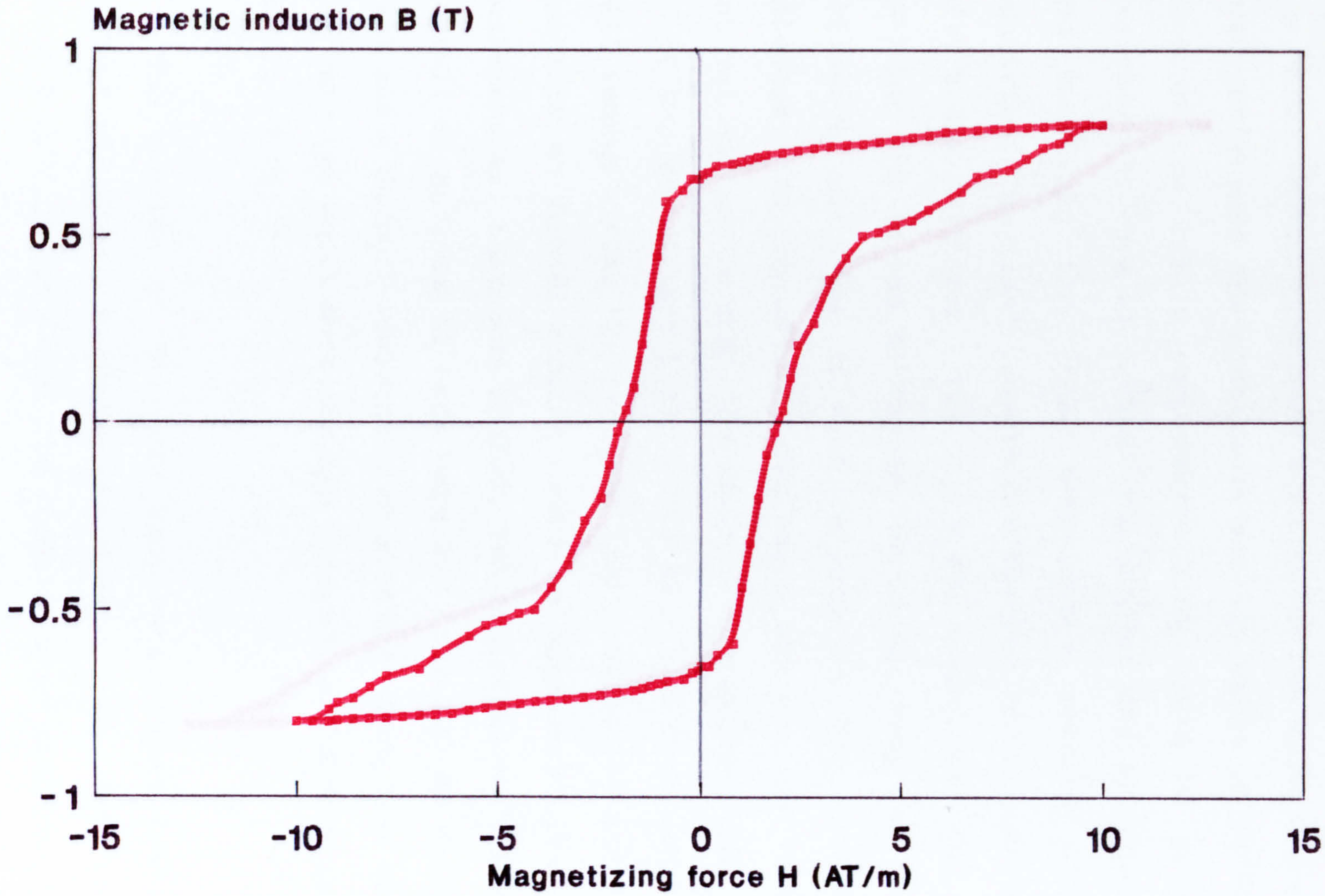

Fig. 7.70 Hysteresis loop of amorphous 2605-S2 treated with adhesive at temperature 100 C flux density 0.8 (T)).

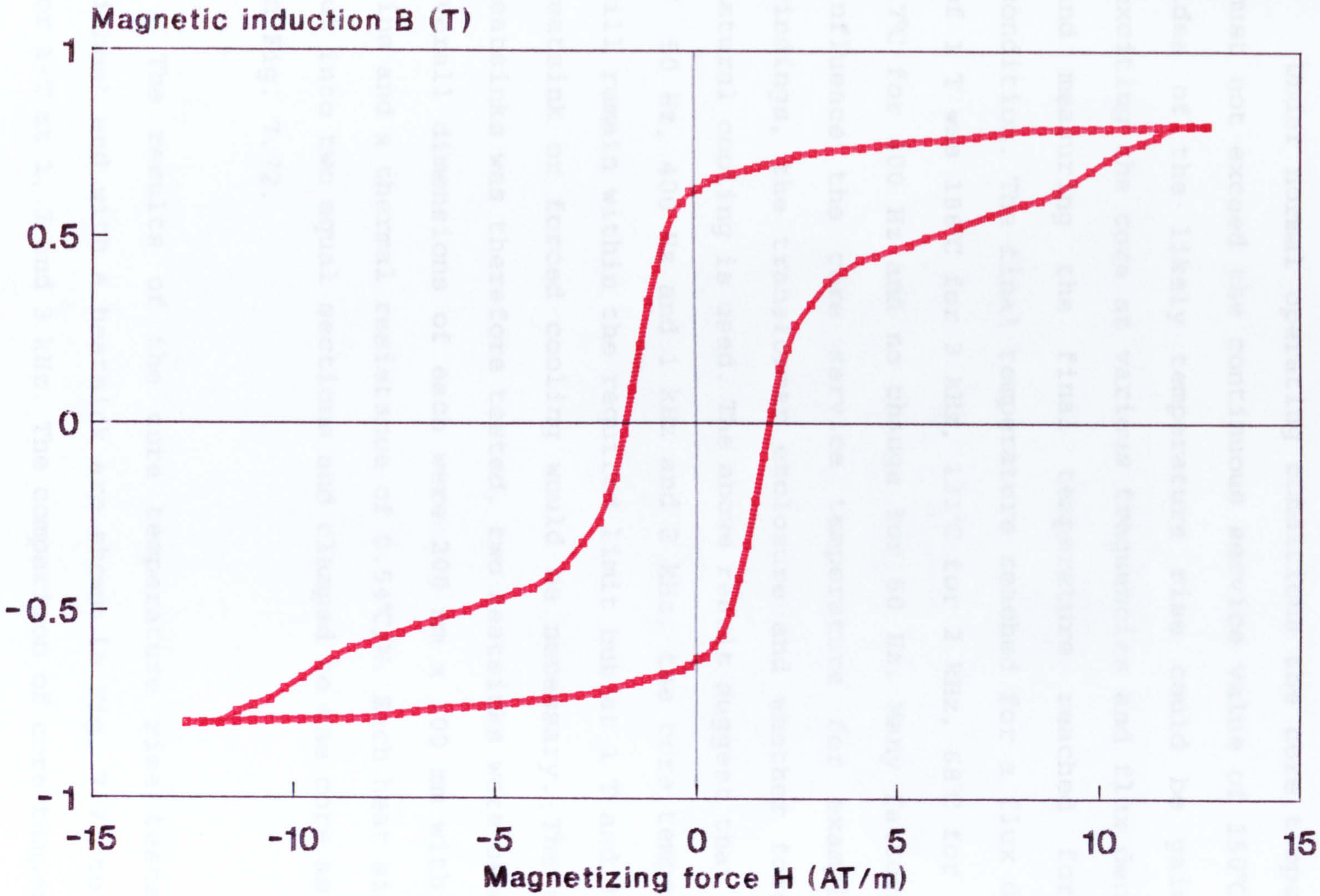

Fig. 7.71 Hysteresis loop of amorphous Metglas 2605-S2 treated with adhesive at 150 C temperature flux density 0.8 (T).

7.15 Core Temperature Rise

7.15.1 Amorphous Metglas 2605-S2 Core

Under normal operating conditions the core temperature must not exceed the continuous service value of 150°C. Some idea of the likely temperature rise could be gained by exciting the core at various frequencies and flux densities and measuring the final temperature reached for each condition. The final temperature reached for a flux density of 1 T was 186°C for 3 kHz, 131°C for 2 kHz, 68°C for 1 kHz, 37°C for 400 Hz and no change for 50 Hz. Many factors will influence the core service temperature for example the windings, the transformer enclosure and whether forced or natural cooling is used. The above result suggest that at 1.0 T 50 Hz, 400 Hz and 1 kHz and 2 kHz, the core temperature will remain within the required limit but at 1 T and 3 kHz a heatsink or forced cooling would be necessary. The use of heatsinks was therefore tested, two heatsinks were used, the overall dimensions of each were 200 mm x 100 mm with 40 mm fins and a thermal resistance of 0.54°C/W. Each heat sink was cut into two equal sections and clamped to the core as shown in Fig. 7.72.

The results of the core temperature rise tests both without and with a heatsink are shown in Fig. 7.73 to 7.75, for 1-T at 1, 2 and 3 kHz. The comparison of core temperature rise without and with heatsink of Metglas 2605-S2 measured are summarized in Table 7.7.

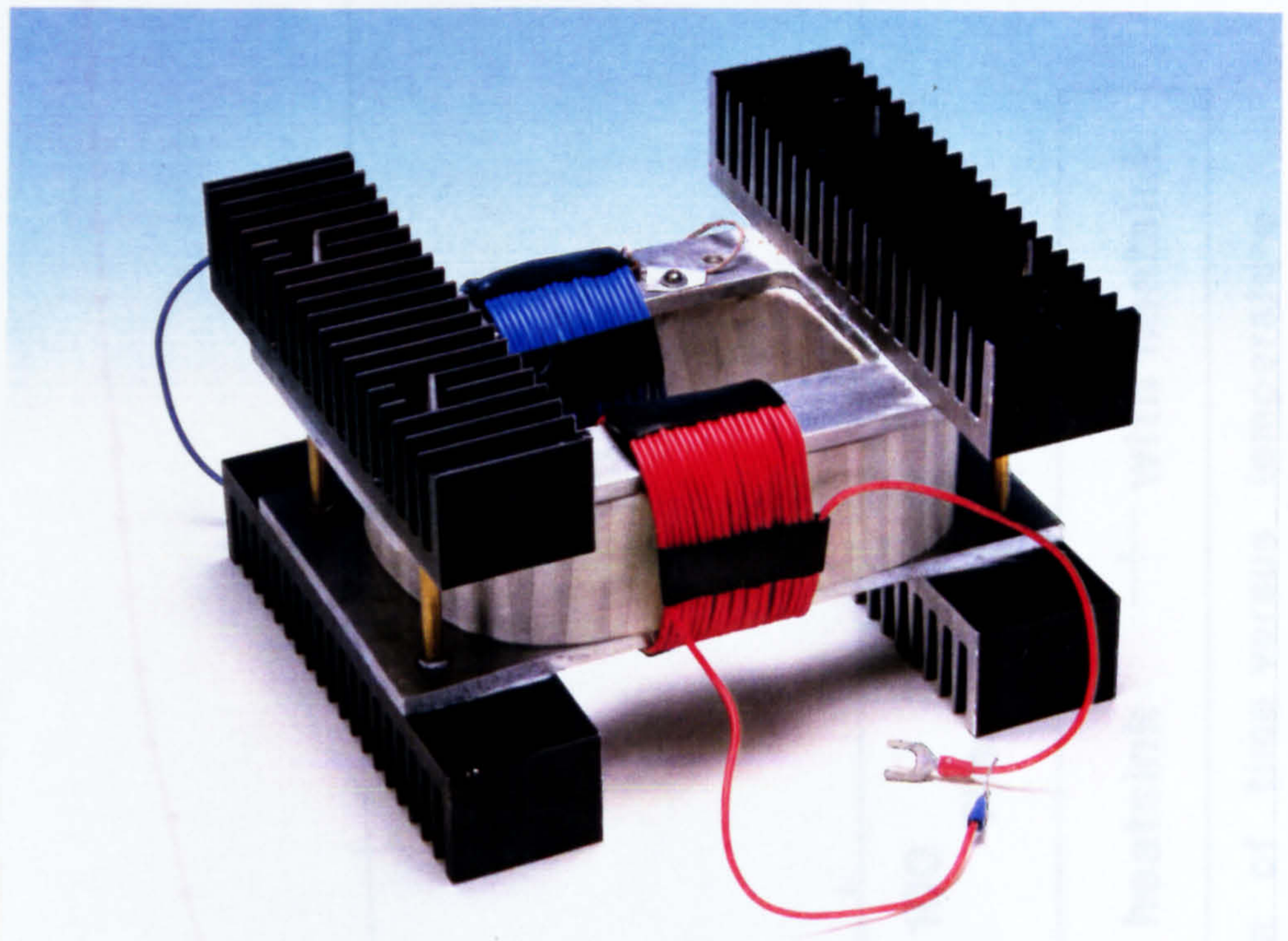

Fig. 7.72 Metglas 2605-S2 core with heatsink attached.

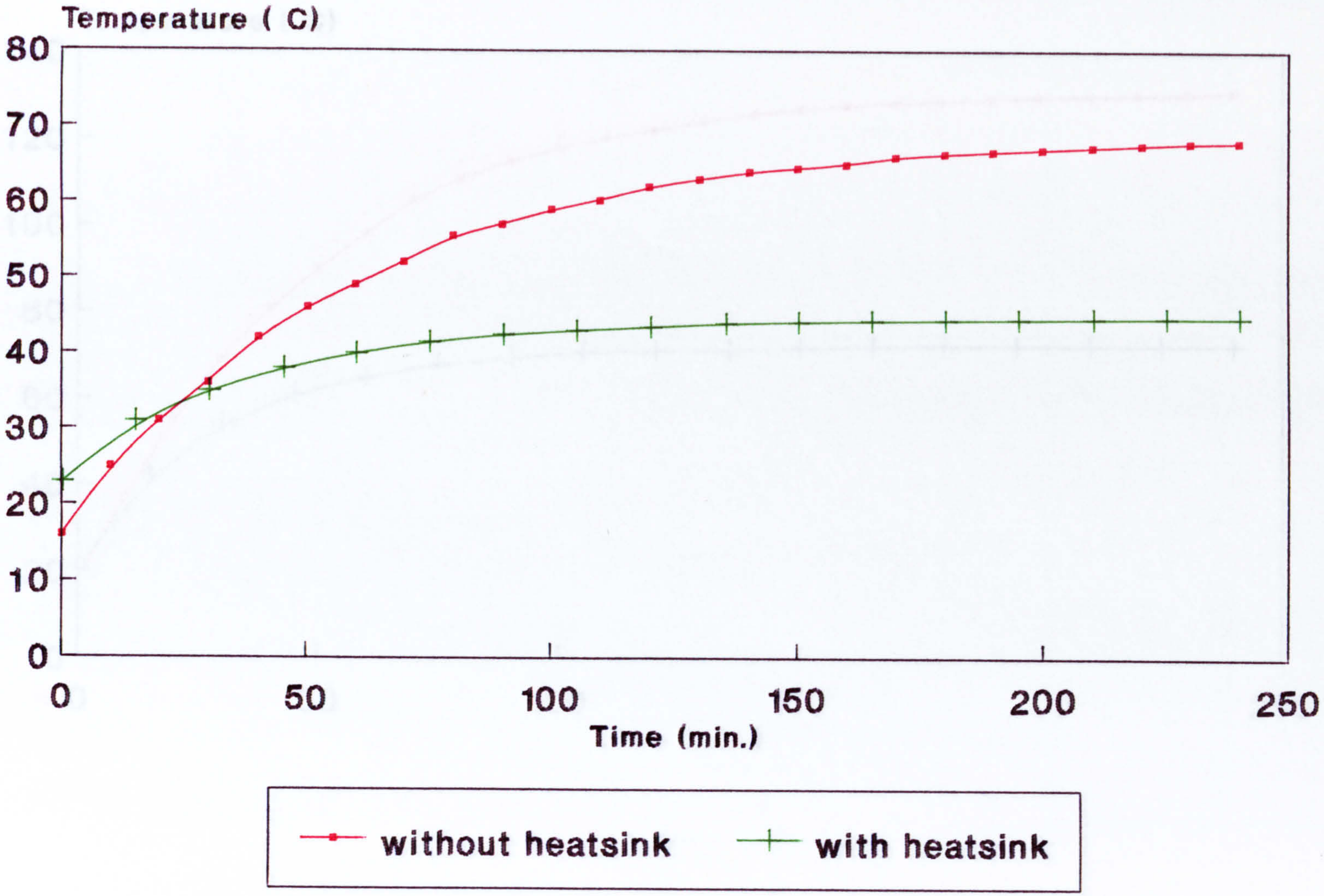

Fig. 7.73 Comparison of time versus temperature Metglas 2605-S2 at 1.0 T, 1000Hz without and with heatsink core No.2.

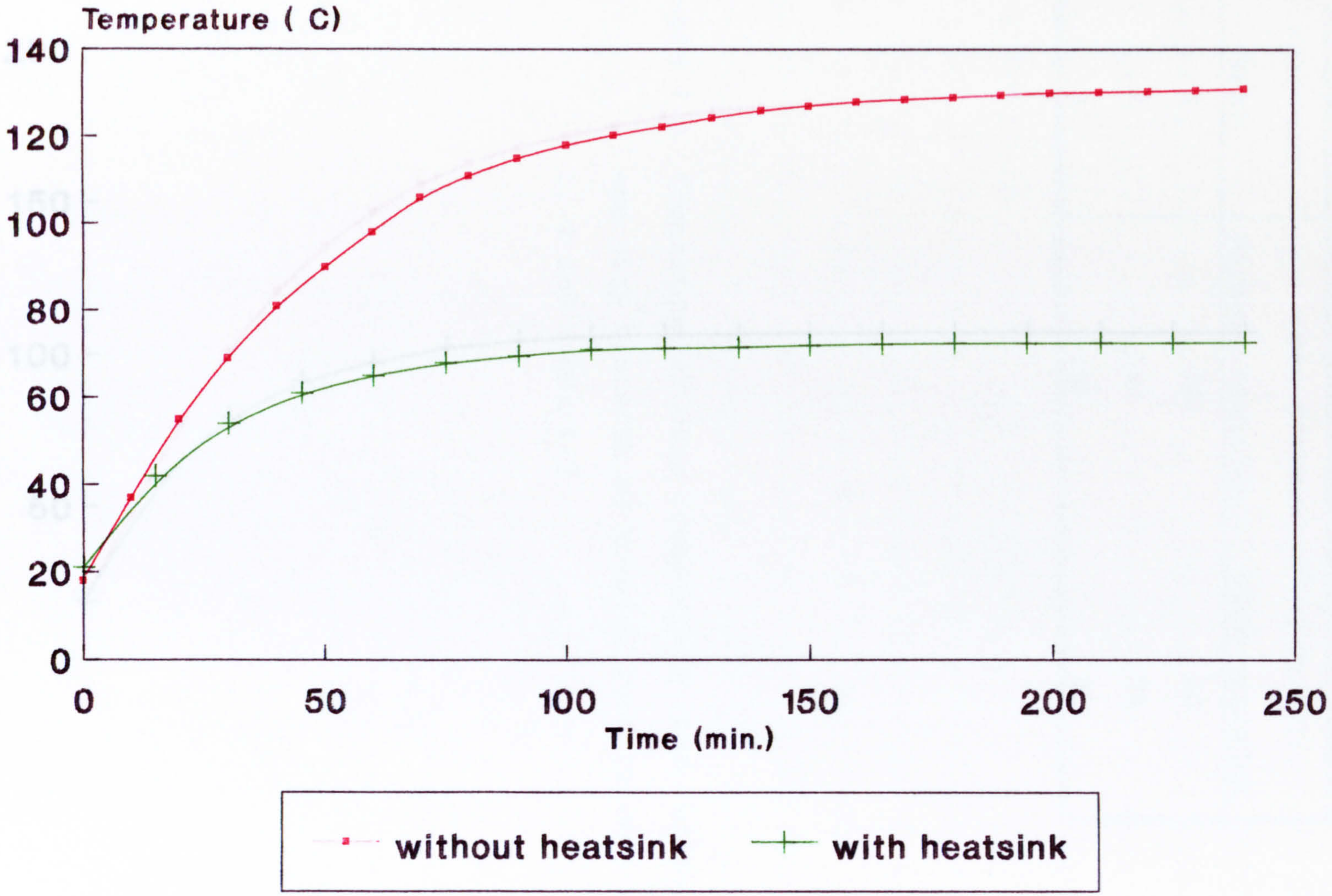

Fig. 7.74 Comparsion of time versus temperature Metglas 2605-S2 at 1 T, 2000 Hz without and with heatsink core No.2.

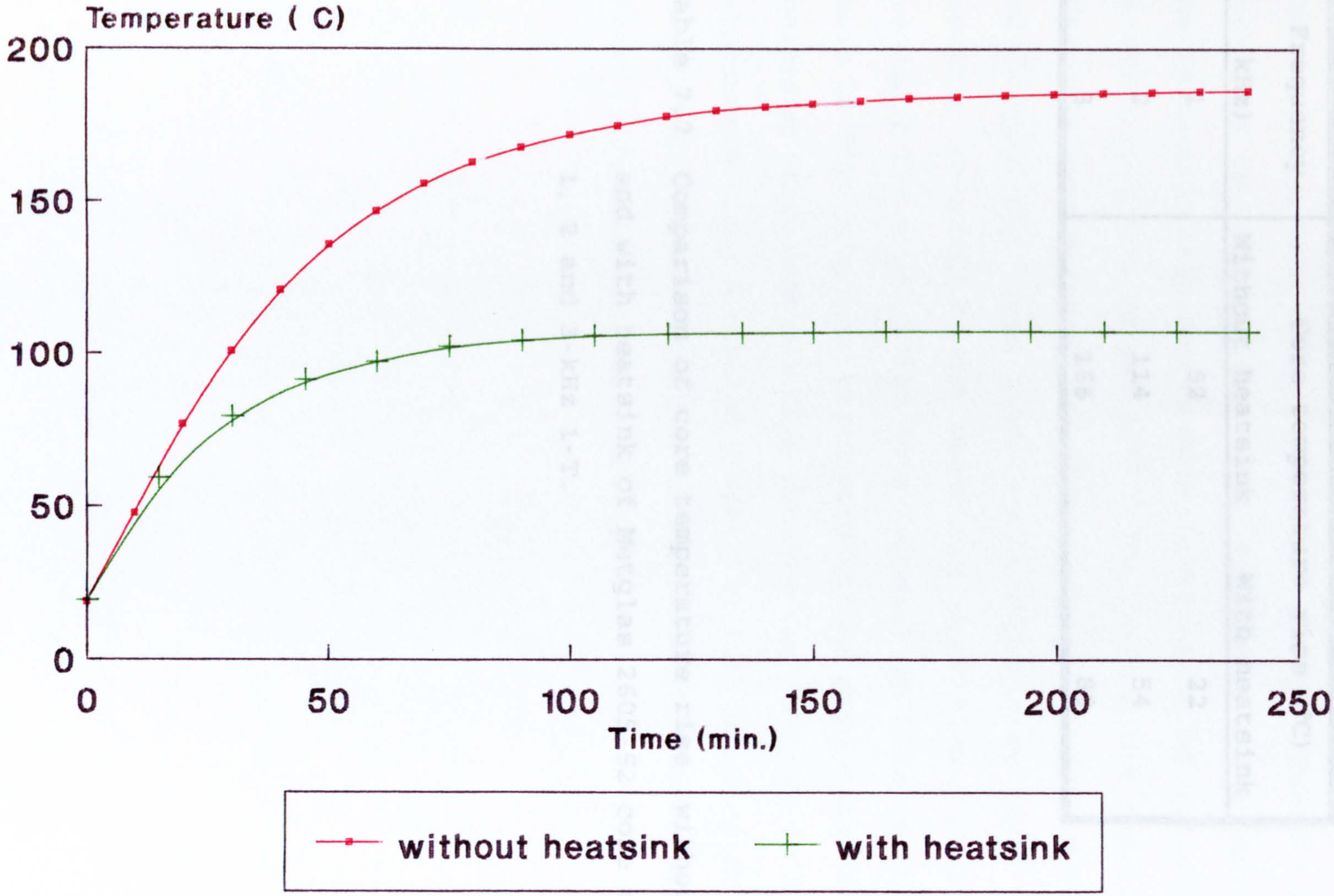

Fig. 7.75 Comparison of time versus temperature Metglas 2605-S2 at 1.0 T 3000 Hz without and with heatsink core No.2.

Frequency (kHz)	Core temperature rise (°C)	
	Without heatsink	With heatsink
1	52	22
2	114	54
3	166	88

Table 7.7 Comparison of core temperature rise without and with heatsink of Metglas 2605-S2 core at 1, 2 and 3-kHz 1-T.

7.15.2 Silicon-iron core

The results of temperature rise test carried out on the uncut silicon-iron core (9.9 kg) are shown in Table 7.8. The core loss as expected decreased when temperature increased. The maximum continuous service temperature of silicon-iron material must not exceed 150°C. The temperature rise of the test core were measured for various operating flux densities and frequencies. From these temperature rise tests it is possible to predict the operating core flux density and frequency for a specified core temperature rise. A graph is shown in Fig. 7.76 from which predictions may be made for the operating frequency and flux density for 80°C and 100°C core temperature rise. A similar graph, fig.7.95 for 2605-S2, gives predictions of operating f and B for various core temperature rises. (see section 7.16.7.)

(a)

Frequency (kHz)	Core loss(W/kg) Ambient Temp.	Core loss(W/kg) Final Temp.	Temp. rise (°C)
1	4.05	3.97	39
2	11.2	9.8	80
3	18.9	15.8	99

(b)

Frequency (kHz)	Core loss(W/kg) Ambient Temp.	Core loss(W/kg) Final Temp.	Temp. rise (°C)
1	8.65	8.08	66
2	22.42	18.68	131

(c)

Frequency (kHz)	Core loss(W/kg) Ambient Temp.	Core loss(w/kg) Final Temp.	Temp. rise (°C)
1	14.0	13.0	101
2	34.06	26.6	170

(d)

Frequency (kHz)	Coreloss(W/kg) Ambient Temp.	Core loss(W/kg) Final Temp.	Temp. rise
1	21.0	17.6	127
2	45.6	-	-

Table 7.8 Temperature rise tests for uncut silicon-iron core. (9.9 kg) for three hours time at (a) 0.4T; (b) 0.6 T; (c) 0.8 T and (d) 1.0 T.

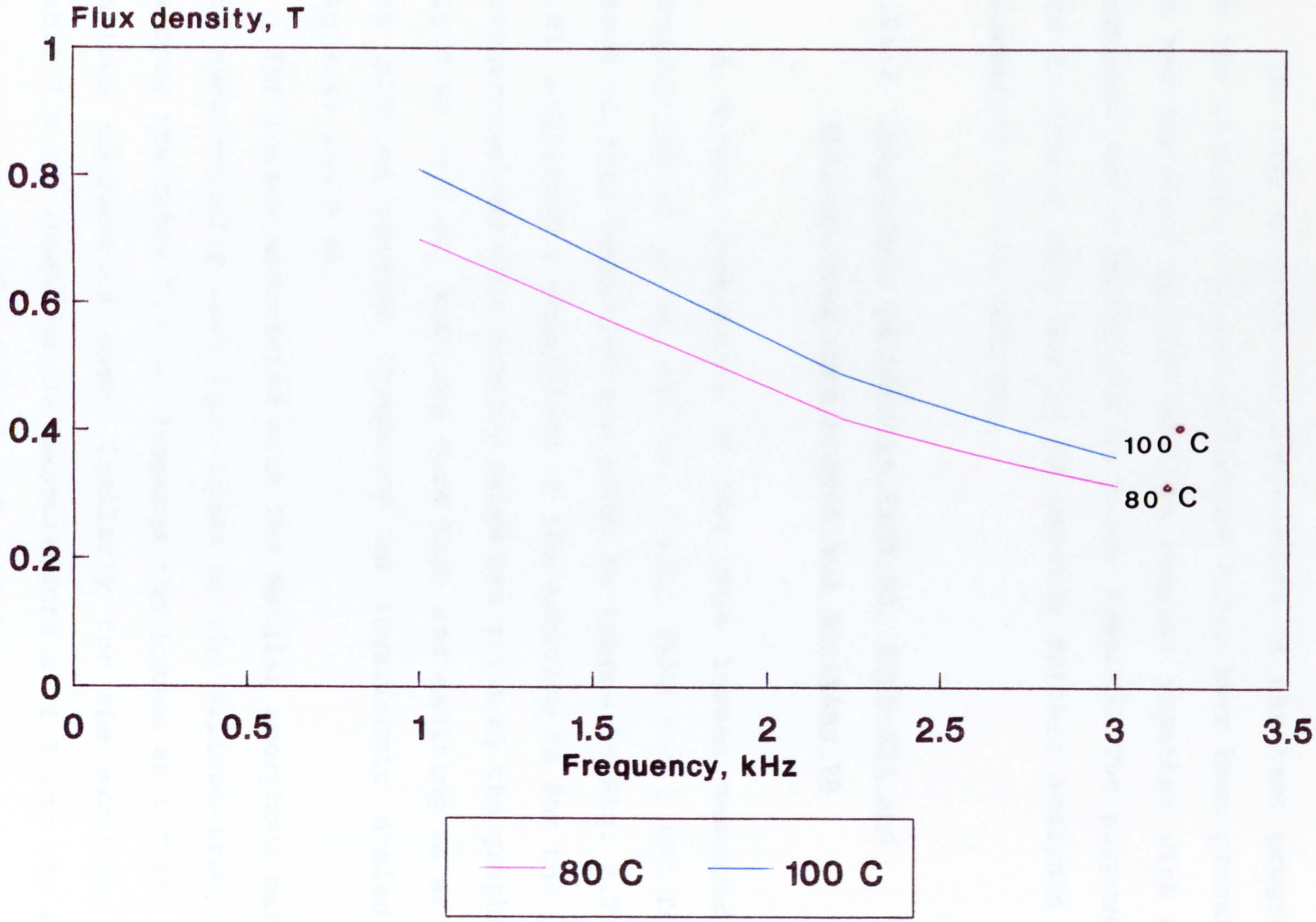

Fig. 7.7 6 Silicon-iron core temperature rise without of heatsink.

7.16 Summary and assessment of Test Results

7.6.1 Introduction

The test methods and the results of the test programme on the silicon-iron and amorphous cores have been presented in the previous section of this chapter together with some comments and observations on those results. The purpose of the following sections is to provide further analysis and assessment of the results.

7.16.2 Comparison of Metglas 2605-S2, 2605-S3A and Silicon-iron Core Losses and Exciting VA

A direct comparison of the core losses measured at frequencies of 50 Hz, 400 Hz, 1 kHz, 2kHz and 3 kHz for a range of flux densities are given by graphs in Fig. 7.77 to 7.81. Similarly a comparison of the exciting VA for the same frequencies and flux density range are given by the graphs of Fig.7.82 to 7.86. Also the core loss and exciting VA at 1 T are plotted against frequency on logarithmic scales in Fig.7.87 and 7.88.

The losses associated with the Metglas amorphous metals are substantially less than those of the silicon-iron, for example the Table 7.9 (a) compares the losses at 1 T for the various frequencies used. Similarly for the exciting VA, Table 7.9 (b) compares the measurements at 1 T for the same frequency range. The losses and exciting VA are the values measured on uncut cores for each of the three core materials.

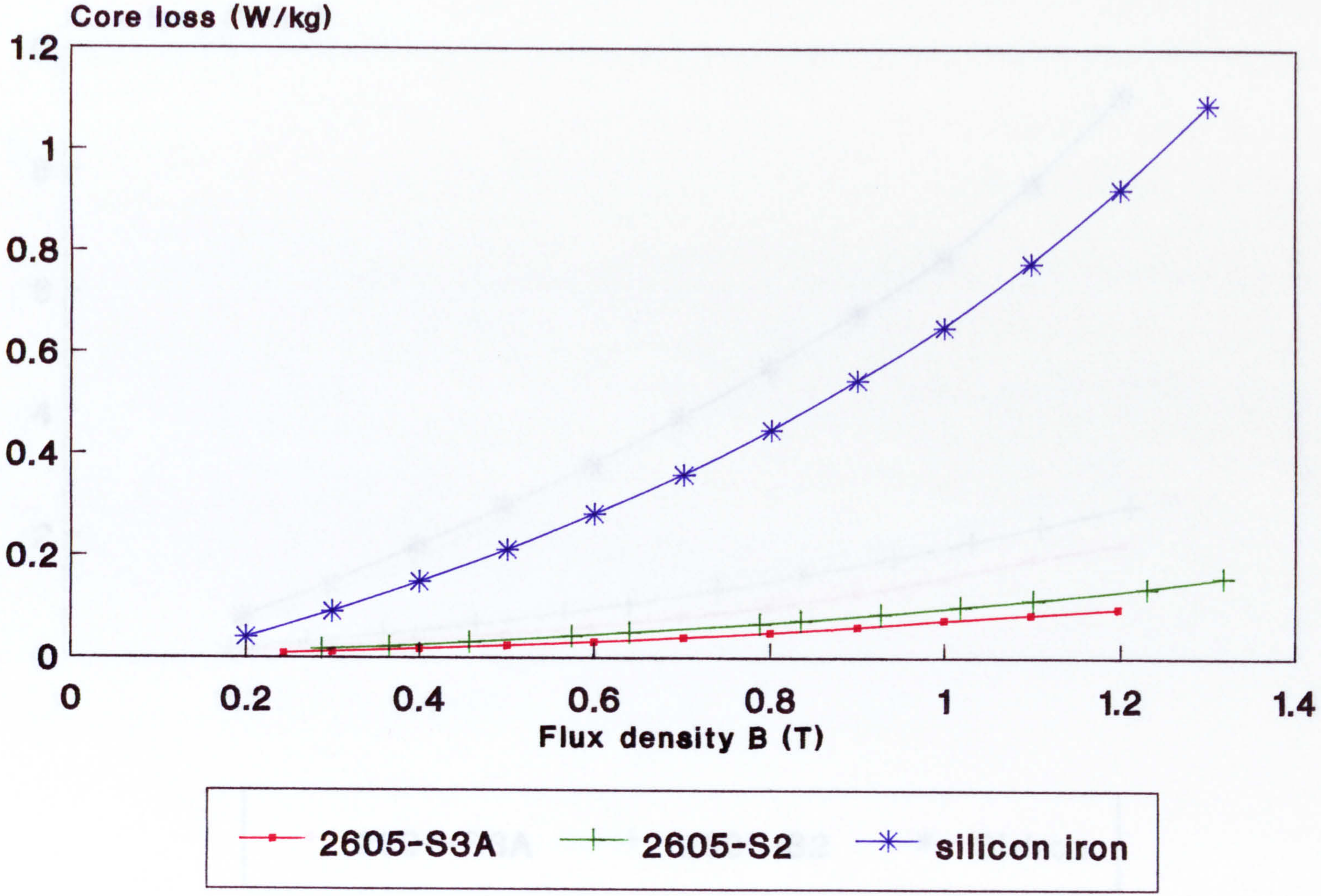

Fig. 7.77 Comparison of core loss of amorphous Metglas 2605-S3A, 2505-S2 with silicon-iron at 50 Hz.

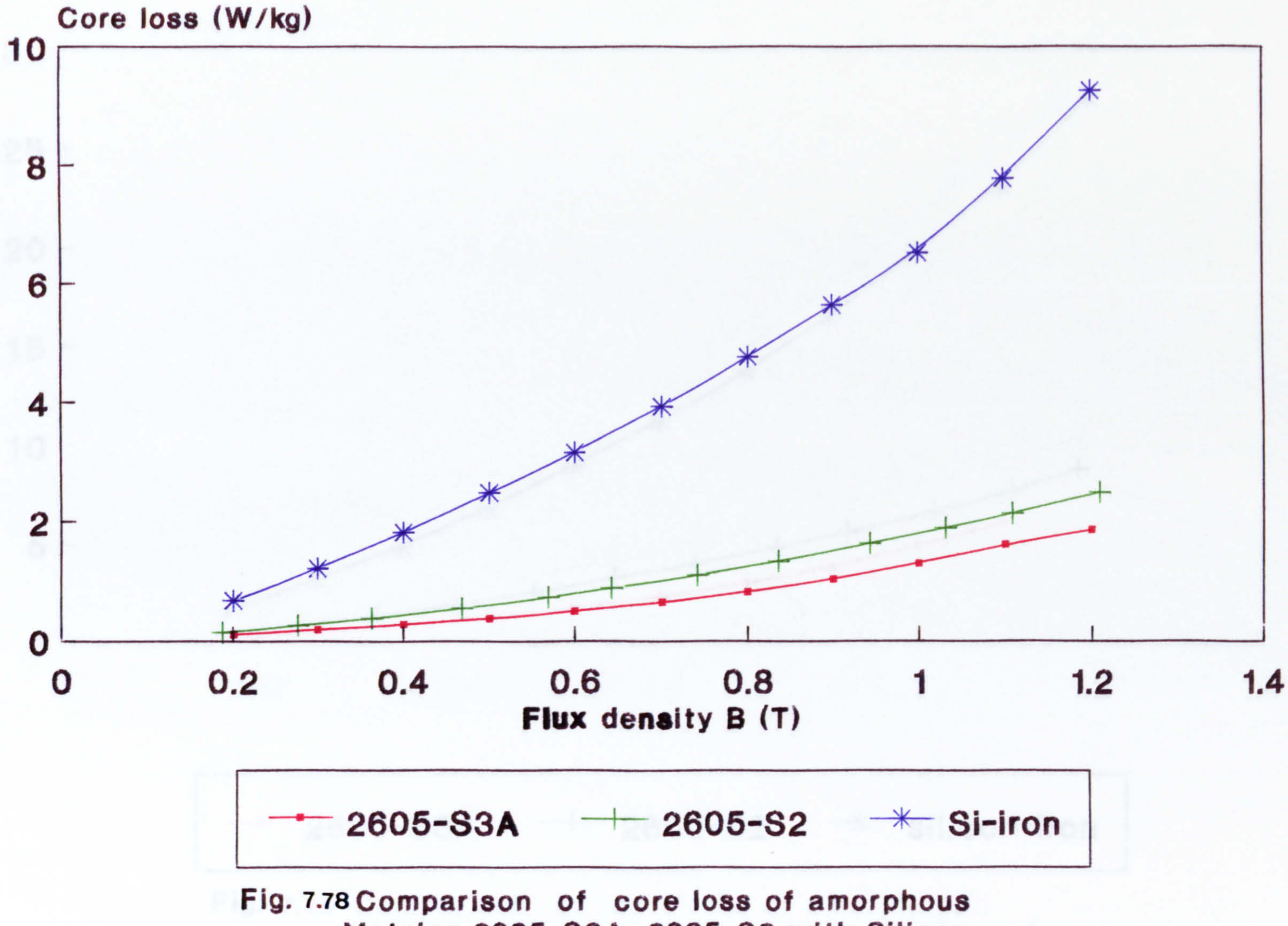

Fig. 7.78 Comparison of core loss of amorphous Metglas 2605-S3A, 2605-S2 with Silicon-iron at 400 Hz.

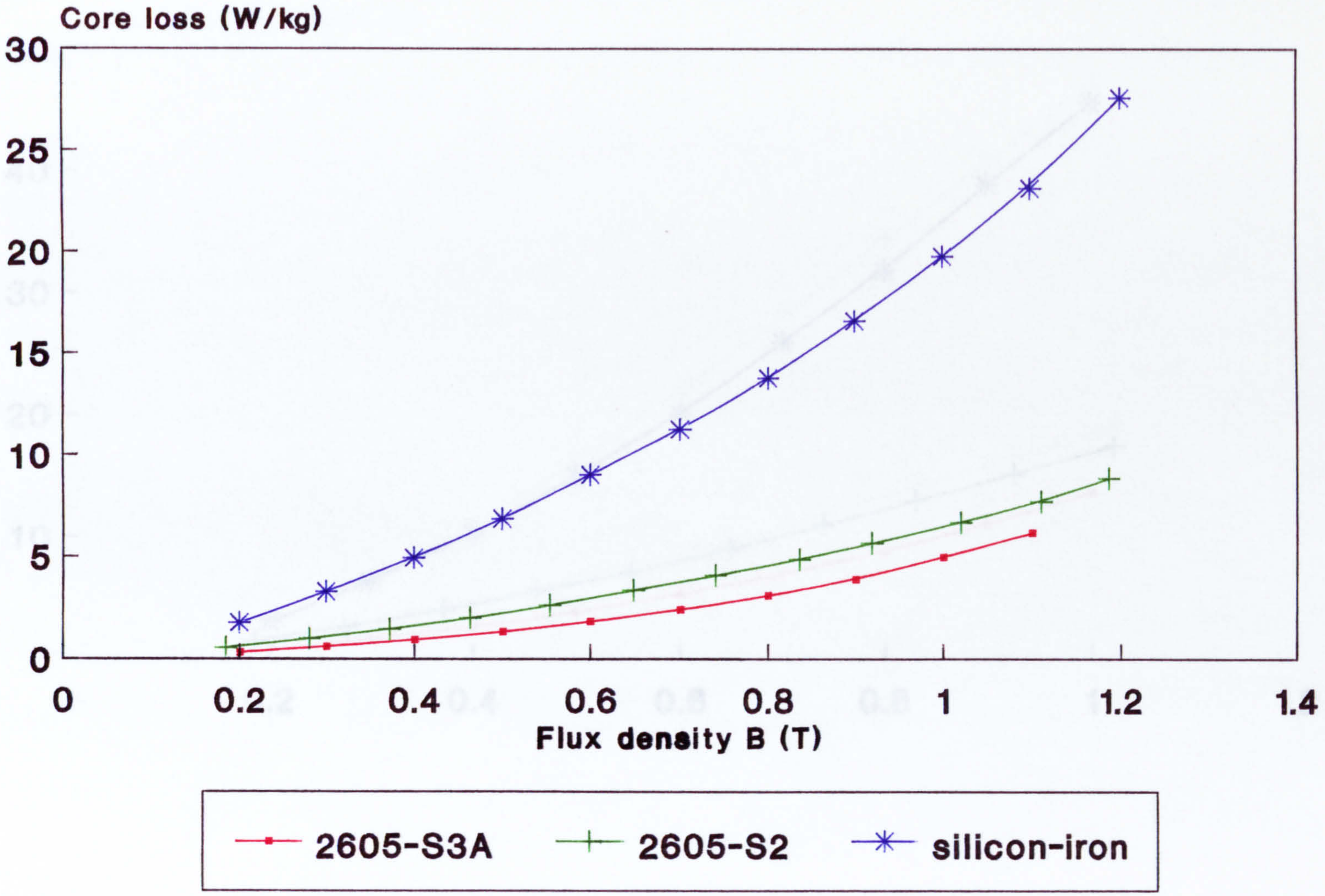

Fig. 7.79 Comparison of core loss of amorphous Metglas 2605-S3A, 2605-S2 with silicon-iron at 1000 Hz.

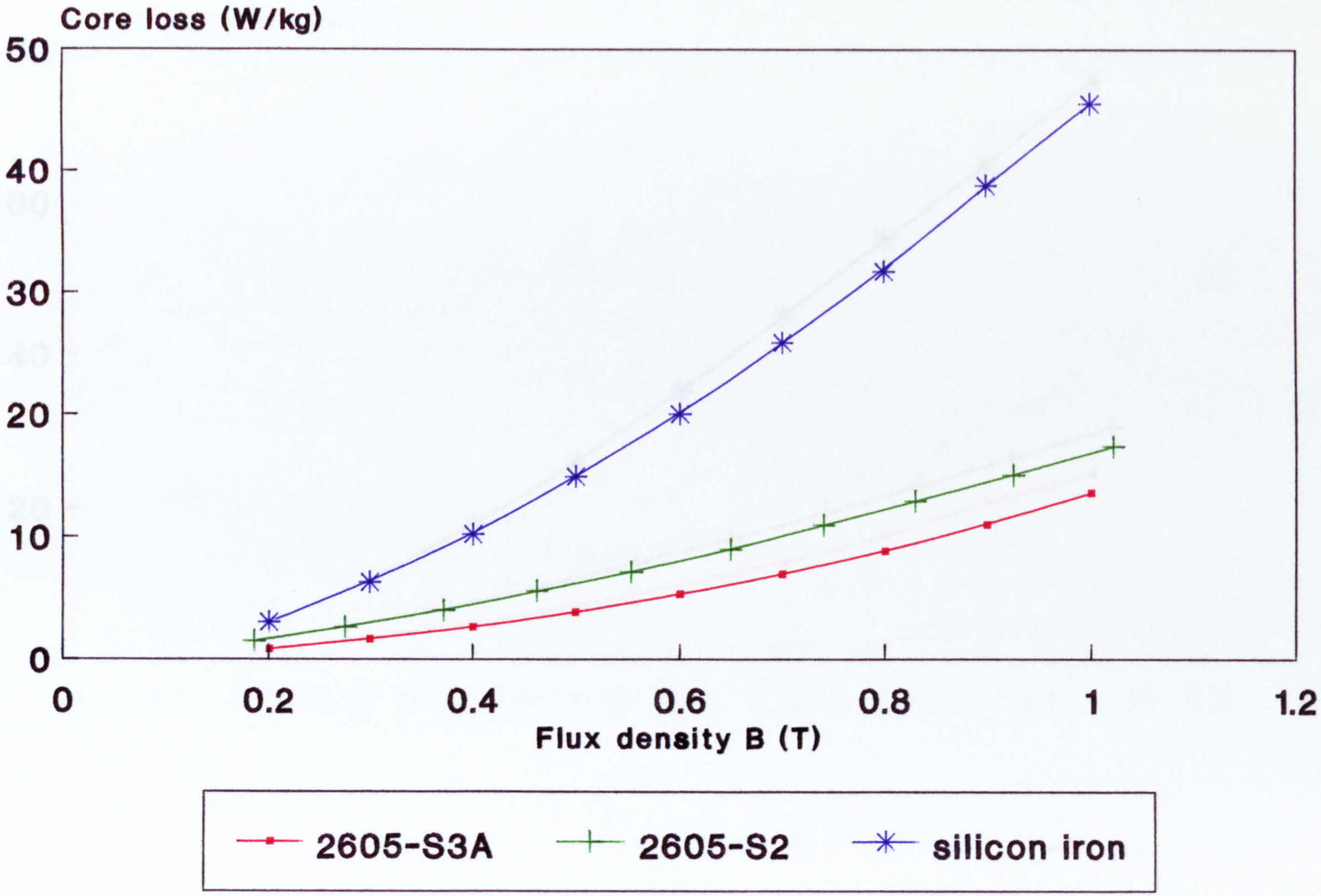

Fig. 7.80 Comparison of core loss of amorphous Metglas 2605-S3A, 2505-S2 with silicon-iron at 2000 Hz.

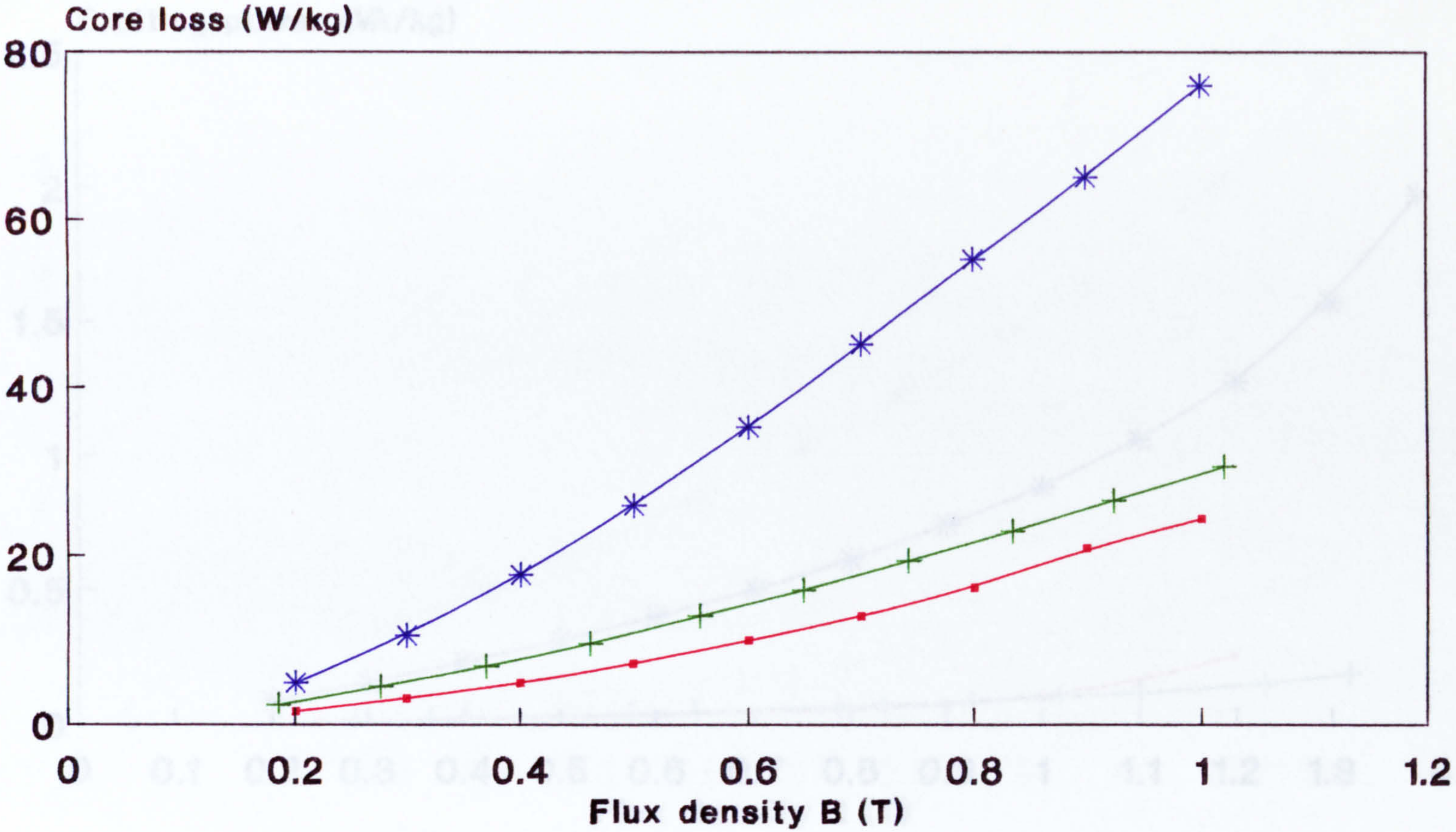

Fig. 7 81 Comparison of core loss of amorphous Metglas 2605-S3A, 2605-S2 with silicon-iron at 3000 Hz.

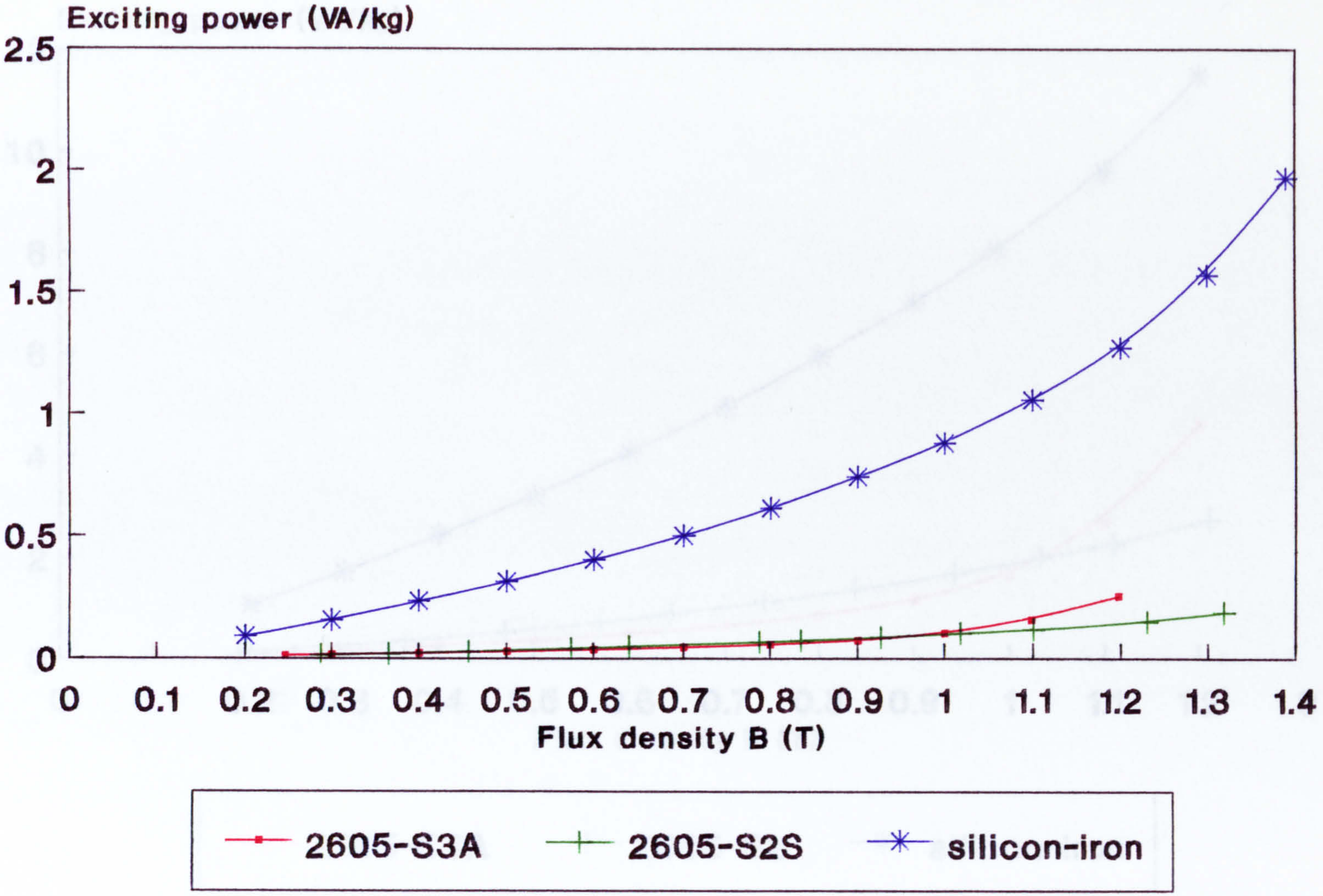

Fig. 7.82 Comparison of exciting VA of amorphous Metglas 2605-S3A, 2605-S2 with silicon-iron at 50 Hz.

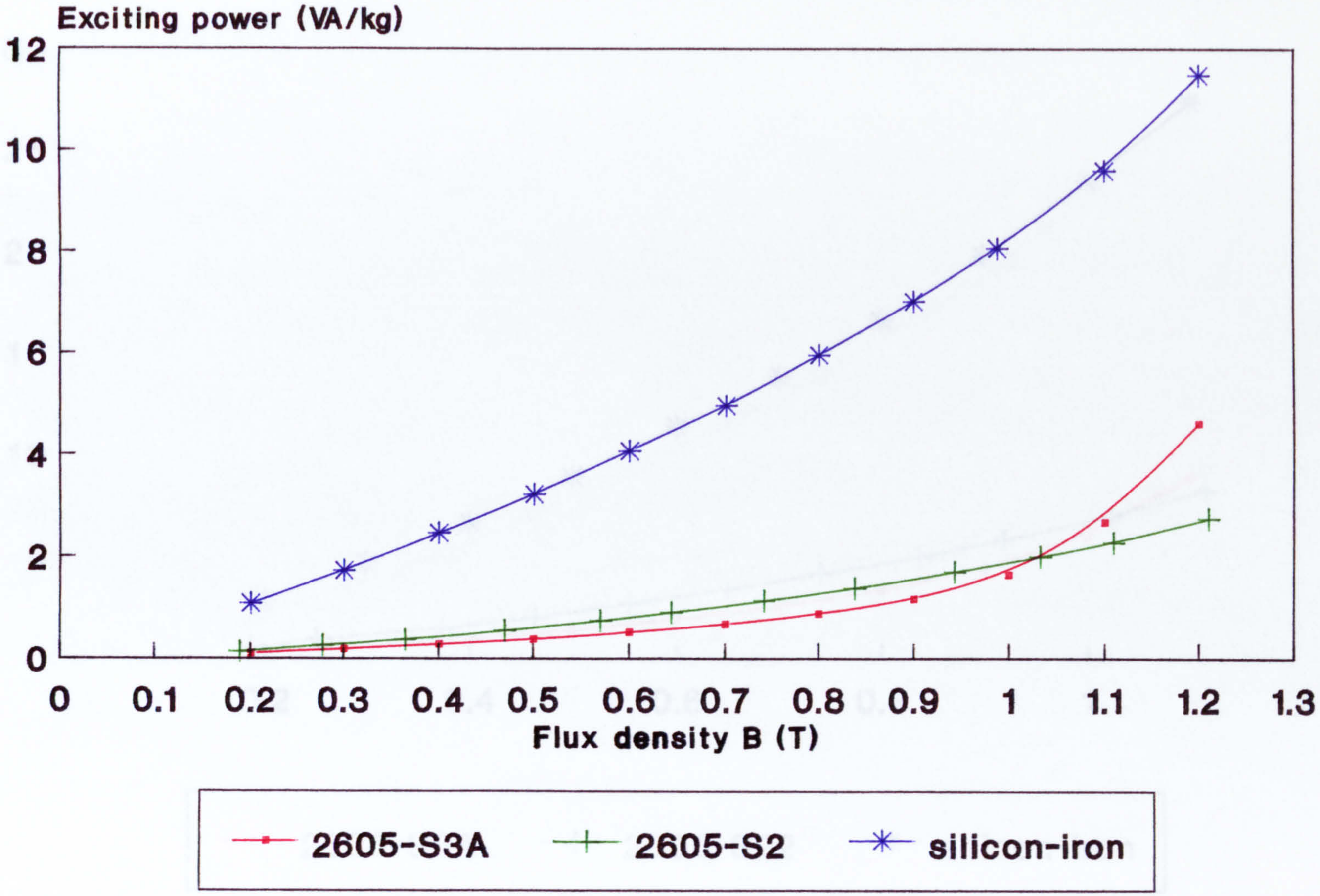

Fig.7.83 Comparison of exciting VA of amorphous Metglas 2605-S3A, 2605-S2 with silicon-iron at 400 HZ.

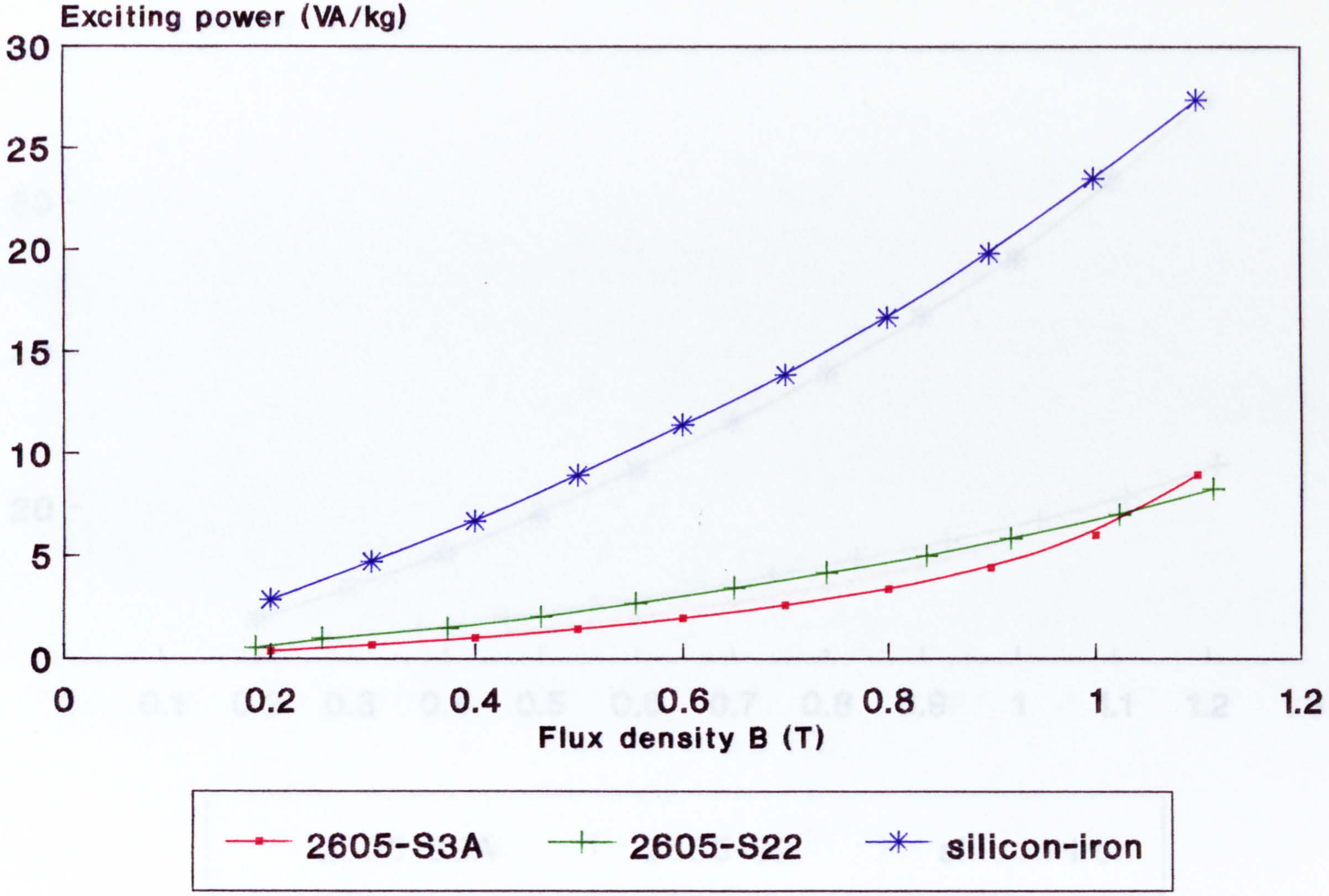

Fig. 7.84 Comparison of exciting VA of amorphous Metglas 2605-S3A, 2605-S2 with silicon-iron at 1000 Hz.

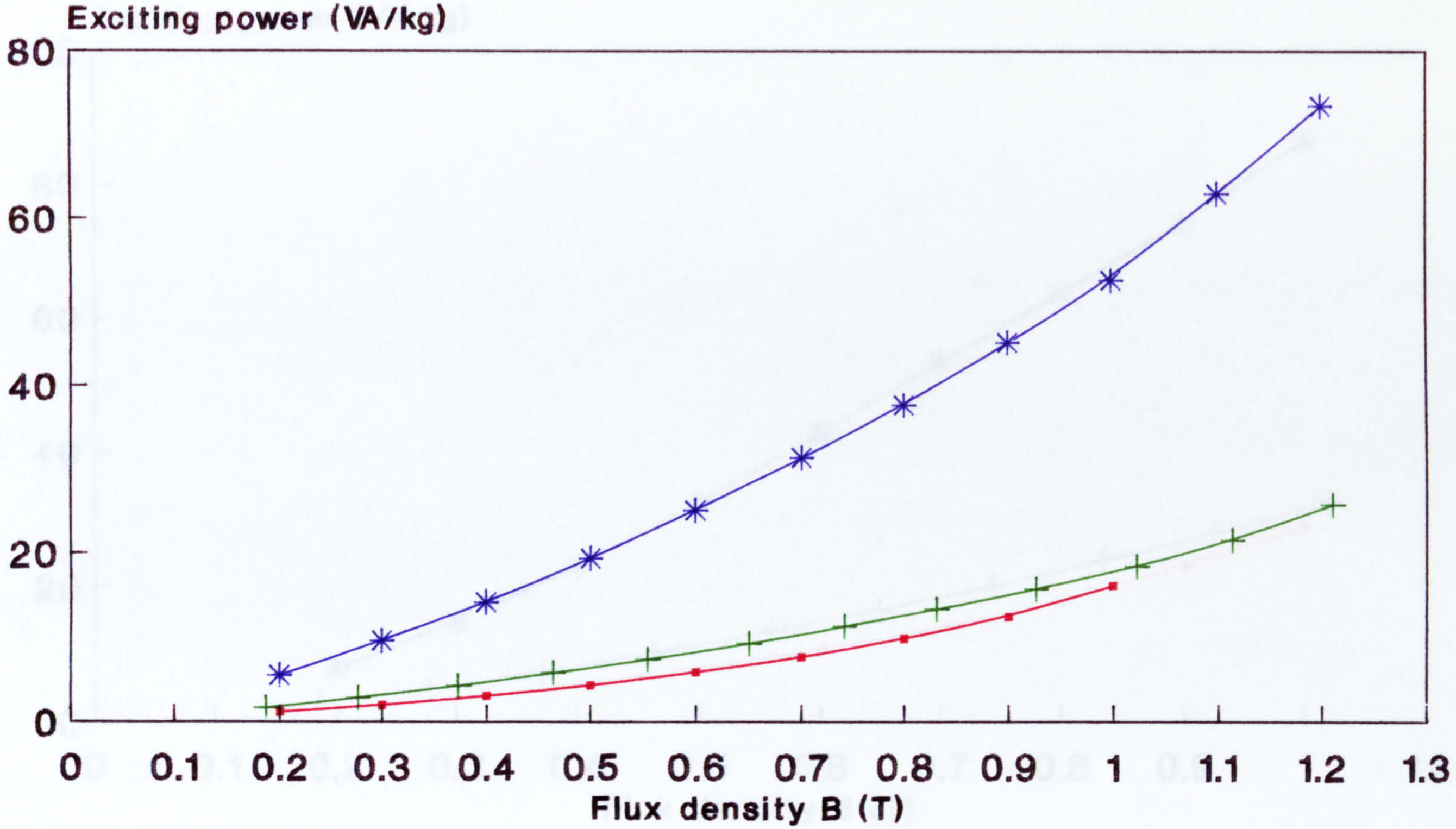

Fig. 7.85 Comparison of exciting VA of amorphous Metglas 2605-S3A, 2605-S2 with silicon-iron at 2000 Hz.

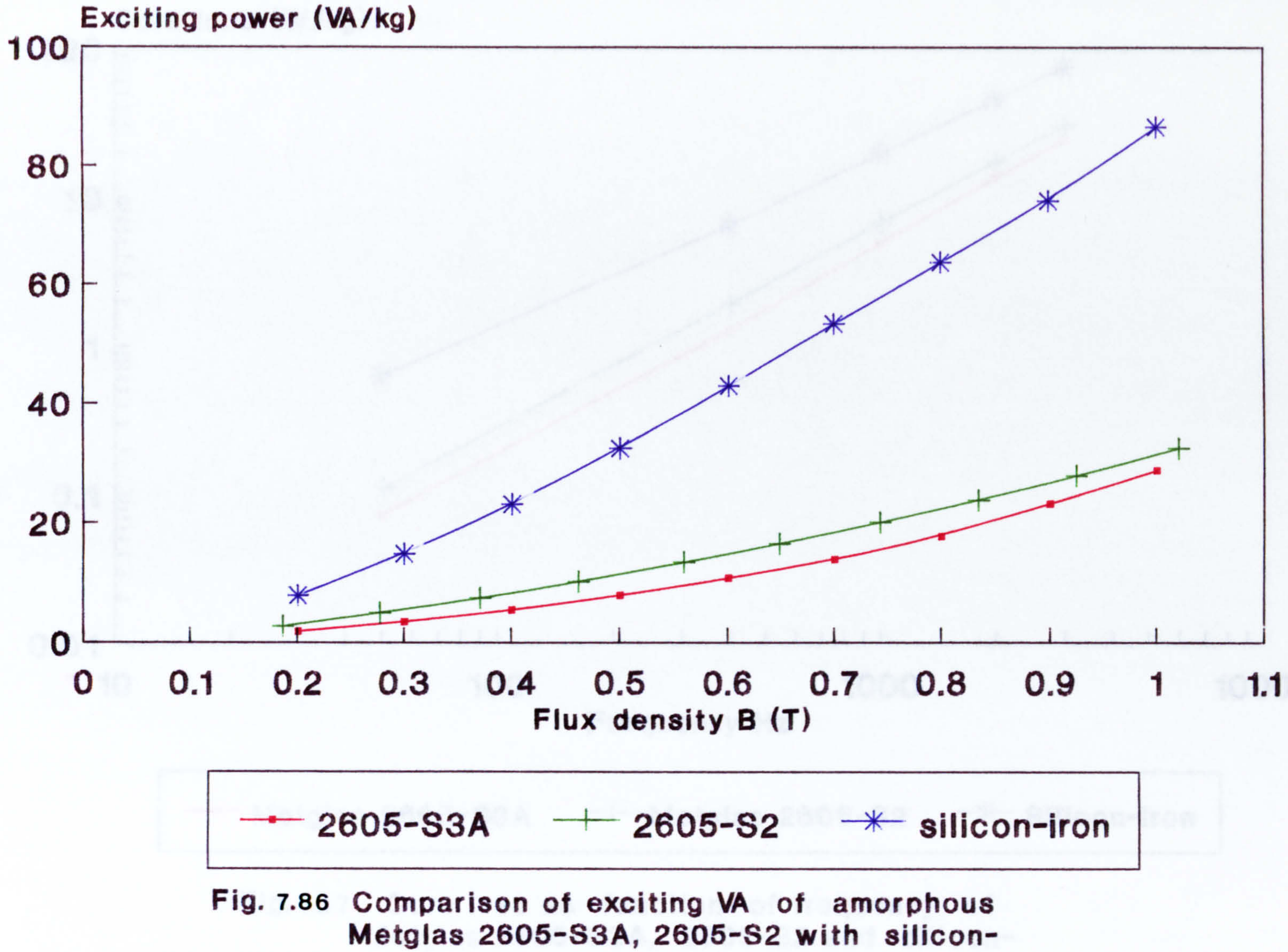

Fig. 7.86 Comparison of exciting VA of amorphous Metglas 2605-S3A, 2605-S2 with silicon-iron at 3000 Hz.

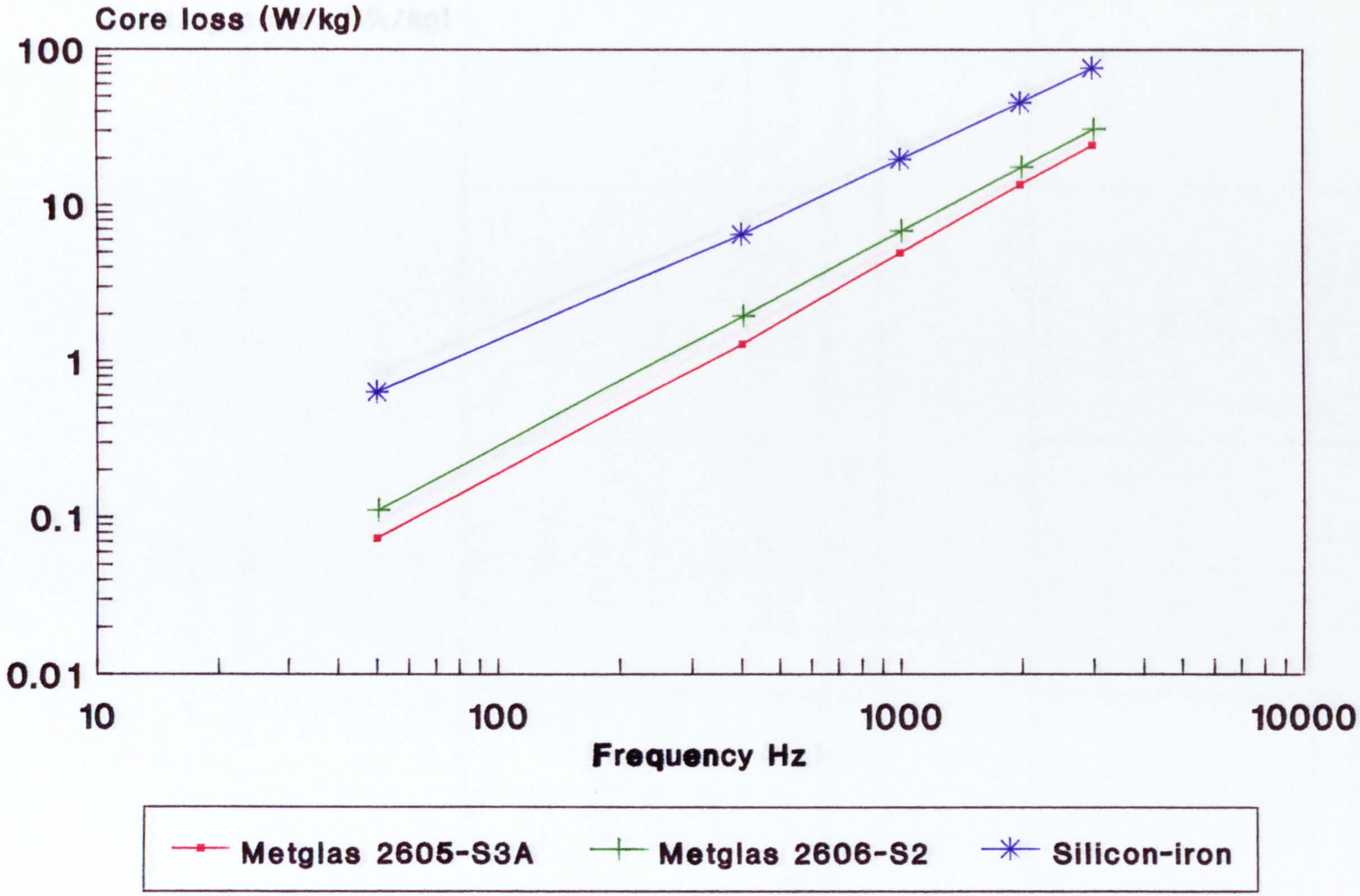

Fig. 7.8 7 Core loss as function of frequency of Metglas 2505-S3A, 2605-S2 and silicon-iron at flux density 1.0-T.

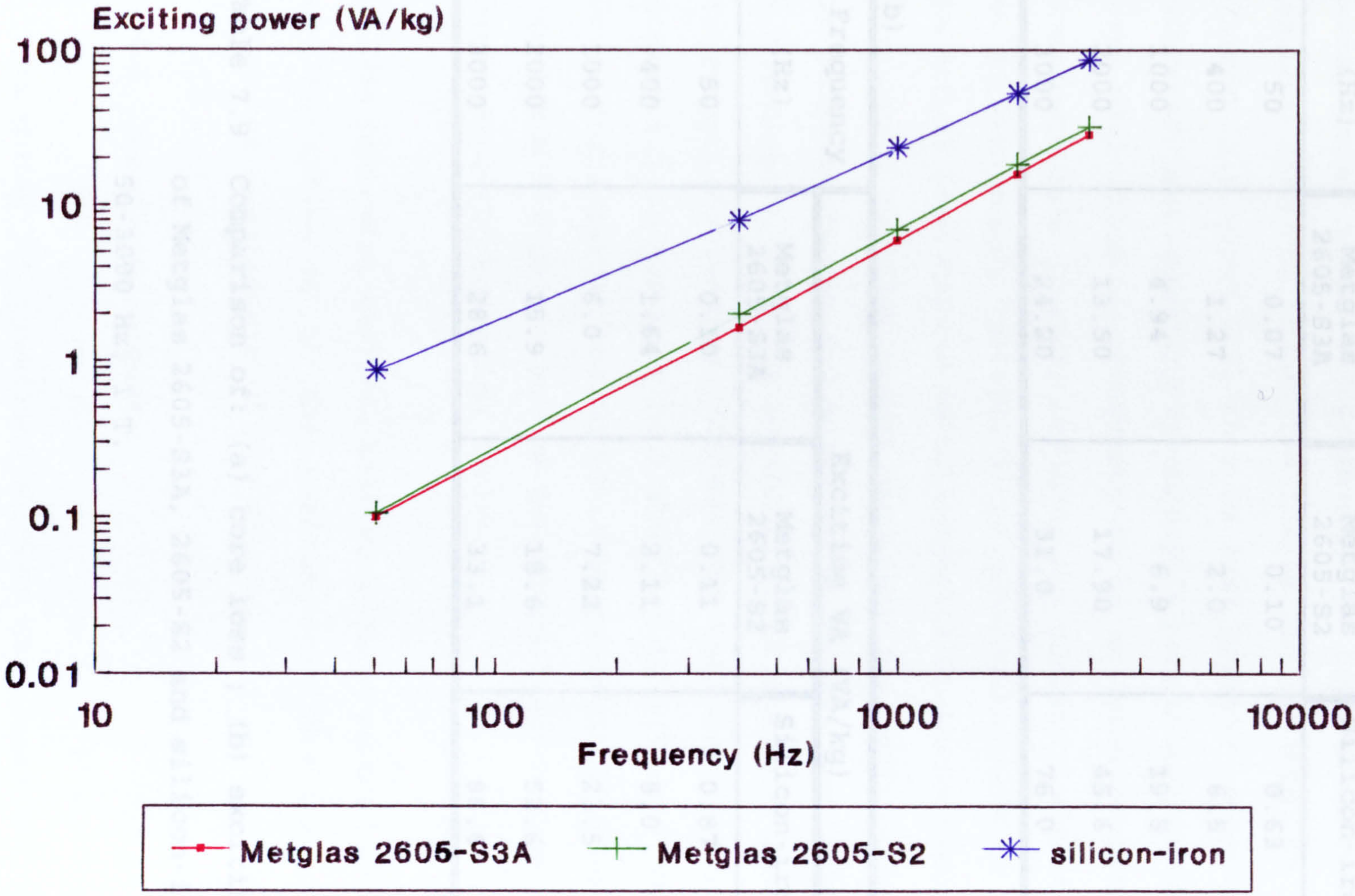

Fig. 7.88 Exciting VA as function of frequency of Metglas 2605-S3A, 2605-S2 with silicon-iron at flux density 1.0-T.

(a)

Frequency (Hz)	Core Loss (W/kg)		
	Metglas 2605-S3A	Metglas 2605-S2	Silicon-iron
50	0.07	0.10	0.63
400	1.27	2.0	6.5
1000	4.94	6.9	19.8
2000	13.50	17.90	45.6
3000	24.20	31.0	76.0

(b)

Frequency (Hz)	Exciting VA (VA/kg)		
	Metglas 2605-S3A	Metglas 2605-S2	Silicon-iron
50	0.10	0.11	0.87
400	1.64	2.11	8.0
1000	6.0	7.22	23.5
2000	15.9	18.6	52.6
3000	28.6	33.1	86.6

Table 7.9 Comparison of: (a) core loss ; (b) exciting VA of Metglas 2605-S3A, 2605-S2 and silicon-iron at 50-3000 Hz, 1 T.

Normally when silicon iron cores are used they are cut to allow for ease of assembly of the windings, the windings having being wound independently on formers before final assembly onto the limbs. The losses and exciting VA for cut silicon iron cores will thus be even greater. When a choice of transformer operating frequency is possible, the amorphous cores will allow the frequency to be at least doubled for a given core loss, thereby reducing the number of winding turns for a given supply voltage. It is interesting also to compare the actual loss and the so called specific loss to obtain the widely used building factor necessary for design purposes. The building factor for uncut silicon cores was found to be in the range 0.74 to 1.3 depending on flux density levels and frequency. For Metglas 2605-S2, the building factor varied between 1.3 to 1.7 at 1 to 3 kHz, 0.3 to 1-T. The buuilding factor for 2605-S3A was found to be higher than 2605-S2 but a reliable figure may not be quoted due to the uncertainies relating to the annealing cycle.

The following sections analyse in more detail the results and the influence of the various conditions encountered during the manufacture of the core.

7.16.3 Annealing Process

According to previous studies the annealing process serves to reduce the losses from those in the as cast state. The ribbon as supplied is in the as cast state and for

optimum results the annealing should be carried out after core manufacture. The annealing will thus relieve the stresses set up during casting as well as during core manufacture.

In addition during the annealing process the application of a magnetic field will further reduce the losses by inducing uniaxial anisotropy.

It is believed that non-field annealing of these amorphous alloys indicates an anisotropy at each domain wall which is caused by local ordering of the metal atoms [124]. This anisotropy tends to pin the domain walls during magnetization and hence degrades magnetic properties. The field annealing process eliminates this anisotropy since the sample is magnetically saturated and atomic ordering at domain walls cannot now occur, hence improved magnetic properties are obtained.

Optimum core loss results will therefore depend on the field annealing cycle, namely the rate of temperature rise, the soak temperature and time of soak, the cooling rate and the magnetic field applied. Previous studies have shown that the application of a magnetic field of a strength at the saturation level produces minimal losses. A small variation in the magnetic field strength about the saturation level is not critical. The soak temperature used during the annealing process can however have considerable influence on the losses

[125]. Crystallisation of the ribbon can occur if the soak temperature is taken too high which in turn has disastrous effects on the magnetic properties and a large increase in power loss may result.

It may be concluded therefore that the soak temperature would most likely be of greatest concern during the annealing process. This is borne out in the results. For Metglas 2605-S2 adequate information is available from the manufacturer of the annealing process including the soak temperature and consistent results were obtained on several cores. However for Metglas 2605-S3A details of the soak temperature were not so specific and the core loss and exciting VA results were disappointing resulting in a large building factor for the one core made.

7.16.4 Mechanical Stresses (Clamping)

The annealing process should relieve the mechanical stresses induced during the casting process and core manufacture. Once annealed the core may be subjected to externally applied mechanical stresses, for example clamping of the core limbs.

Only a small increase in the core losses was measured when a clamping pressure was applied see appendix VI. However there was a significant increase in the exciting VA at flux density levels above 1 T, see figures 7.52 to 7.56. A

comparison of the B/H loops with and without clamping pressure revealed a significant increase in the exciting current required to establish the peak flux density, see figures 7.57 to 7.62.

The results agree with earlier research [126] on a sample of powercore strip (the powercore material comprises several ribbons of amorphous material loosely bonded together in the form of a lamination). A significant increase in exciting VA and less significant increase in losses became evident at high values of B_m (1.4 T) and at high values of pressure (100kPa), these tests refer to a 50 Hz supply. The clamping pressure applied for our small cores was considerably less, 39.6 kPa, values of the order 100 kPa would be appropriate only for large power frequency transformer. It is more than likely that when clamping pressure is applied, compressive stresses are set up in the direction of the applied force and also a righ angles to it, the latter being due to waves in the ribbon layers of each limb.

7.16.5 Core Treated with Adhesive

The effect of the inter-laminar adhesive on the core loss and exciting VA of amorphous Metglas 2605-S2 is shown in Fig.7.89 to 7.94 where direct comparison is made for the same core before and after applying adhesive. The effect of applying adhesive to the core results in an increase of the core loss and exciting VA in the amorphous ribbon. Table 7.10

compares the core losses and exciting VA at 1-T for 1, 2 and 3-kHz.

The increase in the core loss and exciting VA is greater with the adhesive applied when compared with the clamping pressure results. It is likely that the adhesive sets up greater stresses in the ribbon both in the rolling direction and at right angles to the rolling direction.

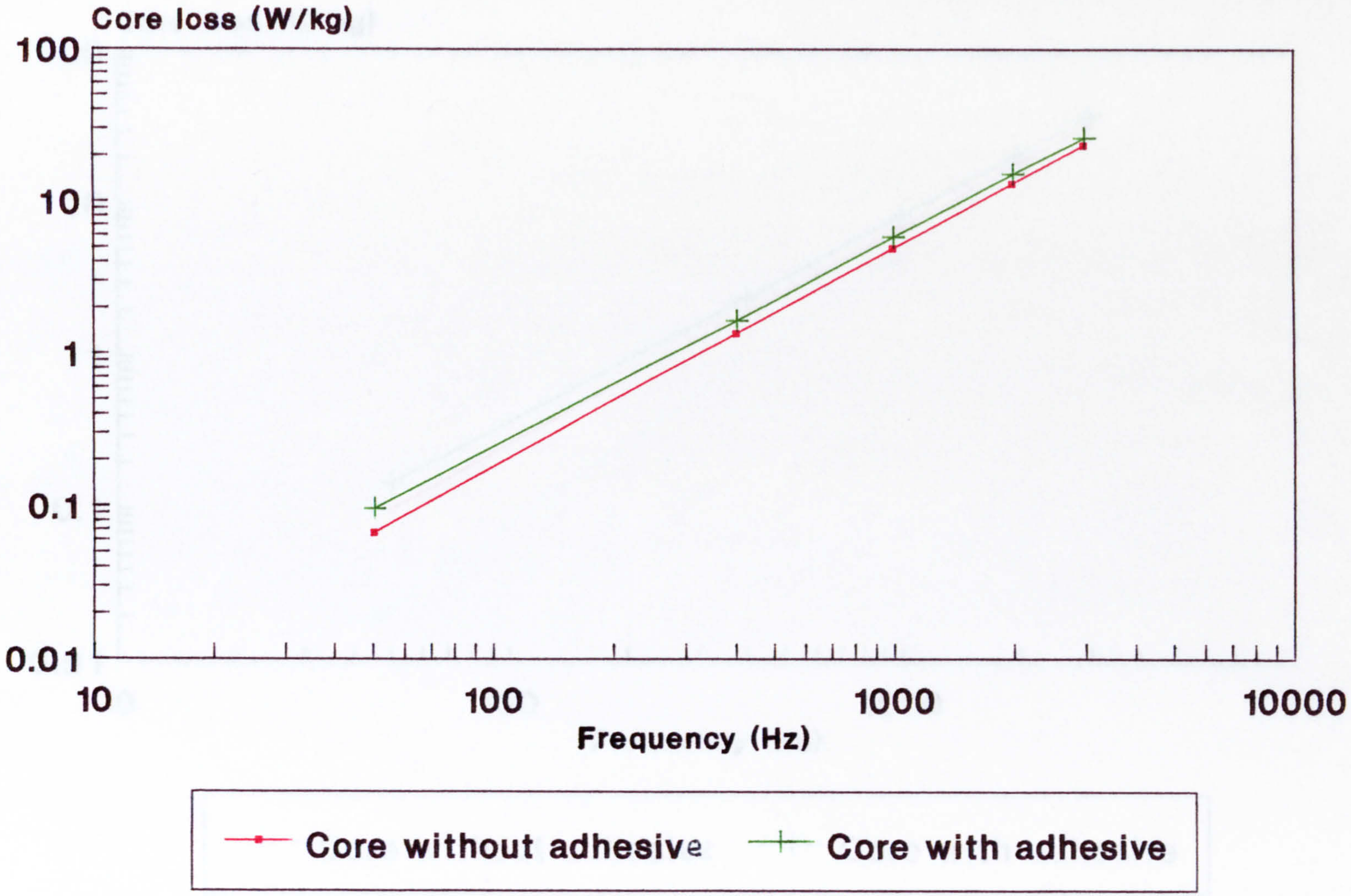

Fig. 7.89 Core loss as a function of frequency of Metglas 2605-S2 without and with applied inter-laminated adhesive at 0.8-T.

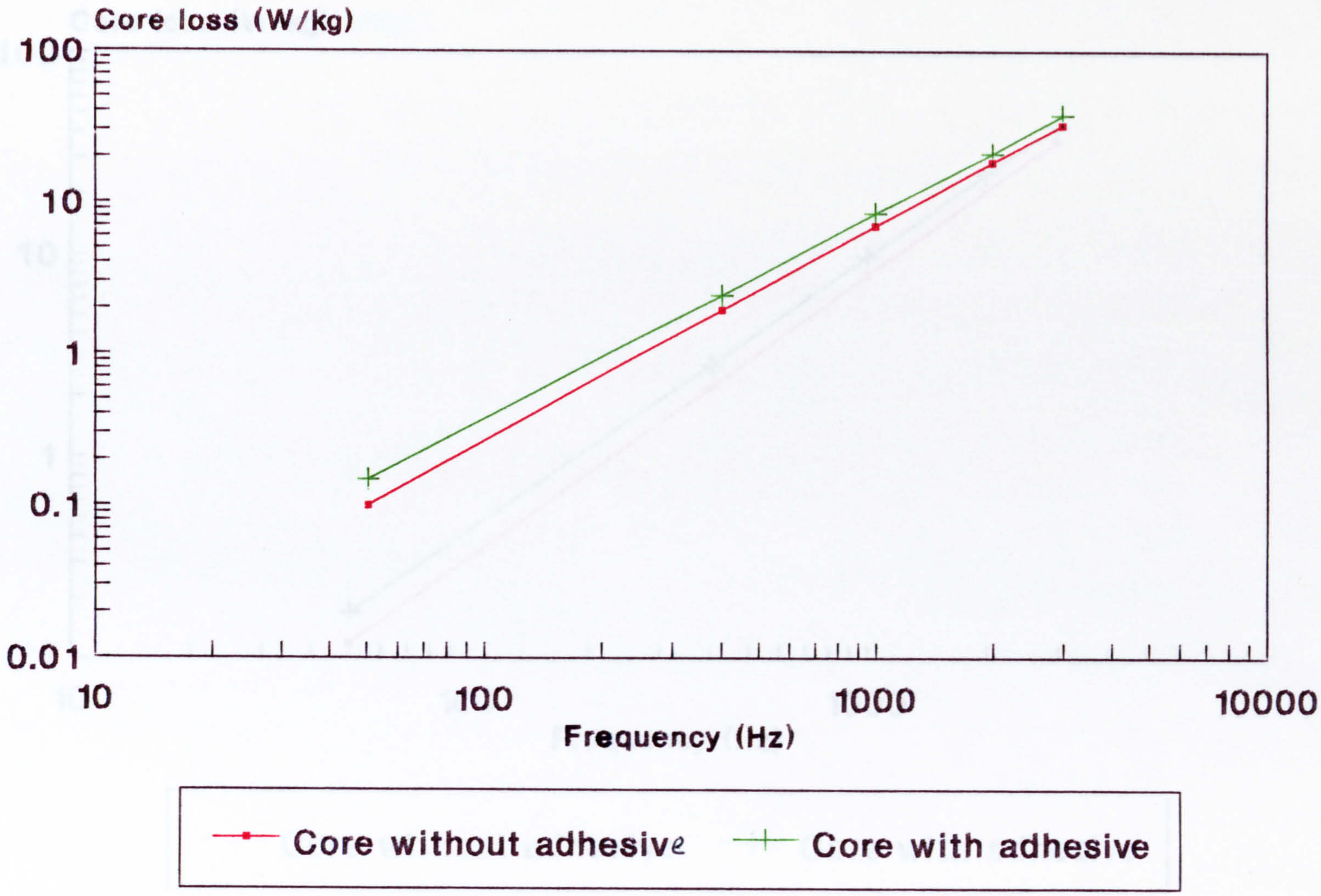

Fig. 7.90 Core loss as a function of frequency of Metglas 2605-S2 without and with applied inter-laminated adhesive at 1.0 T.

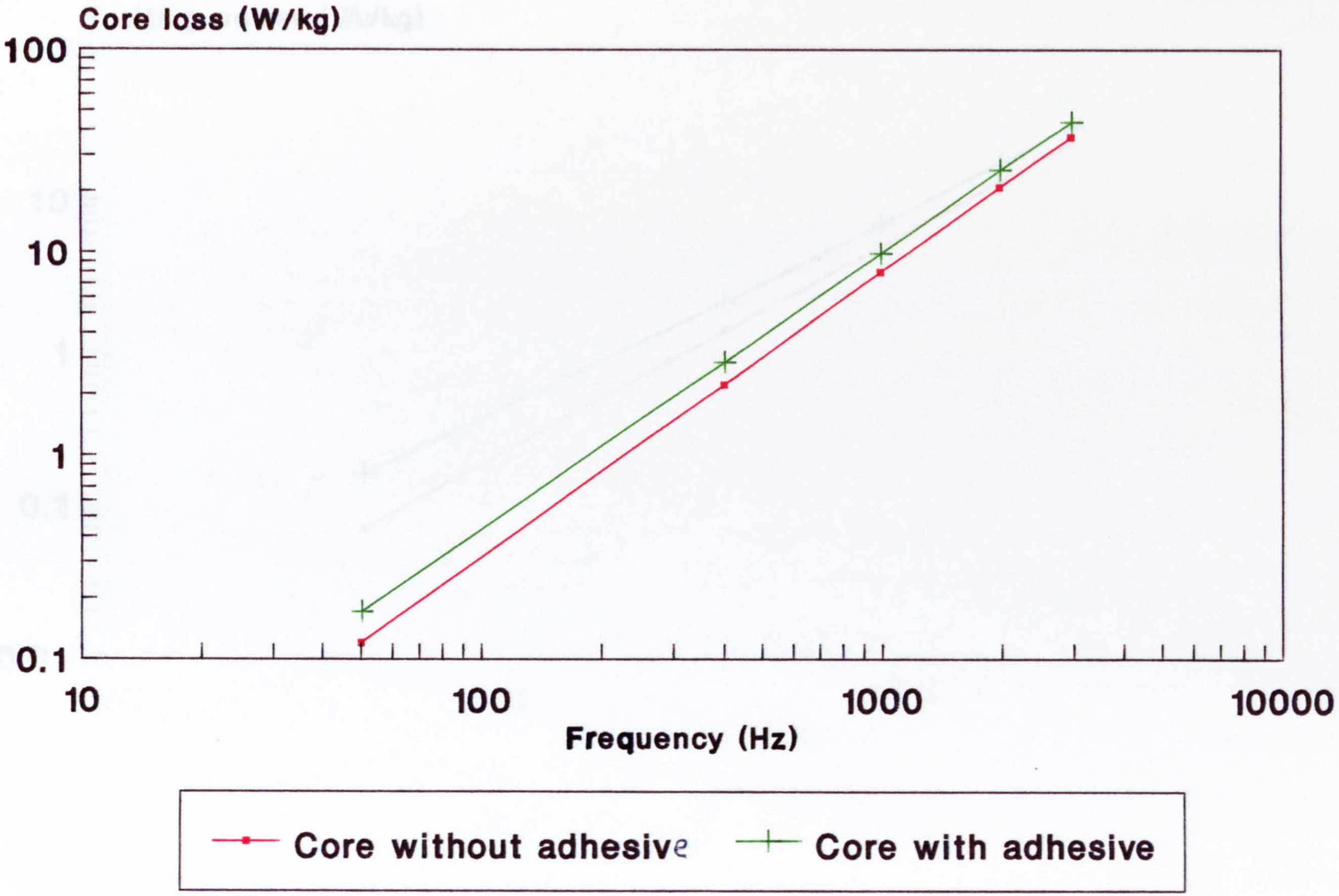

Fig. 7.91 Core loss as a function of frequency of Metglas 2605-S2 without a d with applied inter-laminated adhesive at 1.1 T.

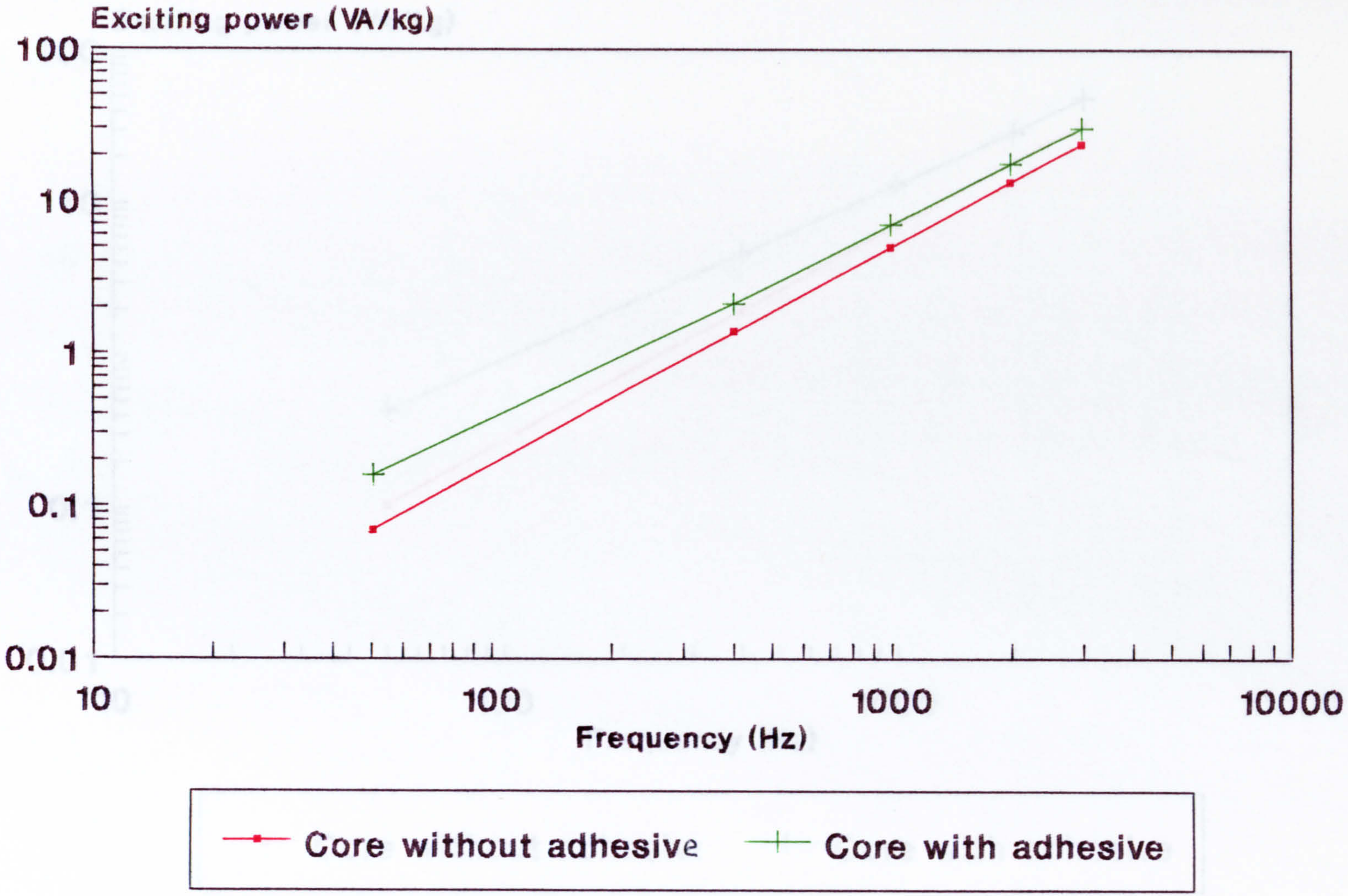

Fig. 7.92 Exciting VA as function of frequency of Metglas 2605-S2 without and with applied inter-laminated adhesive at 0.8-T.

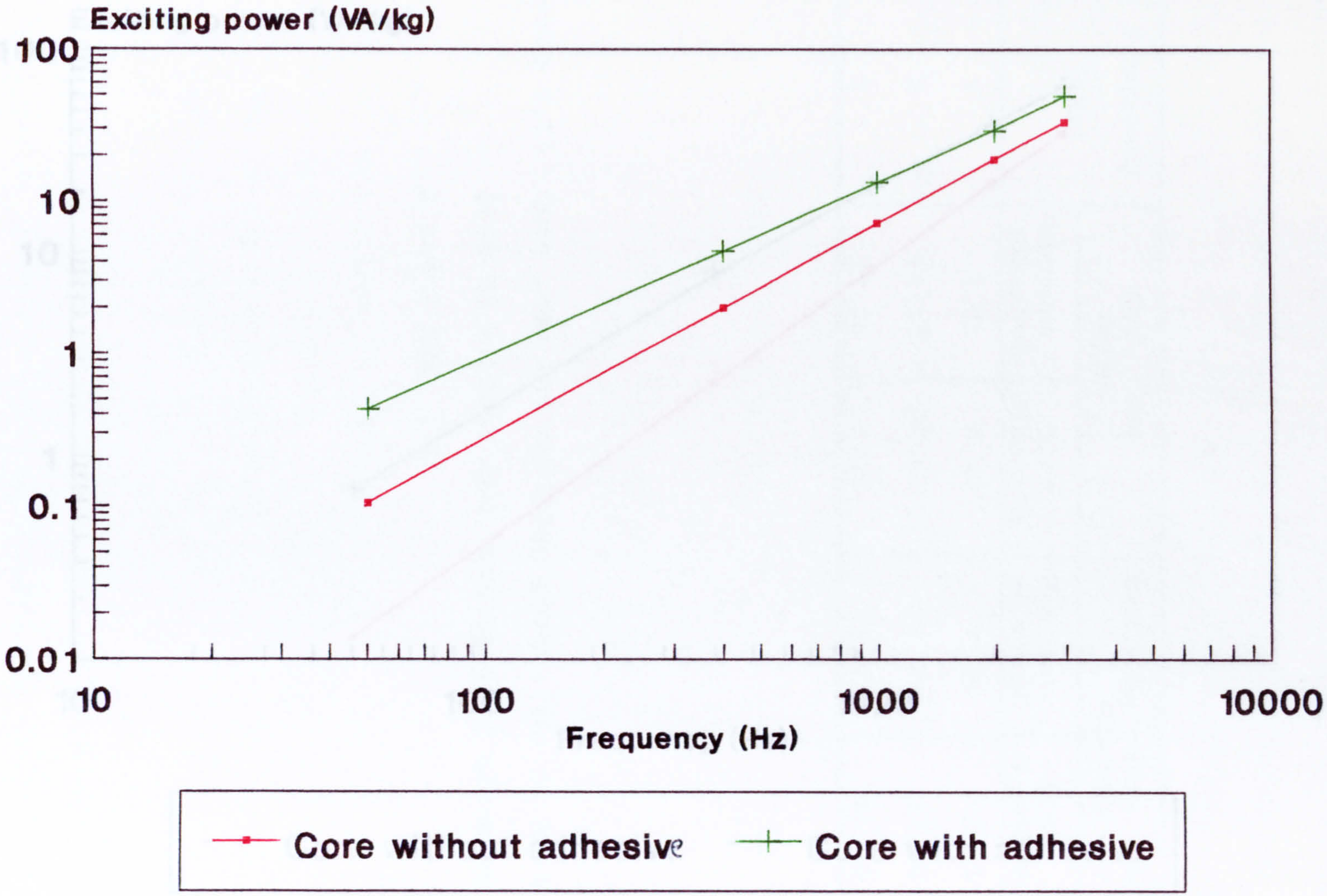

Fig. 7.93 Exciting VA as a function of frequency of Metglas 2605-S2 without and with applied inter-laminated adhesive at 1-T.

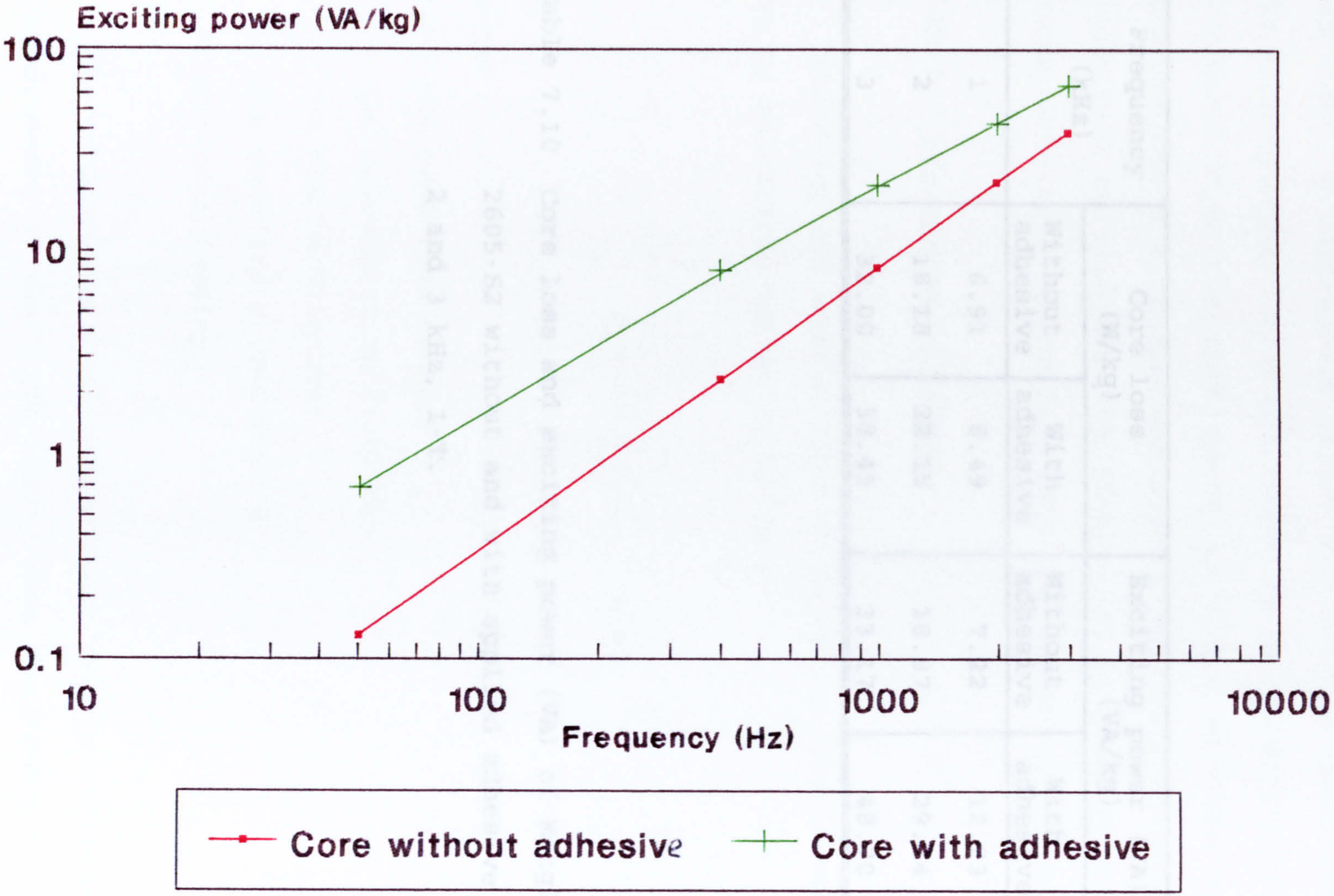

Fig. 7.94 Exciting VA as a function of frequency of Metglas 2605-S2 without and with applied inter-laminated adhesive at 1.1T

Frequency (kHz)	Core loss (W/kg)		Exciting power (VA) (VA/kg)	
	Without adhesive	With adhesive	Without adhesive	With adhesive
1	6.91	8.49	7.22	12.23
2	18.18	22.15	18.87	29.24
3	32.00	38.45	33.17	48.70

Table 7.10 Core loss and exciting power (VA) of Metglas 2605-S2 without and with applied adhesive at 1, 2 and 3 kHz, 1-T.

Previous research has shown that compressive pressures increase the losses whereas extensive pressure lead to a reduction. A compressive stress may well be established in the rolling direction of the ribbon by the interaction of the adhesive. When the core heats up these stresses may be enhanced due to differing expansion properties. However it is impossible to separate the effects of increasing material resistivity with temperature from the changes due to stress.

7.16.6 Separation of Losses

The classical eddy current component of the losses, P_e, can be calculated using the formula:

$$P_e = \frac{(\pi\ B\ f\ t)^2}{6\sigma\rho} \quad W/kg \qquad (7.24)$$

where

B = the peak flux density

f = the magnetization frequency

t = the sample thickness

ρ = the material's resistivity

σ = material density.

The value of the total eddy current loss is obtained from a measurement of the total losses less the hysteresis loss. The value of the excess eddy current or anomalous loss component may be determined and the associated anomaly

factor, η, which is defined in equation 4.22 in chapter 4.2.1.

Table 7.11 gives the values of thickness, t, resistivity, ρ and density, σ, used in this investigation. The value of σ, ρ and thickness were obtained from the literature [127,128]. Table 7.12 to 7.14 show the values calculated of the anomaly factors at 1.0 T, 50-3000 Hz for the Metglas 2605-S2, 2605-S3A and silicon-iron. The anomaly factor for the Metglas 2605-S3A and 2605-S2 is much higher than the anomaly factor measured for the 3 % silicon-iron, for example at 50 Hz magnetization the anomaly factor for (Metglas 2605-S3A) is 286, for Metglas 2605-S2 is 103 and for silicon-iron is 22. However, at higher frequencies the anomaly factors were reduced for example at 3 kHz the anomaly factor for (Metglas 2605-S3A) was, 50, (Metglas 2605-S2) was , 26.7 and (silicon iron), 4.3. The values of anomaly factor are however much higher than those measured in conventional electrical sheet steel.

Material	Thickness t (m)	Resistivity ρ (Ωm)	Density σ (kg/m^3)
Metglas 2605-S2	2.5×10^{-5}	1.37×10^{-6}	7.18×10^{3}
Metglas 2605-S3A	1.77×10^{-5}	1.38×10^{-6}	7.29×10^{3}
Silicon-iron	5×10^{-5}	0.48×10^{-6}	7.65×10^{3}

Table 7.11 Material parameters of the Metglas 2605-S2, 2605-S3A and silicon-iron.

Frequency (Hz)	Total power loss (W/kg)	Hysteresis loss (W/kg)	Excess eddy current loss (W/kg)	Anomaly factor (η)
50	0.107	0.08	0.026	103
400	2.0	0.72	1.26	76.6
1000	6.9	1.82	4.99	48.8
2000	17.90	4.1	13.38	33.0
3000	31.0	5.9	24.1	26.7

Table 7.12 Total power loss, hysteresis loss, excess eddy current loss and anomaly factor of Metglas 2605-S2 at 1.0 T core No.1

Frequency (Hz)	Total power loss (W/kg)	Hysteresis loss (W/kg)	Excess eddy current loss (W/kg)	Anomaly factor (η)
50	0.63	0.55	0.078	22.0
400	6.53	4.4	1.95	12.0
1000	19.8	11.0	7.60	6.9
2000	45.6	22.2	18.90	5.2
3000	76.0	33.30	32.65	4.3

Table 7.13 Total power loss, hysteresis loss, excess eddy current loss and anomaly factor of silicon-iron at 1.0 T.

Frequency (Hz)	Total power loss (W/kg)	Hysteresis loss (W/kg)	Excess eddy current loss (W/kg)	Anomaly factor (η)
50	0.074	0.039	0.034	286
400	1.27	0.31	0.95	123
1000	4.97	0.77	4.16	86
2000	13.50	1.55	11.75	61
3000	24.2	2.32	21.56	50

Table 7.14 Total power loss, hysteresis loss, excess eddy current loss and anomaly factor of Metglas 2605-S3A at 1.0 T.

7.16.7 Core Temperature Rise Without and With a Heat sink

The deciding criteria for the maximum operating frequency and flux density of a core will be the temperature rise of the core. The maximum continuous service temperature of the amorphous material according to the manufacturer of Metglas must not exceed 150°C. The temperature rise of the test cores were therefore measured for various operating flux densities and frequencies both without and with a heat sink being attached. A heat sink was found to be necessary at 1-T, 3-kHz to stop the core temperature exceeding 150°C. The two heat sinks attached to the core yokes, each had a thermal resistance of 0.54°C/W. From these temperature rise tests it is possible to predict the operating core flux density and frequency for a specified core temperature rise. A graph is shown in Fig. 7.95 from which predictions may be made for the operating frequency and flux density for various core temperature rises both without and with a heat sink. The addition of a heat sink permits a significant increase in operating flux density, for example at 3-kHz and a core temperature rise of 80°C, the operating flux density may be increased from 0.5-T to 0.9-T.

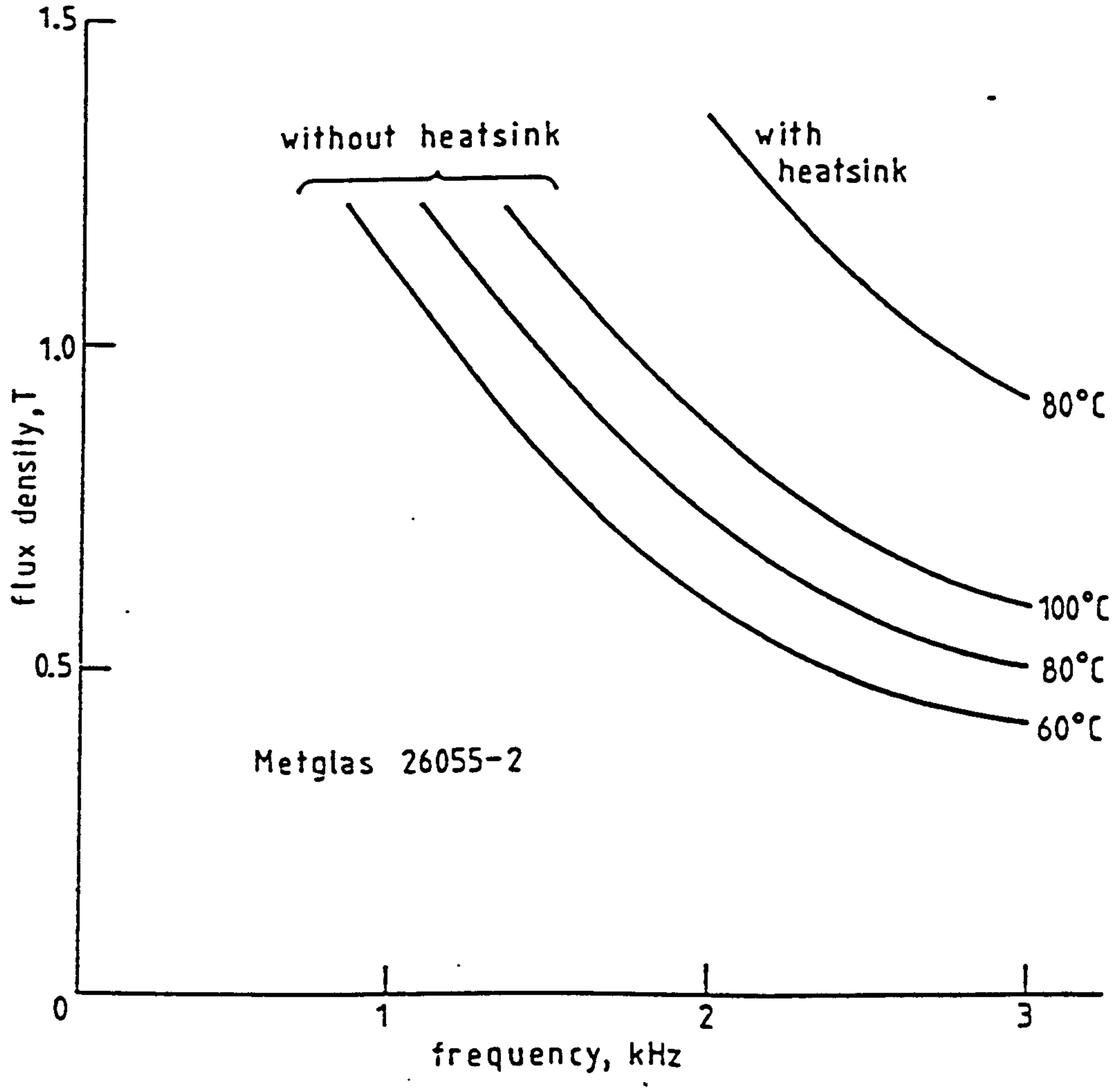

Fig. 7.95 Core temperature rise.

CHAPTER 8

8.0 CONCLUSION

The initial design comparison studies illustrated the advantages of using amorphous metals compared with silicon-iron in medium frequency power transformers. Their apparent ability to operate at high levels of flux density provide the possibility of considerable savings in core size and weight. Similar economies would also result with the winding dimensions. Of the various amorphous alloys available, two iron based alloys were chosen from the range manufactured by Allied Signal. The type 2605-S2 has commonly been used in power frequency transformers and was therefore likely to be the cheapest available. The other type chosen was 2605-S3A which from inspection of its characteristics had lower losses and would therefore be useable at higher frequencies than 2605-S2 with high flux density levels maintained. For the transformer rating chosen for the core design, the research has shown that 2605-S2 may be operated at 1.2 T, 1 kHz and 0.9 T, 3 kHz without excessive core temperature rise occurring. With attention to assisted cooling in the form of heat sinks, forced fan or possibly oil immersion, higher flux densities and frequencies are possible. The other amorphous material investigated, the type 2605-S3A, provided disappointing results, its losses were only about 23% less at 1 T 3 kHz. Although this would permit operation at 1 T 3 kHz, much higher levels would be doubtful. The manufacturers data

indicated a much greater reduction for example 57% at 1 T 3 kHz, when comparing directly the specific loss figures quoted for 2605-S3A and 2605-S2. The cause of the higher than expected losses was almost certainly due to the annealing process carried out, further comment follows later.

The assembly of the wound type cores using the ribbon material posed few problems with only ribbon tension and alignment of mandrel needing careful setting. Uncut cores were deemed essential to minimise losses. The actual cutting of the ribbon would have required special techniques and equipment.

The method of assembly of the core and winding needs careful consideration particularly with regard to the mechanical stresses placed on the core. Essentially there are two possible methods of assembly (a) the conventional arrangement whereby the core supports the windings or (b) the windings are wound onto formers and the core is supported by the windings formers. Another factor to be considered is that following the annealing of the core, the ribbon material is prone to flaking and the core is flexible. After careful assessment, method (b) was chosen, the core being supported by the winding formers. The core itself was protected by wrapping in polyimide tape which is able to sustain temperature in excess of the maximum core temperature allowed. The core was then subjected to minimal externally applied pressure .

An alternative method of core support was tested using adhesive wicked in between the ribbon layers. This produced a very rigid self supporting core. However an increase in the core losses and exciting VA was sustained due most likely to stresses set up in the ribbon by the adhesive. Despite the increased losses the core treated with adhesive cooled better than the untreated type. Extended testing of this type of core would be necessary to assess whether cycling of the core temperature produced any detrimental effects over a long period.

Another feature of core manufacture was the annealing process. For minimal core losses careful attention needs to be paid to heat up rates, soak temperature and cooling rates. Adequate information is available for 2605-S2 annealing cycle but not for 2605-S3A. Consistent results were obtained for several 2605-S2 cores made but the results for 2605-S3A were disappointing. It was likely that the soak temperature for 2605-S3A was not the optimum and insufficient ribbon was available to carry out further investigation.

Summarising, the assembly of an amorphous cored medium frequency power transformer is perfectly feasible without any expensive machinery requirement. The objectives of limiting the core size and weight have been met with operating flux densities of 1 T at 3 kHz. Higher frequencies are likely to be possible with other alloy types.

REFERENCES

(1) Boll, R. and Warlimont, H.IEEE Trans. Mag.Vol. Mag-17,No.6, 3053, Nov.1981.

(2) Datta, A., DeCristoforo N.J. and L.A. Davis, Proc. of 4th Int'l Conf. on Rapidly Quenched Methods, (T.Masumoto and K. Suzuki, eds) Japan Inst. of metals, sendai, 1982, P.1007; R.Hasegawa, G.E. Fish and V.R.V. Romanan, p.1031.

(3) Chen, D.Y.Proc. IEEE Vol.69, p.853, 1981.

(4) Honoma, K.,Nozaawa,T., Kobayashi, IEEE Trans. on Mag. MAG-21, p.1903, 1985.

(5) Salsgiver, J.A Journal of Metals Vov.1, 27, 1986.

(6) Warlimont, H, "Rapidly Quenched Metals", Conf.North-Holland, Amsterdam Vol.II. p.1599, 1985.

(7) Slemon, G.R. and Straughen, A.," Electric Machines", Chapter 2 , 1980.

(8) Crompton, A.B. "Theory of Transformer Design Principles". Chapter 2, Modern Power Transformer Practice. Edited by R. Feinberg, Macmillan Press Ltd., 1979.

(9) Say, M.G. "Alternating Current Machines". Chapter 1, Pitman Publishing Ltd., 1976.

(10) Gordy, T. D., and Somerville, G. G. "Single-Phase Power Transformer Formed Cores", Trans. Am. Inst. Electr. Eng., Vol.69, p.1384, 1950.

(11) Kerr, H.W., "Windings". Chapter 5, in Modern Power Transformer Practice. Edited by R. Feinberg.

Macmillan Press Ltd., 1979.

(12) Cotton, H., "Electrical Technology", Pitman,Ltd, 6th Edition.

(13) Slemon, G.R. and Straughen, A.," Electric Machines", Chapter 1, 1980.(OP.Cit.)

(14) Blundell, M.G., Ph.D. Thesis, University of Wales, pp. 20-32, 84, 85, 1981.

(15) Overshott, K.J., "The Use of Domain observations in Understanding and Improving Magnetic Properties of Transformer Steels", IEEE Trans. Mag.Vol. 12, 1976, pp. 840-845.

(16) Overshott, K.J., "The causes of the Anomalous Loss in Amorphous Ribbon Materials", IEEE Trans. Mag., Vol. 17, No. 6, Nov. 1981, pp. 2698-2700.

(17) Wilkins, J.T. and Thompson, J.E. Elect. Times, Vol. 141, p.233, 1962.

(18) Waker, J.H., Rogers, G.J. and Jackson, R.L. Proc. IEE, p111, 1964.

(19) Bancks, P.J. and Rawlinson, E. IEE, 114, (10), p.1537, 1967.

(20) Brown, W.R., Holt, C. and Thompson, J.E. Proc. IEE, 11, p.183, 1965

(21) Houze, G.L. J. Appl. Phys., Vol.40, p1090, 1969.

(22) Houze, G.L. J. Appl. Phys., Vol.38, p.1089, 1967.

(23) Yamamoto, T. and Nozawa, T. J. Appl. Phys., 41, p.2981, 1970.

(24) Barrent, W.F., Brown, W. and Hadfield, R.A., Sci. Trans. Roy. Dunlin Soc. Vol.7, p.67, 1900.

(25) Hadfield, R.A., U.S. Pat. 745, 829, 1903.

(26) Gumlich, E. and Goerens, P., Trans. Farady Soc. Vol.8, p.98, 1912.

(27) Goss, N.P. U.S. Pat., 1,965,559, 1934.

(28) Nippon Steel Technical Report, No.21, p.127-134, June 1983.

(29) Taguchi, S. and Sakakura, A., U.S. Pat., 3, 159, 511, 1964, Japan, Pat., Sho. 33-4710, 1958.

(30) Taguchi, S., Sakakura, A. and Takashima, H., U.S. Pat., 3. 28, 183, 1966, Japan Pat., Sho. 40-15644, 1965.

(31) Sakakura, A., Taguchi, S., Wada, T., Ueno, K., Yamamoto, T. and Urushiyama, N., U.S. Pat., 3, 636, 579, 1972. Japan. Pat., Sho. 46-23820, 1971.

(32) Taguchi, S. and Skakura, A. J. Appl. Phys., Vol.40,No.3, pp.1539-1541, 1969.

(33) Goto, I., Matoba, I., Imanaka, T., Gotoh, T. and Kan, T. Proc. Soft Mag. Mat. Conf. Vol.2, p262, 1975.

(34) Barison, M. and Candiotti, M. IEEE Trans. MAG-14, p.345, 1978.

(35) Fiedler, H.C. IEEE Trans. MAG-13, p.1433, 1977.

(36) Yamamoto, Y. and Taguchi, S., Proc. Soft Mag. Mat. Conf. Vol.2, 1975.

(37) Hayes, D.M. and Wolford, D.S., U.S. Pat., No.2234968, 1924.

(38) Kuroki, K. and Tanaka, O., Japan. laid open Pat., Sho. 53-137016, 1979.

(39) Nozawa, T., Yamamoto, T., Matsuo, Y. and Ohya, Y.,

IEEE Trans. MAG-15, Vol.2, p.972, 1979.

(40) Ichiyama, T., Yamaguchi, S., Iuchi, T. and Kuroki, K., Japan. laid open Pat., Sho 56-51529, 1981.

(41) Ichijima, I., Nakamura, M., Nozawa, T. and Makata, T., IEEE Trans.MAG-20, No.5, p.1557-1559, 1984.

(42) Graham, Jr. C.D.,"Textured Magnetic Materials". Chapter 15, in Magnetism and Metallurgy. Edited by AMI E. Berkowitz and Eckart Kneller Vol.2, 1969.

(43) Littmann, M.F., J. Appl. Phys., Vol.38, p.1104-1108, 1967.

(44) Yamamoto, T., Taguchi, S., Sakakura, A. and Nozawa, T., IEEE Trans. MAG-8, No.3, p.677-681, 1972.

(45) Taguchi, S., Trans. ISIJ, Vol.17, p.604-615, 1977.

(46) Taguchi, S., Yamamoto, T. and Sakakura, A., Proc. Soft Mag. Mat. Conf., 1973.

(47) Iuchi, T., Yamaguchi, S., Ichiyama, T., Nakamura, M., and Kuroki, K., J. Appl. Phys., Vol.53, No.3, p.2410-2412, 1982.

(48) Eto, K. Japan. laid open Pat., Cho. 55-131124, 1980.

(49) Beckley, P., Snell, D. and Lockhart, C., J. Appl. Phys., Vol.57, No.1, p.4212-4213, 1985.

(50) Krause, R.F. Rauch, G.C., Kasner, W.H. and Miller, R.A., J. Appl., Phys., Vol.55, No.6, p.2121-2123, 1984.

(51) Von Holle, A.L. and Schoen, J.W., J. Appl. Phys., Vol.55, No.6, p.2124-2126, 1984.

(52) Luborsky, F.E., "Amorphous ferromagnets", Chapter

7., North Holland Press, 1977.

(53) Turnbull, D., J. de Physique, Vol.35, C4-1, 1974.

(54) Spaepen, F. and Turnbull, D., "Rapidly Quenched Metals", Section 1., p.205 MIT Press, Cambridge, Mass., 1976.

(55) Duwez, P., Willens, R.H. and Klement, W., Jr., J. Appl. Phys., Vol.31, p.1136, 1960.

(56) Duwez, P. and Willens, R.H., Trans. Met. Soc. AIME, Vol.227, p.362, 1963.

(57) Pietrokowsky, P., Rev. Sci. Instr., Vol.34, p.445, 1963.

(58) Cahn, R.W., Krishnanand, K.D., Laridjani, M., Greenholtz, M. and Hill, R., Materials Sci. Eng., Vol.23, p.83, 1976.

(59) Kumar, R. and Sinha, A.N., Trans. Ind. Inst. Metals, Vol.21, p.19, 1968.

(60) Roberge, R. and Herman, H., Materials, Sci. Eng., Vol.3, p.62, 1968.

(61) Moss, M., Smith, D.L. and Lefever, R.A., Appl. Phys. Lett., Vol.5, p.120, 1964.

(62) Pond, R. Jr. and Maddin, R., Trans. Met. Soc. AIME, Vol.245, p.2475, 1969.

(63) Chen, H.S. and Miler, C.E., Rev. Sci. Instrum., Vol.41, p.1237, 1970.

(64) Babic, E., Girt, E., Kisnik, R. and Leontic, B., J. Phys. Sci. Instrum., Vol.3, p.1015, 1970.

(65) Liebermann, H.H. and Graham, Jr. C.D., IEEE Trans. Mag., MAG-12, p.921, 1976.

(66) Liebermann, H.H., Proc. 3rd Int. Conf. on Rapidly Quenched Metals, Univ. of Sussex, pp.34-40, 1978.

(67) Daniels, M., "Design Domain" Phys. World, Vol.1, pp.33-36, Dec. 1988.

(68) Douglas, J., "Transformer with Lower Losses", EPRI Journal p.26, Oct. Nov. 1987.

(69) Maringer, R.E. and Mobley, C.E., J. Vac. Sci. Technol., Vol.11, p.1067, 1974.

(70) Mariger, R.E., Mobley, C.E. and Collings, E.W., Quenched Metals, Section 1, p.29 MIT Press, 6 Cambridge, Mass., p.29, 1976.

(71) Fish, G. E. and Smith, C.H., in Proc. Soft and Hard Magnetic Materials with Applications (Proc. Symp., Lake Buena Vista, USA, 1986),American Society for Metals, Choice Book Mfg Co., Mass, USA p, 1-20, 1986.

(72) Luborsky, F.E., "Perspective on Application of Amorphous Alloys in Augnetic" in "Amorphous Magnetism II", Addison Wesley, pp.345-368, 1976.

(73) Luborsky F.E., IEEE Trans. MAG-14, pp.1008-1012, 1978.

(74) Luborsky, F.E., Becker, J.J., Frischmann P.J. And Johnson, L.W., J. Appl. Phys., Vol.49, pp.1760-1774, 1978.

(75) Graham Jr., C.D. and Egami, T., in Proc. 3td Int. Conf. on Rapidly Quenched Metals, Univ. of Sussex, pp.96-108, 1978.

(76) Sacks, T."Amorphous Transformers" Electrical

Review, Vol.224 Pt.6 pp.18-20, 1991.

(77) Johnson, L.A., Cornell, E.P., Bailey, D.J. and Hegvi, S.M., General Electrical Technical Information Series Report No.81, ORD127,Aug. 1981.

(78) Milkovic, M., Luborsky, F.E., Chen, D. and Tiompkins, R. IEEE Trans. Mag. MAG-13, p.1224, 1977.

(79) Raskin. D, and Davies, L.A., IEEE Spectrum pp.28-33, Nov. 1981.

(80) Luborsky, F.E. and Johnson, L.A., in "Application of Magnetic Amorphous Alloy", 4th Int. Conf. on Amorphous Metals, Grenoble, 1980.

(81) Steeb,, S. and Warlimont, 2 Rapidly Quenched Metals", Vol.I and II. Proc. 5th Int. Conf. RQM, Wurzburg, Germany. 1984, North-Holland, Amsterdam 1985.

(82) Lee, P. W., and Carbonara, R.S., "Rapidly Solidified Materials", in Proc. Intl. Conf., San Diego, USA 1985, American Society for Metals, Metals Park, USA. 1985.

(83) Luborsky, F.E., "Glass Current Issues" in Proc. NATO Advanced Study Institute Martinus Nijhoff, BV, Dordrecht, Netherlands P.139, 1985.

(84) Soft Magnetic Materials, Intl. Conf. SMM-7, Blackpool, England 1985, Wolfson Centre for Magnetics Technology, Cardiff, UK. 1986.

(85) Giessen, B.C., Polk, D.E., and Taub, A.J., "Rapidly Solidified Alloys and Their Mechanical and Magnetic

Properties", in Proc. Symp., Boston, USA, p.985, 1985, Materials Research Society, Pittsburgh 1986.

(86) Hernando, A., Madurga, V., Sanchez, M.C., and Vazquez, M., in "Magnetic Properties of Amorphous Metals", Proc. Symposium, Benalmadena, Spain, 1987. North-Holland, Amsterdam 1987.

(87) Duhaj, P., and Mrafko, P., "Amorphous Metallic Materials" in Proc. Conf., Smolenice, Czechoslovalia, 1978, VEDA Publishing House of the Slovak Acda., Bratislava 1980.

(88) Hargitaym, C., Bakonyi, I. and Kemeny, T., "Metallic Glasses, Science and Technology", in Proc. Conf. Budapest, Hungary, 1980, Central Research Institute for Physics, Budapest 1081.

(89) Henkel, O., "Amorphous Metallische Werkstoffe", in Proc. 14 Metalltagung in der DDR, Dresden, GDR, 1981, Zenteralinstitut fur Festkorperphysik und Werstofforschung, Dresden 1981.

(90) Matyja, H., and Zielinski, P.G., "Amorphous Metals", in Proc. Summer School, Wilga, Poland, 1985, World Scientific Publ. Co., Singapore. 1985.

(91) "Metallic and Semiconducting Glasses" in Proc. Intl. Conf. Hyderabad, India, 1986, Published by Trans. Tech. Publ., Switzerland as a special issue of the journal, Engineering Materials, 1987.

(92) Mischler, W.R., Rosenberry, G.M., Frischmann and Tompkins, IEEE PES Meeting Altanta, GA, Paper 81, WM 189-O, 1981.

(93) Fiedler, H.C., Johnson, L.A. and Frischmann, P.G., IEE, Colloquium on "Magnetic Properties and Applications of Amorphous Ribbons", London, Oct. 1981.

(94) Lowdermilk, L.A. and Lee, A.C., "Five years Operating Experience with Amorphous Transformers.", General Electric Company Transformer Business, ASM International Metal Park, Ohio 44073, p.3, Oct.1987.

(95) Douglas, J., "Transformer with Lower Losses", IPRI Journal, p.27, Oct.Nov. 1987.

(96) Frewin, K., "Amorphous Metal Cores", Electrical Review Vol.214 No.20, pp.15-22, June 1984.

(97) Frewin, K., "Amorphous Materials in Distribution Transformers", in GEC Distribution Transformers Ltd, Broadstairs, Kent, UK. 1985.

(98) Sampat, M.P., Lowdermilk, L.A. "Amorphous Metal Distribution Transformers Technology Development at General Electric Company USA" Hickory, NC, pp.1-17, Nov. 25-26, 1988.

(99) Hilzinger, H.R.., IEEE Trans. Mag. MAG-21, 2020, 1985.

(100) Zhang Luo, Lin Guang-Di, Song-Yao, "Rapidly Quenched Metals" in Proc. 5th Intl. Conf. RQM, Wurzburg, Germany, 1984 Vol.II. p.1679North-Holland, Amsterdam 1985.

(101) Inomata, K., IEEE Transl. J.Magn. Jpn., USA TJMJ-Vol.1, 672, 1985.

(102) Mendelsoh, L.I., Nesbitt E.A. and G.R. Bretts, IEEE Trans. Mag., MAG-12, p.924, 1976.

(103) Sellers, G.I. Proc. IEEE Int. Symp. on Electromagnetic Compatibility, p.129, 1977.

(104) Boll, R. and Warlimont, H. "Application of Amorphous Magnetic Materials in Electronics" IEEE Trans. on Magn., Vol. MAG-17, No.6, Nov. 1981.

(105) Shiau, Y., Bridges, J. and Sellers, G.J., Proc. of IEEE Conf., Atlanta, June 1978.

(106) Boll, R. and Borek, L., NTG Fachberichte, Band 76, p.178, 1980.

(107) Arai, K., Tsuya, N., Yamada, N. and Masumoto, T., IEEE Trans. Mag., MAG-12, p.936, 1976.

(108) Shirae, K. and Mashino, K., Intermag Paper 30-11, 1977.

(109) Asc, K. , Vedair, S. Ito, Tamura, H. and Makimo, Y., U.K. Patent Appl. BG2005303A, April 19, 1979.

(110) Tohoku Univ. Jap. Patent 52114-421, Sept.26, 1977.

(111) Sony Corp. German Patent 2839-626, March 22, 1979.
Aso, K., Uchira, A., Murata, H., Ito, M. and Makino, Y. Jap. Patent 5.54-56916, May 8, 1979.

(112) Shiiki, K., Otomo, S. and Kudo, M., Paper EC-10 , in 26th Conf. on Magnetism and Magn. Mat., Dallas, Texas 1980.

(113) Shiiki, K., Otomo, S. and Kudo, M., Paper EC-10 in Proc. 26th Conf. on Magnetism and Magnetic Materials, Dallas, Texas, 1980.

(114) Hayakawa, M., Hotai, K., Aso, K., Uedaira, S.,

Ochiai, Y. and Makino, Y., in Proc. 4th Intern. Conf. on Rapidly Quenched Metals, Japan Inst. Met. 1981.

(115) Raskin D. and Daviies L.A. "Metallic Glasses: a Magnetic Alternative" IEEE Spectrum, pp.28-33, Nov.1981.

(116) Nathasingh, D.M. and Liebermann, H.D."Transformer Applications of Amorphous Alloys in Power Distribution Systems" IEEE Trans. on Power Delivery Vol.2, No.3, July 1987.

(117) Allied-signal Inc. USA, "Metglas Transformer Core Alloy, Core Construction Methods" Technical Report 1988.

(118) Allied-Signal Inc. USA Metglas Magnetic Alloys Technically Superior, 1988.

(119) Marits, R.J.J., "Amorphous Alloys as Transformer Core Materials" Introduction Fabrication Compsition and Properties Annealing Treatement Thermal Stibility Powercore.(no date)

(120) Nathasingh, D.M., Smith, C.H. and Dutta, A. IEEE, Trans. Magn. MAG-20, p.1332, 1984.

(121) Tadashi Sasaki, Takashi Hosokawa and Shunji Takada "Annealing Dependencies of Magnetic and Mechanical Properties in Iron Based Amorphous Ribbons" Physica. Vol. 39, pp.655-657, 1989.

(122) British Standard "Magnetic Materials" Part 2. Methods of Measurement of Magnetic, Electrical and Physical Properties of Magnetic Sheet and Strip,BS

6404, 1985.

(123) Reissland U Martin, "Electrical Measurements" Fundamentals Concepts Application, Wiley Eastern Limited, p.289, 1989.

(124) Fujimori, H.Kato, T., Masumoto, T. and Morita, H. in Proc. 3rd Int. Conf. on "Rapidly Quenched Metals", Brighton, UK, Vol. 2, p240, 1978.

(125) Nathasingh, D. and Smith, C. "A new High, Low-Loss Magnetic for High Frequency Application" Powercon 7, Proc. of the 7th National Solid state Power Convention, Sen Diego, Ca., p.B2-4 March 1980.

(126) Technical literature, Interborder Metals Ltd., Newport, Gwent, UK. "Metglas Amorphous Transformer Core Alloys", 1989.

(127) Luborsky, F.E. "Amorphous Magnetism II", Plenum Press, New York, p.345, 1977.

(128) Technical literature, British Steel Corporation Electrical Sheet Works, Newport Gewent ,"ALPHASIL, Grain Oriented Electrical Steel" [n.d].

AMORPHOUS METAL CORES FOR USE IN MEDIUM FREQUENCY POWER TRANSFORMERS

(To be published in 28th Universities Power Engineering Conference in Stafford, U.K., Sept. 1993)

K.T. Williams, G.H. Cooke, A.B. Crompton, M. Razaz, A. Benhama

University of Salford, UK

ABSTRACT

The low loss associated with amorphous metal has been utilised in the design of a medium frequency power transformer. The ability of being able to operate at high levels of flux density, with tolerable core losses, leads to significant economies in the size and weight of the transformer compared with those using ferrite or silicon material. The design and construction of an amorphous cored transformer is described. The results of a comprehensive test programme on the core are given.

1. INTRODUCTION

With the advancement in the switching speeds, current and voltage capabilities of power semiconductor devices, high power inverters are now possible, typically 10-kW with operating frequencies in the region of 10-kHz. For higher power ratings where gate turn off thyristors are used, the inverter frequencies are much lower. These inverters are often used in conjunction with isolating transformers and inductors. The core materials available for use in these components include the various types of low loss silicon steels, the amorphous metals and ferrites. A comparison of these materials would indicate the suitability of the amorphous metals for high power ratings in the frequency range 0.5-kHz to 3-kHz and possibly up to 6-kHz. Their particular advantage at these frequencies is their ability to be operated at high flux density levels with tolerable core losses leading to economies of both size and weight of the transformer.

2.0 TRANSFORMER DESIGN STUDIES

For the frequency range of 0.5-kHz to 3-kHz and inverter power ratings of say 20-kW where the switching devices are likely to be gate turn off thyristors, low loss silicon steels and the amorphous metals are two possible choices for the core material of any transformers or inductors in the circuit.
A tentative design comparison has therefore been carried out to assess the advantages of utilising the higher operating flux densities of the amorphous metals.

2.1 DESIGN COMPARISON OF AMORPHOUS METAL AND SILICON STEEL

A 20-kW, 800/600-V, transformer rating was used for the comparison at two operating frequencies, 1-kHz for design No 1 and 3-kHz for design No 2. In the case of the silicon steel designs, data relating to Alphasil TO50 (0.05mm thick laminations), a cold rolled grain oriented silicon steel was used. The flux density levels chosen were those commonly employed at the frequencies being addressed. For the amorphous core designs, data provided by Allied Signal for their Metglas range of alloys was used. A number of different amorphous alloys are available of which the iron based alloys appear to be the most suitable for use in the frequency band of 0.5-kHz to 6-kHz. The Metglas alloy 2605S-2 was chosen for the comparison and following inspection of the material data, a maximum operating flux density of 1.4-T was considered to be feasible at 1-kHz and 1-T at 3-kHz.
The results of the design comparison are given in Table 1.

Table 1 Design Comparison of Amorphous and Silicon Steel

Core material	Metglas 2605S-2	
	Design 1	Design 2
Freq kHz	1.0	3.0
Flux den T	1.4	1.0
Core wt kg	6.8	4.8
Specific loss W/kg :-		
	10	26
Core material	**Silicon steel**	
	Design 1	Design 2
Freq kHz	1.0	3.0
Flux den T	1.0	0.4
Core wt kg	14.0	25.0
Specific loss W/kg :-		
	23	19

The higher flux densities possible with the amorphous metal produce a significant reduction in core weight compared with silicon steel. This is particularly evident at 3-kHz where the operating flux density level of the silicon steel has to be reduced to 0.4-T to maintain tolerable core losses.

2.2 CHOICE OF AMORPHOUS CORE MATERIAL

Amorphous metal alloys are produced in ribbon form by rapid cooling and solidification of the molten metal on a fast moving drum before the atoms crystallise. The result is a metal alloy of glass like atomic structure. Their characteristics vary according to the composition of the alloy, i.e. iron based, nickel iron based and cobalt based alloys are available. The iron based alloys are best suited to frequencies in the range 50-Hz to 200-kHz. Of the iron based alloys produced by Allied Signal, both Metglas 2605S-2 and 2605S-3A are likely to be suitable. Metglas 2605S-2 has already been used for the core material in power frequency transformers and its use may extend up to 3-kHz before its losses give rise to excessive core temperatures, necessitating a reduction in the operating flux density. In comparison, the lower core losses of Metglas 2605S-3A at frequencies above 1-kHz suggest it may be used with advantage without excessive core temperatures occurring at frequencies up to 6-kHz.
As a preliminary exercise, several uncut cores were wound using Metglas 2605S-2, in the weight range 4-5kg. The measured core losses per kg are compared in Table 2 with the core loss data supplied by Metglas. The building factor quoted in the table is the ratio of the measured loss per kg on the finished core to the loss per kg data provided by Allied Signal. Only sufficient Metglas 2605S-3A material was available to wind one 5-kg core, its measured losses are also included in Table 2 together with the losses from Metglas

data.

Table 2 Measured Core Losses

Core material 2605S-2		
Flux density T	1.0	1.0
Frequency kHz	1.0	3.0
Measured loss W/kg	6.9	32.0
Metglas loss W/kg	5.2	26.0
Building Factor	1.33	1.23
Core material 2605S-3A		
Flux density T	1.0	1.0
Frequency kHz	1.0	3.0
Measured loss W/kg	4.85	24.7
Metglas loss W/kg	3.0	11.0
Building Factor	1.62	2.2

From the core losses measured, the building factor for Metglas 2605S-3A was much higher than expected although the annealing cycle used may not have been the optimum for minimum losses. The precise details of the annealing cycle were not readily available and further experimentation is required.

3.0 GENERAL DESIGN CONSIDERATIONS FOR A 3-kHz TRANSFORMER

Following the preliminary design studies, the research has concentrated on the assembly of an amorphous cored 3-kHz, 100/200-V, 20-kW transformer. Metglas 2605S-2 ribbon was chosen for the core material and wound to form a rectangular uncut core. The windings have been wound directly onto both legs through the core window. Foil windings have been used rather than multistrand Litz type wire, it was considered that foil would be easier to wind and the larger eddy current losses associated with foil would not be excessive at 3-kHz.

4.0 TRANSFORMER CORE

A number of cores were wound and subjected to various tests to establish the best method of core manufacture and transformer assembly. The cores were built to the following dimensions:- core window...125mm(leg) x 85mm(yoke), net csa...1275mm^2.

4.1 CORE ASSEMBLY DETAILS

The 50mm wide amorphous ribbon (2605S-2) was wound onto a mandrel made to the dimensions of the core window. The mandrel was mounted in a lathe and rotated to draw the ribbon from a pay off spool. The pay off spool had an adjustable friction brake to tension the ribbon. The core was then annealed in an inert atmosphere with a magnetic field applied in accordance with the manufacturers recommendations.

4.2 CORE LOSS AND EXCITING VA

The core losses and exciting VA of Metglas 2605S-2 measured at 1-T at frequencies from 50-Hz to 3-kHz are listed in Table 3.

Table 3 Core Loss and Exciting VA at 1-T

Frequency	Core loss	Exciting VA
Hz	W/kg	VA/kg
50	0.1	0.1
400	1.9	1.98
1000	6.9	7.2
2000	18.2	18.9
3000	32.0	33.2

4.3 SEPARATION OF CORE LOSSES

Some idea of the relative magnitudes of the eddy current and hysteresis losses were of interest with a view to the need for inter turn insulation of the ribbon. The B/H loop of the core was thus measured and the hysteresis loss calculated for each frequency. The eddy current loss was then obtained by subtracting the hysteresis loss from the total loss measured. This method was considered accurate enough for general conclusions to be made. Table 4 lists the separated losses at frequencies of 50-Hz, 400-Hz, 1-kHz, 2-kHz, 3-kHz for a flux density of 1-T.

Table 4 Separation of Core Losses

Frequency Hz	Hysteresis loss(W/kg)	Eddy current loss(W/kg)
50	0.08	0.02
400	0.64	1.25
1000	1.60	5.31
2000	3.2	15.0
3000	4.8	27.2

The eddy current loss at 3-kHz does suggest a need to consider insulating between the layers of ribbon, however such insulation will seriously affect the core space factor, particularly so with the large number of turns of thin ribbon making up the core. For the cores wound, the number of turns for 2605S-2 was about 1000 and for 2605S-3A about 1400 for the same net csa.

4.4 EFFECT OF CLAMPING CORE LIMBS

The transformer core may be subjected to mechanical stresses caused by the method used to support the core and winding. To evaluate the effect of pressure on the limbs, both limbs were clamped and various pressures applied to compress the ribbons together. The effect on core losses was found to be negligible, however a measurable increase in exciting VA was noted at flux density levels above 0.8-T, for example at 1-T:-

Clamping pressure,kN/m^2	0.0	38.6
Exciting VA/kg at 1-kHz	7.2	9.4
Exciting VA/kg at 3-kHz	33.2	38.0

The B/H loop measured with the core clamped showed an increase in the exciting current at the peak flux density but little change in loop area.

4.5 EFFECT OF TEMPERATURE ON CORE LOSSES AND EXCITING VA

The results given so far all relate to ambient temperature, however under normal operating conditions the core temperature will be significantly above ambient. Table 5 compares the core losses and exciting VA at ambient and at 150°C, the maximum recommended core temperature. As expected, both were found to decrease with increasing core temperature.

Table 5 Effect of Temperature on Core Loss and Exciting VA

At 1-T and 1-kHz :-

	Ambient		150°C
Core loss W/kg	6.9	6.1	
Exciting VA/kg	7.2		6.7

At 1-T and 3-kHz :-

	Ambient	150°C
Core loss W/kg	32.0	27.2
Exciting VA/kg	33.2	28.8

4.6 CORE TEMPERATURE RISE WITHOUT AND WITH A HEATSINK

The deciding criteria for the maximum operating frequency and flux density will be the temperature rise of the core, the maximum continuous service temperature of the amorphous material must not exceed 150°C.The temperature rise of the test cores were measured for various operating flux densities and frequencies both without and with a heatsink being attached. The two heatsinks attached to the core yokes, each had a thermal resistance of 0.54°C/W. From these temperature rise tests it is possible to predict the operating core flux density and frequency for a specified core temperature rise. A graph is shown in figure 1 from which predictions may be made for the operating frequency and flux density for various core temperature rises both without and with a heatsink. The addition of a heatsink permits a significant increase in operating flux density, for example at 3-kHz and a core temperature rise of 80°C, the operating flux density may be increased from 0.5-T to 0.9-T.

4.7 CORE PROTECTION POSTANNEAL

The amorphous metal cores after annealing were slightly flexible and prone to flaking. The method of assembly of the core and winding needs careful consideration particularly with regard to cooling provisions and any mechanical stress placed on the core. Essentially there are two methods of assembly (a) the conventional arrangement whereby the core supports the windings or (b) the winding formers support both the core and the windings.

For method (a) the core could be wrapped in fibreglass tape and then coated with a castable epoxy to provide a suitable foundation for the windings. However, such a coating would inhibit heat dissipation and the use of a low viscosity anaerobic adhesive was tried as an alternative. The adhesive was allowed to wick in between the ribbon layers and after curing a very rigid core was formed. The measured core loss and exciting VA were both found to increase, the results are given in Table 6. The increases may be attributed to the mechanical stresses set up in the ribbon by the interaction of the adhesive between the ribbon layers. These stresses would be further enhanced by any changes in the core temperature.

Table 6 Effect of Adhesive on Core Loss and Exciting VA

	Without adhesive	With adhesive
Core loss at 1-T/1-kHz	6.9 W/kg	8.5 W/kg
Core loss at 1-T/3-kHz	32.0 W/kg	38.5 W/kg
Exciting VA at 1-T/1-kHz	7.2 VA/kg	12.2 VA/kg
Exciting VA at 1-T/3-kHz	33.2 VA/kg	48.7 VA/kg

Despite the increased losses, the core was found to dissipate its heat more efficiently. For example, the core loss and temperature rise measured on the same core before and after applying adhesive at 1-T, 1-kHz were:-

	Core loss	Temp. rise
Without adhesive	6.5 W/kg	62°C
With adhesive	7.8 W/kg	58°C

Similarly at 1-T, 2-kHz:-

Without adhesive	15.8 W/kg	136°C
With adhesive	19.6 W/kg	122°C

Method (b) was subsequently adopted for the transformer assembly in which the core was supported by the winding former. The core was protected by wrapping with polyimide tape which was found to have little effect on heat dissipation.

5.0 TRANSFORMER WINDINGS

For high frequency and high current transformers, the multistrand Litz type of conductor could be used to limit the eddy current losses in the windings. At frequencies of up to 3-kHz, the copper foil type of winding is likely to be a feasible alternative, offering the benefits of a higher winding space factor, better heat dissipation and simplified winding manufacture. The foil type of winding was therefore chosen. The method of core support and winding assembly used is illustrated in figure 2. A comprehensive analysis of the foil windings has been carried out and will be the subject of a future publication.

6.0 CONCLUSIONS

The advantages of using amorphous metal for the cores of medium frequency power transformers has been proved with regard to the reduction in size and weight when compared with silicon steel types. For the transformer built, an operating frequency of 3-kHz and a flux density of 1-T was about the limit for acceptable core loss and temperature rise using Metglas 2605S-2. Lower temperatures could have been obtained by further attention to the cooling provided or by the use of Metglas 2605S-3A.
The winding formers provide the main support structure of the transformer, leaving the core mechanically unstressed. Both the winding of the uncut core and the assembly of the foil windings by winding through the core window, posed few problems. The rigid core produced by the application of a low viscosity adhesive deserves further evaluation despite its higher losses. This core requires minimal external protection and the windings may be supported by the core on less substantial formers.

ACKNOWLEDGEMENTS

The research was supported by a SERC Cooperative grant with NEI Controls of Gateshead. In addition the authors also wish to acknowledge the valuable assistance of BBH Coils of Bishop Auckland and the facilities provided by the Electronic and Electrical Engineering Departments of the Universities of Salford and Northumberland.

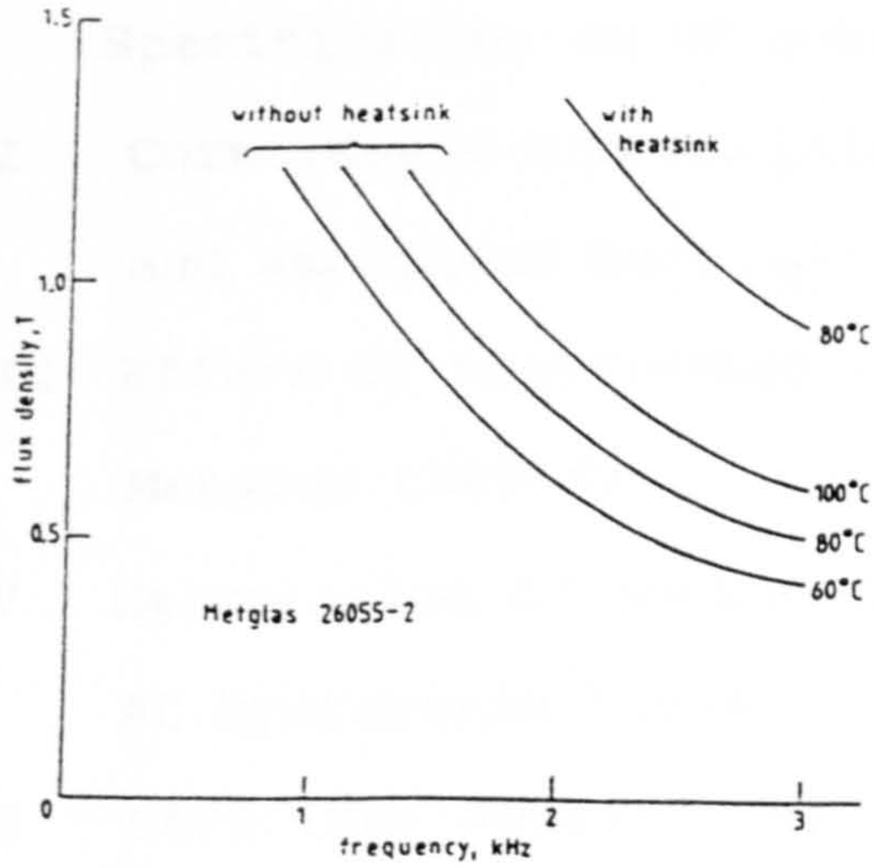

Fig. 1 Core temperature rise.

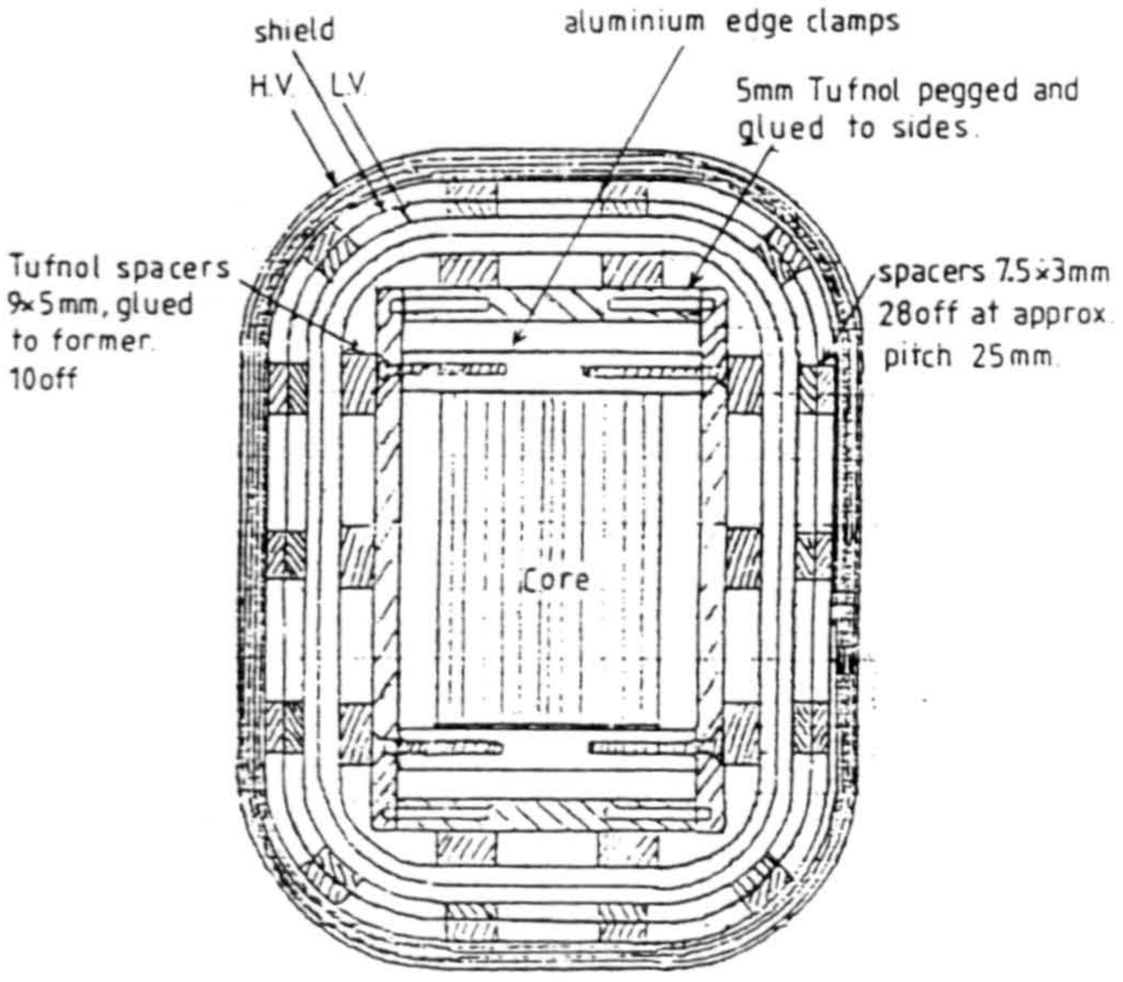

Fig. 2 Cross-section of Leg.

APPENDIXES

Appendix I	Specification of AC power analyser PM 1000	301
Appendix II	Core losses and exciting VA of silicon-iron and amorphous Metglas	303
Appendix III	Effect of temperature on B/H loop of amorphous Metglas 2605-S2	314
Appendix IV	Calculation of area of hysteresis loops	327
Appendix V	AC hysteresis loops	331
Appendix VI	Core loss sensitivity of amorphous Metglas with pressure	341

APPENDIX I

Specification of AC power analyser PM 1000

Voltage (V_{rms})	Range		2V to 700V rms
	Frequency range		DC and 5Hz to 20kHz
	Accuracy 23 ± 5°C Sine Wave	5Hz to 1kHz	± 0.25% of reading
		1kHz to 20kHz	± 0.40 of reading
	Input Impedance		8MΩ
Current (A_{rma})	Range		20mA to 20A rms
	Frequency range		DC and 5Hz to 20kHz
	Accuracy 23 ± 5°C Sine Wave	5Hz to 1kHz	± 0.5% of reading
		1kHz to 20kHz	± 0.8% of reading
	Input Resistance		0.05Ω max inc.fuse circuit
Power (W)	Range		40mW to 14kW
	Frequency range		DC and 5Hz to 20kHz
	Accuracy 23 ± 5°C Sine Wave	5Hz to 1kHz	PF 1.0 to 0.3 ± 0.75% PF 0.3 to 0.1 ± 1.5%
		1kHz to 20kHz	PF 1.0 to 0.1 ± 1.5% of VA
Apparent Power (VA)	Range		40mVA to 14kVA
	Frequency range		DC and 5Hz to 20kHz
	Accuracy 23 ± 5°C Sine Wave	5Hz to 1kHz	± 0.75% of reading
		1kHz to 20kHz	± 1.2% of reading
Power Factor (PF)	Range		0.000 to ± 1.000
	Accuracy 23 ± 5°C Sine Wave	5Hz to 1kHz	± 0.75% of reading
		1kHz to 20kHz	± 1.2% of reading
AC Supply Frequency (FREQ)	Range		5Hz to 20kHz
	Accuracy		± 0.2% of reading
Harmonic Analysis (HARM)	RMS Current Range		20ma to 20A rms
	Harmonic Freq. Range		5Hz to 20kHz
	Accuracy AC Components 23 ± 5°C DC Component		± 0.8% of reading± 2mA ± 0.8% of reading± 5mA

Table A.1 Specification of AC power analyser PM 1000

APPENDIX II

Core losses and exciting VA of silicon-iron and amorphous Metglas

B_{max} (T)	V_{rms} (V)	$I_{pri.}$ (A)	P_T Total Core loss (W)	Core Loss (W/kg)	Exciting Power (VA)	Exciting Power (VA/kg)
0.10	1.07	0.326	0.114	0.011	0.354	0.035
0.20	2.02	0.435	0.403	0.040	0.883	0.089
0.30	3.04	0.508	0.892	0.090	1.54	0.155
0.40	4.09	0.566	1.48	0.149	2.32	0.234
0.50	5.07	0.608	2.10	0.212	3.10	0.313
0.60	6.08	0.654	2.79	0.281	3.97	0.401
0.70	7.08	0.695	3.54	0.357	4.92	0.496
0.80	8.09	0.748	4.41	0.445	6.04	0.610
0.90	9.11	0.801	5.39	0.544	7.31	0.738
1.00	10.11	0.863	6.44	0.650	8.68	0.876
1.10	11.14	0.940	7.71	0.778	10.45	1.055
1.20	12.15	1.045	9.15	0.924	12.66	1.27
1.30	13.16	1.176	10.81	1.09	15.54	1.57
1.40	14.14	1.38	12.83	1.29	19.58	1.97
1.50	15.21	1.71	15.34	1.46	25.90	2.61

Table A.2 Total and per kg core loss and exciting power of 3% silicon iron at 50 Hz.

B_{max} (T)	V_{rms} (V)	$I_{pri.}$ (A)	P_T Total Core loss (W)	Core Loss (W/kg)	Exciting Power (VA)	Exciting Power (VA/kg)
0.10	8.10	0.541	1.97	0.198	4.40	0.44
0.20	16.21	0.662	6.78	0.684	10.78	1.08
0.30	24.30	0.708	12.11	1.22	17.20	1.73
0.40	32.47	0.753	18.16	1.83	24.46	2.47
0.50	40.60	0.785	24.35	2.49	31.89	3.22
0.60	48.60	0.825	31.28	3.159	40.13	4.05
0.70	56.70	0.864	38.81	3.92	49.00	4.94
0.80	64.90	0.908	47.14	4.76	59.00	5.95
0.90	72.95	0.952	55.96	5.65	69.48	7.01
1.00	80.10	0.998	64.70	6.53	79.93	8.07
1.10	89.10	1.067	77.21	7.79	95.06	9.60
1.20	97.23	1.169	91.70	9.26	113.67	11.48

Table A.3 Total and per kg core loss and exciting power of 3% silicon iron at 400 Hz.

B_{max} (T)	V_{rms} (V)	$I_{pri.}$ (A)	P_T Total Core loss (W)	Core Loss (W/kg)	Exciting Power (VA)	Exciting Power (VA/kg)
0.10	18.25	0.685	5.11	0.516	12.49	1.26
0.20	36.50	0.791	17.39	1.75	28.82	2.91
0.30	54.67	0.866	32.60	3.29	47.30	4.77
0.40	72.76	0.918	49.20	4.96	66.91	6.75
0.50	91.20	0.972	68.19	6.88	88.77	8.96
0.60	109.4	1.033	89.17	9.00	112.70	11.38
0.70	127.8	1.070	110.9	11.20	137.26	13.86
0.80	145.8	1.136	136.0	13.73	165.52	16.71
0.90	164.1	1.20	164.2	16.58	196.90	19.88
1.00	182.4	1.28	196.0	19.79	233.20	23.55
1.10	200.6	1.357	229.0	23.13	271.4	27.41
1.20	219.8	1.47	273.0	27.57	326.1	32.93

Table A.4 Total and per kg core loss and exciting power of 3% silicon iron at 1000 Hz.

B_{max} (T)	V_{rms} (V)	I_{pri} (A)	P_T Total Core loss (W)	Core Loss (W/kg)	Exciting Power (VA)	Exciting Power (VA/kg)
0.10	18.34	1.16	8.06	0.814	21.29	2.15
0.20	36.45	1.50	30.32	3.06	54.56	5.51
0.30	54.81	1.74	62.77	6.34	95.16	9.61
0.40	72.90	1.93	101.77	10.27	140.59	14.20
0.50	91.20	2.10	147.70	14.91	191.70	19.36
0.60	109.34	2.26	197.8	19.97	247.40	24.98
0.70	127.70	2.42	256.50	25.90	309.20	31.23
0.80	145.90	2.55	315.0	31.81	372.10	37.58
0.90	164.20	2.71	385.0	38.88	447.00	45.15
1.00	182.22	2.87	451.3	45.58	521.10	52.63
1.10	201.00	3.09	536.2	54.16	623.30	62.95
1.20	219.60	3.31	617.3	62.35	727.00	73.43

Table A.5 Total and per kg core loss and exciting power of 3% silicon iron at 2000 Hz.

B_{max} (T)	V_{rms} (V)	$I_{pri.}$ (A)	P_T Total Core loss (W)	Core Loss (W/kg)	Exciting Power (VA)	Exciting Power (VA/kg)
0.10	21.41	1.19	12.30	1.24	25.61	2.58
0.20	42.70	1.84	49.00	4.94	78.51	7.93
0.30	63.76	2.32	104.81	10.58	148.26	14.97
0.40	85.08	2.70	175.90	17.76	230.0	23.23
0.50	106.4	3.02	256.2	25.87	321.0	32.42
0.60	127.8	3.31	348.3	35.18	425.0	42.92
0.70	149.0	3.56	447.3	45.18	529.6	53.49
0.80	170.4	3.72	548.1	55.36	632.8	63.91
0.90	191.6	3.84	644.4	65.09	735.2	74.26
1.00	212.7	4.03	752.3	75.98	858.0	86.66

Table A.6 Total and per kg core loss and exciting power of 3% silicon iron at 3000 Hz.

B_{max} (T)	V_{rms} (V)	$I_{pri.}$ (A)	P_T Total Core loss (W)	Core Loss (W/kg)	Exciting Power (VA)	Exciting Power (VA/kg)
0.31	0.71	0.12	0.085	0.014	0.09	0.015
0.4	0.9	0.14	0.125	0.021	0.132	0.022
0.5	1.12	0.16	0.177	0.029	0.183	0.03
0.6	1.37	0.18	0.246	0.041	0.257	0.043
0.7	1.58	0.20	0.306	0.051	0.320	0.053
0.81	1.83	0.22	0.395	0.066	0.414	0.069
0.92	2.08	0.25	0.499	0.083	0.533	0.089
1.0	2.27	0.27	0.582	0.097	0.625	0.105
1.13	2.55	0.31	0.721	0.121	0.784	0.131
1.22	2.76	0.33	0.842	0.141	0.943	0.158
1.3	2.92	0.36	0.936	0.157	1.06	0.178
1.4	3.16	0.40	1.10	0.184	1.29	0.216

Table A.7 Total and per kg core loss and exciting power, in core assembled from amorphous material type Metglas 2605-S2 core No.3 at 50Hz.

B_{max} (T)	V_{rms} (V)	$I_{pri.}$ (A)	P_T Total Core loss (W)	Core Loss (W/kg)	Exciting Power (VA)	Exciting Power (VA/kg)
0.194	3.6	0.25	0.86	0.14	0.89	0.15
0.30	5.42	0.32	1.72	0.28	1.77	0.29
0.40	7.20	0.38	2.70	0.45	2.77	0.46
0.50	9.02	0.43	3.87	0.65	4.00	0.67
0.60	10.80	0.48	5.07	0.85	5.24	0.88
0.70	12.6	0.52	6.40	1.07	6.63	1.11
0.80	14.5	0.57	7.94	1.33	8.20	1.37
0.90	16.21	0.61	9.57	1.60	9.98	1.67
1.00	18.0	0.65	11.28	1.89	11.82	1.98
1.10	19.82	0.70	13.08	2.19	13.83	2.32
1.20	21.78	0.76	15.43	2.59	16.67	2.80
1.30	23.45	0.82	17.55	2.94	19.38	3.25
1.40	25.11	0.92	20.00	3.36	23.00	3.86

Table A.8 Total and per kg core loss and exciting power, in core assembled from amorphous material type Metglas 2605-S2 core No.3 at 400Hz.

B_{max} (T)	V_{rms} (V)	$I_{pri.}$ (A)	P_T Total Core loss (W)	Core Loss (W/kg)	Exciting Power (VA)	Exciting Power (VA/kg)
0.20	9.13	0.41	3.64	0.611	3.74	0.628
0.30	13.64	0.515	6.87	1.154	7.04	1.183
0.40	18.08	0.592	10.49	1.763	10.70	1.798
0.50	22.51	0.657	14.57	2.448	14.80	2.487
0.60	27.0	0.715	18.99	3.191	19.45	3.268
0.70	31.63	0.772	23.91	4.018	24.48	4.114
0.80	36.0	0.826	29.08	4.887	29.78	5.00
0.90	40.40	0.880	34.50	5.798	35.46	5.959
1.00	45.28	0.947	41.15	6.915	43.00	7.226
1.10	49.50	1.01	47.26	7.942	50.00	8.403
1.20	54.12	1.10	54.57	9.171	59.72	10.036
1.30	58.30	1.21	62.00	10.42	70.56	11.858

Table A.9 Total and per kg core loss and exciting power, in core assembled from amorphous material Type Metglas 2605-S2 core No.3 at 1000 Hz.

B_{max} (T)	V_{rms} (V)	$I_{pri.}$ (A)	P_T Total Core loss (W)	Core Loss (W/kg)	Exciting Power (VA)	Exciting Power (VA/kg)
0.20	18.10	0.594	10.49	1.76	10.79	1.81
0.30	27.18	0.727	19.40	3.26	19.76	3.32
0.40	36.02	0.814	28.68	4.82	29.33	4.92
0.50	45.04	0.888	39.00	6.55	39.88	6.70
0.60	54.10	0.958	50.40	8.47	51.87	8.71
0.70	63.10	1.02	63.14	10.61	64.94	10.91
0.80	72.20	1.09	77.26	12.98	79.46	13.35
0.90	81.27	1.17	92.30	15.51	95.20	16.00
1.00	90.07	1.24	108.20	18.18	112.30	18.87
1.10	99.30	1.32	125.16	21.03	131.54	22.10
1.20	108.2	1.42	143.80	24.18	153.50	25.79

Table A.10 Total and per kg core loss and exciting power, in assembled core from amorphous material type Metglas 2605-S2 core No.3 at 2000 Hz.

B_{max} (T)	V_{rms} (V)	$I_{pri.}$ (A)	P_T Total Core loss (W)	Core Loss (W/kg)	Exciting Power (VA)	Exciting Power (VA/kg)
0.20	27.10	0.753	19.59	3.29	20.4	3.42
0.30	40.65	0.874	34.27	5.75	35.63	5.98
0.40	54.20	0.973	51.13	8.59	52.7	8.85
0.50	67.84	1.070	71.28	11.97	72.76	12.22
0.60	81.20	1.155	92.46	15.53	93.64	15.73
0.70	94.60	1.220	113.47	19.07	115.83	19.46
0.80	108.2	1.30	138.0	23.19	140.42	23.6
0.90	121.9	1.38	163.8	27.52	167.56	28.16
1.00	132.2	1.463	190.5	32.01	197.40	33.17
1.10	148.6	1.56	220.4	37.04	231.40	38.89
1.20	162.5	1.676	252.8	42.48	272.90	45.86

Table A.11 Total and per kg core loss and exciting power, in core assembled from amorphous material type 2605-S2 core No.3 at 3000Hz.

APPENDIX III

Effect of temperature on B/H loop of amorphous Metglas

2605-S2

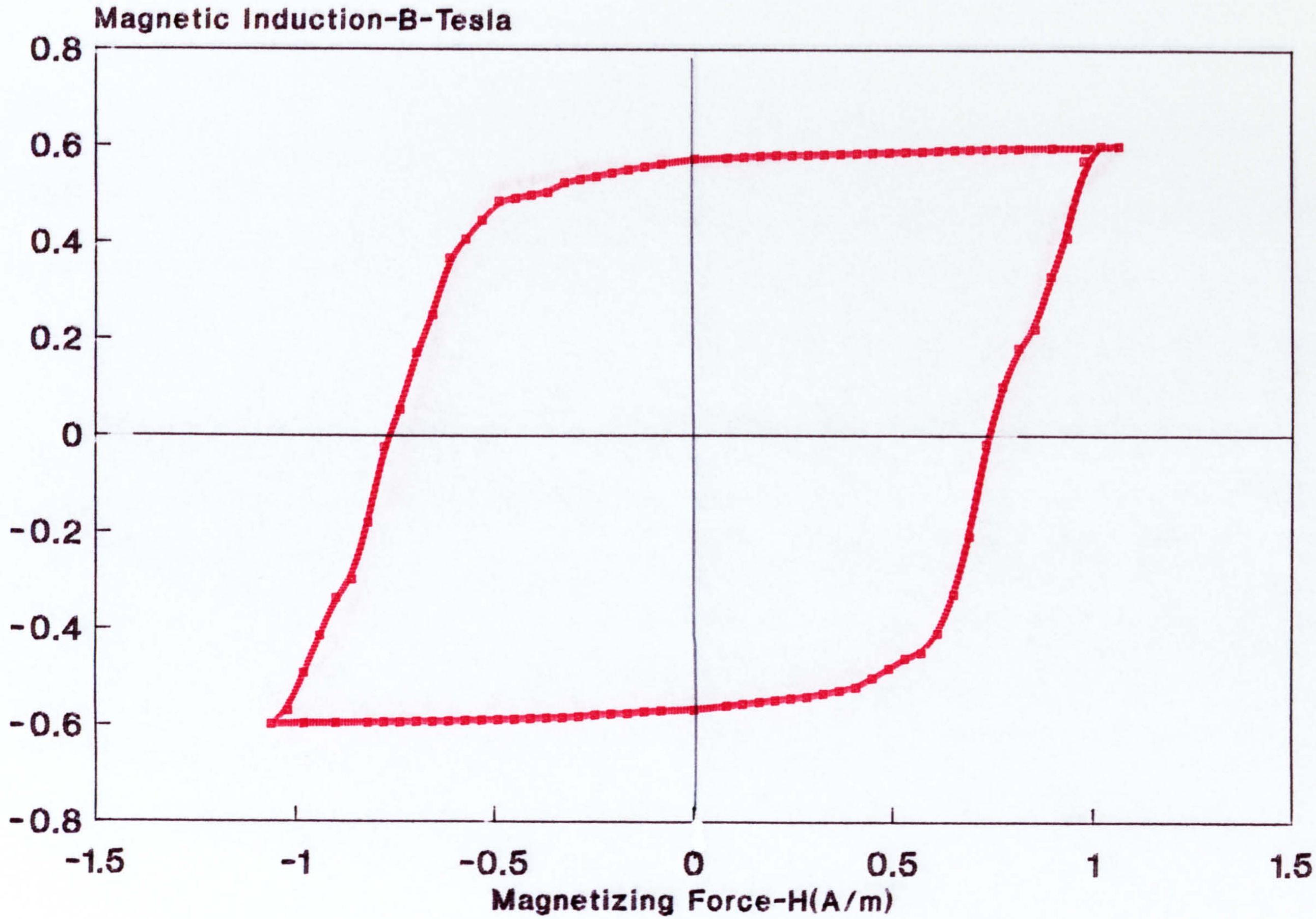

Fig. A.1 B/H loop of Metglas 2605-S2 at flux density 0.6 T at ambient temperatue.

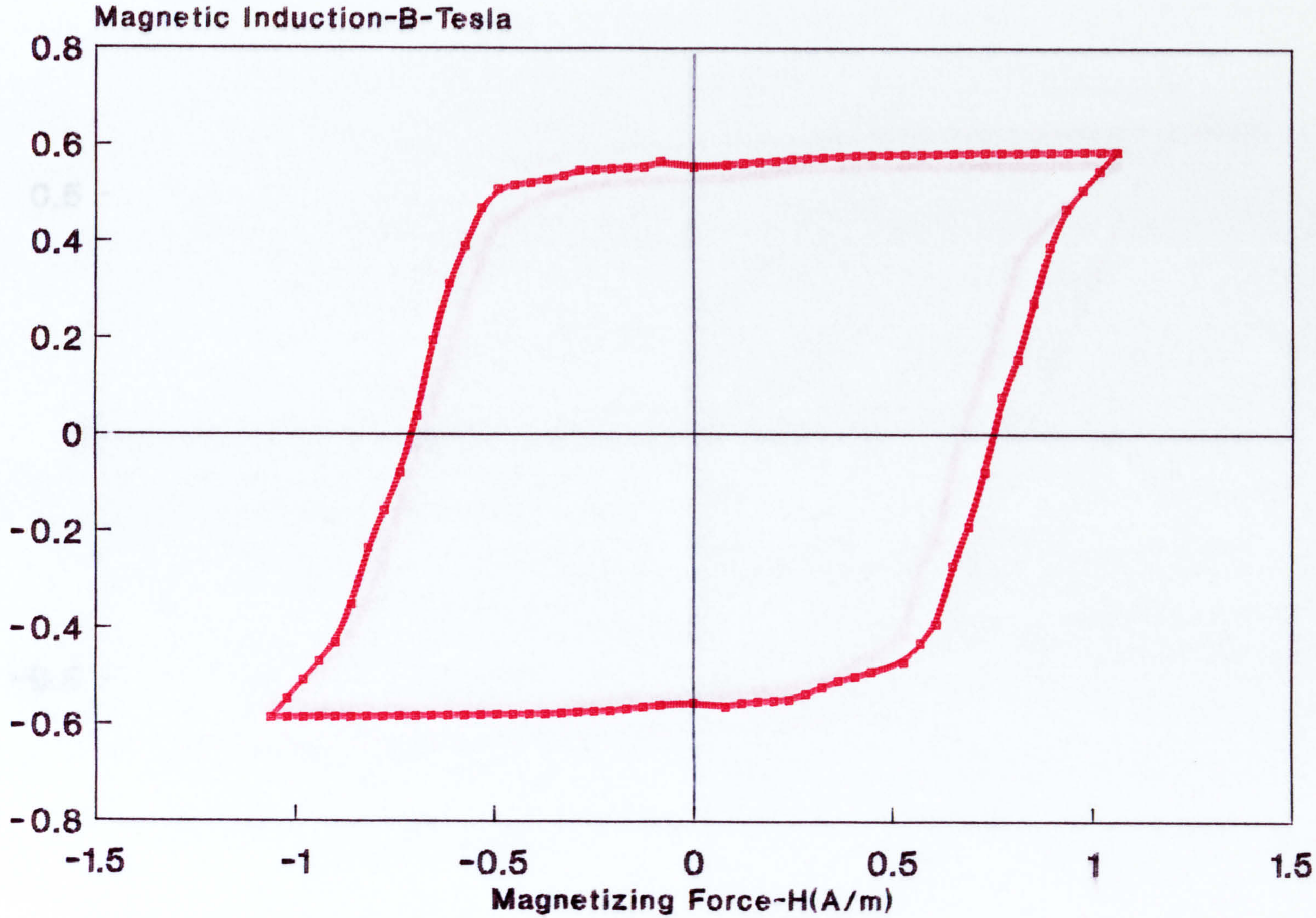

Fig. A.2 B/H loop of Metglas 2605-S2 at flux density 0.6 T at 100 C.

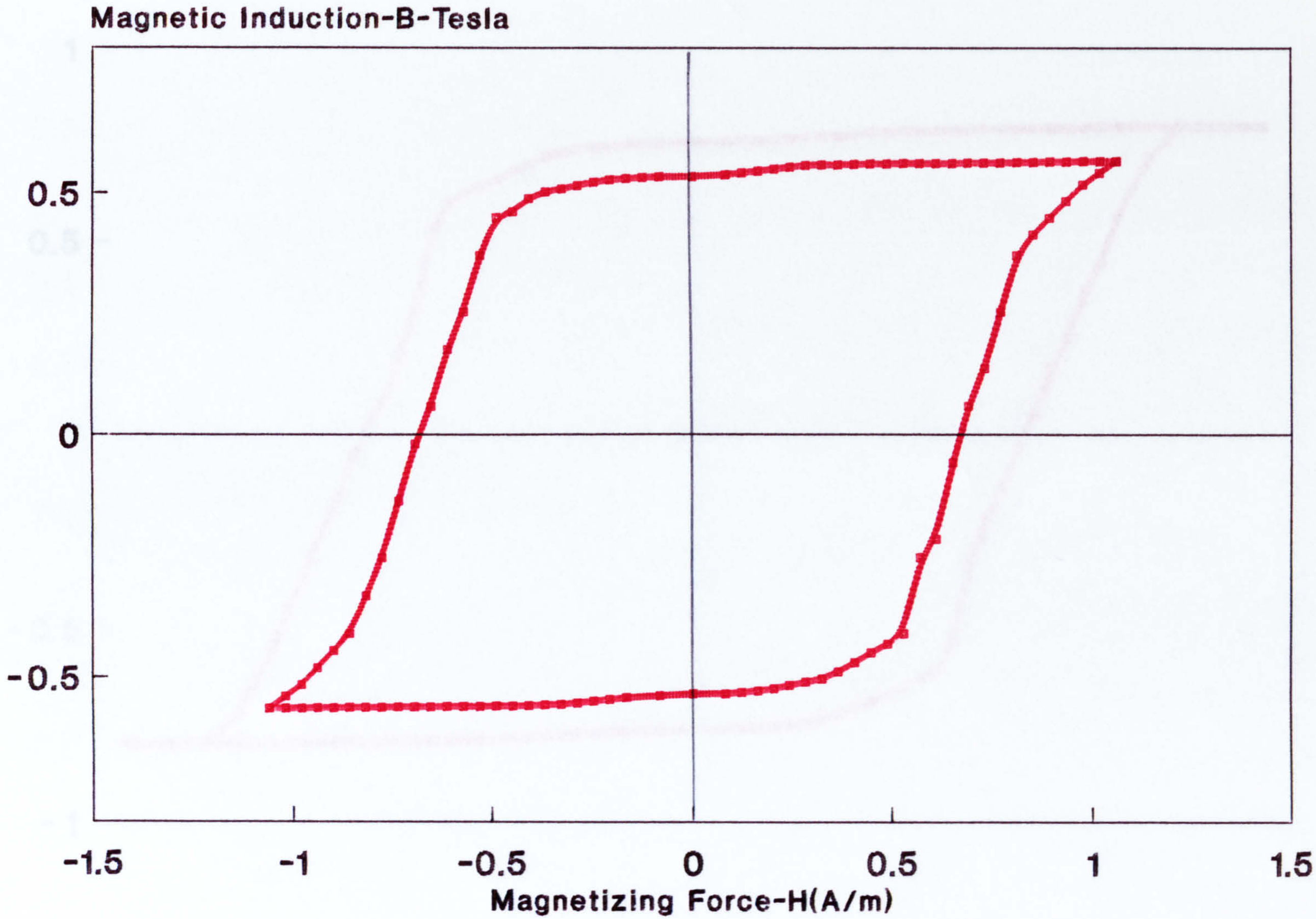

Fig. A.3 B/H loop of Metglas 2605-S2 at flux density 0.6 T at 150°C.

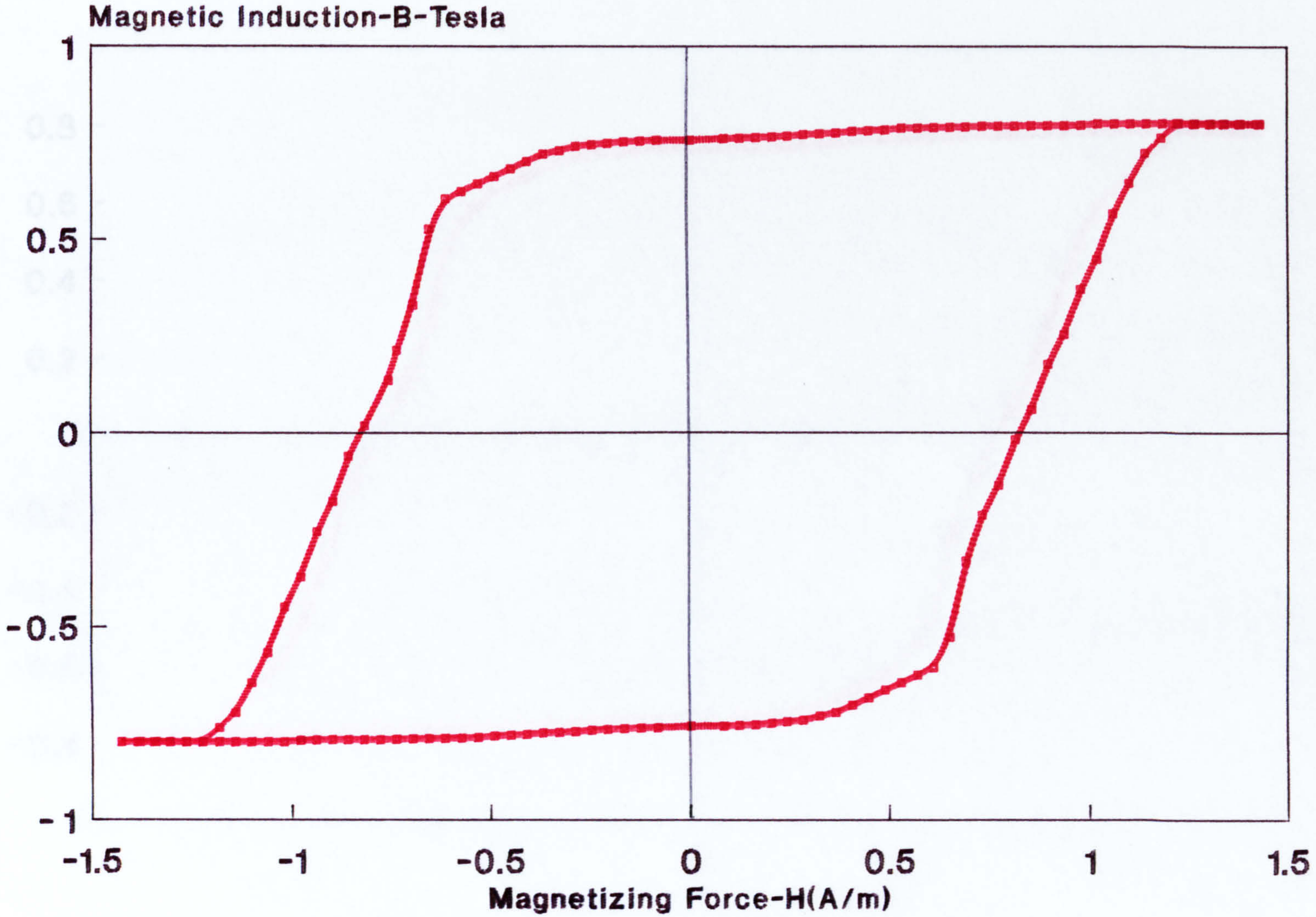

Fig. A.4 B/H loop of Metglas 2605-S2 at flux density 0.8 T at ambient temperature.

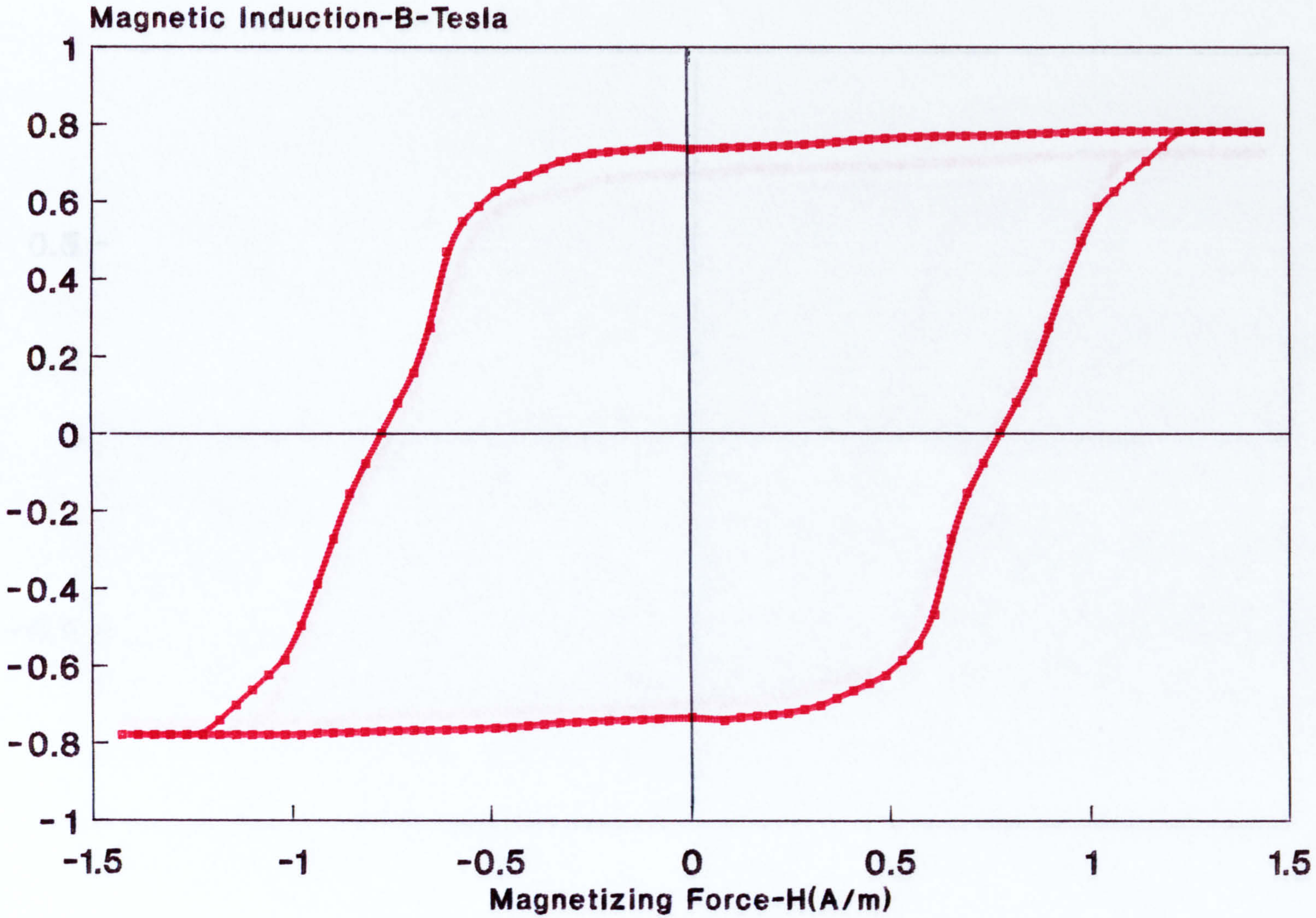

Fig. A.5 B/H loop of Metglas 2605-S2 at flux density 0.8 T at 100°C.

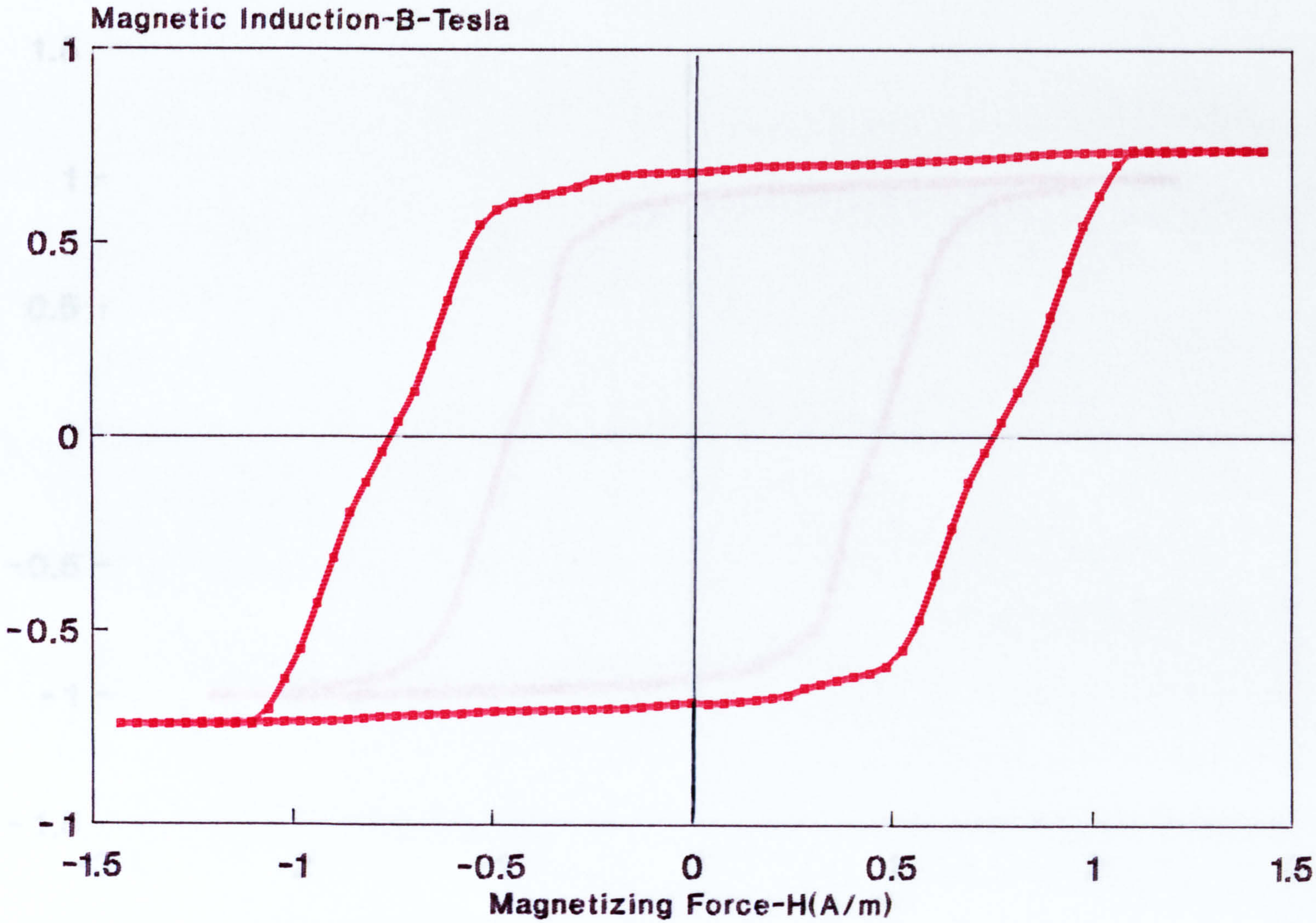

Fig. A.6 B/H loop of Metglas 2605-S2 at flux density 0.8 T at 150°C.

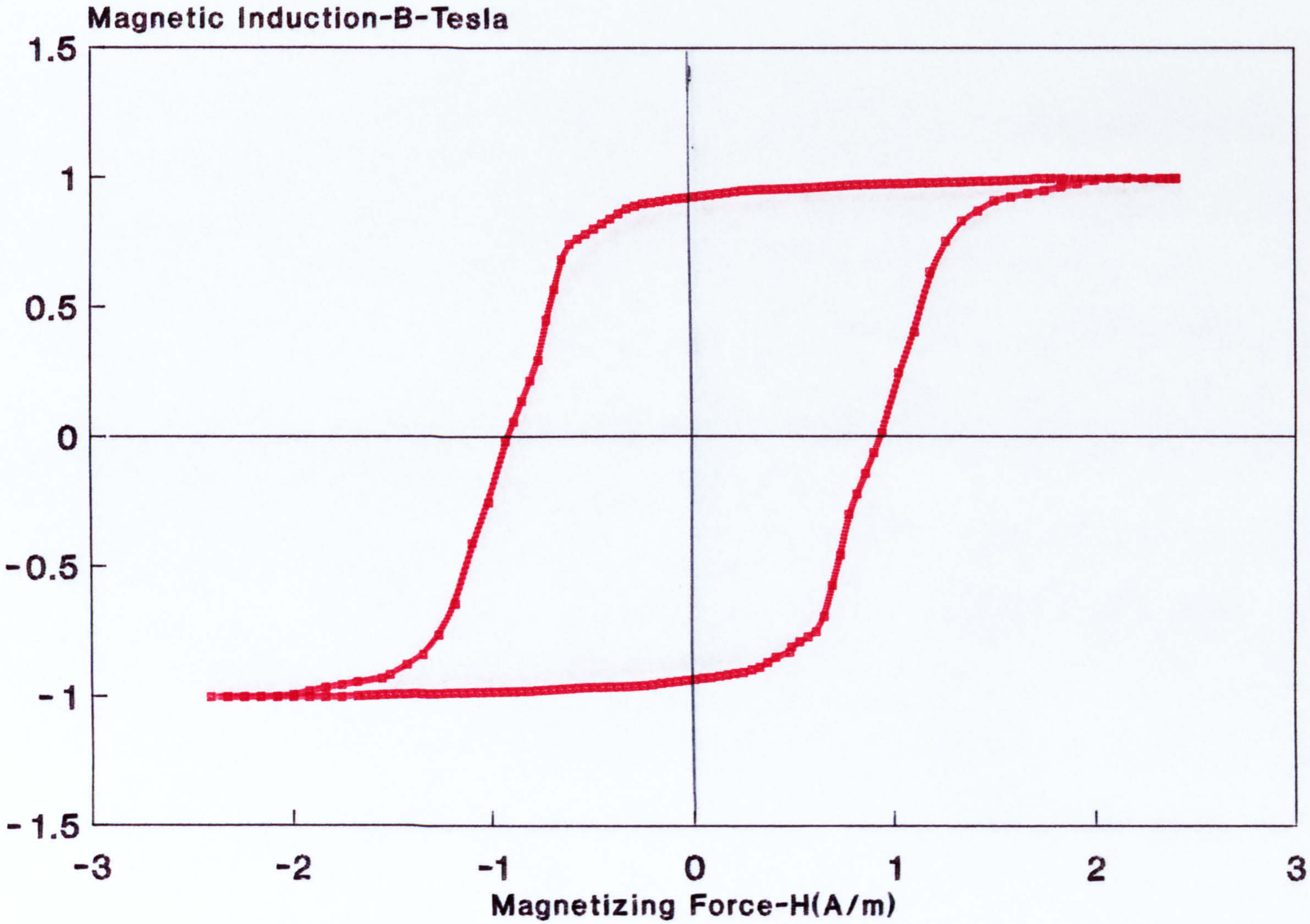

Fig. A.7 B/H loop of Metglas 2605-S2 at flux density 1.0 T at ambient temperature.

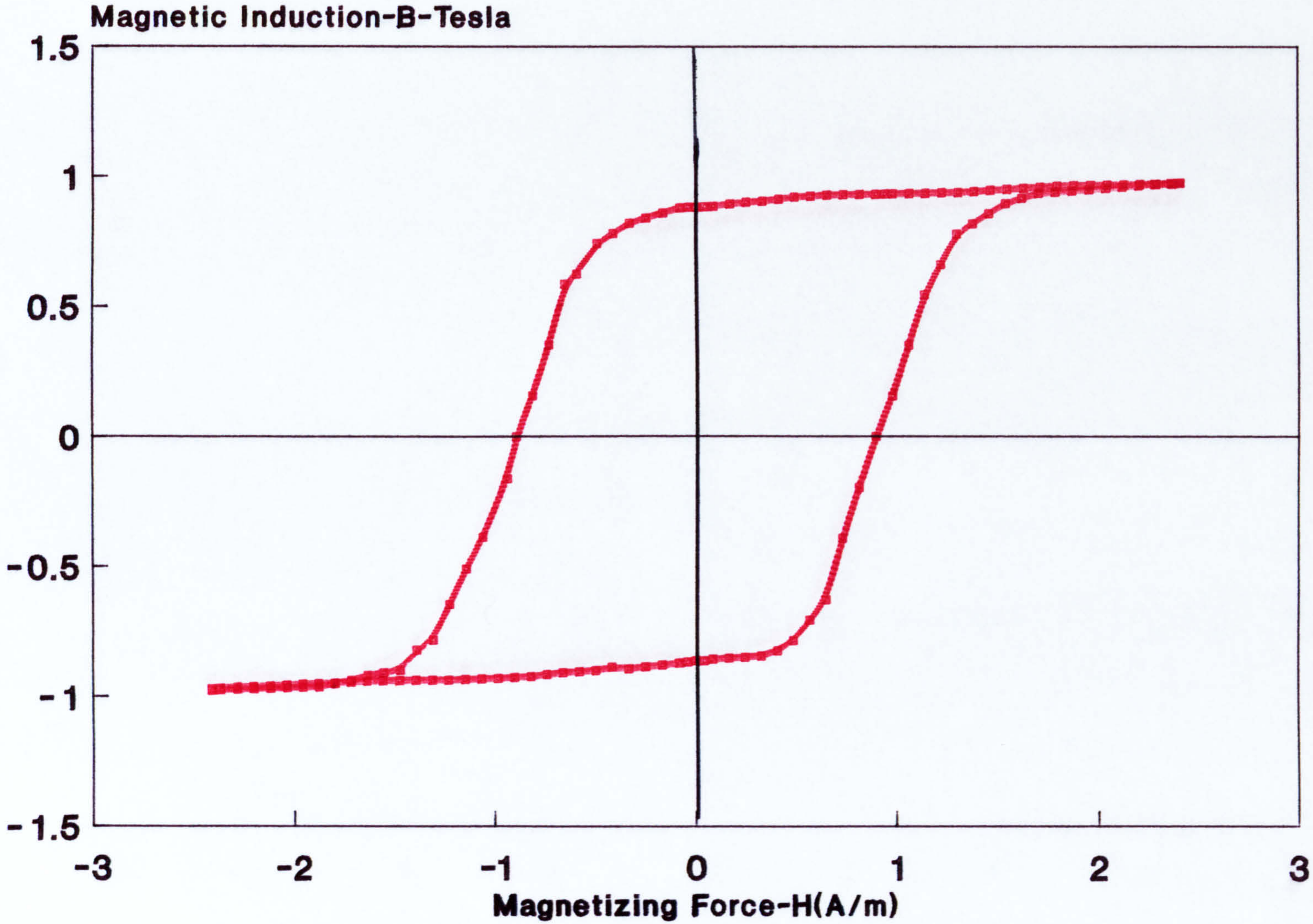

Fig. A.8 B/H loop of Metglas 2605-S2 at flux density 1.0 T at 100°C.

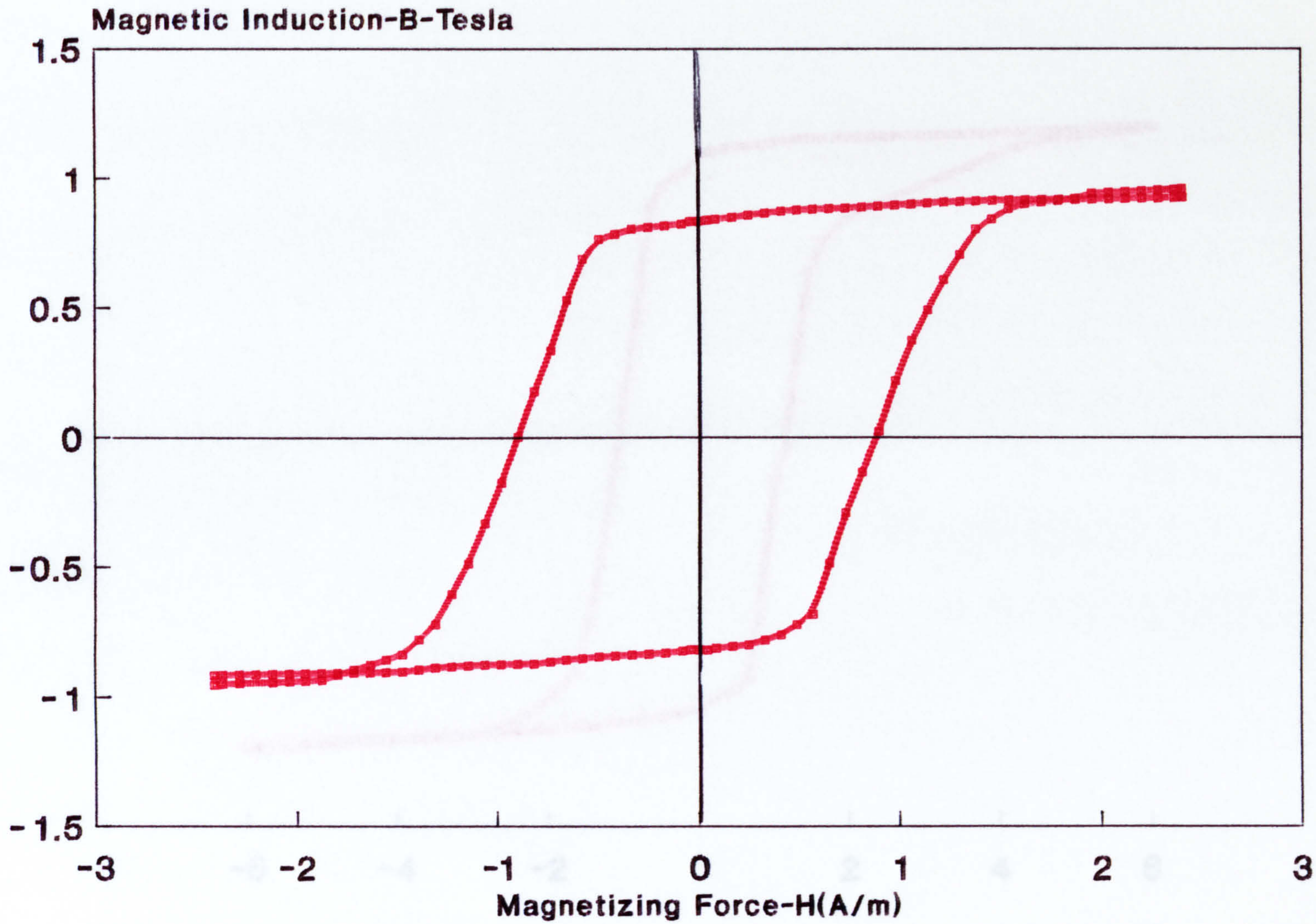

Fig. A.9 B/H loop of Metglas 2605-S2 at flux density 1.0 T at 150°C.

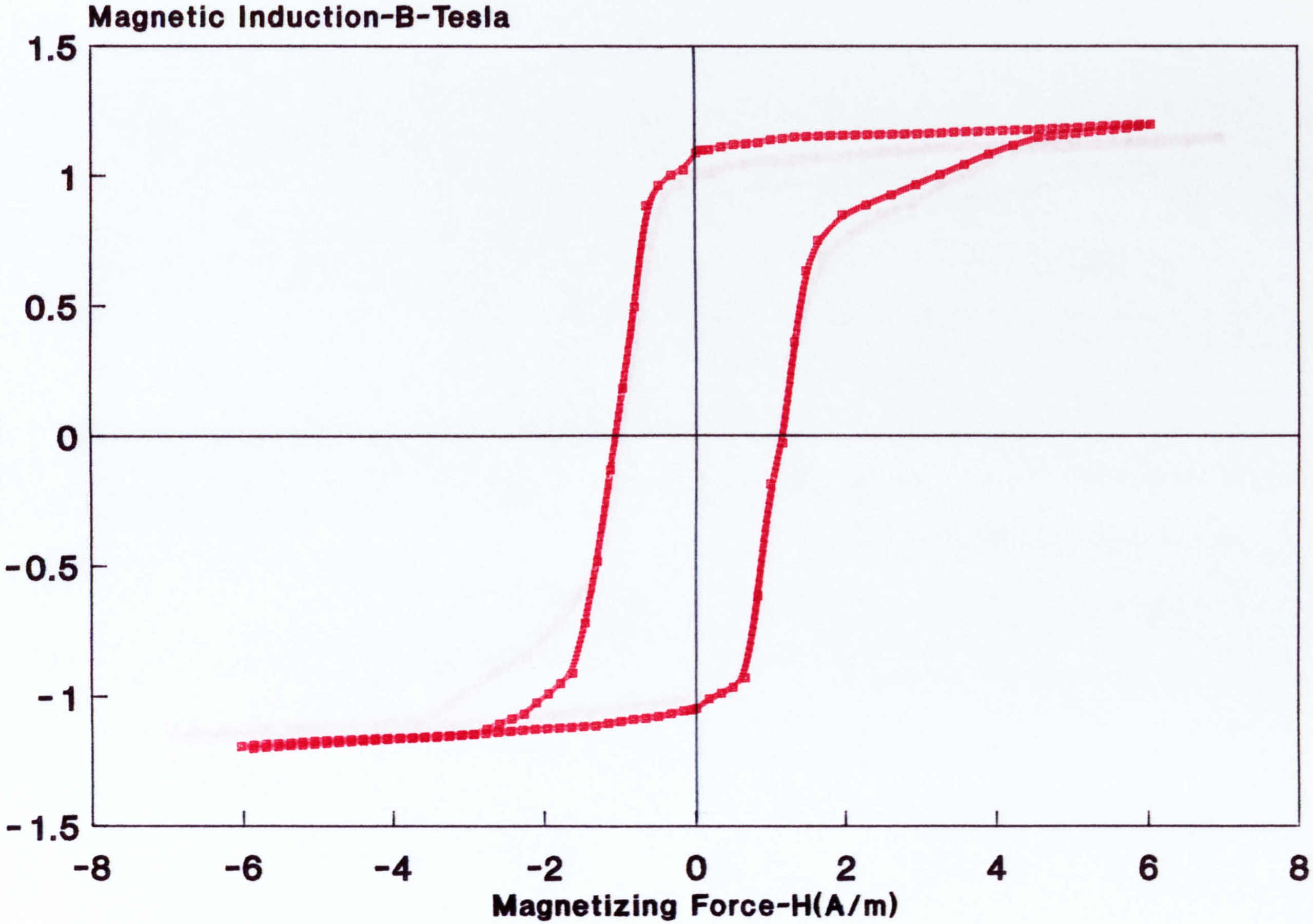

Fig. A.10 B/H loop of Metglas 2605-S2 at flux density 1.2T at ambient temperature.

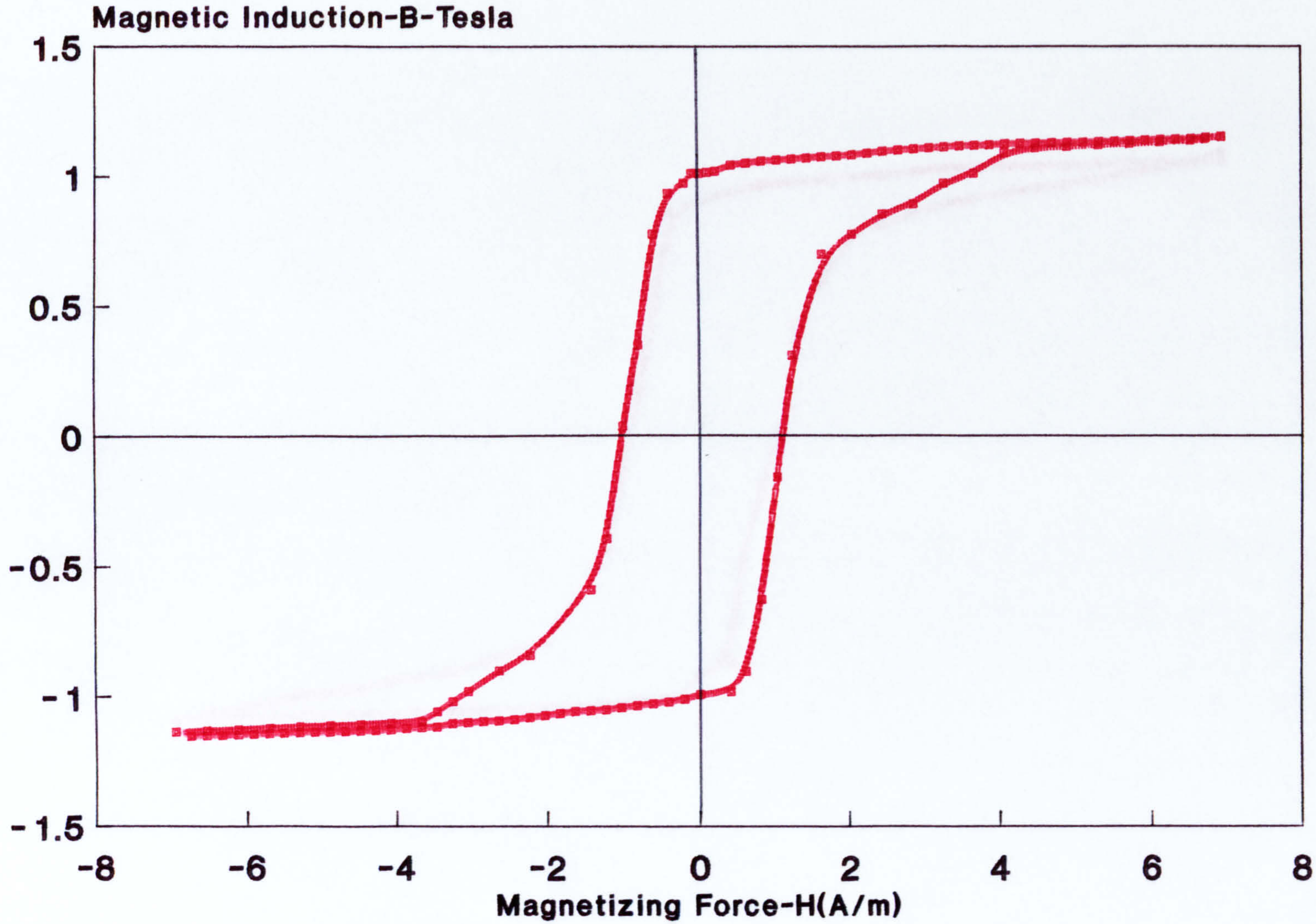

Fig. A.11 B/H loop of Metglas 2605-S2 at flux density 1.2 T at 100°C.

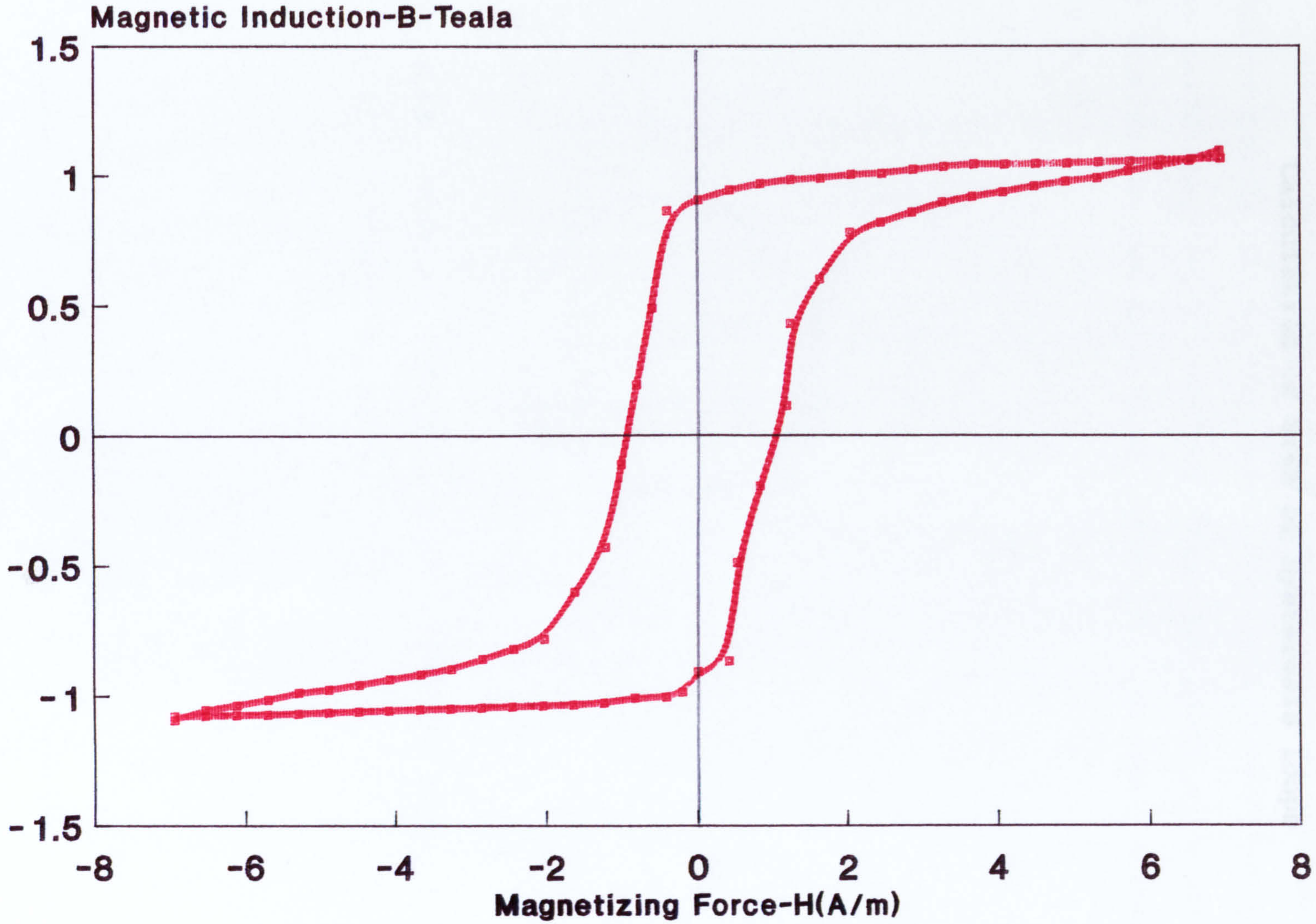

Fig. A.12 B/H loop of Metglas 2605-S2 at flux density 1.2 T at 150° C.

APPENDIX IV

Calculation of area of hysteresis loops

Appendix IV

Calculation of Area of Hysteresis loops

Using a Bitpad digitiser to obtain (x,y) co-ordnates of various points around the curve. The area within the curve was calculated using a Fortran programme based on summation of the areas see page 330 Area of a polygon shown in Fig.A.13

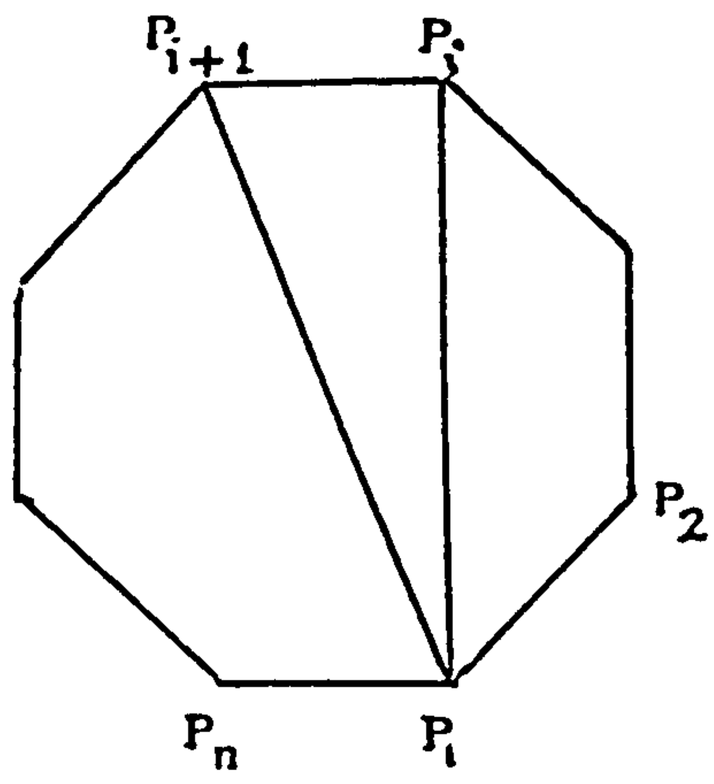

Fig. A.13 Polygon, using for calculating the area of the hysteresis loops.

Number the vertices anti-clock wise as shown in the diagram. The area of the polygan, g, is the summation of the areas of triangles formed as $P_1P_iP_{i+1}$ that is,

$$g = \sum a_i \qquad (A.1)$$

where a_i is the area of triangle $P_1P_iP_{i+1}$

Thus,

$$g = \frac{1}{2} \sum [y_1(x_{i+1} - x_i) + y_i(x_1 - x_{i+1}) + y_{i+1}(x_i - x_1)] \qquad (A.2)$$

```
C  Program to find the area enclosed by a set of points, given
C  (x,y) co-ordinates.  The (x,y) values must be in a file, in
C  the order in which they are taken from the curve, in going
C  around it in an anti-clockwise direction...
C
C     X1  Y1                                          o  (X1, Y1)
C     X2  Y2                    (X2, Y2)   o
C       .
C       .                     (X3, Y3) o
C       .                                             o  (Xn, Yn)
C     Xn  Yn
C                                                o  X5, Y5)
C                         (X4, Y4) o
C
C  Note that the points follow each other around the curve.
C  The last point (Xn,Yn) must not be a duplicate of the first
C
C
      real  x(1000), y(1000), area
      integer  i
      character*80  fname

      write (*, *) 'Please type name of data file:'
      read (*, '(a)')  fname
      open (file=fname, status='old', unit=5, err=4)
      do 1 i = 1, 1000
         read (5, *, end=2)  x(i), y(i)
         n = i
1     continue

2     area = 0.0
      do 3 i = 2, n-1
3     area = area + 0.5 * (y(i) * (x(1) - x(i+1))
     1                     - y(1) * (x(i) - x(i+1))
     1                     + y(i+1) * (x(i) - x(1)))

      write (*, '(a, G12.4)')  'Area of enclosed figure is', area
      stop
4     write (*, *) 'Could not open your data file'
      end
```

APPENDIX V

AC hysteresis loops

(a)

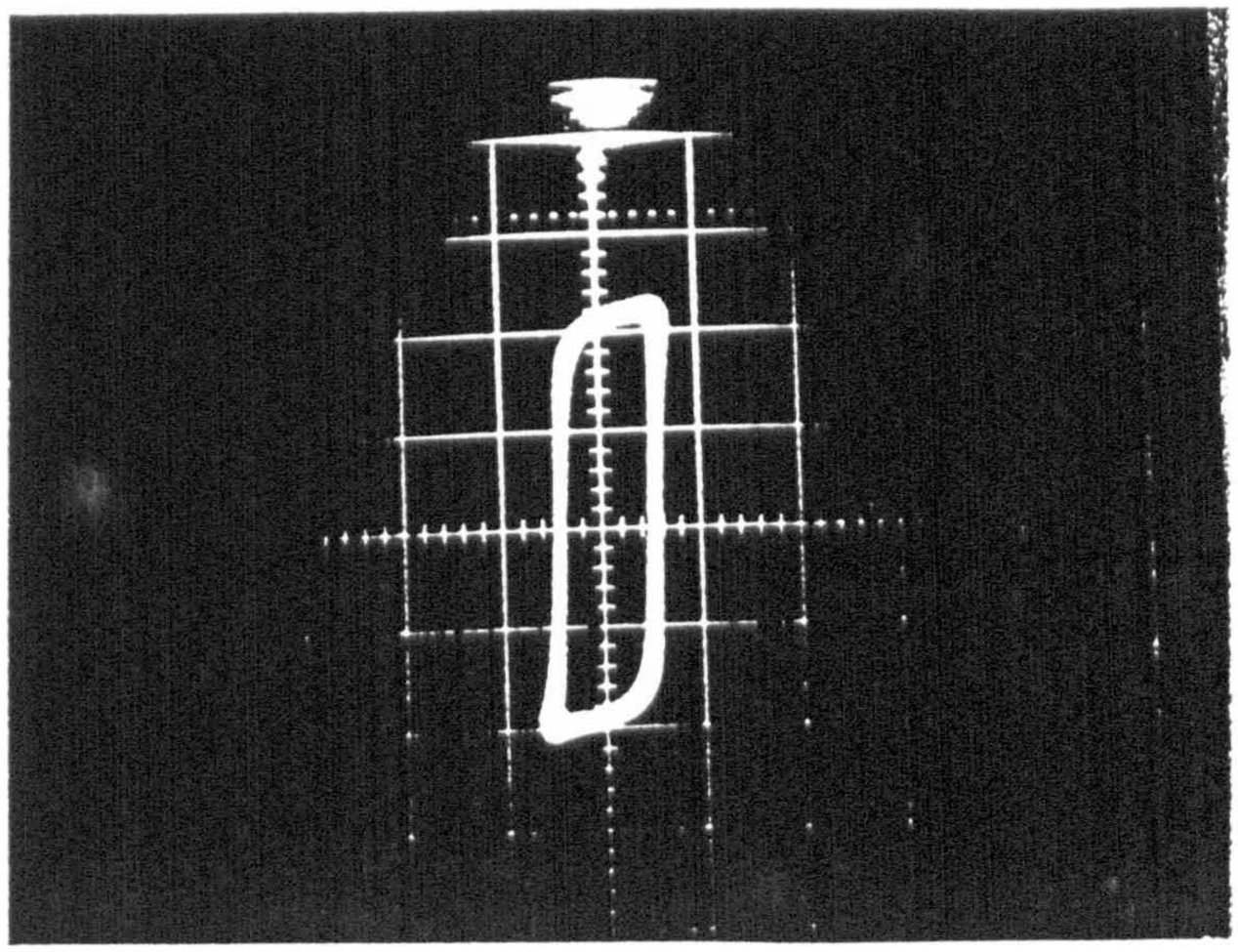

(b)

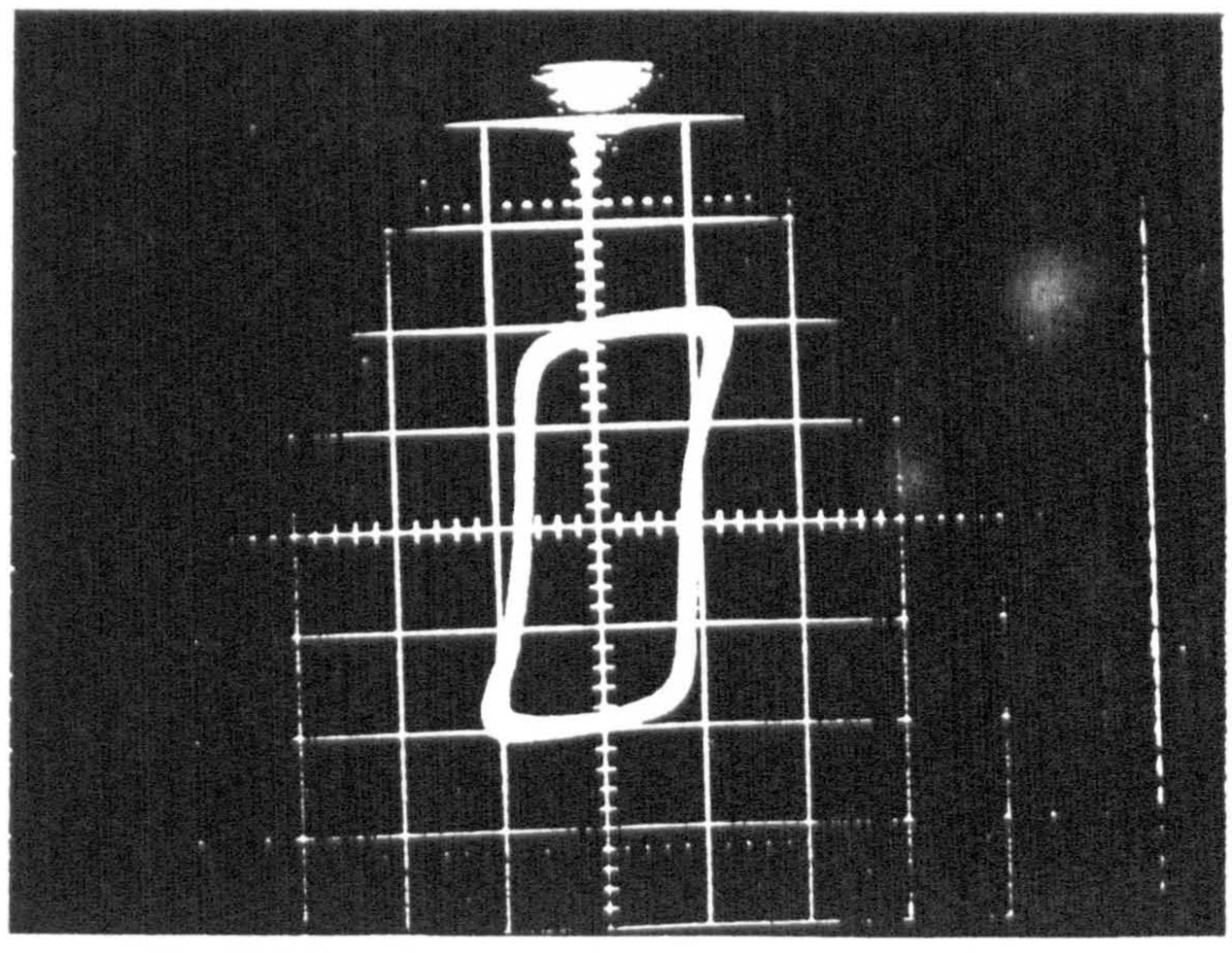

Fig. A.14 AC hysteresis loops of Metglas 2605-S2 (a) 50 Hz; (b) 400 Hz; (c) 1000 Hz; (d) 2000 Hz and (e) 3000 Hz at B_m = 1 T.

(c)

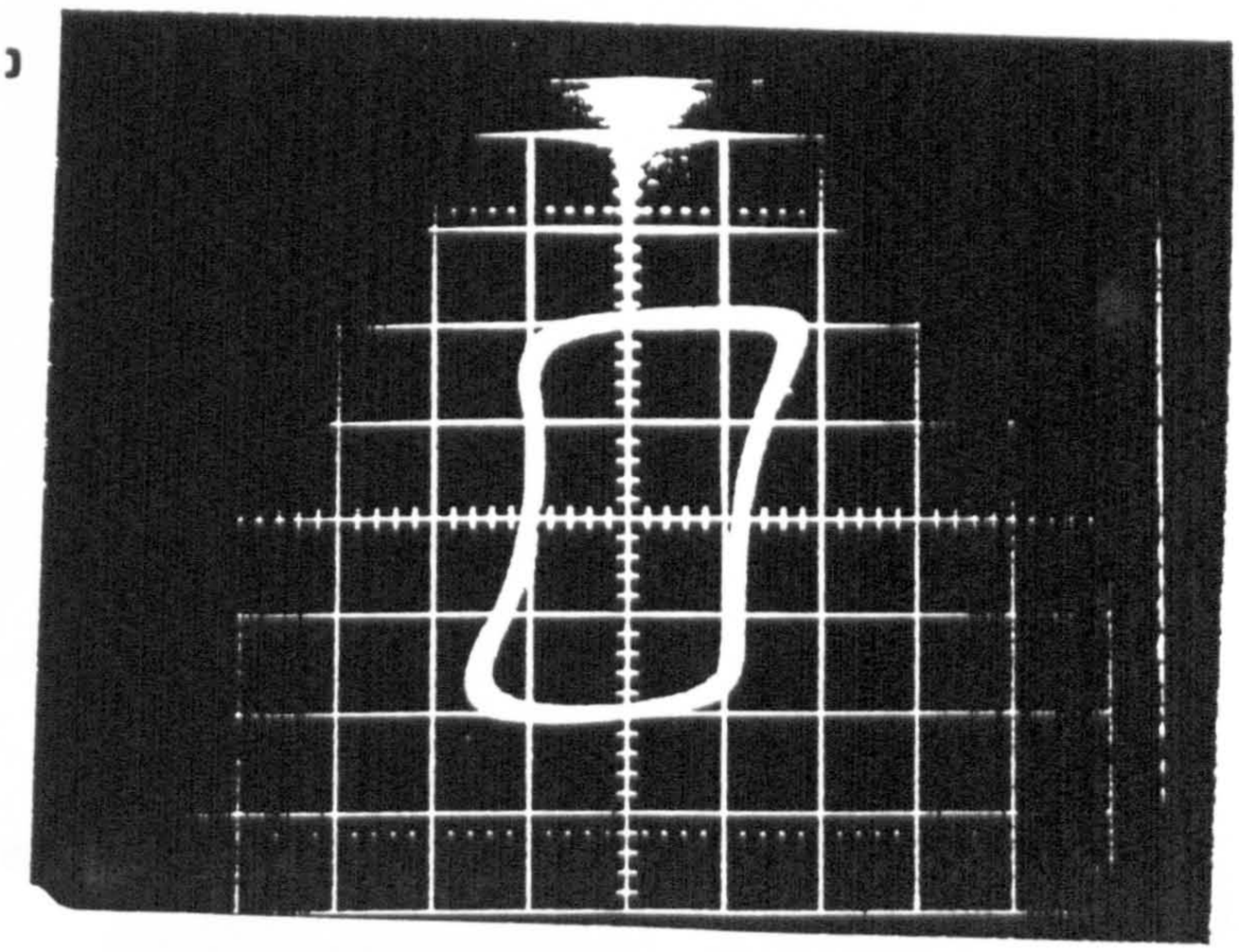

(d)

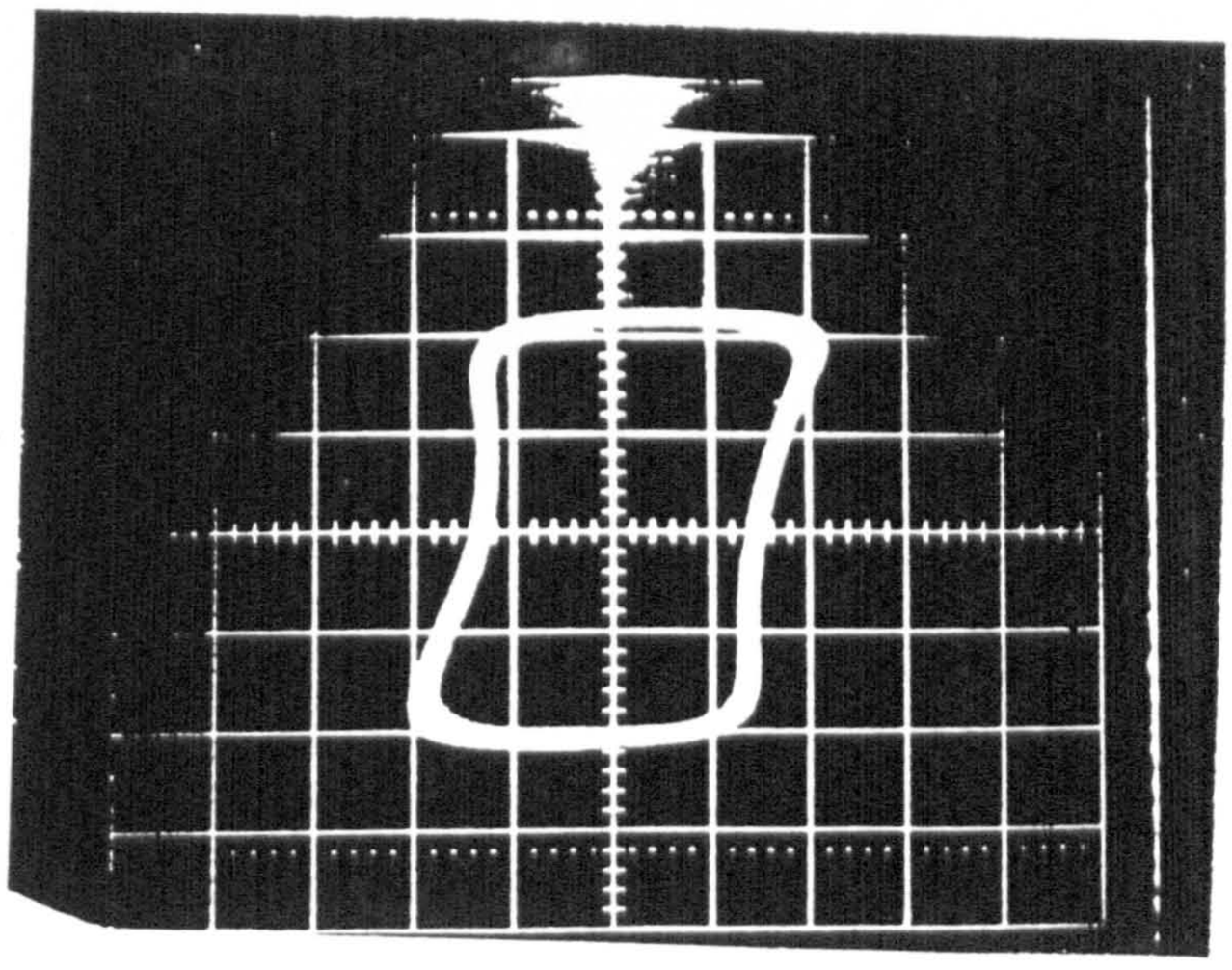

(e)

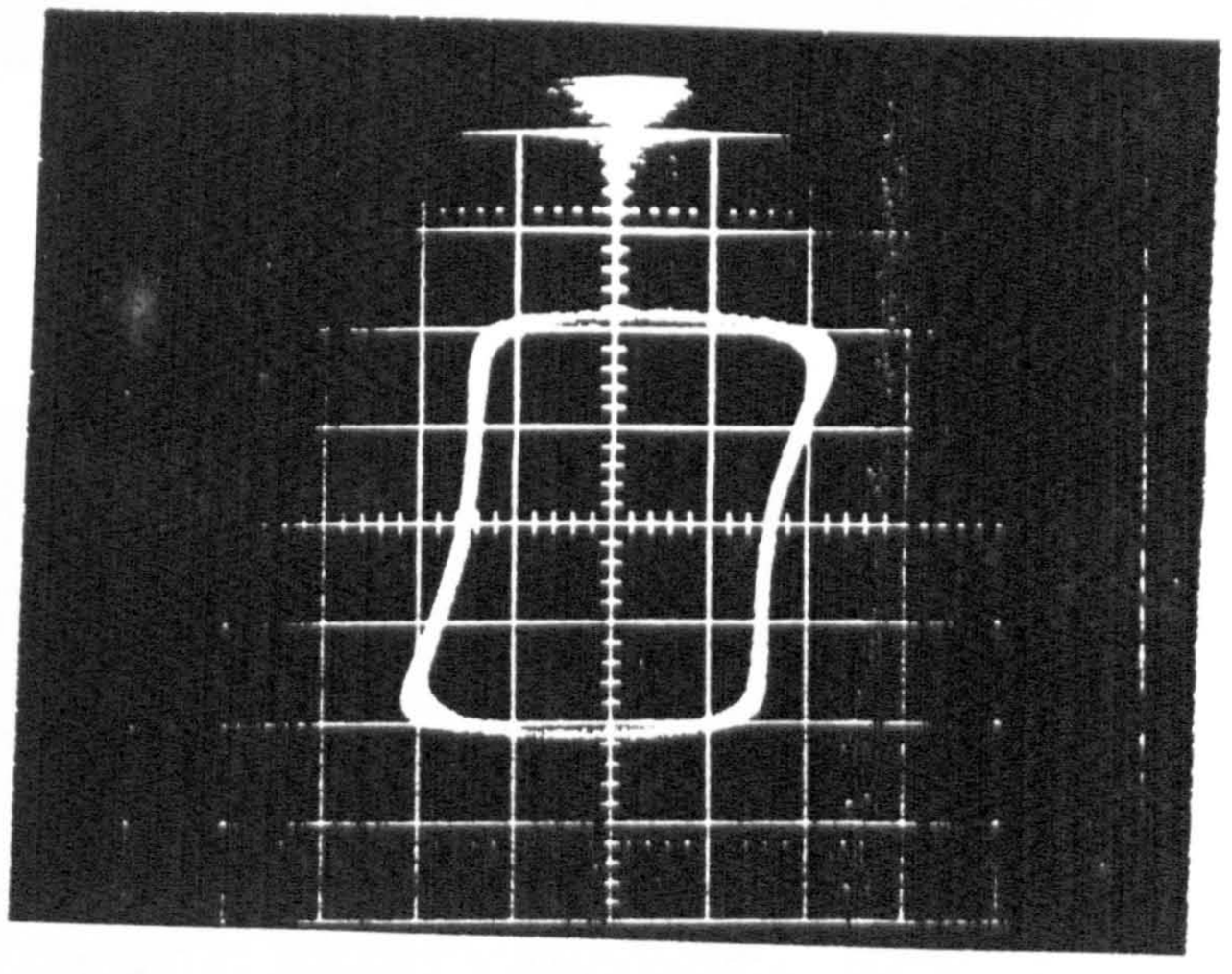

(a)

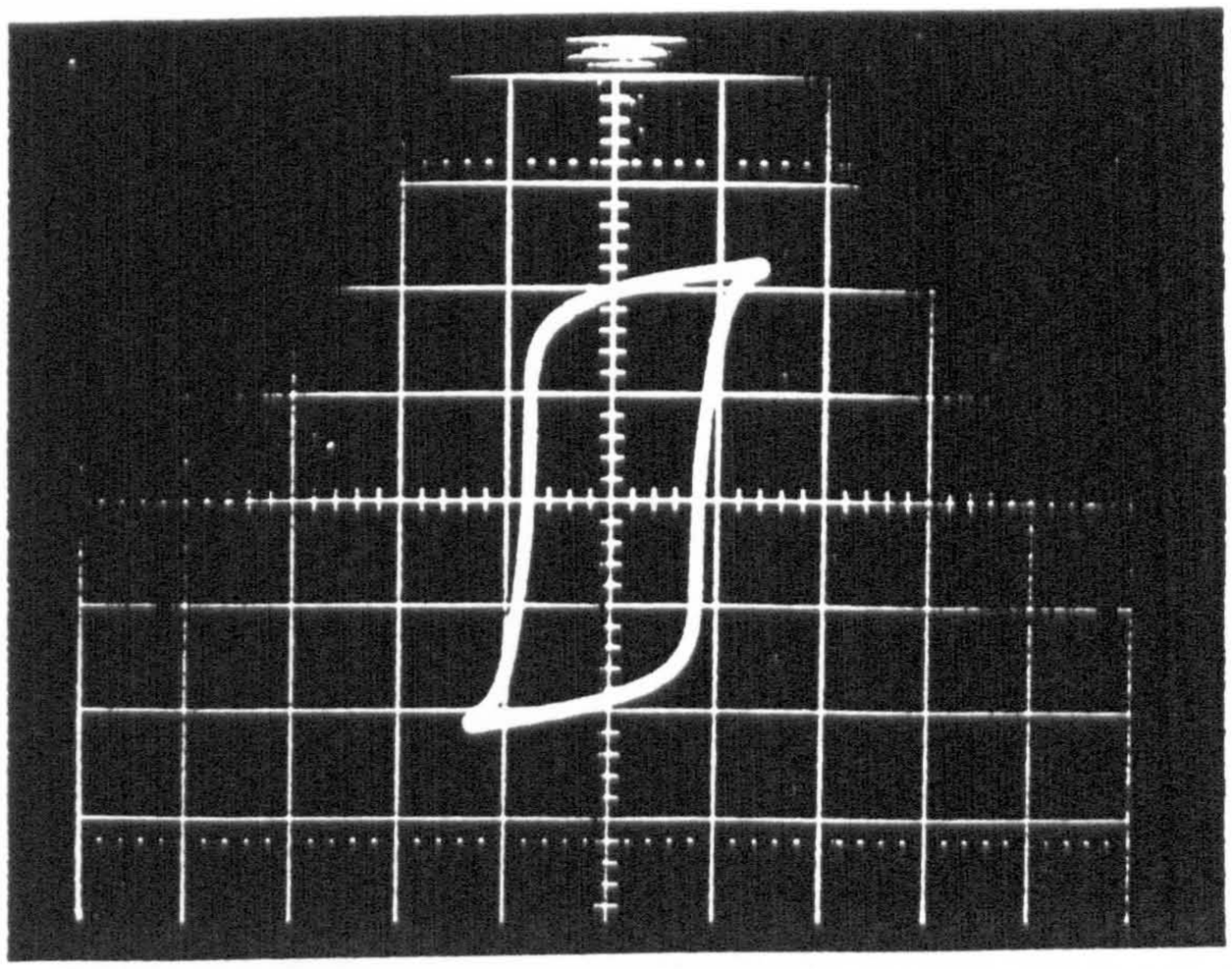

(b)

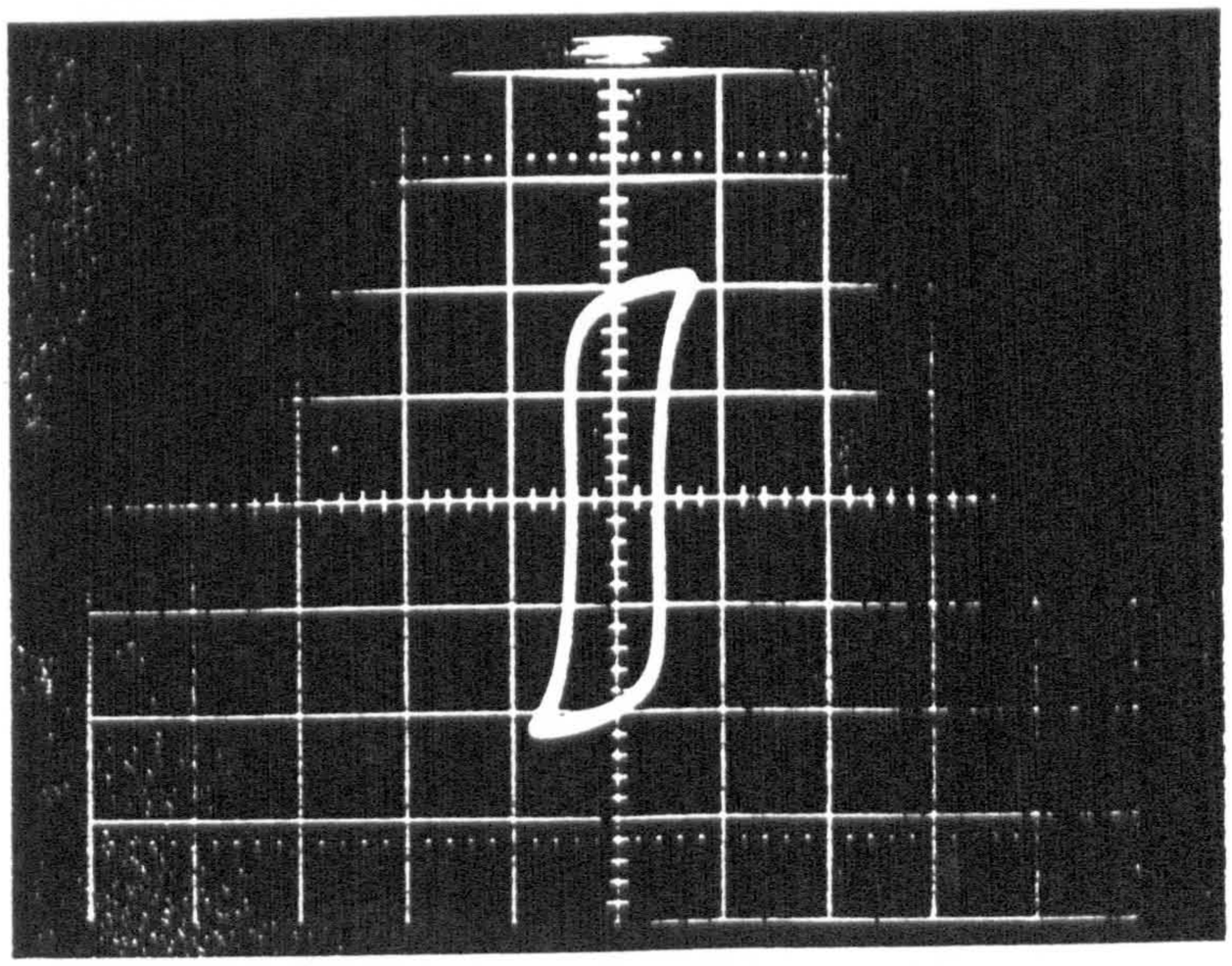

Fig. A.15 AC hysteresis loops of Metglas 2605-S3A (a) 50 Hz; (b) 400 Hz; (c) 1000 Hz; (d) 2000 Hz and (e) 3000 Hz at B_m = 1 T.

(c)

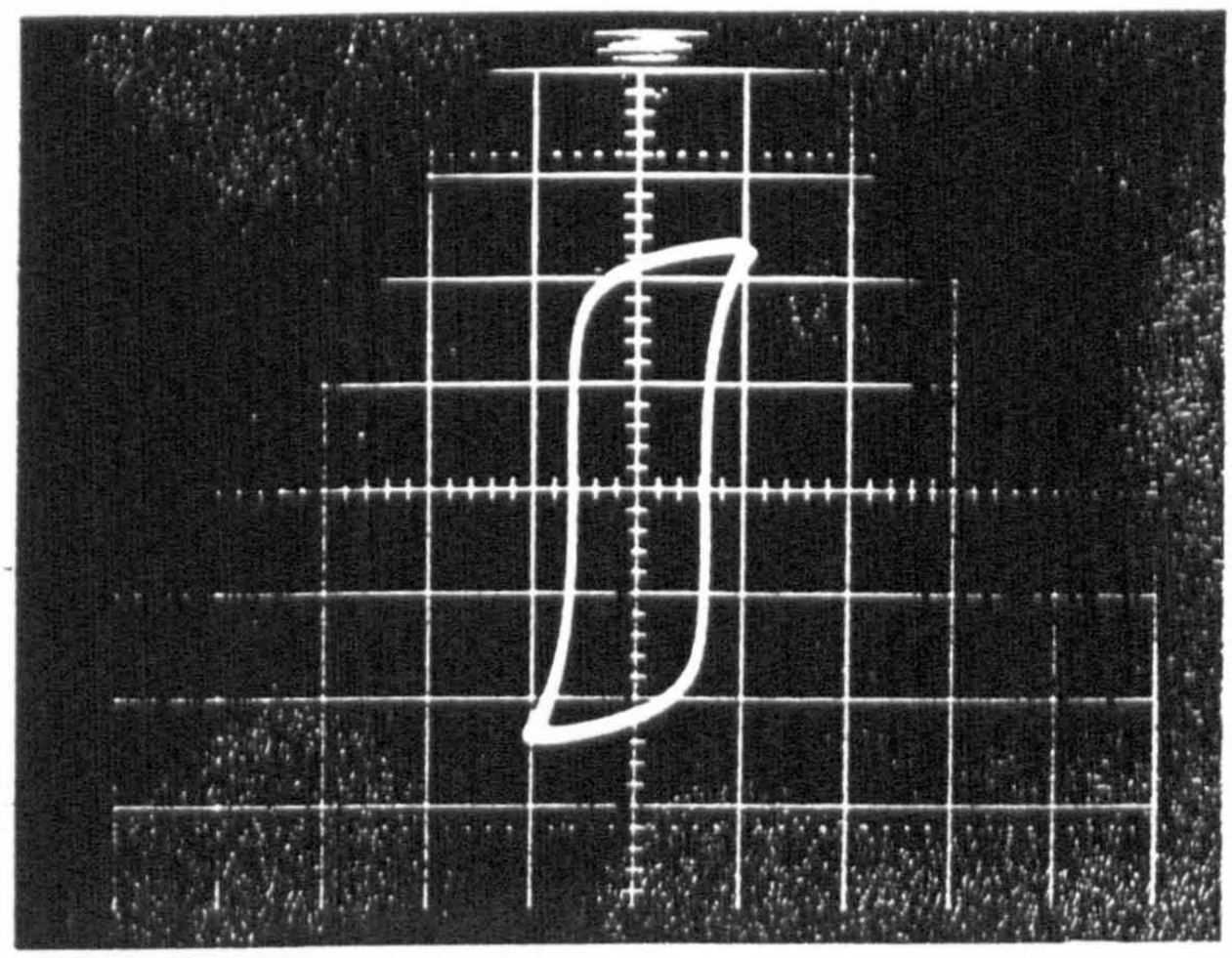

(d)

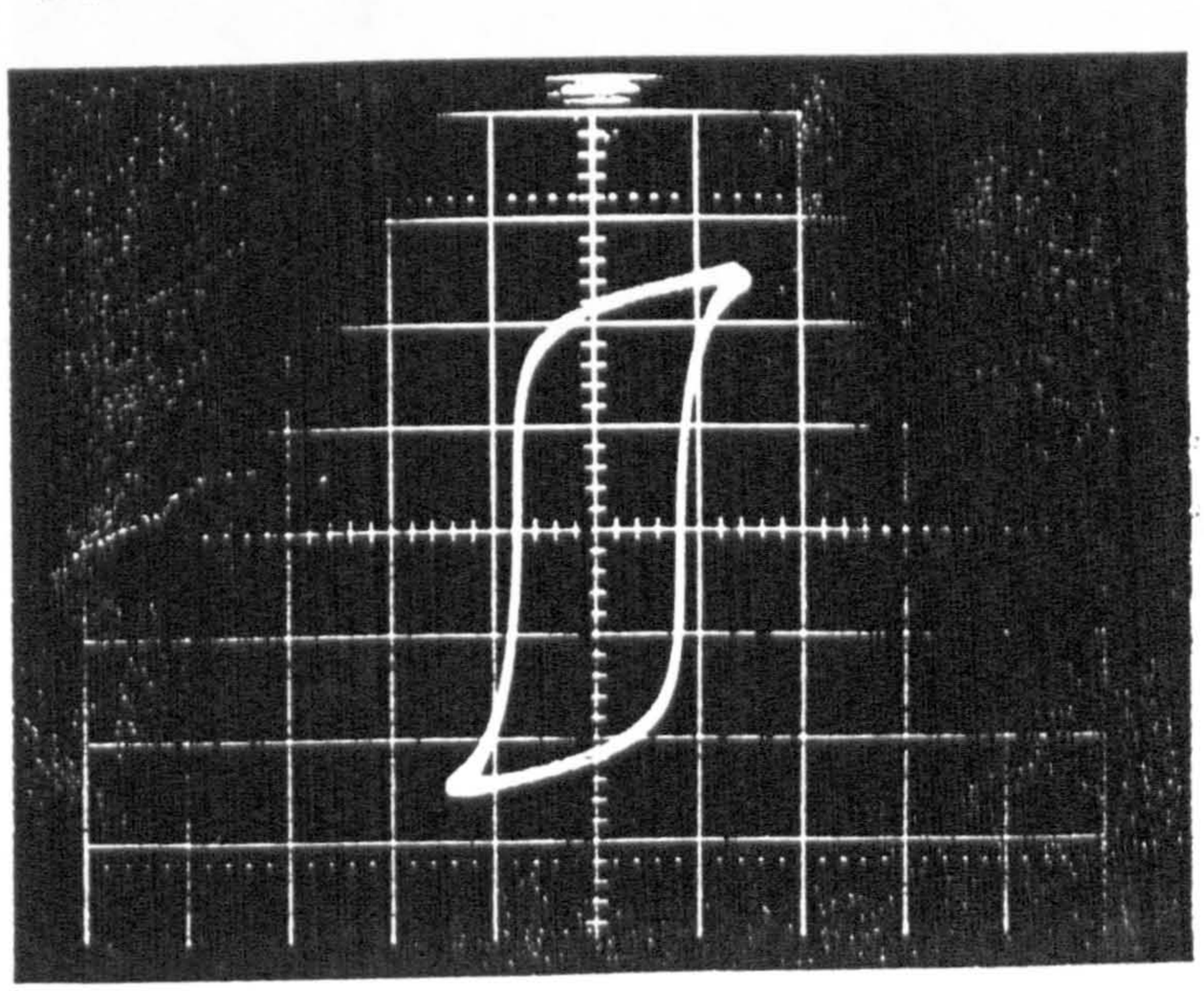

(e)

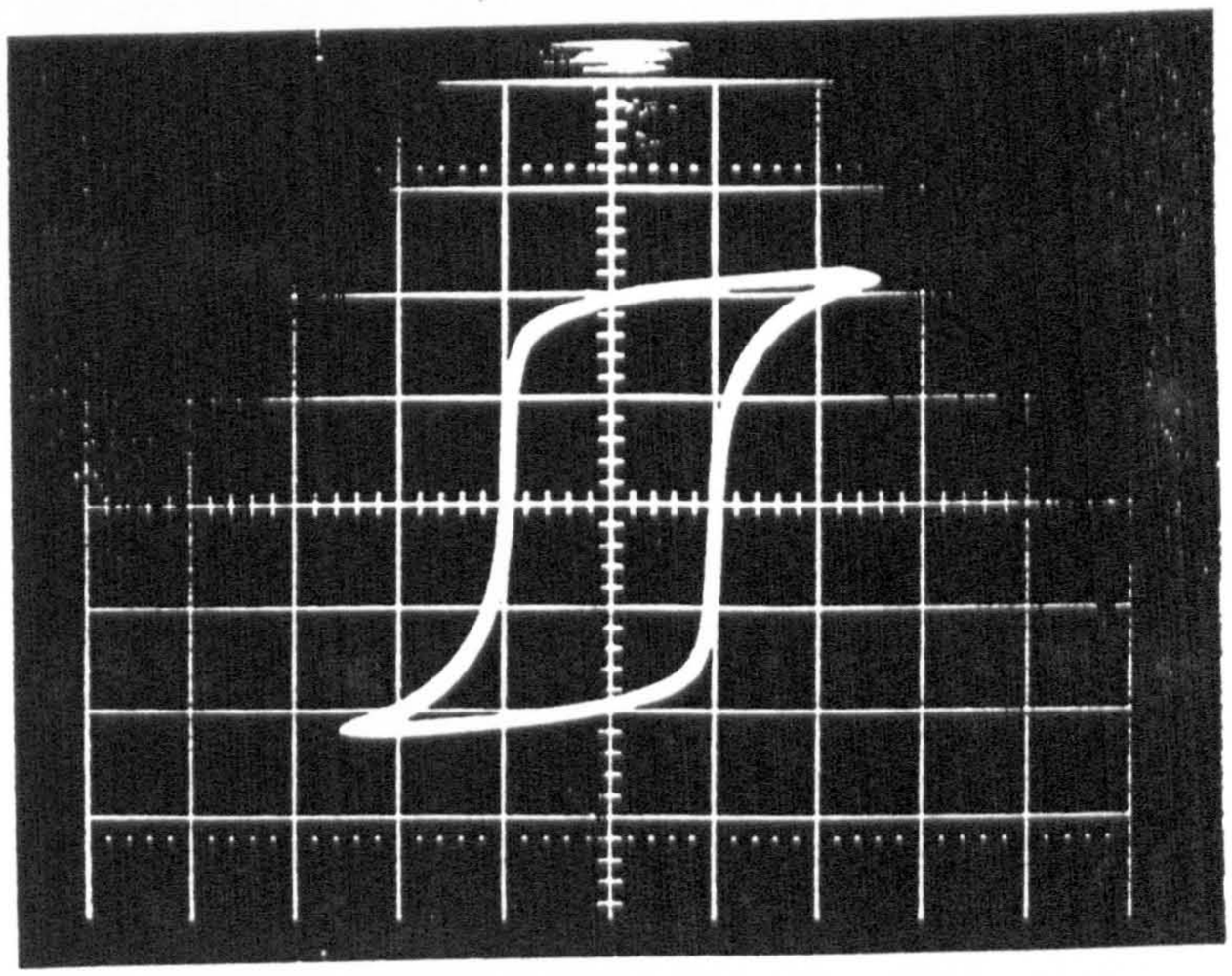

(a)

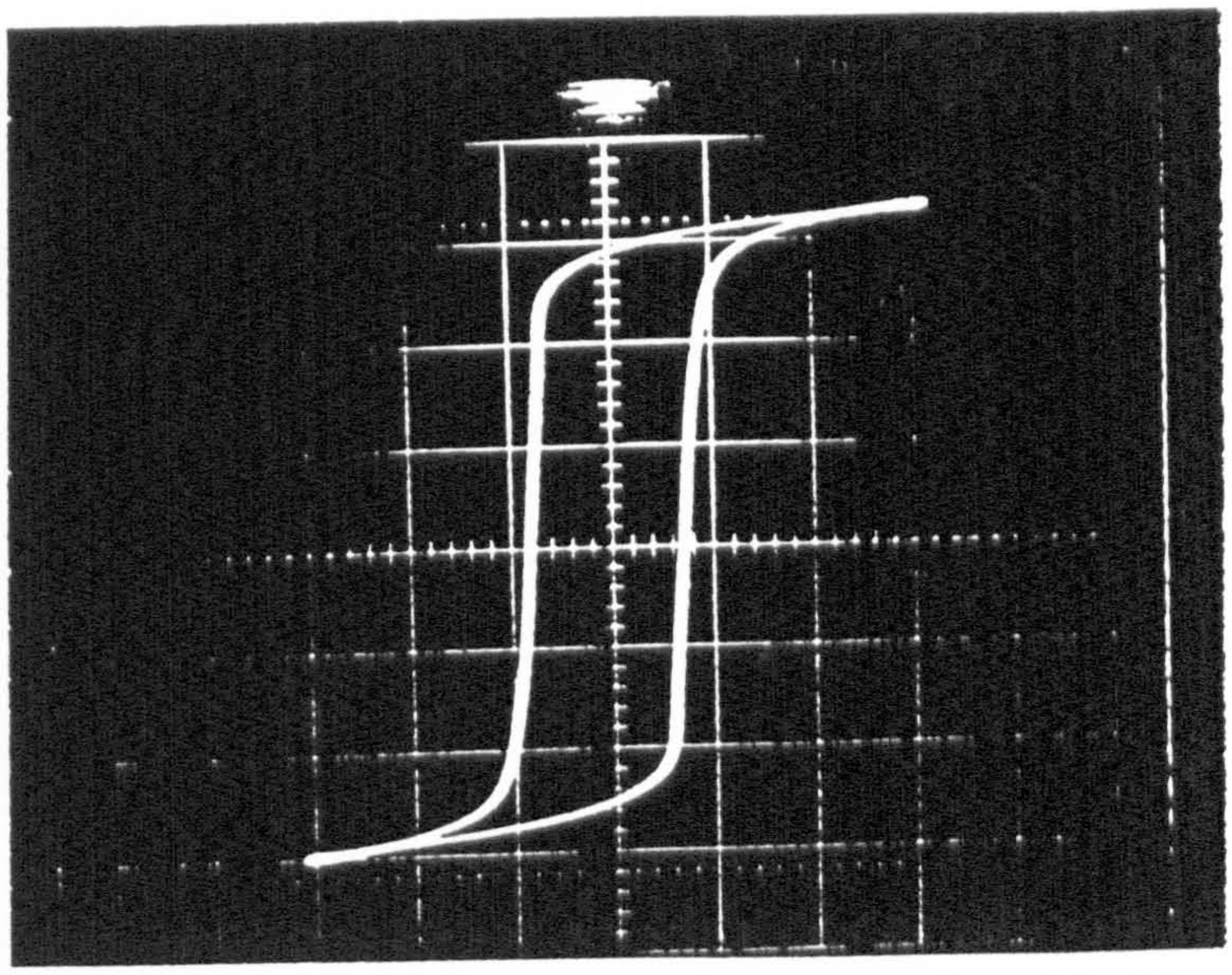

(b)

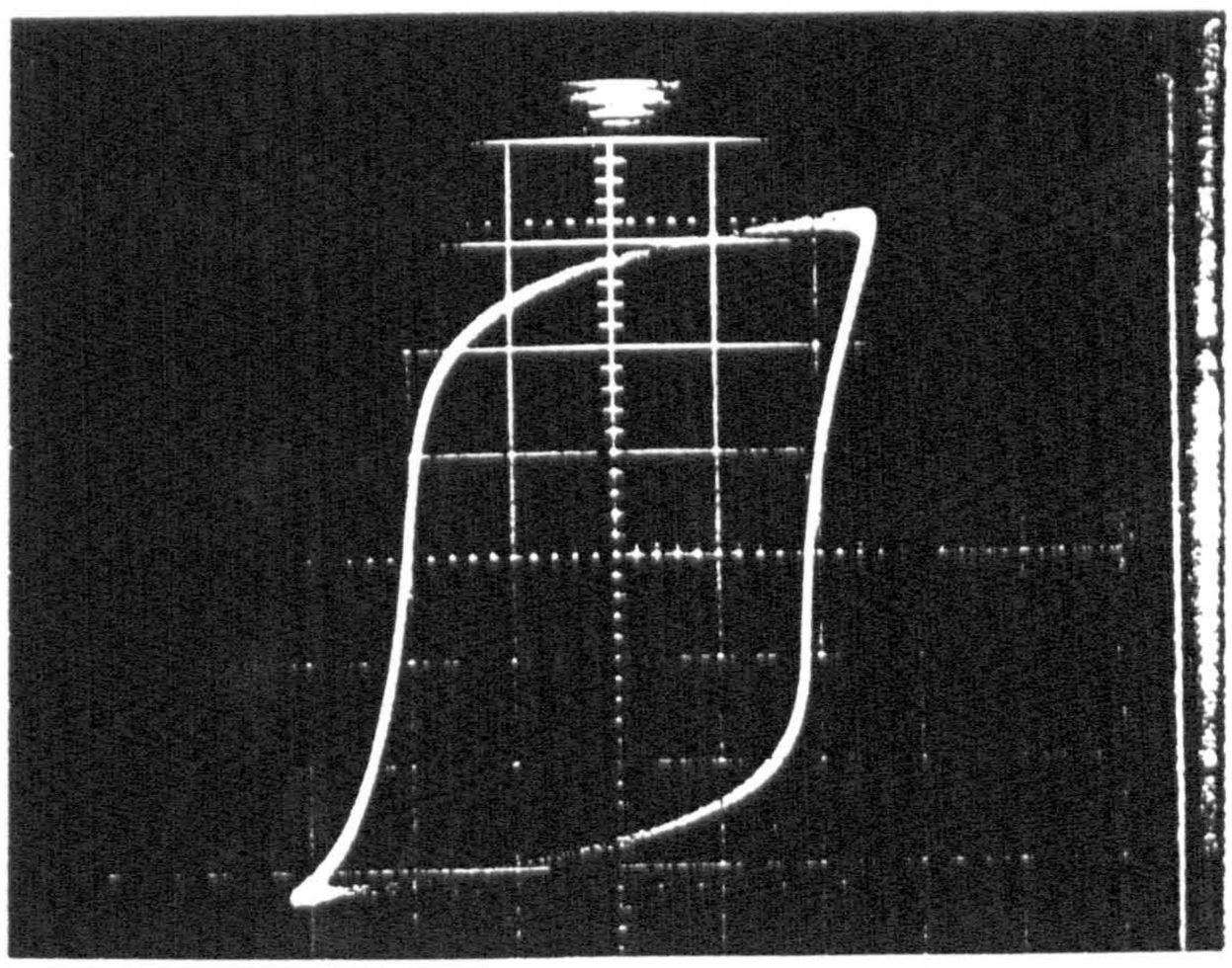

Fig. A.16 AC hysteresis loops of silicon-iron (a) 50 Hz 1.6 T; (b) 400 Hz 1 T; (c) 1000 Hz 0.8 T; (d) 2000 Hz 0.6 T and (e) 3000 Hz 0.4 T.

(c)

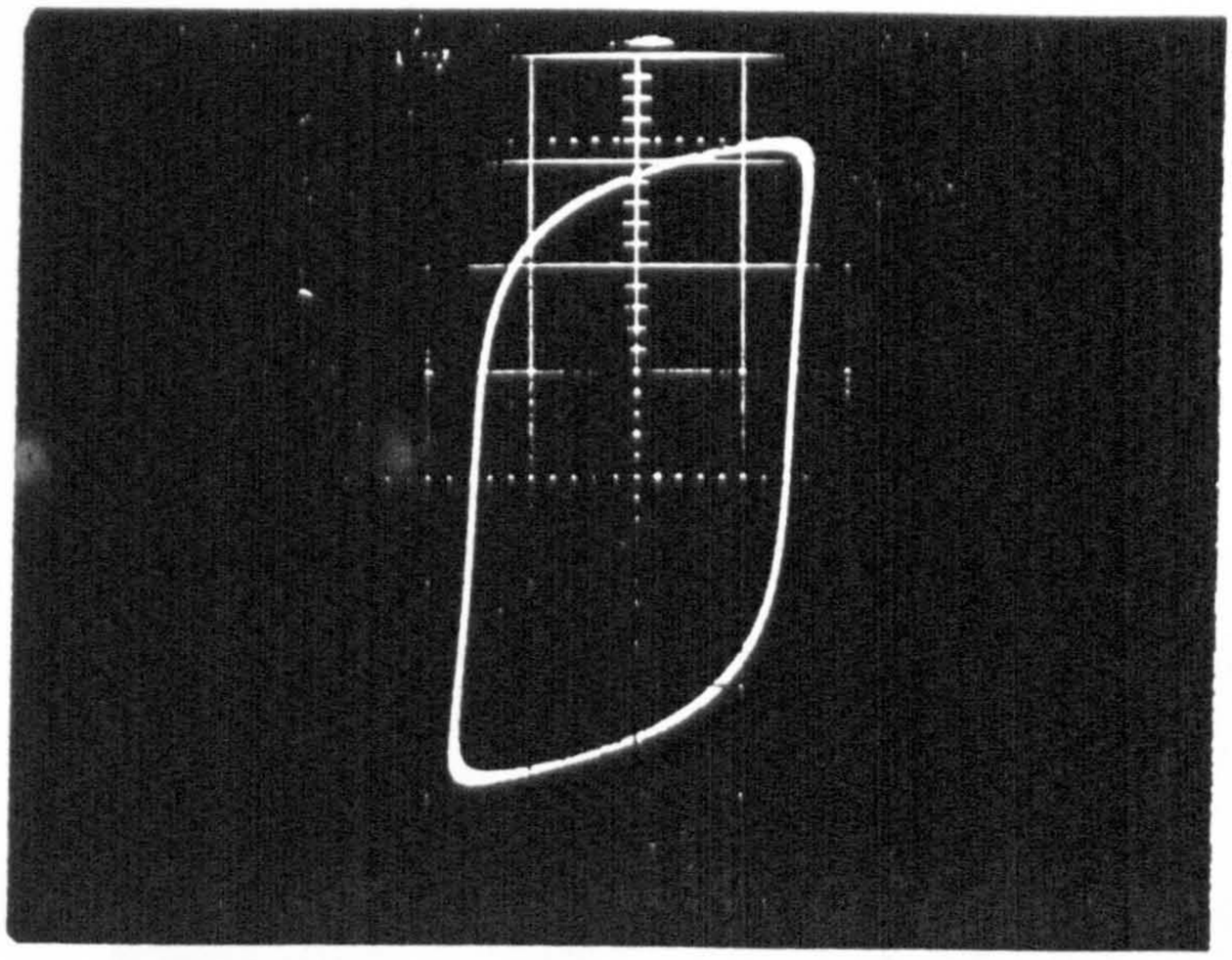

(d)

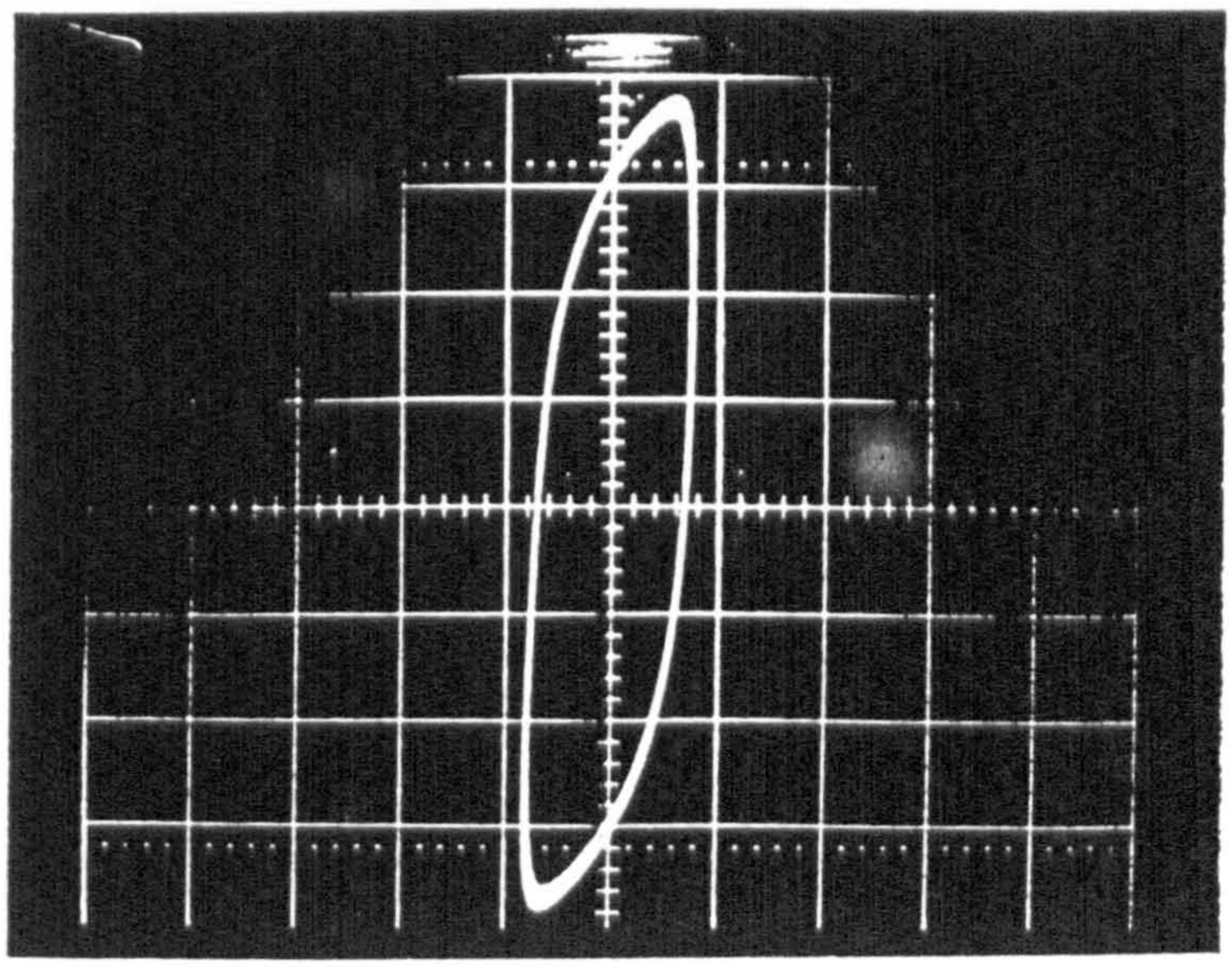

(e)

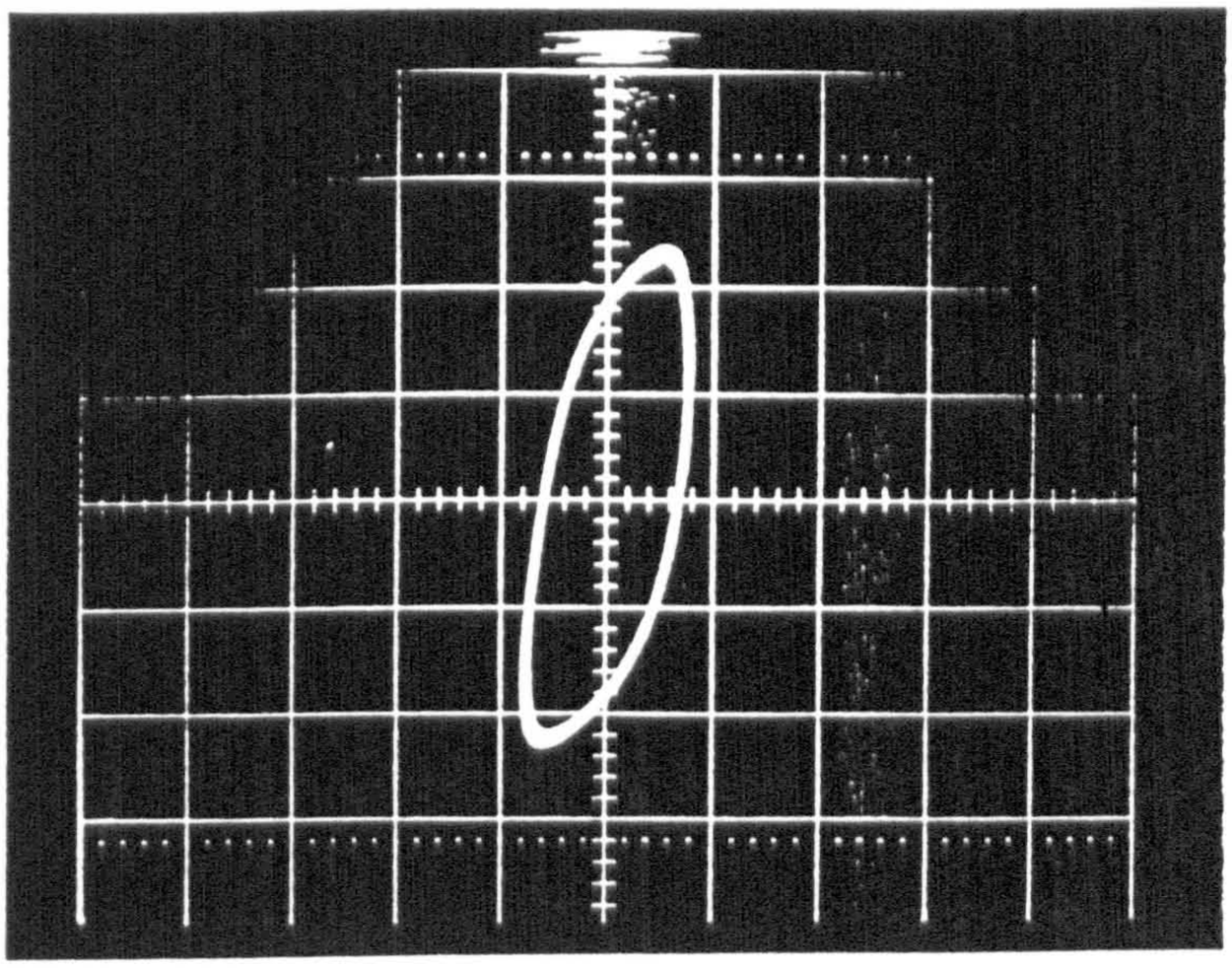

APPENDIX VI

Core loss sensitivity of amorphous Metglas with pressure

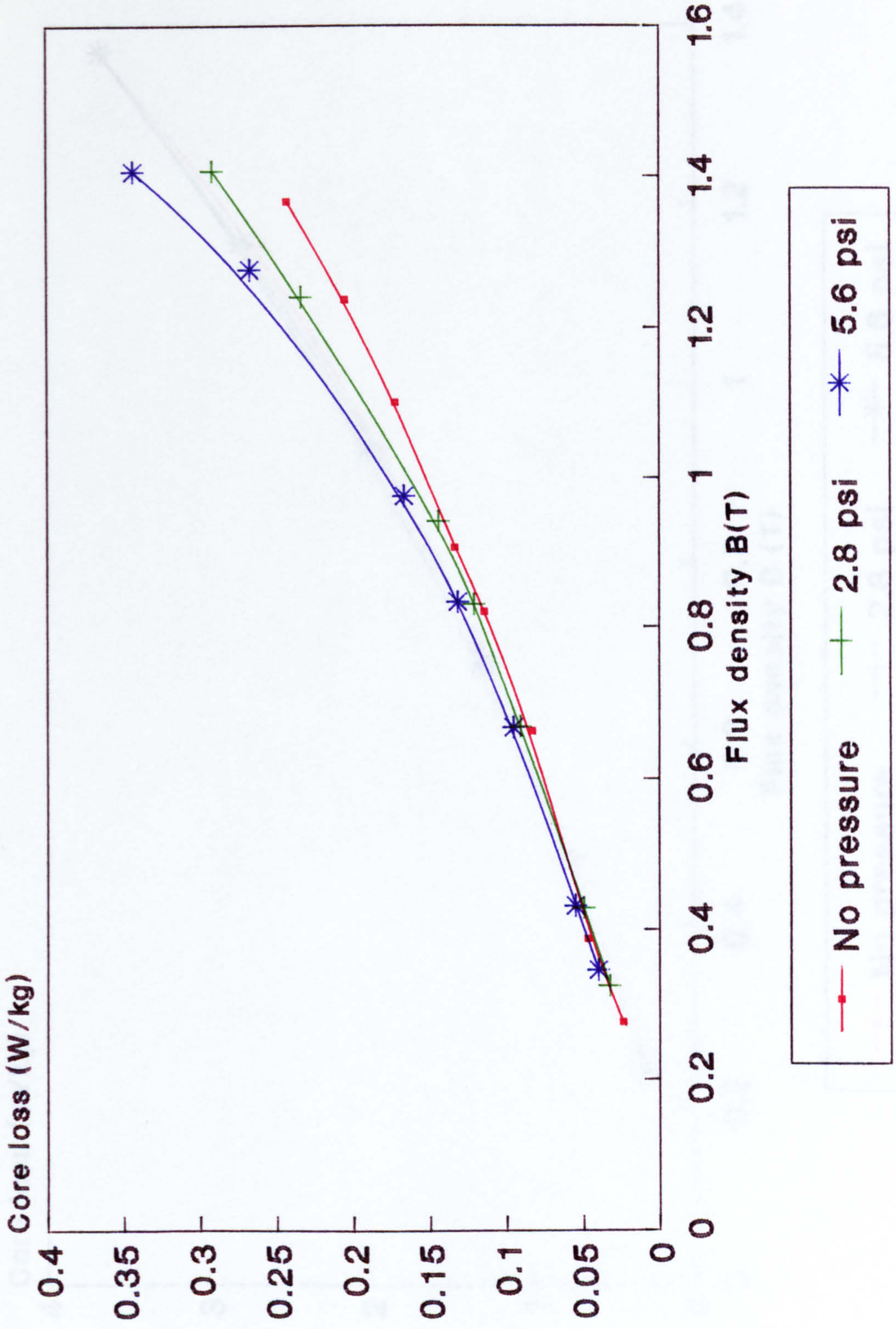

Fig. A.17 Core loss sensitivity of Metglas 2605-S2 with pressure of 0, 2.8, 5.6psi at 50 Hz core No.1.

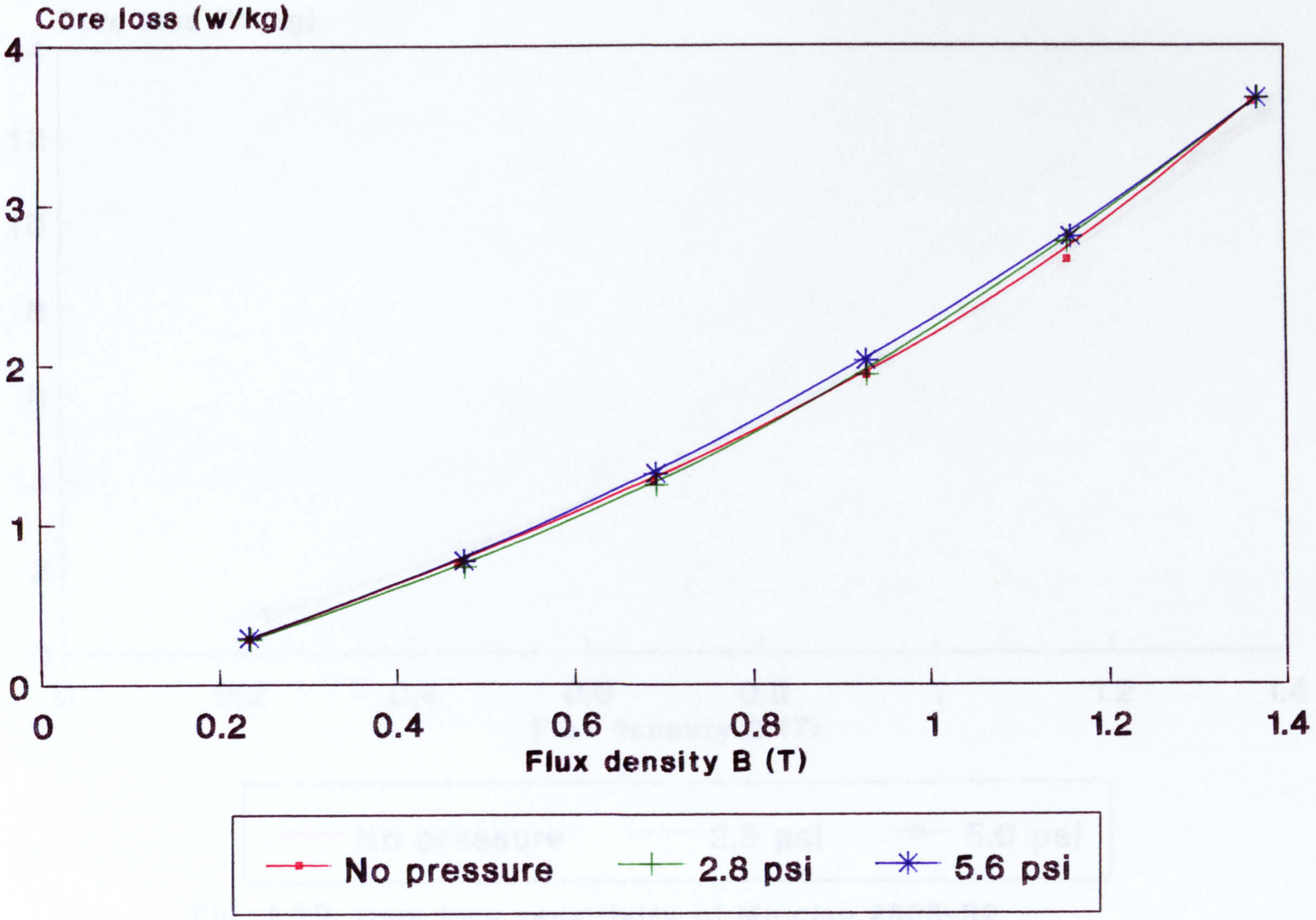

Fig. A.18 Core loss sensitivity of Metglas 2605-S2 of 0, 2.8 and 5.6 psi at 400Hz core no.1

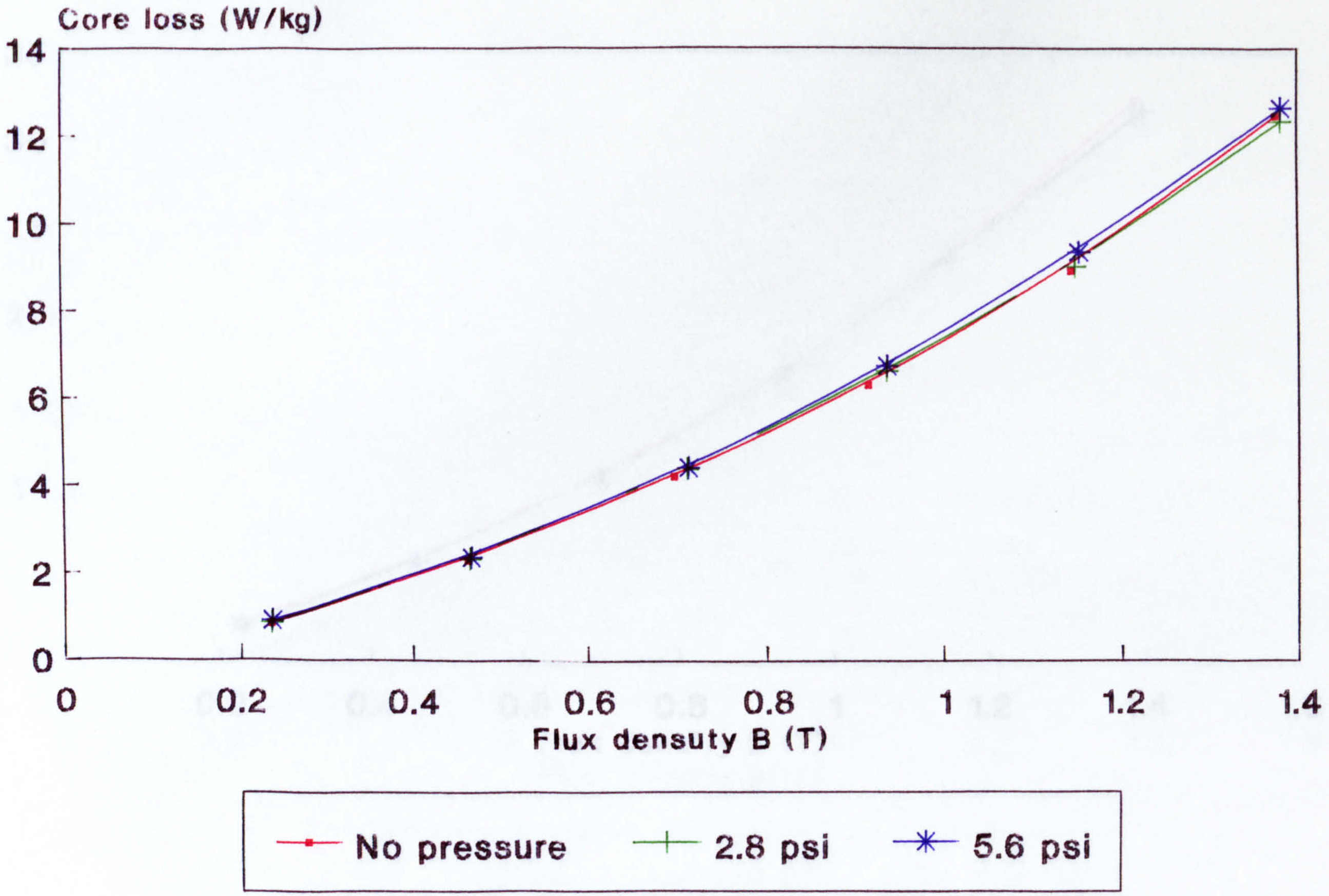

Fig. A.19 Core loss sensitivity of Metglas 2605-S2 of 0, 2.8 and 5.6 psi at 1000 Hz core No.1.

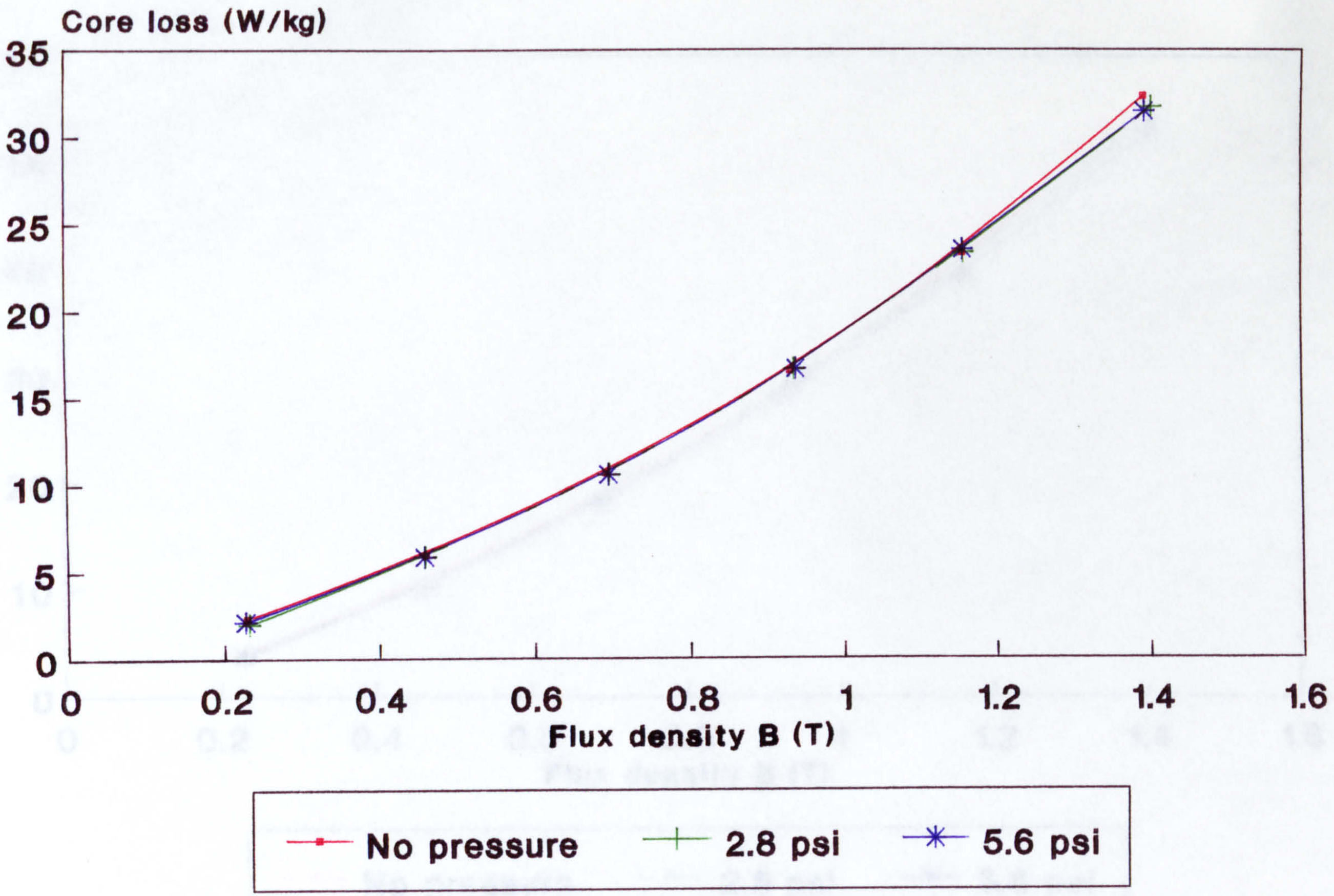

Fig. A.20 Core loss sensitivity of Metglas 2605-S2 of 0, 2.8 and 5.6 psi at 2000 Hz core No.1.

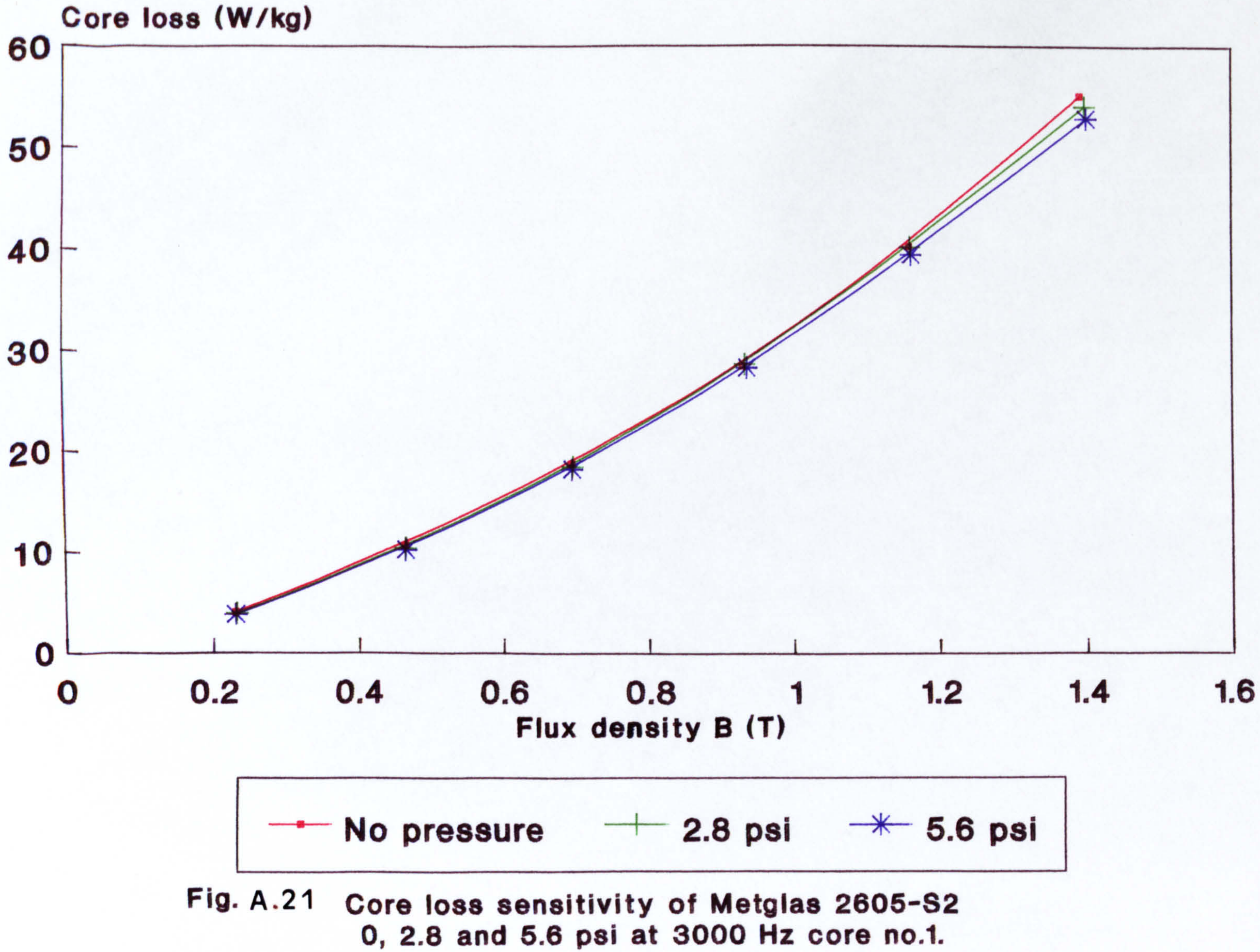

Fig. A.21 Core loss sensitivity of Metglas 2605-S2 0, 2.8 and 5.6 psi at 3000 Hz core no.1.